

Breaking the Symmetry
with
Helicating Oligopyridines

Inauguraldissertation

zur

Erlangung der Würde eines Doktors der Philosophie
vorgelegt der
Philosophisch-Naturwissenschaftlichen Fakultät
der Universität Basel

von

Inger Annette Hougen

aus St. Antönien-Ascharina, Graubünden

Basel, 2004

Genehmigt von der Philosophisch-Naturwissenschaftlichen Fakultät

auf Antrag von

Prof. Dr. Edwin C. Constable

Prof. Dr. Katharina M. Fromm

Basel, den 6. Juli 2004

Prof. Dr. Marcel Tanner
Dekan

Never as dark as just before dawn

Acknowledgements

Prof. Dr. Edwin C. Constable and Prof. Dr. Catherine E. Housecroft for offering me the opportunity to do this research and for supervision

Prof. Dr. Katharina M. Fromm for acting as co-referee for the thesis and acting as coexaminer

Prof. Dr. Hanspeter Huber for chairing the exam

My parents Nils Henrik and Elisabeth Hougen-Lötscher

My brother Lukas Fridtjof Hougen

Haluk Yilmaz for cooking at any hour in the day and for moral support

Ayten Sezen for her kindness

Christian Markert for giving me the Stille coupling conditions and literature about $\text{Pd}(\text{Ph}_3\text{P})_2\text{Cl}_2$ and LiCl

Dr. Jürgen Müller, Dr. Torsten Kulke, Dr. Alain Schneider and François Raymond Ph.D. from American Dye Source, Inc., Baie d'Urfé, Quebec, Canada for fruitful discussions

Dr. Christopher Smith 'Chris' many thanks for setting up crystallisations which gave the crystals of $[\text{Cu}_2(\text{mp})_2][\text{PF}_6]_3$, and for many fruitful discussions, help with the computer, proof reading and for being a great friend

Dr. Niamh McMahon and Dr. Conor Brennan for help writing in English

Prof. Dr. Peter Belser for sending me the literature used for synthesising 2-bromo-6'-carboxy-4'-(4-methoxyphenyl)-2,2'-bipyridine¹

Dr. Reza Fallahpour for the Jameson literature^{2,3}

Dr. Egbert Figgemeier for electrochemical measurements and for help with the LaTeX programme

Dr. Olimpia Mamula for catalyst activation of $\text{Pd}(\text{Ph}_3\text{P})_4$ ethanol diethylether, and for helping me to submit for international conferences

Herr Nadig for EI and FAB mass spectrometric measurements

Herr Kirsch for microanalyses

Dr. Gerd Scherer and Dr. Daniel Häussinger for NMR measurements on the 600 MHz spectrometer

Dr. Klaus Kulike, for measuring COSY on the 500 MHz NMR-spectrometer

Lukas Scherer and Sarah Chow for Maldi-TOF measurements and for fruitful discussions

Dr. Valérie Jullien for helping me with software problems (ChemDraw) and proof reading

Barbara Brisig for the spin only and paramagnetic susceptibility NMR methods literature

Leo Merz, Markus Honegger, Dr. Markus Weitzer and Emanuela Bianchi for help with LaTeX

Dr. Bernhard Jung for general computer support

All the members of the past and present Constable-Housecroft group and everyone in the former 'Institut für Anorganische Chemie' for the good atmosphere

The Swiss National Fonds, the University of Basel and the 'Freiwillige Akademische Gesellschaft' FAG for funding

Summary

Chapter 1 enters into the field of research in which this thesis is placed. It summarises relevant concepts and introduces the chemical systems studied in this thesis.

Chapter 2 describes the ligand synthesis steps to the 2,2':6',2'':6'',2''':6''',2''''-quinquepyridine (**qnp**) derivatives, and includes their characterisation as well as the characterisation of the intermediate substances.

Chapter 3 describes the synthetic steps of linking two identical **qnp** moieties together into one new ligand. The linked ligands are characterised.

Chapter 4 describes the metal directed assembly of mono- and double-helicates of new (**qnp**) and linked ligands. Complexations with copper(II), cobalt(II) and nickel(II) are described, and the species formed are characterised. Two NMR-titrations with D₂O are discussed briefly and two are discussed in detail.

Chapter 5 describes the synthetic pathway to a new terminally substituted 2,2':6',2'':6'',2'''-quaterpyridine (**qtp**) derivative, and includes characterisation of this ligand, as well as the new intermediate products.

Chapter 6 summarises the achievements and conclusions, and offers a perspective of future work on these or similar systems.

Chapter 7 contains the experimental details on the syntheses, characterisations and general experimental data.

Contents

Acknowledgements	iv
Summary	v
Abbreviations	xviii
1 Introduction	1
1.1 Supramolecular chemistry	1
1.1.1 Definition	1
1.1.2 Placing supramolecular chemistry	2
1.2 Metallosupramolecular chemistry	3
1.2.1 Definition	3
1.2.2 The coordinate bond	3
1.3 The helical motif	5
1.3.1 Helicates	7
1.4 Going asymmetric	9
1.5 The projects in this thesis	9
2 Unsymmetrically substituted quinquepyridine ligands	15
2.1 Overview	15
2.1.1 Different approaches and mechanisms of the 2,6-oligopyridine synthesis	15
2.1.2 The synthetic pathway to the qnp _y derivatives qp, mp and pp	15
2.2 2,6-Diacetylpyridine	18
2.2.1 Synthesis and characterisation	18
2.3 Mono- and bis-chalcones	18
2.3.1 General synthesis	18
2.3.2 Differences and crucial points	18
2.3.3 Characterisation	19
2.4 qnp _y derivative ligands: qp, mp and pp	24
2.4.1 Synthesis	24
2.4.2 Characterisation	24

3	Unsymmetrically linked quinquepyridine ligands	33
3.1	Overview	33
3.1.1	Expected features of the linked ligands comprising two qnpy domains	33
3.1.2	Synthetic route to the qnpy derivatives qcq, mcm and pcp	34
3.2	Linked qnpy ligands: qcq, mcm and pcp	35
3.2.1	Synthesis	35
3.2.2	Crucial point	35
3.2.3	Characterisation	36
4	Complexes of unsymmetrically substituted quinquepyridine and linked quinquepyridine type ligands with copper(II), copper(I), cobalt(II) and nickel(II)	47
4.1	Tools for the characterisation of the coordination compounds	47
4.1.1	¹ H-NMR method for paramagnetic compounds	47
4.2	Copper complexes	49
4.2.1	Synthesis	49
4.2.2	Crystallographic analysis	55
4.2.3	Comparison with other substituted quinquepyridine complexes	74
4.2.4	Electrochemistry	81
4.2.5	UV-Vis spectra and spectroelectrochemistry	83
4.2.6	Summary and conclusions	88
4.3	Cobalt complexes	92
4.3.1	Synthesis and characterisation of mononuclear complexes	92
4.3.2	Synthesis and characterisation of dinuclear complexes	96
4.3.3	Electrochemistry	113
4.3.4	Summary	114
4.4	Nickel complexes	117
4.4.1	Synthesis and characterisation	117
5	Synthesis of a quaterpyridine to be linked at the 4-position of the terminal ring	119
5.1	Overview	119
5.2	Reaction steps to 4-(4-methoxyphenyl)-2,2':6',2'':6'', 2'''-quaterpyridine (4MeOphqtpy)	120
5.2.1	6,6'-Bromo-2,2'-bipyridine	120
5.2.2	6-Bromo-2,2'-bipyridine	120
5.2.3	6-Tributylstannyl-2,2'-bipyridine	120
5.2.4	3-(4'-Methoxyphenyl)-1-oxo-2-butenoic acid	121
5.2.5	<i>N</i> -[1-Oxo-1-(6-bromo-2-pyridyl)eth-2-yl]pyridinium iodide (Br-PPI)	121
5.2.6	6'-Bromo-6-carboxylate-4-(4-methoxyphenyl)-2,2'-bipyridine	121
5.2.7	6-Bromo-4'-(4-methoxyphenyl)-2,2'-bipyridine	122
5.2.8	4-(4-Methoxyphenyl)-2,2':6',2'':6'', 2'''-quaterpyridine	122
5.3	Alternative reaction steps to 4MeOphqtpy	123
5.3.1	(2,2'-6-bipyridyl)-4,4,5,5-tetramethyl-1,3,2-dioxaborolan	124
5.3.2	4-(4-Methoxyphenyl)-2,2':6',2'':6'', 2'''- quaterpyridine	124
5.4	Conclusions about the syntheses	124
5.5	Summary and outlook	125

6	Conclusions and perspectives	129
7	Experimental Details	131
7.1	The synthesis of 4'-(<i>tert</i> -butylphenyl)-4'''-(4-hydroxyphenyl)-2,2':6',2'':6'',2''':6''',2''''-quinquepyridine (qp) and complexes	131
7.1.1	Diethyl 2,6-dipicolinate	131
7.1.2	2,6-Diacetylpyridine	131
7.1.3	2-Acetyl-6-[3-(4-hydroxyphenyl)-1-oxoprop-2-enyl]pyridine	132
7.1.4	2-[3-(4- <i>tert</i> -Butylphenyl)-1-oxoprop-2-enyl]-6-[3-(4-hydroxyphenyl)-1-oxoprop-2-enyl]pyridine	133
7.1.5	Side product of the synthesis above: 2,6-di-[3- <i>tert</i> -butylphenyl]-1-oxoprop-2-enyl]pyridine	133
7.1.6	<i>N</i> -[1-Oxo-1-(2-pyridyl)-eth-2-yl]pyridinium iodide (PPI)	134
7.1.7	4'-(4- <i>tert</i> -Butylphenyl)-4'''-(4-hydroxyphenyl)-2,2':6',2'':6'',2''':6''',2''''-quinquepyridine (qp)	134
7.1.8	[Cu ₂ (4'-(4- <i>tert</i> -Butylphenyl)-4'''-(4-hydroxyphenyl)-2,2':6',2'':6'',2''':6''',2''''-quinquepyridine) ₂][PF ₆] ₃ , [Cu ₂ (qp) ₂][PF ₆] ₃	135
7.2	The synthesis of 1,17-di(4-(4'-(4- <i>tert</i> -Butylphenyl)-2,2':6',2'':6'',2''':6''',2''''-quinquepyridyl)-phenoxy)-3,6,9,12,15-pentaoxaheptadecane (qcq) and complexes	136
7.2.1	Hexaethylene glycol ditosylate (Tos ₂ Heg)	136
7.2.2	1,17-di(4-(4'-(4- <i>tert</i> -Butylphenyl)-2,2':6',2'':6'',2''':6''',2''''-quinquepyridyl)phenoxy)-3,6,9,12,15-pentaoxaheptadecane (qcq)	136
7.2.3	[Cu ₂ (1,17-di(4-(4'-(4- <i>tert</i> -Butylphenyl)-2,2':6',2'':6'',2''':6''',2''''-quinquepyridyl)-phenoxy)-3,6,9,12,15-pentaoxaheptadecane)][PF ₆] ₃ , [Cu ₂ qcq][PF ₆] ₃	137
7.2.4	[[Co ₂ (1,17-di(4-(4'-(4- <i>tert</i> -butylphenyl)-2,2':6',2'':6'',2''':6''',2''''-quinquepyridyl)-phenoxy)-3,6,9,12,15-pentaoxaheptadecane)(OAc)][PF ₆] ₃ , [Co ₂ (qcq)(OAc)][PF ₆] ₃	138
7.2.5	[Co ₂ (1,17-bis(4-(4'-(4- <i>tert</i> -Butyl phenyl)-2,2':6',2'':6'',2''':6''',2''''-quinquepyridyl)phenoxy)-3,6,9,12,15-pentaoxaheptadecane)(H ₂ O) ₂ (MeOH) ₂][OAc][PF ₆] ₃ , [Co ₂ (qcq)(OH ₂) ₂ (MeOH) ₂][PF ₆] ₄	138
7.3	The synthesis of the 4'-(methoxyphenyl)-4'''-(4-hydroxyphenyl)-2,2':6',2'':6'',2''':6''',2''''-quinquepyridine (mp) and complexes	139
7.3.1	2-Acetyl-6-[3-(4-methoxyphenyl)-1-oxoprop-2-enyl]pyridine	139
7.3.2	Side product of the synthesis above: 2,6-bis[3-(4-methoxyphenyl)-1-oxoprop-2-enyl]pyridine	140
7.3.3	2-[3-(4-methoxyphenyl)-1-oxoprop-2-enyl]-6-[3-(4-hydroxyphenyl)-1-oxoprop-2-enyl]pyridine	140
7.3.4	4'-(4-Methoxyphenyl)-4'''-(4-hydroxyphenyl)-2,2':6',2'':6'',2''':6''',2''''-quinquepyridine (mp)	141
7.3.5	[Cu ₂ (4'-(4-methoxyphenyl)-4'''-(4-hydroxyphenyl)-2,2':6',2'':6'',2''':6''',2''''-quinquepyridine) ₂][PF ₆] ₃ , [Cu ₂ (mp) ₂][PF ₆] ₃	142
7.3.6	[Nickel ₂ (4'-(4-methoxyphenyl)-4'''-(4-hydroxyphenyl)-2,2':6',2'':6'',2''':6''',2''''-quinquepyridine) ₂ (OAc)][PF ₆] ₃ , [Ni ₂ (mp) ₂ (OAc)][PF ₆] ₃	143
7.3.7	Drying cobalt(II) acetate	144
7.3.8	[Cobalt ₂ (4'-(4-methoxyphenyl)-4'''-(4-hydroxyphenyl)-2,2':6',2'':6'',2''':6''',2''''-quinquepyridine) ₂ (OH ₂)(OH)][PF ₆] ₃ , [Co ₂ (mp) ₂ (OH ₂)(OH)][PF ₆] ₃	144

7.3.9	[Cobalt(4'-(4-methoxyphenyl)-4'''-(4-hydroxyphenyl)-2,2':6',2'':6'',2''':6''',2''''-quinquepyridine)(H ₂ O) ₂][PF ₆] ₂ , [Co(mp)(OH ₂) ₂][PF ₆] ₂	144
7.4	The synthesis of 1,17-Bis(4-(4'-(4-methoxyphenyl)-2,2':6',2'':6'',2''':6''',2''''-quinquepyridyl)phenoxy)-3,6,9,12,15-pentaoxaheptadecane (mcm) and complexes	145
7.4.1	1,17-Bis(4-(4'-(4-methoxyphenyl)-2,2':6',2'':6'',2''':6''',2''''-quinquepyridyl)phenoxy)-3,6,9,12,15-pentaoxaheptadecane (mcm)	145
7.4.2	[Cu ₂ (1,17-Bis(4-(4'-[4-methoxyphenyl]-2,2':6',2'':6'',2''':6''',2''''-quinquepyridyl)phenoxy)-3,6,9,12,15-pentaoxaheptadecane)][PF ₆] ₄ , [Cu ₂ mcm][PF ₆] ₃	146
7.5	The Synthesis of 4'-(4-hydroxyphenyl)-4'''-phenyl-2,2':6',2'':6'',2''':6''',2''''-quinquepyridine (pp) and complexes	147
7.5.1	2-[3-(4-Hydroxy)-1-oxoprop-2-enyl]-6-[3-phenyl-1-oxoprop-2-enyl]pyridine	147
7.5.2	4'-(4-Hydroxyphenyl)-4'''-phenyl-2,2':6',2'':6'',2''':6''',2''''-quinquepyridine (pp)	147
7.5.3	[Cu ₂ (4'-(4-hydroxyphenyl)-4'''-phenyl-2,2':6',2'':6'',2''':6''',2''''-quinquepyridine)] ₂ [PF ₆] ₃ , [Cu ₂ (pp) ₂][PF ₆] ₃	148
7.6	The synthesis of 1,17-Bis-4-(4'-(4'''-phenyl-2,2':6',2'':6'',2''':6''',2''''-quinquepyridyl)phenoxy)-3,6,9,12,15-pentaoxaheptadecane (pcp) and complexes	149
7.6.1	1,17-Bis-4-(4'-(4'''-phenyl-2,2':6',2'':6'',2''':6''',2''''-quinquepyridyl)phenoxy)-3,6,9,12,15-pentaoxaheptadecane (pcp)	149
7.6.2	[Cu ₂ (1,17-di-4'(4'''-phenyl-2,2':6',2'':6'',2''':6''',2''''-quinquepyridyl)phenoxy)-3,6,9,12,15-pentaoxaheptadecane)][PF ₆] ₃ , [Cu ₂ pcp][PF ₆] ₃	150
7.7	On the way to 5-(4-methoxyphenyl)-2,2':6',2'':6'',2'''-quaterpyridine (5qtpy)	151
7.7.1	3- <i>N,N</i> -Dimethylamino-1-oxo-1-(2-pyridyl)-2-propene	151
7.7.2	2-Acetyl-6-bromopyridine	151
7.7.3	2-Bromo-6-(3'-dimethylammonio-1'-oxopropyl)pyridine chloride	152
7.7.4	2-Ethylthiopyridine	152
7.7.5	2-Bromo-6-(2-methyl-1,3-dioxolan-2-yl)pyridine	153
7.7.6	6-Bromo-2,2':6',2''-terpyridine	153
7.7.7	6-(<i>n</i> -Butyl)-2,2':6',2''-terpyridine	154
7.7.8	Test boronation reaction of 2-bromopyridine: comparing the effects of <i>n</i> -BuLi and PhLi	155
7.7.9	4-Methoxyphenylboronic acid	156
7.7.10	Dimethoxyl-4-methoxyphenyl borate	157
7.7.11	Diisopropyl-4-methoxyphenyl borate	157
7.7.12	Test on which side of the 2,5-dibromopyridine the lithiation occurs	158
7.7.13	2-Bromo-5-pyridylboronic acid	158
7.7.14	Two approaches to 2-bromo-5-(4-methoxyphenyl)pyridine	159
7.7.15	5-Bromo-2-(4-methoxyphenyl) pyridine	160
7.7.16	Diisopropyl-2-(4-methoxyphenyl)-5-pyridyl borate	162
7.8	The synthesis of 4-(4-methoxyphenyl)-2,2':6',2'':6'',2'''-quaterpyridine (4MeOphqtpy)	163
7.8.1	6,6'-Dibromo-2,2'-bipyridine	163
7.8.2	6-Bromo-2,2'-bipyridine	163
7.8.3	6- <i>n</i> -Butyl-2,2'-bipyridine	164
7.8.4	6-Tributylstannyl-2,2'-bipyridine	165

7.8.5	3-(4'-Methoxyphenyl)-1-oxo-2-butenoic acid	166
7.8.6	<i>N</i> -[1-Oxo-1-(6-bromo-2-pyridyl)eth-2-yl]pyridinium iodide (Br-PPI)	166
7.8.7	6'-Bromo-4-(4-methoxyphenyl)-2,2'-bipyridine-6-carboxylic acid	167
7.8.8	6-Bromo-4'-(4-methoxyphenyl)-2,2'-bipyridine	168
7.8.9	4-(4-Methoxyphenyl)-2,2':6',2'':6'',2''':6''',2''''-quaterpyridine	169
7.8.10	Alternative synthesis of 6-bromo-4'-(4-methoxyphenyl)-2,2'-bipyridine	170
7.9	Alternative synthesis of 4-(4-methoxyphenyl)-2,2':6',2'':6'',2''':6''',2''''- quaterpyridine	171
7.9.1	(2,2'-bipyrid-6-yl)-4,4,5,5-tetramethyl-1,3,2-dioxaborolane	171
7.9.2	4-(4-Methoxyphenyl)-2,2':6',2'':6'',2''':6''',2''''- quaterpyridine	172
7.10	General Experimental	173
A	Crystal Structures of Helicates	175
A.1	[Cu ₂ (mp) ₂][PF ₆] ₃	175
A.2	[Cu ₂ pcp][PF ₆] ₃	186
B	Crystal Structures of the qtpy-ligand: 4MeOphqtpy	197
B.1	4MeOphqtpy	197
C	Crystal Structures of Helicand precursors	201
C.1	2-Acetyl-6-[3-(4-methoxyphenyl)-1-oxoprop-2-enyl]pyridine	201
C.2	6-Bromo-[4'-(4-methoxyphenyl)]-2,2'-bipyridine	204
C.3	5-Bromo-2-(4-methoxyphenyl)pyridine	207
C.4	6'-Bromo-6-carboxyl-4-(4-methoxyphenyl)-2,2'-bipyridine	209
C.5	4-Methoxyphenylboronic acid	211
D	Crystal structures of minor quality	213
D.1	2,6-di-[3- <i>tert</i> -butylphenyl]-1-oxoprop-2-enyl]pyridine	213
D.2	Dibenzo-18-crown-6	214

List of Figures

1.1	Molecular orbital diagram for a first row transition metal octahedral complex with a σ -donor ligand.	5
1.2	Molecular orbital diagram for a first row transition metal octahedral complex with a σ - and π -donor ligand.	6
1.3	Molecular orbital diagram for a first row transition metal octahedral complex with a σ -donor and π -acceptor ligand.	6
1.4	Molecular orbital diagram for a first row transition metal tetrahedral complex with a σ -donor ligand.	7
1.5	Energetically best available orbitals, with which pyridine may interact.	8
1.6	The first designed dinuclear double helicate, formed by preorganised qtpy derivatives.	9
1.7	Schematic picture of the two helical enantiomers, shown in the example of a dinuclear double helicate.	10
1.8	Formula of 2,2':6',2'':6'',2''':6'''-quaterpyridine (qtpy) and 2,2':6',2'':6'',2''':6''',2''''-quinquepyridine (qnpq). qtpy consists of four, qnpq of five pyridine rings.	10
1.9	Schematic picture of the different possible isomers with unsymmetrically substituted quinquepyridine type ligands and two non-equivalent metal ions (octahedral and tetrahedral) in a dinuclear double helicate, showed on the example of a Cu(II)/Cu(I) complex of unsymmetrical qnpq.	11
1.10	A qnpq with different substituents in two positions. A linker is introduced in the 4'''-position. All six ligands have been fully characterised.	11
1.11	qtpy and qnpq with a substituent in any position on one of the terminal pyridine rings. A linker introduced at this substituent position is strategically placed for forming hair-pin helicates.	12
1.12	Schematic picture of the HT enantiomers of [Cu ₂ pcp] ³⁺	13
1.13	Schematic picture of a HH- and a HT-dinuclear double helicate isomer with a terminally linked qtpy derivative ligand.	13
2.1	Last step in the Hantzsch pyridine synthesis versus completion of the Kröhnke cyclisation	16
2.2	Overview of the synthesis of the qnpq derivatives and ligands qp, mp and pp, R = <i>tert</i> -butyl, methoxy and H for qp, mp and pp respectively.	17
2.3	General labels of the qnpq derivatives and ligands, R = <i>tert</i> -butyl, methoxy and H for qp, mp and pp respectively.	24
2.4	The UV absorption spectra of the three qnpq derivatives qp, mp and pp.	26
2.5	600 MHz ¹ H-NMR spectrum of mp.	28
3.1	Tris-bipy with chiral template	33

3.2	Overview of the synthesis of the linked qnpy derivatives and ligands qcq, mcm and pcp, R = <i>tert</i> -butyl, methoxy and H for qcq, mcm and pcp respectively.	34
3.3	General labels of the qnpy derivatives and ligands, R = <i>tert</i> -occur, methoxy and H for qcq, mcm and pcp respectively.	35
3.4	The UV absorption spectra of the three linked qnpy derivatives qcq, mcm and pcp. . .	37
3.5	600 MHz ¹ H-NMR spectrum of qcq.	45
3.6	¹ H ¹⁵ N-HMBC NMR spectrum of the unsymmetrically linked qnpy derivative qcq. . .	46
4.1	Formation of dinuclear copper complexes with an unsymmetrical qnpy derivative and with an unsymmetrically linked qnpy derivative.	50
4.2	600 MHz ¹ H-NMR spectrum of [Cu ₂ (mp) ₂][PF ₆] ₃ acetonitrile-d ₃ solution.	52
4.3	A cut of the 600 MHz ¹ H-NMR spectra of [Cu ₂ (pp) ₂][PF ₆] ₃ , [Cu ₂ (mp) ₂][PF ₆] ₃ and [Cu ₂ (qp) ₂][PF ₆] ₃ acetonitrile-d ₃ solution.	53
4.4	A cut of the 600 MHz ¹ H-NMR spectra of [Cu ₂ pcp][PF ₆] ₃ , [Cu ₂ mcm][PF ₆] ₃ and [Cu ₂ qcq][PF ₆] ₃ acetonitrile-d ₃ solution.	54
4.5	Crystal structure of the cation in [Cu ₂ (mp) ₂][PF ₆] ₃ · 1.5 acetone: sideways view. . . .	56
4.6	Crystal structure of the cation in [Cu ₂ (mp) ₂][PF ₆] ₃ · 1.5 acetone: view along the Cu-Cu axis.	57
4.7	Crystal structure of the cation in [Cu ₂ pcp][PF ₆] ₃ · 2.5 acetone: sideways view.	58
4.8	Crystal structure of the cation in [Cu ₂ pcp][PF ₆] ₃ · 2.5 acetone: view along the Cu-Cu axis.	59
4.9	Crystal structure: one coordinated ligand strand of [Cu ₂ mp ₂][PF ₆] ₃ , emphasizing the terpy and bipy domains.	60
4.10	Crystal structure: one coordinated ligand strand' of [Cu ₂ mp ₂][PF ₆] ₃ , emphasizing the terpy and bipy domains.	60
4.11	Crystal structure: one coordinated ligand strand of [Cu ₂ pcp][PF ₆] ₃ , emphasizing the terpy and bipy domains.	62
4.12	Crystal structure: one coordinated ligand strand' of [Cu ₂ pcp][PF ₆] ₃ , emphasizing the terpy and bipy domains.	62
4.13	N-Cu-N angles of the octahedrally coordinated Cu(II) and the tetrahedrally coordinated Cu(I) in Cu ₂ (mp) ₂ ³⁺	71
4.14	N-Cu-N angles of the octahedrally coordinated Cu(II) and the tetrahedrally coordinated Cu(I) in Cu ₂ pcp ³⁺	71
4.15	Well centred copper(II) and copper(I) in the complex [Cu ₂ (mp) ₂] ³⁺	72
4.16	Well centred copper(II) and copper(I) in the complex [Cu ₂ pcp] ³⁺	73
4.17	UV spectra of the qnpy-type copper complexes in the region 200nm-450nm in acetonitrile.	84
4.18	Vis spectra of the qnpy-type copper complexes in the region 450nm-800nm in acetonitrile.	85
4.19	The UV absorption spectra of the three qnpy derivatives qp, mp and pp in chloroform and their copper(II/I) helicate complexes in acetonitrile solutions.	86
4.20	The UV absorption spectra of the three linked qnpy derivatives qcq, mcm and pcp in chloroform and their copper(II/I) helicate complexes in acetonitrile solutions.	87
4.21	A copper(I) trinuclear tris-bipy double helicate.	87
4.22	Spectroelectrochemistry of [Cu ₂ (mp) ₂][PF ₆] ₃ in acetonitrile, applied potential of +800mV.	88
4.23	Spectroelectrochemistry of [Cu ₂ (mp) ₂][PF ₆] ₃ in acetonitrile, applied potential of -400mV.	89
4.24	Spectroelectrochemistry of [Cu ₂ pcp][PF ₆] ₃ in acetonitrile, applied potential of +1100mV.	90

4.25	Spectroelectrochemistry of $[\text{Cu}_2\text{pcp}][\text{PF}_6]_3$ in acetonitrile, applied potential of -100mV.	91
4.26	Formation of mononuclear complexes with an unsymmetrical qnpy derivative and with an unsymmetrically linked qnpy derivative.	92
4.27	600 MHz $^1\text{H-NMR}$ spectrum of $[\text{Co}(\text{mp})(\text{OH}_2)_2][\text{PF}_6]_2$ in acetonitrile- d_3 , the region of least shifted protons.	93
4.28	600 MHz $^1\text{H-NMR}$ spectrum of $[\text{Co}(\text{mp})(\text{OH}_2)_2][\text{PF}_6]_2$ in acetonitrile- d_3	94
4.29	250 MHz $^1\text{H-NMR}$ spectrum of $[\text{Co}_2(\text{qcq})(\text{OH}_2)_2][\text{PF}_6]_4$ in acetonitrile- d_3	94
4.30	Formation of dinuclear complexes with an unsymmetrical qnpy derivative and with an unsymmetrically linked qnpy derivative.	96
4.31	250 MHz $^1\text{H-NMR}$ spectrum of the dinuclear double helicate $[\text{Co}_2(\text{qcq})(\text{OAc})][\text{PF}_6]_3$ in acetonitrile- d_3	97
4.32	600 MHz $^1\text{H-NMR}$ spectrum of $[\text{Co}_2(\text{mp})_2(\text{OAc})][\text{PF}_6]_3$ in acetonitrile- d_3	98
4.33	A possible mechanism for the transition from dinuclear double helicate to mononuclear helicate.	103
4.34	600 MHz $^1\text{H-NMR}$ titration of $[\text{Co}_2(\text{mp})_2(\text{OAc})][\text{PF}_6]_3$ in acetonitrile- d_3 with D_2O , the area of most shifted protons.	104
4.35	600 MHz $^1\text{H-NMR}$ titration of $[\text{Co}_2(\text{mp})_2(\text{OAc})][\text{PF}_6]_3$ in acetonitrile- d_3 with D_2O , the area of next most shifted protons.	105
4.36	600 MHz $^1\text{H-NMR}$ titration of $[\text{Co}_2(\text{mp})_2(\text{OAc})][\text{PF}_6]_3$ in acetonitrile- d_3 with D_2O , the area of next least shifted protons.	106
4.37	600 MHz $^1\text{H-NMR}$ titration of $[\text{Co}_2(\text{mp})_2(\text{OAc})][\text{PF}_6]_3$ in acetonitrile- d_3 with D_2O , the area of least shifted protons.	106
4.38	600 MHz $^1\text{H-NMR}$ titration of $[\text{Co}_2\text{qcq}(\text{OAc})][\text{PF}_6]_3$ in acetonitrile- d_3 with D_2O , the area of the most shifted protons.	108
4.39	600 MHz $^1\text{H-NMR}$ titration of $[\text{Co}_2\text{qcq}(\text{OAc})][\text{PF}_6]_3$ in acetonitrile- d_3 with D_2O , the area of the medium shifted protons.	110
4.40	600 MHz $^1\text{H-NMR}$ titration of $[\text{Co}_2\text{qcq}(\text{OAc})][\text{PF}_6]_3$ in acetonitrile- d_3 with D_2O , the area of the least shifted protons.	111
4.41	600 MHz $^1\text{H-NMR}$ of $[\text{Co}_2\text{qcq}(\text{H}_2\text{O})_2][\text{PF}_6]_4$ in acetonitrile- d_3 after 2 days, area from 145 to 0ppm.	112
4.42	Redox potentials of $[\text{Co}_2(\text{mp})_2(\text{OAc})][\text{PF}_6]_3$ versus ferrocene: differential pulse voltammetry in acetonitrile (abs), with tetrabutylammonium hexafluorophosphate (0.1M) as electrolyte.	113
4.43	Cyclovoltammogram of $[\text{Co}_2(\text{mp})_2(\text{OAc})][\text{PF}_6]_3$ in acetonitrile with tetrabutylammonium hexafluorophosphate (0.1M) as electrolyte.	114
4.44	600 MHz $^1\text{H-NMR}$ of $[\text{Ni}_2(\text{mp})_2(\text{OAc})][\text{PF}_6]_3$ in acetonitrile- d_3 at ambient temperature.	117
5.1	Overview over the synthesis of 4-(4-methoxyphenyl)-2,2':6',2'':6'',2'''-quaterpyridine.	126
5.2	Two partially alternative reaction pathways to 5-(4-methoxyphenyl)-2,2':6',2'':6'',2'''-quaterpyridine.	127
5.3	A possible Kröhnke cyclisation mechanism to the unsymmetrical bipy derivative with and without a substituent in the 6 position.	128
7.1	Diethyl 2,6-dipicolinat	131
7.2	2,6-Diacetylpyridine	132
7.3	2-Acetyl-6-[3-(4-hydroxyphenyl)-1-oxoprop-2-enyl]pyridine	132

7.4	2-[3-(4- <i>tert</i> -Butylphenyl)-1-oxoprop-2-enyl]-6-[3-(4-hydroxyphenyl)-1-oxoprop-2-enyl]pyridine	133
7.5	2,6-Bis[3-(4-methoxyphenyl)-1-oxoprop-2-enyl]pyridine	133
7.6	<i>N</i> -[1-Oxo-1-(2-pyridyl)-eth-2-yl]pyridinium iodide (PPI)	134
7.7	4'-(4- <i>tert</i> -butylphenyl)-4'''-(4-hydroxyphenyl)-2,2':6',2'':6'',2''':6''',2''''-quinquepyridine	135
7.8	Hexaethyleneglycol ditosylate	136
7.9	1,17-Bis(4-(4'-(4- <i>tert</i> -butylphenyl)-2,2':6',2'':6'',2''':6''',2''''-quinquepyridyl)phenoxy)-3,6,9,12,15-pentaoxaheptadecane	136
7.10	2-Acetyl-6-[3-(4-methoxyphenyl)-1-oxoprop-2-enyl]pyridine.	139
7.11	2,6-Bis[3-(4-methoxyphenyl)-1-oxoprop-2-enyl]pyridine	140
7.12	2-[3-(4-Methoxyphenyl)-1-oxoprop-2-enyl]-6-[3-(4-hydroxyphenyl)-1-oxoprop-2-enyl]pyridine	141
7.13	4'-(4-Methoxyphenyl)-4'''-(4-hydroxyphenyl)-2,2':6',2'':6'',2''':6''',2''''-quinquepyridine	142
7.14	1,17-Bis(4-(4'-(4-methoxyphenyl)-2,2':6',2'':6'',2''':6''',2''''-quinquepyridyl)phenoxy)-3,6,9,12,15-pentaoxaheptadecane	145
7.15	2-[3-(4-Hydroxy)-1-oxoprop-2-enyl]-6-[3-phenyl-1-oxoprop-2-enyl]pyridine	147
7.16	4'-(4-Hydroxyphenyl)-4'''-phenyl-2,2':6',2'':6'',2''':6''',2''''-quinquepyridine	148
7.17	1,17-Bis-4-(4'-(4'''-phenyl-2,2':6',2'':6'',2''':6''',2''''-quinquepyridyl)phenoxy)-3,6,9,12,15-pentaoxaheptadecane	149
7.18	5-(4-Methoxyphenyl)-2,2':6',2'':6'',2''''-quaterpyridine	151
7.19	3- <i>N,N</i> -Dimethylamino-1-oxo-1-(2-pyridyl)-2-propene	151
7.20	2-Acetyl-6-bromopyridine	152
7.21	2-Bromo-6-(3'-dimethylammonio-1'-oxopropyl)pyridine chloride	152
7.22	2-Ethylthiopyridine	153
7.23	2-Bromo-6-(2-methyl-1,3-dioxolan-2-yl)pyridine	153
7.24	6-Bromo-2,2':6',2''-terpyridine	153
7.25	6-2,2':6',2''-Terpyridylboronic acid	154
7.26	6-(<i>n</i> -Butyl)-2,2':6',2''-terpyridine	155
7.27	2-Pyridylboronic acid	155
7.28	4-Methoxyphenylboronic acid	156
7.29	Dimethoxyl-4-methoxyphenyl boronate	157
7.30	Diisopropyl-4-methoxyphenyl borate	157
7.31	2-Bromo-5-pyridylboronic acid	158
7.32	2-Bromo-5-(4-methoxyphenyl)pyridin	159
7.33	5,5'-Di-(4-methoxyphenyl)-2,2'-bipyridine	159
7.34	6,6'-Di-(4-methoxyphenyl)-3,3'-bipyridine (dmp)	160
7.35	5-Bromo-2-(4-methoxyphenyl)pyridine	161
7.36	2,5-Di-(4-methoxyphenyl)pyridine	161
7.37	Diisopropyl-2-(4-methoxyphenyl)-5-pyridyl borate	162
7.38	6,6'-Dibromo-2,2'-bipyridine	163
7.39	6-Bromo-2,2'-bipyridine	163
7.40	6-Pyridyl-1,3,2-dioxaborolane	164

7.41	6- <i>n</i> -Butyl-2,2'-bipyridine	164
7.42	6-Tributylstannyl-2,2'-bipyridine	165
7.43	3-(4'-Methoxyphenyl)-1-oxo-2-butenic acid	166
7.44	<i>N</i> -[1-Oxo-1-(6-bromo-2-pyridyl)eth-2-yl]pyridinium iodide (Br-PPI)	166
7.45	6'-Bromo-4-(4-methoxyphenyl)-2,2'-bipyridine-6-carboxylic acid	167
7.46	6-Bromo-4'-(4-methoxyphenyl)-2,2'-bipyridine	168
7.47	4-(4-Methoxyphenyl)-2,2':6',2'':6'',2'''-quaterpyridine	169
7.48	4-Methoxycinnamaldehyde	170
7.49	1-(1,3-Dioxolan-2-yl)-2-(4-methoxyphenyl)ethene	170
7.50	(2,2'-Bipyrid-6-yl)-4,4,5,5-tetramethyl-1,3,2-dioxaborolane	171
A.1	Crystal structure of the complex cation in [Cu ₂ (mp) ₂][PF ₆] ₃ · 1.5 acetone.	175
A.2	Crystal structure of one of the ligand strands in [Cu ₂ (mp) ₂][PF ₆] ₃ · 1.5 acetone.	175
A.3	Crystal structure of the other of the ligand strands in [Cu ₂ (mp) ₂][PF ₆] ₃ · 1.5 acetone.	176
A.4	Crystal structure of the complex cation of [Cu ₂ pcp][PF ₆] ₃ · 2.5 acetone.	186
A.5	Crystal structure of the two ligand strands of [Cu ₂ pcp][PF ₆] ₃ · 2.5 acetone.	196
B.1	Crystal structure of 4MeOphqtpy.	197
C.1	Crystal structure of 2-acetyl-6-[3-(4-methoxyphenyl)-1-oxoprop-2-enyl]pyridine.	201
C.2	Crystal structure of 6-bromo-4'-(4-methoxyphenyl)-2,2'-bipyridine.	204
C.3	Crystal structure of 5-bromo-2-(4-methoxyphenyl)pyridine.	207
C.4	Crystal structure of 6'-bromo-6-carboxyl-4-(4-methoxyphenyl)-2,2'-bipyridine.	209
C.5	Crystal structure of 4-methoxyphenylboronic acid.	211
D.1	Pluto plot of 2,6-di-[3- <i>tert</i> -butylphenyl]-1-oxoprop-2-enyl]pyridine.	213
D.2	Crystal structure of dibenzo-18-crown-6.	214

Abbreviations

abs. / (abs)	absolute, dry
approx.	approximately
asym.	asymmetrical
bipy	2,2'-bipyridine
bis-chalcone	term used in this thesis as a short general name for any symmetrically and unsymmetrically substituted 2,6-bis(phenyl-1-oxoprop-2-enyl)pyridine compounds
bromo-phenyl-bipy	6-bromo-4'-(4-methylphenyl)-2,2'-bipyridine
Br-PPI	<i>N</i> -[1-Oxo-1-(6-bromo-2-pyridyl)eth-2-yl]pyridinium iodide
BuLi	<i>n</i> -butyllithium
c	concentration
CA	Chemical Abstracts
chalcone ^{4,5} / mono-chalcone	benzal-acetophenone, or benzylidene-acetophenone, used in this thesis as a short general name for the 2-acetyl-6-phenyl-1-oxoprop-2-enylpyridine compounds (with any substituent on the phenyl)
COSY	Correlated spectroscopy, term used in this thesis for two-dimensional H,H-spectra
cp ₂ qnpy	4',4''''-di-(4-chlorophenyl)-2,2':6',2''':6'',2''''':6''''',2''''''-quinquepyridine
d	doublet
DCM	dichloromethane
dd	doublet times doublet
ddd	doublet times doublet times doublet
dmp	6,6'-di-(4-methoxyphenyl)-3,3'-bipyridine
dop ₂ qnpy	4',4''''-di-(4- <i>n</i> -decyl-oxyphenyl)-2,2':6',2''':6'',2''''':6''''',2''''''-quinquepyridine
dt ₂ qnpy	4',4''''-di-(4-methylphenyl)-2,2':6',2''':6'',2''''':6''''',2''''''-quinquepyridine
ds ₂ qnpy	4',4''''-di-(<i>n</i> -decylthio)-2,2':6',2''':6'',2''''':6''''',2''''''-quinquepyridine
dt	doublet times triplet
DMF	<i>N,N</i> -dimethylformamide
EI-MS	electron impact mass spectrometry
esd value	estimated standard deviation
EtOAc	ethyl acetate
FAB-MS	fast atom bombardement
FT-IR	fourier transformation-infrared spectroscopy
h	hour or hours
hetcor	heteronuclear correlation, term used in this thesis for two dimensional C,H and N,H spectra
HH	head-to-head
HMBC	heteronuclear multiple bond correlation
HMQC	heteronuclear multiple quantum coherence
HSQC	heteronuclear single quantum coherence
hp ₂ qnpy	4',4''''-di-(4-hydroxyphenyl)-2,2':6',2''':6'',2''''':6''''',2''''''-quinquepyridine
HT	head-to-tail
HV	high vacuum
IR	infrared spectroscopy
EI	electron impact
Maldi-TOF	Matrix-assisted laser desorption and ionisation time-of-flight
m	in infrared spectroscopy: medium, in NMR spectroscopy: multiplet
mcm	1,17-Bis(4-(4'-(4-methoxyphenyl)-2,2':6',2''':6'',2''''':6''''',2''''''-quinquepyridyl)-phenoxy)-3,6,9,12,15-pentaoxaheptadecane
4MeOphqtpy	4-(4-methoxyphenyl)-2,2':6',2''':6'',2''''-quaterpyridine
5MeOphqtpy	5-(4-methoxyphenyl)-2,2':6',2''':6'',2''''-quaterpyridine
MeOH	methanol
min.	minute or minutes
MLCT	metal-to-ligand charge transfer
mono-chalcone	see chalcone
mop ₂ qnpy	4',4''''-di-methoxyphenyl-2,2':6',2''':6'',2''''':6''''',2''''''-quinquepyridine
mp	4'-(4-methoxyphenyl)-4''''-(4-hydroxyphenyl)-2,2':6',2''':6'',2''''':6''''',2''''''-quinquepyridine

ms ₂ qnpq	4',4'''-di-methylthio-2,2':6',2'':6'',2''':6''',2''''-quinquepyridine
ms ₂ sxpy	4',4'''-di-(methylthio)-2,2':6',2'':6'',2''':6''',2''''-sexipyridine
NBA	3-nitrobenzyl-alcohol
NMR	nuclear magnetic resonance
NOESY	nuclear Overhauser enhancement spectroscopy
OAc	acetate
oct	octahedron / octahedral
OMe	methoxy
ph ₂ qnpq	4',4'''-diphenyl-2,2':6',2'':6'',2''':6''',2''''-quinquepyridine
pcp	1,17-Bis-4-(4'''-phenyl-2,2':6',2'':6'',2''':6''',2''''-quinquepyridyl)phenoxy)-3, 6,9,12,15-pentaoxaheptadecane
pp	4'-(4-hydroxyphenyl)-4'''-phenyl-2,2':6',2'':6'',2''':6''',2''''-quinquepyridine
PPI	<i>N</i> -[1-Oxo-1-(2-pyridyl)eth-2-yl]pyridinium iodide
prim.	primary
ps ₂ qnpq	4',4'''-di-(propylthio)-2,2':6',2'':6'',2''':6''',2''''-quinquepyridine
q	quartett in the NMR
qcq	1,17-Bis(4-(4'- <i>tert</i> -butylphenyl)-2,2':6',2'':6'',2''':6''',2''''-quinquepyridyl)phenoxy)-3,6,9,12,15-pentaoxaheptadecane
qnpq	2,2':6',2'':6'',2''':6''',2''''-quinquepyridine
qp	4'-(4- <i>tert</i> -Butylphenyl)-4'''-(4-hydroxyphenyl)-2,2':6',2'':6'',2''':6''',2''''-quinquepyridine
qtpy	2,2':6',2'':6'',2'''-quaterpyridine
quar.	quaternary
quinquepy	2,2':6',2'':6'',2''':6''',2''''-quinquepyridine
qnpq	2,2':6',2'':6'',2''':6''',2''''-quinquepyridine
ROESY	rotating frame Overhauser enhancement spectroscopy
rotavap	rotary evaporator
s	in NMR spectroscopy: singlet, in infrared spectroscopy: strong
sexipyridine	2,2':6',2'':6'',2''':6''',2''''-sexipyridine
sixpy	2,2':6',2'':6'',2''':6''',2''''-sexipyridine
sh	shoulder
Solv	solvent molecule
subst.	substituted
sym.	symmetrical / symmetrically
<i>t</i> -Bu	<i>tert</i> -butyl
t	triplet
tbpcpqnpq	4'-(4- <i>tert</i> -Butylphenyl)-4'''-(4-chlorophenyl)-2,2':6',2'':6'',2''':6''',2''''-quinquepyridine
tbp ₂ qnpq	4',4'''-Bis-(4- <i>tert</i> -butylphenyl)-2,2':6',2'':6'',2''':6''',2''''-quinquepyridine
td	triplet times doublet
td	tetrahedron / tetrahedral
terpy	2,2':6',2'':6'',2'''-terpyridine
THF	tetrahydrofuran
tos ₂ heg	hexaethylene glycol ditosylate
vb	very broad
v ₂ qnpq	4',4'''-divinyl-2,2':6',2'':6'',2''':6''',2''''-quinquepyridine
vs	very strong
w	weak

Chapter 1

Introduction

1.1 Supramolecular chemistry

1.1.1 Definition

In the last centuries, chemical scientists have learned how to describe salts, minerals and molecules, and the ionic and covalent bonds that hold them together. Today it is possible to synthesise large and complicated molecules from simple starting materials. The last century brought new knowledge about biological systems and advances in biochemistry that showed that molecules are not only able to interconvert, but are also able to interact and communicate with each other. For example, lipids only form cell membranes and thus make life possible⁶ because they organise themselves into double layers, while retaining their identity as molecules. The causes and mechanisms of self-organisation and self-organising systems are the subject of interest and study in supramolecular chemistry.

Inorganic chemistry started to imitate nature using synthetic systems. Maybe the first of those experiments was the formation of crown-ether coordination compounds by Pedersen in the beginning of the sixties. His experiments showed that, depending on the size of the crown-ether, it specifically bound different alkali metal ions. 18-Crown-6 for instance, bound K^+ selectively in presence of Na^+ and Li^+ . In spite of this high selectivity, the interaction between metal ion and crown-ether is not a predominantly covalent bond. Pedersen, Lehn and Cram received the Nobel prize for chemistry in 1987 for the development of molecules that undergo this kind of interaction. In his Nobel address, Lehn formulated an accepted definition of the term supramolecular chemistry^{7,8} as "... the chemistry of the intermolecular bond, concerning the structure and functions of the entities formed by the association of two or more chemical species".⁹ This was when Supramolecular Chemistry was born as an individual discipline. Supramolecular chemistry relates to organised complex entities, held together by interactions like hydrogen bonding, electrostatic interactions (ion pairing), steric complementary forms (where van-der-Waals interactions are optimised), hydrophilic and hydrophobic interactions, so called π - π -stacking, and donor-acceptor interactions. These interactions are used in synthetic systems, but exactly the same interactions are vital in biology.

An important requirement for specific supramolecular assemblies to form, is *molecular recognition*. The term means that molecules or ions taking part in a supramolecular assembly are able to mutually recognise each other, by e.g. their size and shape, positions of hydrogen bonding partners, specifically placed charges, etc. In an ideal supramolecular system, even from a mixture of many partners, the supramolecular assembly forms spontaneously and specifically by the mutual recognition of the partners. For the recognition to be successful, of course the shapes, hydrogen bonding partners and specifically placed charges must be placed *complementary* in the partners.

The complementary placed recognition features of the components partaking in the assembly, is the foundation for *self-organisation* of the components. The matching of the complementary features makes the system reach a thermodynamic minimum when the components organise into, and build up the

supramolecular assembly. This makes the process spontaneous. With mixtures of (many) components, often several arrangements and supramolecular assemblies give local thermodynamic minima, and often these minima are similar in energy. It is a condition of strict self-assembly, that the process must be fully reversible¹ and that the final product lies in a thermodynamic minimum. Then mixtures in solution exist in dynamic equilibrium, and structures may crystallise from them, that were not foretold. In order to be able to control which supramolecular assembly will be favoured, just one way in which the partners can assemble should be most favoured. Or the desired assembly may form in a mixture from which it can be extracted by tools, such as a template, that drive the reaction towards the desired outcome.

1.1.2 Placing supramolecular chemistry

The crucial point about the intermolecular bonds that assemble the supramolecular structures, is the fact that they are weak. This makes them important, for example, in biology. Weak bonds may be broken easily, and this allows change. A system may react upon interference from outside, like temperature rise and fall, changing of pH, or others, because the thermodynamic minimum may differ, depending on the conditions. Absolutely closed systems, that allow no exchange of matter or energy, will strive to reach the overall thermodynamic minimum (and a maximum in entropy). Our supramolecular assemblies, and biological systems however consist of components with specific sites that may interact with partners of complementary features at complementary sites, and they are receiving free enthalpy from the outside, in form of matter and energy.¹⁰

An example from molecular biology, that illustrates how important this new research area is, are the proteins. When solely considering covalent bonds, they are just long molecule strands. They are acting specifically, for example as enzymes, only when they are folded correctly, and their folding is a supramolecular process. Recent headlines were made about a special protein, the prion that causes BSE. The reason for it being toxic, lies in a wrong folding. If it were folded correctly, it would be perfectly harmless.¹¹⁻¹³

A fascinating experiment about self-organisation was conducted by Breivik.¹⁴ He built a macroscopic model for self-replication that should show how genetic information may have arisen spontaneously. The model consisted of ferromagnetic objects that self-organised into polymers due to environmental fluctuations in temperature. The polymers that formed then template-replicated themselves. The system was reminiscent of DNA, except for employing just two kind of subunits instead of four different nucleotides. The units were macroscopic close-to rectangular plastic bits of two kinds with complementary recognition and binding features, floating freely in liquid. They could partner each other via the short side in the strong bond (permanent magnets) or via the long side in a weak bond (temporary magnets with Curie temperature near the ambient temperature). The stronger magnets corresponded to the phosphate bridge for the nucleotides, and the weaker ones to the base pairs. The experiment was performed with constant liquid turbulence and cyclic variation of the temperature between 60°C and 15°C.

The building blocks started to bond together via the strong magnet when the temperature was high, and the units of the thread began to pair up with the complementary units when the temperature was low. Then the paired complementary units were encouraged into binding with each other, in the arrangement in which they had paired up with the firstly growed strand, to form a complimentary strand. Upon returning to high temperature, the paired polymer split up again, giving now two complementary chains which in turn, upon cooling, paired with new unbound complementary units, and so on. The units built up a polymer and replicated, simply by having the correct features at the correct sites for weak and stronger binding. The evolving polymers carried information, not only about their line of related structures, but also about the environment that allowed them to propagate by the sequential information. The latter was not programmed into the design of the system, but self-organised from chaotic interactions exclusively driven by fluctuations in heat and turbulence.

This experiment certainly mimics the functionality of biology, and a macroscopic model like this is a step into merging the disciplines of physics, biology and chemistry. The weaker magnets, that were

¹There are some other examples of supramolecular assemblies, like interlocked rings, where a chemical bond would have to break in order for the rings to be able to detach from each other. These are special cases, and not discussed here.

turned off by the increase in temperature, and thus correspond to a weak bond or interaction between molecules or ions and thus modeled supramolecular chemistry.

Presently, physical,- material- and nano-scientists are working on miniaturisation of machines (computers, telephones, cameras, etc.), and the smallest imaginable would consist of single molecules as functional components. Instead of ‘engineering down’ to smaller and smaller pieces, the supramolecular approach of the chemical scientists is ‘engineering up’, by building supramolecular assemblies with functions of a machine,^{15,16} like e.g. molecular wires,¹⁷⁻²¹ switches,²²⁻²⁴ energy converters²⁵ or sensors.²⁶ The result may be miniaturisation *par excellence* when machines are ‘engineered-up’ by supramolecular construction.

So supramolecular chemistry may be placed between chemistry, biology, physics, material- and nano-science. It is an important new research field, that promises better understanding and control of dynamic biological processes, but also materials with new properties, that form spontaneously by self-assembly/disassembly or exchange.^{27,28}

1.2 Metallosupramolecular chemistry

1.2.1 Definition

One of the newest trends, and rapidly developing subdiscipline of supramolecular chemistry, is the use of transition metal centres to control formation of new supramolecular structures.²⁹ The key tools for assembly in metallosupramolecular chemistry are donor-acceptor interactions between transition metal atoms or ions, and molecules. This interaction is called the coordinative bond, and atoms, ions and molecules that bind this way are called central atom(s) (ion(s)) and ligands.

As well as displaying a rich chemistry, the metal ions have properties important for coordination chemistry. In particular, the different preferred coordination geometries and number, but also different sizes, oxidation states and charges, electrochemical, magnetic and optical properties. There is a range of different binding forms and strengths, and the coordinative bond may be labile or inert depending on the combination of metal ion and ligand. The metal ions are the structural motif, and are able to direct suitable ligands into a three-dimensional metallosupramolecular aggregate. The spatial arrangement of the ligands around this motif determines the overall three-dimensional architecture obtained.³⁰

The ligands’ ability to differentiate between various metal ions (depending on donor atom type, number and spatial distribution) will determine the number and position of metals to be bound. Therefore, the matching of ligand and the preferred coordination requirements of the metal, directs the system into the spatial distribution. The reactive species are said to bear complementary sets of information. This is often referred to as the ‘intrinsic information’.³⁰ To control, which coordination compound is formed, it is therefore important to match the intrinsic information of central atom and ligand, in a way that only the desired assembly may form, or a mixture of assemblies with similar thermodynamic minima, from which the desired assembly can be extracted by e.g. a template.

1.2.2 The coordinate bond

The words ‘complex’ and ‘coordination compound’ originate from before electronic structures were known and described compounds in which not only atoms or ions, but also molecules could bind in various ratios. Historically most important were ammin complexes of cobalt and platinum ions.³¹

Alfred Werner³² is generally considered to be the founder of modern coordination chemistry since he first postulated the idea of a metal ion having both a primary and a secondary valence. In modern terminology the primary valence is called oxidation number and the secondary valence coordination number. A coordination compound is formed when a number of ions or molecules (ligands) combine with a central atom or atoms to form an entity. The number of atoms attached to the central atom(s) is independent of the oxidations state of that atom(s). The coordination number of the central atom or ion,

is the maximum number of ligands which may arrange in regular order around it. It is a number from 1 to 12, and 6 is the most common.^{4,33}

Over time, models have been evolved and improved in order to explain the nature of the bonding between ligand and central atom. In the first theory for bonding in a coordination compound, it was assumed, that ligand molecules donated an electron pair for the bond with the central atom/ion. It considered the ligand as a Lewis base (electron pair donor), and the central atoms as a Lewis acid (electron acceptor).

A further development was the valence bond theory that assumed unoccupied hybrid orbitals for the central atom/ion (e.g. six d^2sp^3 hybrid orbitals for an octahedral complex). More modern theories for bonding in a coordination compound are derived from the crystal field theory. There the donor atom/ion from the ligand, and the central atom/ion were considered as point charges. There is a repulsion between the negative charged electron clouds of the donor atoms and an electron in a d-orbital of the metal. In an isolated metal atom/ion, the d-orbitals are degenerate in energy, but in the presence of ligands they are split. The splitting depends on the orientation of the ligands around the metal (octahedral, tetrahedral,...), see Figures 1.1 and 1.4. The crystal field was extended to the ligand field theory by taking into account the mutual repulsion of bonding electrons with the additional d-electrons. But most extensive is the molecular orbital theory. It describes bonding in a first approximation as covalent and only secondly as polar, with 'bonding', 'non-bonding' and 'anti-bonding' molecular orbitals for different types of bonds, including also coordinative bonds with some covalent character.

Octahedral complexes According to molecular orbital theory, in an octahedral complex symmetry adjusted combinations of σ -ligand orbitals overlap with the metal 4s-, the three 4p- and the $3d_{x-y}$ - and $3d_{z^2}$ -orbitals. $3d_{xy}$ -, $3d_{xz}$ - and $3d_{yz}$ -orbitals do not take part in any σ -molecular orbital (σ -bond). But they may take part in a π -bond, see Shriver³⁴ pages 228-229.

Figure 1.1 shows the molecular orbital diagram of an octahedral complex with just σ bonding and no π -bonding.³⁴

In the octahedral complex, the six bonding orbitals are occupied completely by the six electron pairs of the ligand donor atoms. The valence electrons of the central atom occupy the non bonding t_{2g} orbitals and the antibonding e_g orbitals. The energy difference between the two orbital groups is Δ_o . For each metal ion, different ligands give a different value for Δ_o , and the spin-pairing energy P is typically around 200kJ/mol but the exact value depends on the metal. Electron transitions between these two metal centred orbitals may be seen in the visible region of the UV-Vis absorption spectra. Of the metal ions Cu(II) d^9 , Cu(I) d^{10} , Co(II) d^7 and Ni(II) d^8 , that were used in this thesis, only Co(II) has the choice between high and low spin. In the spectrochemical series for metals, Co(II) gives a rather small Δ_o , while oligopyridine stands on the side of the spectrochemical series for ligands that give rather big Δ_o . In such cases, it is not clear in advance of the experiment whether a high- or a low-spin configuration will be adopted.

Figure 1.2 show qualitatively the effect of π bonding with a π -donor ligand and Figure 1.3 shows qualitatively the effect of π -bonding with a π -acceptor ligand, see Shriver³⁴ pages 228-229.

Tetrahedral complexes In a tetrahedral complex, the e orbitals d_{z^2} and $d_{x^2-y^2}$ are lower than the t_2 orbitals d_{xy} , d_{xz} and d_{yz} . The magnitude in splitting Δ_t is only just below half of the splitting between the t_2 and e orbitals in the octahedron, and the energy barrier for the electrons to pair up becomes bigger than Δ_t . The molecular orbital diagram is given in Figure 1.4, see Shriver³⁴ page 237. This explains why only high spin tetrahedral complexes are known. The only tetrahedrally coordinated metal ion used in this thesis is Cu(I), and with its d^{10} configuration all the electrons are paired.

The principal interaction between a metal and a coordinated pyridine residue is the sigma-bond which results from a vacant orbital on the metal interacting with the HOMO orbital of the pyridine ring, see Figure 1.5. The other two orbitals that are best accessible in energy, are the LUMO and the HOMO-1 orbital, both of which have an appropriate symmetry for π -bonding at the nitrogen donor atom, forming a π -acceptor bond by accepting d-electrons from the metal into the LUMO, or forming a π -donor bond by donating electrons from the HOMO-1 into the vacant metal d-orbitals. Thus, the oligopyridines should be able to stabilise low oxidation states on a metal, by interaction of filled metal d-orbitals, with

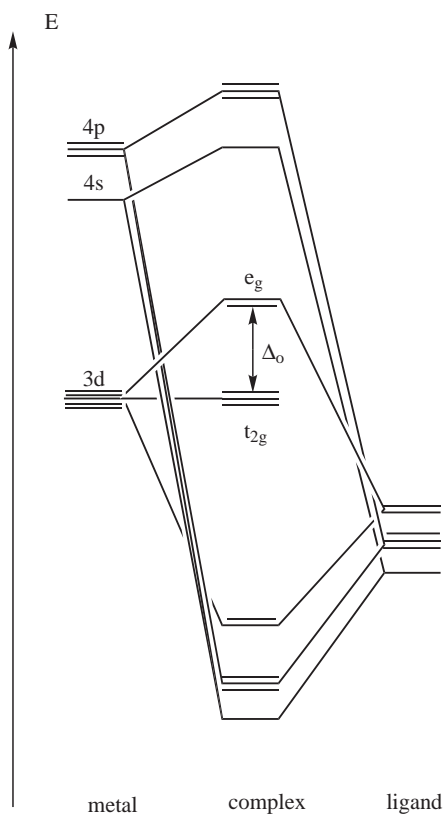


Figure 1.1: Molecular orbital diagram for a first row transition metal octahedral complex with a σ -donor ligand, see Shriver³⁴ pages 228-229.

their vacant LUMO orbital, and high oxidation states on a metal by interaction of empty metal orbitals with the filled HOMO-1, see Figure 1.5. In practice, oligopyridines tend to stabilise lower oxidation states more readily than higher ones,³⁵⁻⁴³ and this may be because the LUMO is energetically closer to the d-orbital energies, and therefore a resulting molecular binding orbital would be stabilised much better.

The bond strength of a coordinative bond is in between the covalent bond and van-der-Waals bonds, and varies strongly. Many coordination compounds, for example of Co(II), are very labile, and ligand exchange is rapid. Returning to the definition of a supramolecule given earlier, we can see that a coordination compound is indeed a supramolecule, as it can be broken down into its constituent ligands and central atom/ion without breaking covalent bonds.

1.3 The helical motif

Definition

A helix is the figure generated by the trace of a point moving at a constant distance around and along an axis (the helical axis). The linear movement along the helical axis needed for a 360° turn (projected on a perpendicular plane to it), defines the helical pitch as the height along the helical axis.^{44,45} In the discussion of the crystallographic analysis on page 55, 'the pitch' was used as a synonym for the length of the double helical complexes, even though they did not reach a 360° turn. A helix is always chiral, because it may either turn clockwise or anticlockwise about the helical axis. When viewing along this axis and moving away from the observer along the helix strand, the clockwise motion corresponds to a plus (P or Δ), and the anti-clockwise motion to a minus (M or Λ) helix.

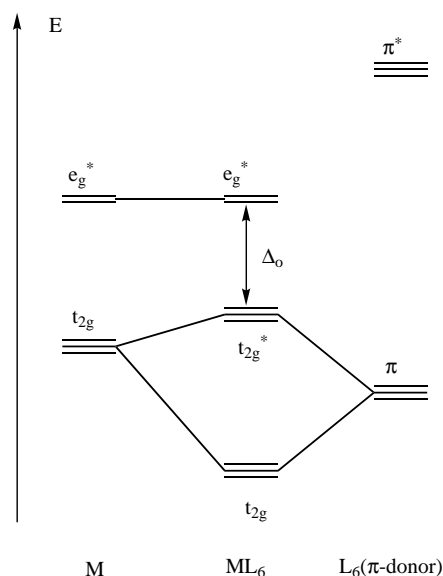


Figure 1.2: Molecular orbital diagram for a first row transition metal octahedral complex with a σ - and π -donor ligand.³⁴

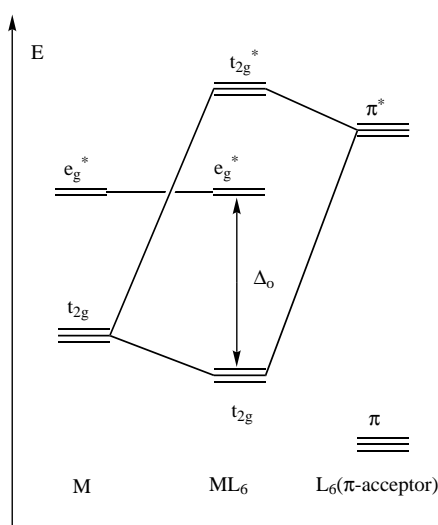


Figure 1.3: Molecular orbital diagram for a first row transition metal octahedral complex with a σ -donor and π -acceptor ligand.³⁴

Natural helices

Linus Pauling received the Nobel Prize in chemistry in 1954 for his work on mesomerism and on the structure of proteins. The secondary structure of proteins is in some cases α -helical.^{46,47} In nails (and horns), the α helix of keratin is held together by intramolecular hydrogen bonds. In hair, three protein helices, containing cysteine, are intertwined and held together by disulfide bridges between the cysteine amino acids, see Hart⁴⁸ on pages 389–394. α -amylose, the non-branched form of starch also forms an α helix. It consists of 50-300 maltose units, that are bound via a 1-4- α -bonds. About six units form a total turn of a helix. In solution it may incorporate small molecules (like iodine), in its hydrophobic interior, see Hart⁴⁸ pages 357–388.

Since the publication of Watson and Crick's ground-breaking papers^{49,50} in 1953, the term "double helix" instantly brings to mind the structure of DNA – the molecule responsible for the encryption of genetic information in cells. Each molecule of DNA is comprised of two right handed polynucleotide chains formed by deoxyribose and a purine or pyrimidine base and bound through a phosphate. They are coiled around a common axis to form a double helix. The purine and pyrimidine bases are on the inside of the helix, whereas the phosphate and deoxyribose units are on the outside. The diameter of the helix is 20Å and a full turn is completed every 10 bases, equivalent to 34Å along the helical axis. The two strands are held together in their helical conformation by the hydrogen bonding interactions of the purine – pyrimidine base pairing.^{48,51}

Yet another example for a helix is the tobacco mosaic virus (TMV). The TMV particle consists of 2130 protein subunits wrapped in a helical ribbon around a single strand of RNA 6390 nucleotides long. Rather than adding one protein subunit at a time, aggregates of subunits are added. The formation of the protein subunits into discs through weak, though numerous, non-covalent (e.g. salt bridges) interactions, is a dynamic self-assembly process. If the assembly process goes wrong, it is easily broken down into the units and then repaired.⁵¹⁻⁵³ With all these examples of natural occurring helices, the structures are controlled by (numerous) non-covalent bonds, and thus can be described as supramolecules.

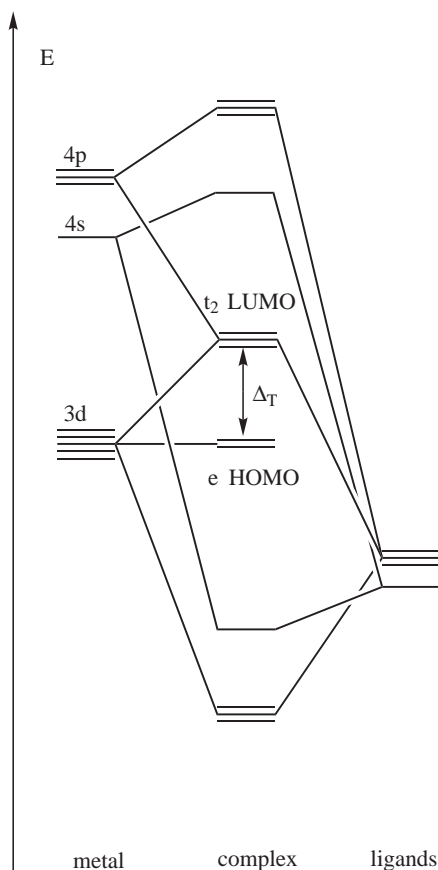


Figure 1.4: Molecular orbital diagram for a first row transition metal tetrahedral complex with a σ -donor ligand, see Shriver³⁴ page 237.

1.3.1 Helicates

Helicate is a generally accepted term defined by Lehn⁵⁴ as helices, which form by coordination of molecular threads to metal centres. The molecular threads (or strands) that form helicates are called helicands, and are multidentate bridging ligands; or in other words extended molecules which contain at least two separate domains that can coordinate to different metal centres.

Helicate self-assembly represents the first example of designed metallosupramolecular chemistry,^{30,55} and an example of which the crystal structure was solved, is presented in Figure 1.6.

That the supramolecular assemblies that form are helicates, depends on the flexibility of the ligand strands, the number and arrangement of their donor atoms inside them, and also on the geometrical preference of the metal ions that are used. In this example, the quaterpyridine ligand was substituted strategically with methyl groups, to preorganise the ligands sterically, and so forcing the helical structure to adopt, rather than a planar conformation. In order to obtain a double-helicate with copper(I), this preorganisation of the quaterpyridine ligand by substitution is not really necessary, but that was not discovered until later. The substituents did not enhance double helicate formation, but rather influenced the helical pitch and metal–metal distance in the helicate.³⁸

When a ligand coordinates to more than one metal ion at the same time, its donor atoms may be viewed as split into sets. The donor sets may consist of different numbers of donor atoms, but they must match the coordination number preference, and to some degree the geometry preference of the metal. In order to obtain a helical arrangement of ligands, between the donor-sets, they must be flexible by rotation at least. Otherwise side-to-side structures, grids or ladders are expected, where the ligand

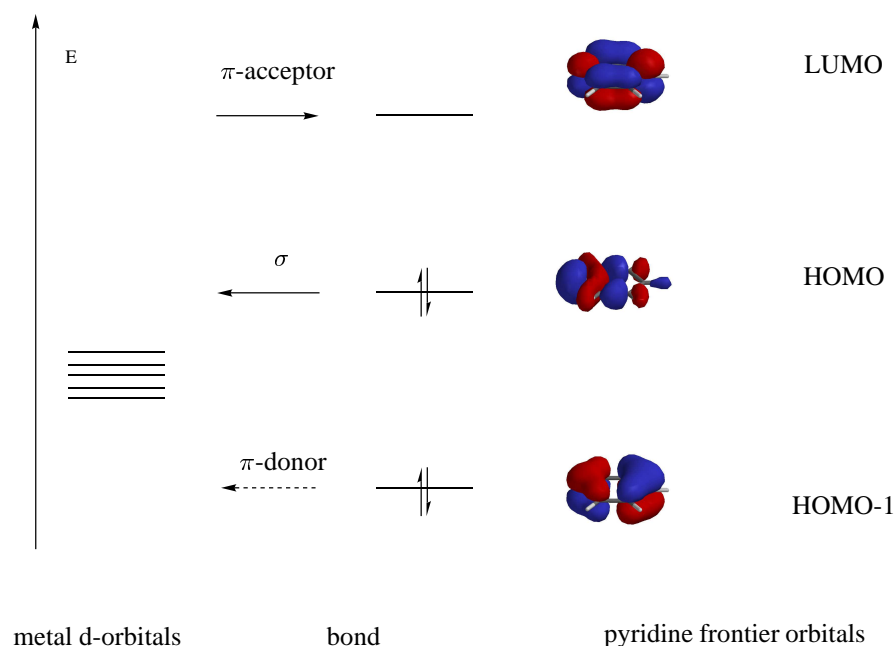


Figure 1.5: Energetically best available orbitals, with which pyridine may interact.

strands must be rigid.^{56,57} But even when the ligand design is correct for helicate formation, other structures sometimes form, with double helicates as subunits, or double helical ring systems, side-by-side structures, catenates² and other.⁵⁶⁻⁶¹

As all helices, helicates exist in two isomer forms and may be left-handed or right-handed, see Figure 1.7.

Classification of helicates prepared in this thesis:^{30,62} In this thesis, helicates were synthesised that contained one or two metal ions. Those containing one metal ion are termed ‘mononuclear’, and those containing two are termed ‘dinuclear’ helicates. The helicates contained one or two ligand strand, and the corresponding names are mono-helicate and double-helicate. The helicates synthesised here that are mononuclear are also mono-helicates, and the dinuclear ones are double-helicates. But this is not a general rule, as the number of ligands and the number of central atoms do not have to be the same. The coordination preference of the central atom may be saturated in many different ways.

Helicates may contain more than one kind of central metal atom, and then it is called heterometallic as opposed to homometallic. It is also possible for the metal ions to be the same, but of different oxidation state. Such helicates are called ‘mixed oxidation state’ or ‘mixed valence’ helicates.

A helicate may consist of repetitive binding units along the ligand strand, and this is called homotopic. When the binding units along the ligand strand are different, it is a heterotopic helicate. For instance is a double helicate of qtpy with two tetrahedral metal centres, a homotopic helicate, as each ligand strand consists of two “bipy” binding units, and a double helicate of qnpy with an octahedral and a tetrahedral metal centre a heterotopic helicate, as each ligand strand consists of a “bipy” and a “terpy” binding unit, see Figures 1.8, 1.6 and 1.7.

Helicates may also form with different ligand strands in one complex. These complexes are called heterostranded (or heteroleptic, if there also are no other additional ligand molecules or ions). Homostranded helicates are favoured, if they match the metal preference, and may form even from mixtures of ligands.⁶³ All complexes synthesised in this thesis are homostranded.

²Catenates are supramolecular knots by coordination bond of the ligands with a transition metal ion.

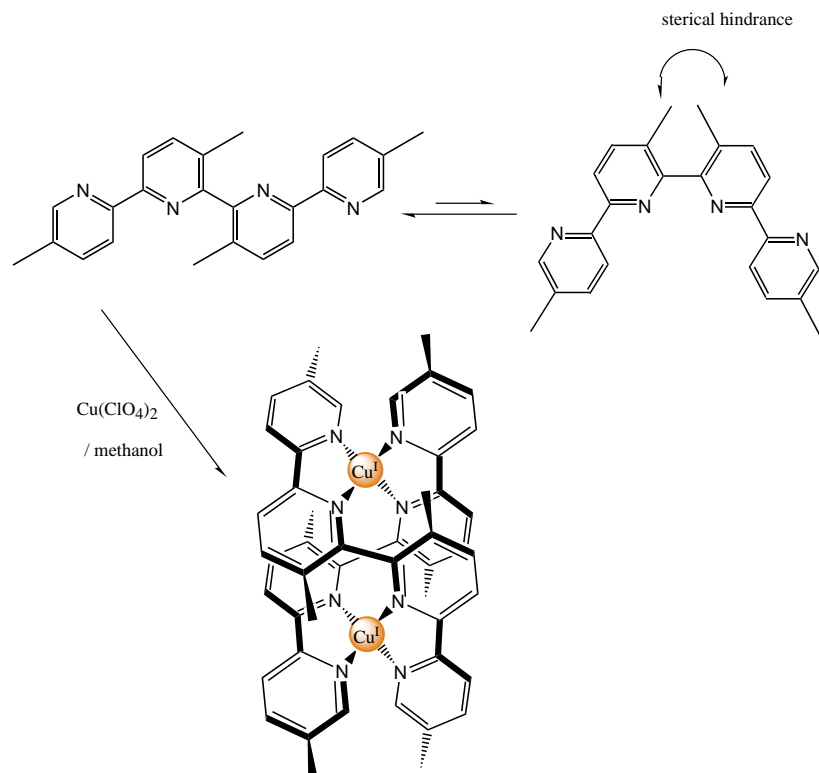


Figure 1.6: The first designed dinuclear double helicate, formed by preorganised qtpy derivatives. The structure was confirmed by X-ray diffraction analysis.⁵⁵

1.4 Going asymmetric

When the ligand strands are asymmetric, the mono helicates will still only exist as the two enantiomers P and M. The double helicates however, will have the possibility of having additional head-to-head (HH) and head-to-tail (HT) isomerism, depending on whether the ligand strands are oriented parallel or anti-parallel along the helical axis, for example, when unsymmetrically substituted qtpy ligands form a double helicate with two Ag^+ or two Cu^+ ions. But if the metal ions in a dinuclear complex are different, e.g. two different metal ions in a complex with unsymmetrical qtpy, then two different HH isomers are possible, in addition to the HT isomer. This is true with the qnpy complexes made in this thesis. Although, the metal ions are the same, in some cases the oxidation states are mixed, and in every case, they are coordinated in a different fashion by the qnpy ligands. In the double helicates of the qnpy ligands, one metal ion in the dinuclear complex is coordinated by two “terpy”-units and the other by two “bipy”-units of the two qnpy, see Figure 1.7 and 1.9. It would be interesting to see, if the asymmetric substituents may make one of the HH isomers favoured over the other, in the way that the most electron-withdrawing side predominantly coordinates to the metal ion of lower oxidation state. The study of asymmetric ligands gives more possible outcomes of supramolecular assemblies, and allows therefore a more detailed study of the self-assembly outcomes. Redox processes and electron transitions should be finely-tuned by the different substituents.

1.5 The projects in this thesis

As the title suggests, the aim of the work described here, was to make and study unsymmetrical helicates. Oligopyridines and their derivatives had already proven to be versatile ligands for various transition metal ions, and 2,6-linearly linked quaterpyridine (qtpy), quinquepyridine (qnpy) and their derivatives

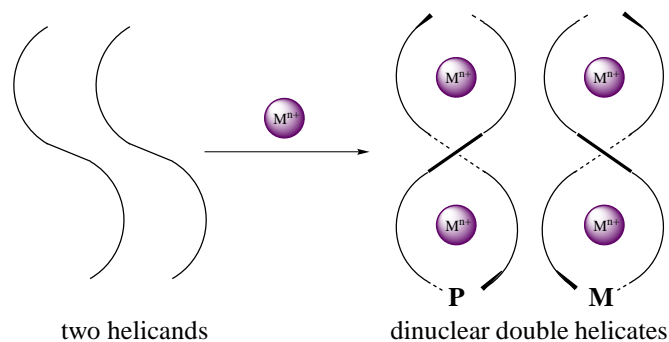


Figure 1.7: Schematic picture of the two helical enantiomers, shown in the example of a dinuclear double helicate.

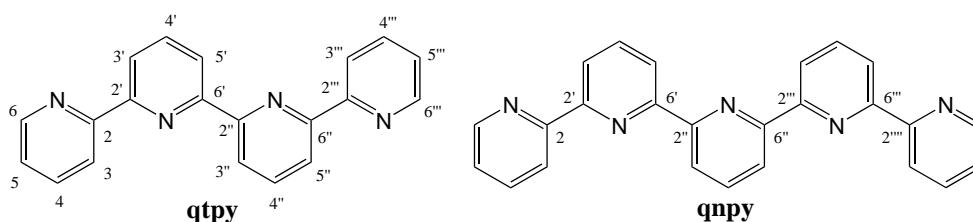


Figure 1.8: Formula of 2,2':6'',2'':6''',2''':6''',2''':6''',2''':6''''-quaterpyridine (qtpy) and 2,2':6'',2'':6''',2''':6''',2''':6''''-quinquepyridine (qnpq). qtpy consists of four, qnpq of five pyridine rings.

had been shown by crystal structure, to form dinuclear double helicates with AgI and CuI for qtpy,^{36,38} and Cu(II), Cu(II)/(I), Ag(I), Co(II), Ni(II) and Pd(II) for qnpq.^{37,40-43,64-70} The qtpy ligand is then split up into two bipy units, and the qnpq ligand into a bipy and a terpy unit.

Both qtpy and qnpq also coordinate as close to planar tetra- and pentadentate ligands, with Ni(II), Co(II), Mn(II), Fe(II), Fe(III) and some second and third row transition metal ions for qtpy,^{36,71-77} and with Cd(II) but also with Co(II) for qnpq.^{64,66,78} With zinc(II), qnpq may coordinate differently.⁷⁹

Substituent effects in the symmetrically substituted ligands had only significant effects on the helicate formation when in the 6,6''''-positions, and would act sterically hindering in a mononuclear mono-helicate.^{69,79} Other substituents did not seem to prevent double helicate formation. The synthesis, characterisation and study of new asymmetrical double helicates was the aim of this work, and quater- and quinquepyridine were target ligands. Substitution at the 6- and 6''''-position of the qnpq, and 6, and 6'''-position of the qtpy ligands was omitted, to rule out additional steric effects.

The helicans

4',4''''-substituted qnpq derivatives The helicans of the first project were unsymmetrically substituted qnpq derivatives, with a 4-*tert*-butylphenyl, a 4-methoxyphenyl and a phenyl group at the 4' position on the qnpq backbone, and a 4-hydroxyphenyl group at the 4''''-position on the qnpq backbone, see Figures 1.8, and 1.10. The substituents on the 4'-position are only slightly different, as the phenyl ring, closest to the qnpq backbone is always slightly electron withdrawing. The *tert*-butyl group has an inductive electron pushing effect, while the methoxy group has an inductive withdrawing effect, but an electron pushing mesomeric effect that is stronger than the inductive effect.

Linked helicans The 4-hydroxyphenyl group of the 4',4''''-substituted qnpq derivatives was used to link two together by a flexible linker, that would still allow the two qnpq units to coordinate to the same two metal ions.

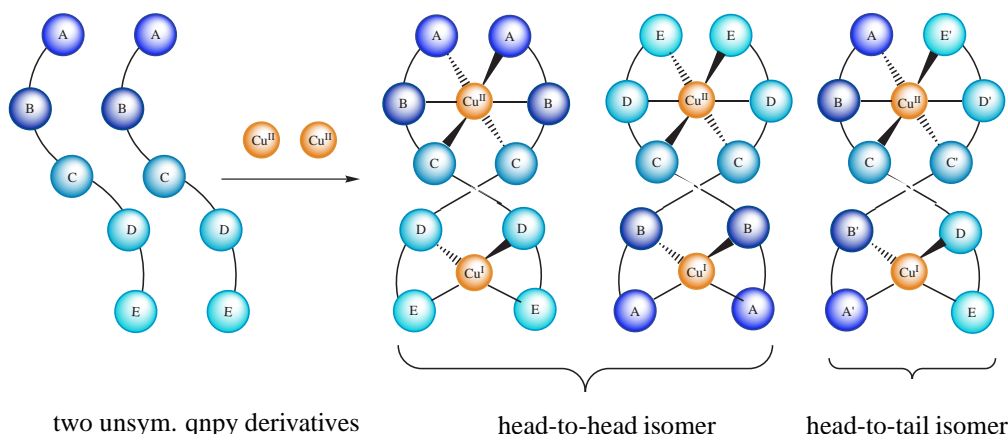


Figure 1.9: Schematic picture of the different possible isomers with unsymmetrically substituted quinquepyridine type ligands and two non-equivalent metal ions (octahedral and tetrahedral) in a dinuclear double helicate, showed on the example of a Cu(II)/Cu(I) complex of unsymmetrical qnp. The blue spheres each represent a pyridine ring. If the 'A'-ends of the two ligand strands forming one dinuclear complex both coordinate to the same copper ion, and the 'E'-ends to the other copper ion, a so-called head-to-head isomer is formed. If however one ligand strand coordinates the opposite way, a head-to-tail complex is formed. A crystal structure of such a complex is discussed on page 55.

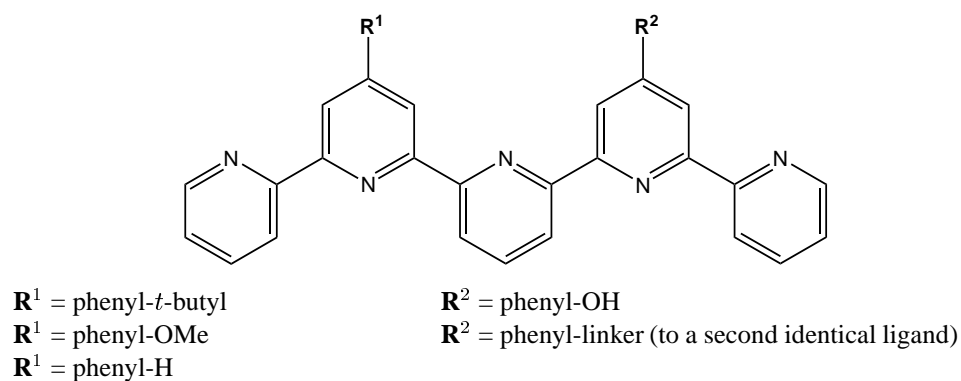
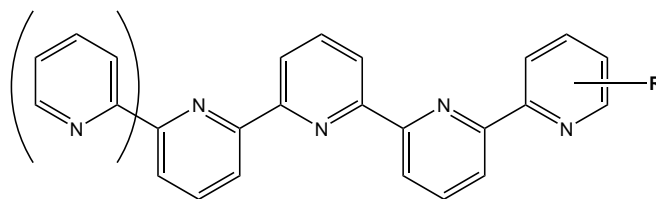


Figure 1.10: A qnp with different substituents in two positions. A linker is introduced in the 4'''-position. All six ligands have been fully characterised.

4-substituted qtpy or qnp derivatives It was the aim to link two helicands together at the terminal pyridine ring, in the 4- or 5- position, rather than the next to terminal ring, see Figure 1.11.

Transition-metal ion directed self-assembly

Metal ions that had proven to direct double helicates with oligopyridines were chosen as the most promising for getting this arrangement also with the new qnp-derivatives. Copper(II), and mixed valence copper(II/I) double helicates had been studied extensively with symmetrically substituted qnp's, and new results would be comparable. The ambiguity of Co(II) helicates, and the good possibility of distinguishing between mononuclear monohelicate and dinuclear double helicate, by the shifted protons in the $^1\text{H-NMR}$ spectroscopy, encouraged us to study the coordination compounds of the qnp derivatives with Co(II) as well.



1. steps: **R** = phenyl-OMe
2. step: **R** = phenyl-OH
3. step: **R** = phenyl-linker (to a second identical ligand)

Figure 1.11: qtpy and qnpy with a substituent in any position on one of the terminal pyridine rings. A linker introduced at this substituent position is strategically placed for forming hair-pin helicates. The 4-(4-methoxyphenyl)qtpy has been fully characterised, see page 122.

The helicates

All double helicates would be expected to form as racemates. As a heterotopic ligand, the qnpy-derivatives would coordinate to two octahedral metal ions with a “terpy” unit each. The remaining “bipy” units would not saturate the coordination sphere of a second octahedral metal ion, so an auxiliary ligand coordinates alongside the two “bipy” units. This is the case with some of the Cu(II), Ni(II) and Co(II) complexes synthesised in this thesis. In the mixed valence helicates with a Cu(II) and a Cu(I), the Cu(I) with its full d-shell, has no real preferences for coordination, and two remaining “bipy” units that are left when the “terpy” units have coordinated to the Cu(II), may bind to Cu(I) in a tetrahedral orientation. Then no additional ligands are needed.

The unsymmetrically substituted qnpy ligands, two HH and one HT isomer are possible, but the slightly different electronic properties of the substituents, may lead to preferred formation of one of the HH isomers, especially in the mixed valence coordination compounds. Helicate formation with the linked qnpy's, may be directed by the different linker conformation for head-to-head and head-to-tail isomers, and one or both of the HH isomers, or the HT isomer might be favoured. When the linker is attached to the next to terminal ring, it would have to stretch out in the HH isomer, while it may be folded up in the HT isomer, see Figure 1.12. When the linker is attached to the terminal ring of the qnpy' ligands however, the linker may fold in both the HH and in the HT isomer, and an influence or control by the linker on which isomer is formed, becomes less likely.

The quaterpyridine derivatives would coordinate to copper(I) and silver(I) by splitting into two “bipy” domains and forming a double helicate. With two equal metal ions in the double helix (homometallic), only one HH and one HT isomer may form. A linker was planned to connect the terminal rings, and would be folded in the HH isomer, but stretched out in the HT isomer. The HH isomer would then resemble a hairpin, with the linker folded up in the direction of the metal-metal axis, see Figure 1.13.

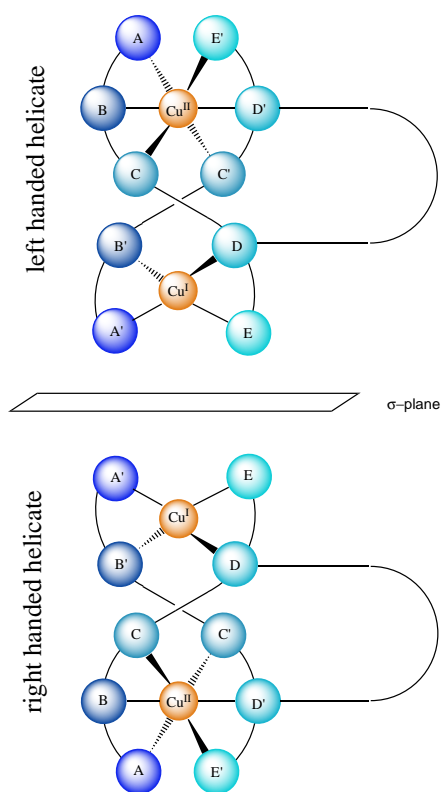


Figure 1.12: Schematic picture of the HT enantiomers of $[\text{Cu}_2\text{pcp}]^{3+}$. The structure was solved by X-ray diffraction and is discussed in detail in the chapter of the coordination compounds on page 55.

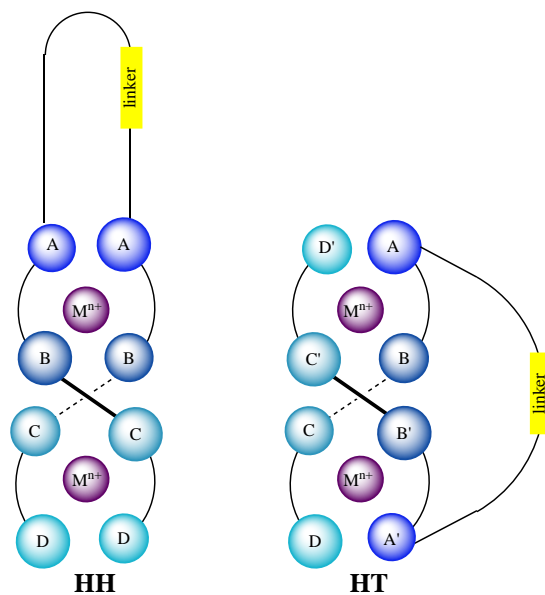


Figure 1.13: Schematic picture of a HH- and a HT-dinuclear double helicate isomer with a terminally linked qtpy derivative ligand. The HH isomer resembles a hairpin, with the linker folded in the direction of the metal-metal axis.

Chapter 2

Unsymmetrically substituted quinquepyridine ligands

2.1 Overview

2.1.1 Different approaches and mechanisms of the 2,6-oligopyridine synthesis

2,2':6',2''-Terpyridines and higher oligopyridines were first synthesised in 1938 by Burstall using the Ullmann reaction in which aromatic halides are coupled upon reaction with metallic copper.^{80,81} This reaction type has been further developed by lithiating the aromatic halides and using metal salts in ether suspension. It is very efficient in making symmetrical 2,6-oligopyridines,^{55,82-84} and was applied in this thesis to make 6,6'-dibromo-2,2'-bipyridine (see page 163 in the experimental part).

However, most of the 2,6-oligopyridine target ligands described in this thesis are unsymmetrical, and with this reaction, any approaches would result in mixtures. It is therefore much more convenient to do specific reactions giving one asymmetric main product.

Already in 1882, Hantzsch published a pyridine ring synthesis by condensation of a β -ketoester, followed by an oxidation, see Name Reactions⁸⁵ on page 168–172. Kröhnke in 1976 published a much improved synthesis by introducing the pyridinium salt PPI. As pyridine is latent as a good leaving group, incorporated as pyridinium in PPI, the oxidation step of the Hantzsch's synthesis becomes superfluous and enhances the overall yields.

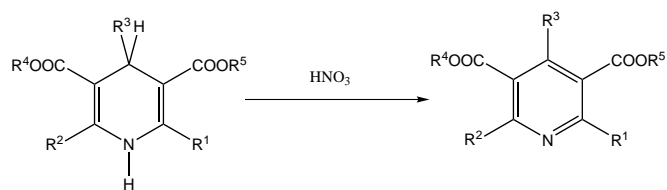
Instead of a β -ketoester, Kröhnke used α,β -unsaturated ketones or alternatively, β -keto mannich bases. The latter undergo cleavage of the dimethylamino group as dimethylamine (in alkaline to weakly acidic solutions) and may react just as α,β -unsaturated ketones.⁸⁶⁻⁸⁸ Using a pyridinium rest was not entirely new, as it was already mentioned in the synthesis of nicotellin by Thesing in 1956.⁸⁸ But Kröhnke was the first to employ it systematically, by introducing this group already via the starting material PPI. Figure 2.1 show the difference between the Kröhnke and Hantzsch intermediate ring, before oxidation/dehydrogenation.

Potts *et al.* found a novel way of synthesising 2,6-disubstituted 4-(methylthio)-pyridines (and thus 2,6-oligopyridines), with a 1,5-enedione, that performs ring closure with ammonium acetate analogous to the Kröhnke method. The synthetic equivalent to the α,β -unsaturated ketones or mannich-base, is the α -oxoketene dithioacetal reagent.⁸⁹

2.1.2 The synthetic pathway to the qnpy derivatives qp, mp and pp

Since qp had already been synthesised by Whall,⁵¹ and similar qnpy derivatives by Whall and Walker,^{90,91} the same synthetic pathway that was successful then was followed. In general, this was the way described by Kröhnke.⁹² Figure 2.2 shows the way to qp, mp and pp. The α,β -unsaturated

Last step of the Hantzsch pyridine synthesis



Last in situ step in the Kröhnke pyridine synthesis



Figure 2.1: Last step in the Hantzsch pyridine synthesis versus completion of the Kröhnke cyclisation

ketones were obtained by aldol reaction in varying yields, followed by ring closure with PPI and elimination of the built in oxidant pyridinium as pyridine.

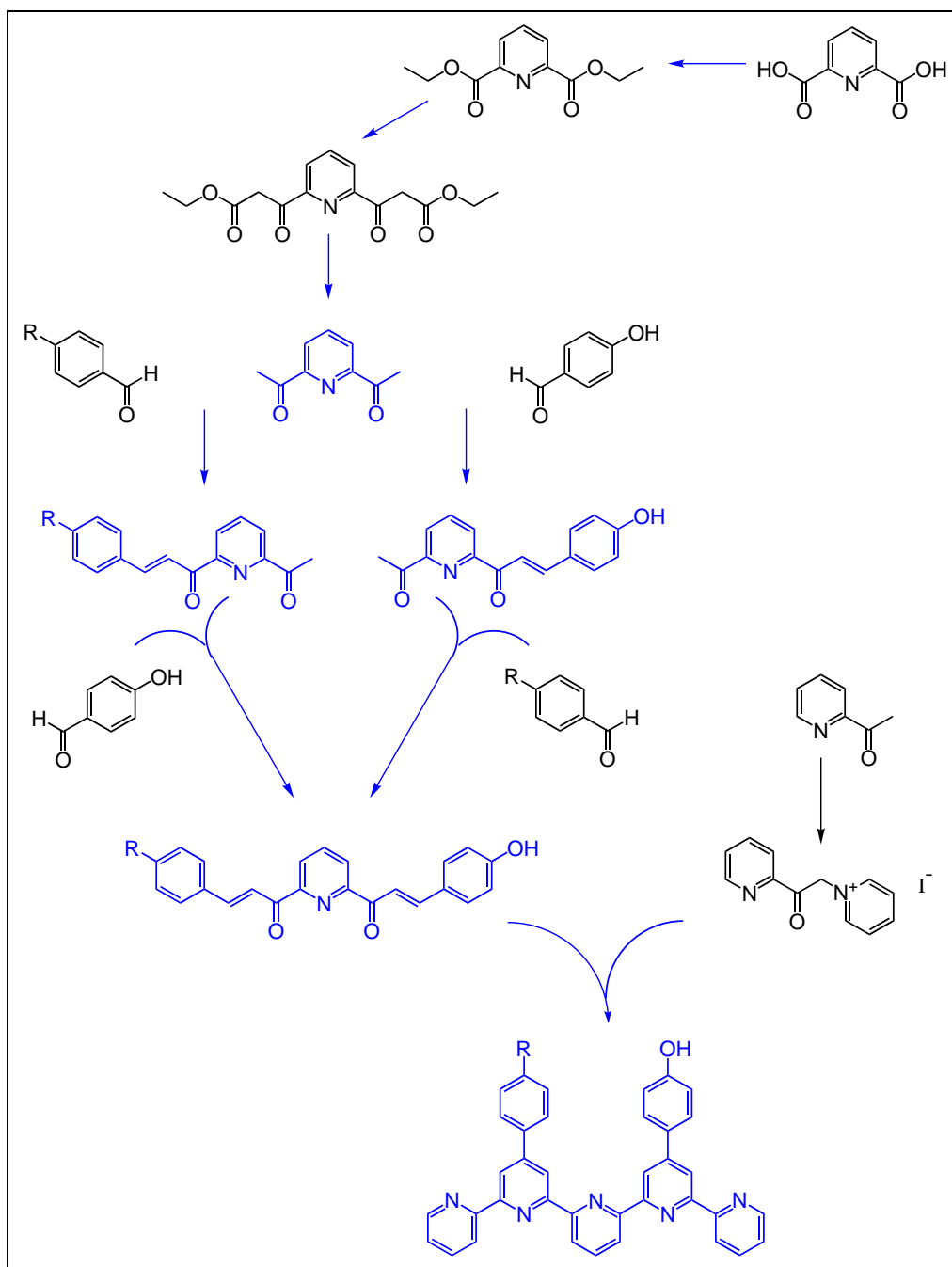


Figure 2.2: Overview of the synthesis of the qnpy derivatives and ligands qp, mp and pp, R = *tert*-butyl, methoxy and H for qp, mp and pp respectively. The reactions and products discussed below are drawn in blue colour.

2.2 2,6-Diacetylpyridine

2.2.1 Synthesis and characterisation

Although this compound is commercially available, it is cheaper to synthesise in the lab. The procedure of Smith was followed,⁹³ see Figure 2.2 on page 17. The reaction comprises three steps, starting with making the ethyl ester of the 2,6-pyridinedicarboxylic acid with thionyl chloride followed by ethanol. (The reaction conditions for this step were improved in 2001 by a Chinese group.⁹⁴) In a second step, the enolate of ethyl acetate replaces the alcohol part of the ester by nucleophilic attack. Finally, in acidic conditions, the new ester is hydrolysed, and CO₂ is eliminated. The 2,6-diacetylpyridine could be extracted with ether. Purification by recrystallisation from hexane gave pure product in an overall yield of 41%. It was characterised by ¹H-NMR. (Another synthetic pathway was patented in 2003.⁹⁵)

2.3 Mono- and bis-chalcones

2.3.1 General synthesis

Under the conditions of the weak base diethylamine in 1-propanol, an aldol reaction takes place between the 2,6-diacetylpyridine and the appropriately substituted benzaldehyde when heated. When using a one to one ratio, the product is the mono-chalcone. If however the ratio of 2,6-diacetylpyridine to benzaldehyde is 1 : 2, the symmetrical bischalcone is made.⁵¹ One such symmetrical bischalcone was obtained as a side product, see Figure 7.5 on page 133 and 7.11 on page 140. In order to make the unsymmetrical bischalcone, the monochalcone was put through the same kind of reaction, this time with a different benzaldehyde derivative (see overview in Figure 2.2 on page 17. The yields of these reactions varied between 20–41%.

2.3.2 Differences and crucial points

No differences in the yield could be observed whether the diethylamine was added quickly in the beginning or added slowly under reflux. But, when the diethylamine was in contact with the aldehyde too long before reaction, a yellow precipitate formed, that was insoluble in common solvents. It happened most with 2-Acetyl-6-[3-(4-hydroxyphenyl)-1-oxoprop-2-enyl]pyridine and 4-methoxybenzaldehyde, and the latter was employed in large excess. Because the amount of precipitate that formed, and because its melting point (231–236 °C) is much higher than that of benzoic acid (185 °C) or 2,6-diacetylpyridine (79–82 °C), it is assumed, that it may be an salt of benzoic acid (oxidised benzaldehyde) and protonated diethylamine. The reaction times were varied between 3 and 18 h without affecting the efficiency of the reaction. The main reason for the varying yield lay in the difficulties of purifying the crude by column chromatography, because of poor solubility in the eluent. In all eluents used, the bands were partly overlapping. The following mixtures in different ratios were tried as eluents:

- DCM : MeOH (50 : 1), (40 : 1), (30 : 1), (20 : 1) and (3 : 1)
- DCM : MeOH : Et₂NH (40 : 1 : 1), (20 : 1 : 1), (20 : 1 : 0.1)
- DCM : *t*-butyl methylether (1 : 2)
- ethyl acetate : petrol ether (1 : 1)
- hexane : ethyl acetate : diethylamine (5 : 1 : 0.1)
- toluene : ethyl acetate : diethylamine (5 : 1 : 0.1)

Partly pure fractions from the column could be obtained pure by recrystallisation from methanol, except when the impurity was another mono- or bis-chalcone.

2.3.3 Characterisation

The chalcones used on the way to qp as well as the symmetrical 2,6-di-[3-*tert*-Butylphenyl]-1-oxoprop-2-enyl]pyridine, that had been obtained here as a side product, had already been fully characterised by Whall.⁵¹ The micro analyses of the new proposed mono- and bischalcones (unsymmetrical as well as symmetrical) all fitted the formula. With the exception of 2-[3-(4-hydroxy)-1-oxoprop-2-enyl]-6-[3-phenyl-1-oxoprop-2-enyl]pyridine, water was present in the samples, see the pages 139, 140, 141 and 147 in the experimental chapter.

Mass spectrometry

All the new chalcones, plus the 2,6-di-[3-*tert*-Butylphenyl]-1-oxoprop-2-enyl]pyridine that had already been characterised by Whall,⁵¹ were measured with the EI-mass spectrometer. Every sample showed the M⁺ signal plus typical fragments like e.g. (M-OCH₃)⁺, (M-C(CH₃)₃)⁺ or M-(M-hydroxyphenyl)⁺.

NMR example and table for all

¹H-NMR assignment of 2-[3-(4-methoxyphenyl)-1-oxoprop-2-enyl]-6-[3-(4-hydroxyphenyl)-1-oxoprop-2-enyl]pyridine in CDCl₃ δ: In the COSY, cross peaks are seen as expected between H4 and H3/H5, between a and b, between a' and b', between o and m and between o' and m'. See Figures 7.3, 7.10, 7.12, 7.15 for labeling. The ROESY showed a cross peak between the methoxy and the m-proton. It also shows the signals belonging to the a, b and o, m systems separate from the a', b' and o', m' systems. Proton 3 and 5 show ROESY contact to 4 and also to a, a', but not to b, b'.

¹³C-NMR assignment of 2-[3-(4-methoxyphenyl)-1-oxoprop-2-enyl]-6-[3-(4-hydroxyphenyl)-1-oxoprop-2-enyl]pyridine in CDCl₃ δ: With HMQC, the protonated carbon atoms could be assigned. HMBC then showed cross peaks for

- CH₃O and Co with Cp
- Ho' with Cp'
- Ho with Co, Cb and Cp
- Hm/m' with Cm/m' on the other side of the phenyl ring, and with Cv and Cv' at 128
- Hb/Hb' with Co and Co' and C = O
- H4 with C2/C6
- Ha and Ha' with Cv and Cv'
- H3/H5 with C5/C3

Only ¹H-NMR were recorded of the other mono- and bis-chalcones, and the ¹H-chemical shifts of these synthesised compounds are listed in Table 2.1.

IR table and discussion

The C = O frequencies of the mono- and bis-chalcones synthesised in this thesis are very characteristically shifted to lower wavenumbers for the carbonyl stretch where enone groups were attached to the pyridine ring, compared to the carbonyl stretch of methylketone (see table 2.2). The C = O in the 2,6-diacetylpyridine is directly attached to pyridine, and the shift of $-15 \pm 5 \text{ cm}^{-1}$ from 1715 is very characteristic for C = O groups in vicinity to an aromatic ring. Substitution leading to α, β -unsaturated systems lowers the wavenumber of this absorption for about $38 \pm 6 \text{ cm}^{-1}$ according to standard books,^{96,97} and this is illustrated again by these compounds.

	chemical shift δ														
	OH	H3	H5	Ha	Ha'	H4	Hb	Hb'	Ho	Ho'	Hm	Hm'	Hp	CH ₃	H _{Substituent}
		8.23	8.37	8.23	-	8.03	7.96	-	7.65	-	6.92	-	-	2.88	-
	-	8.22	8.36	8.23	-	8.018	7.98	-	7.68	-	6.97	-	-	2.87	CH ₃ O 3.87
	9.54	8.36		8.324	8.319	8.07	8.00	7.99	7.72	7.68	6.98	6.92	-	-	CH ₃ O 3.89
	-	8.37		8.33		8.07	8.00		7.73			-	-	CH ₃ O 3.89	
		8.53-8.29				8.11-7.96			7.81-7.73	7.69	7.49-7.45	6.91	7.49-7.45	-	-
		8.45-8.30				8.11-8.00			7.73-7.68		7.48	6.91	-	-	t-Bu 1.38
	-	8.38		8.48		8.08	8.03		7.74		7.50		-	-	t-Bu 1.38

Table 2.1: ¹H-NMR: chemical shifts δ of the protons in mono- and bis-chalcones

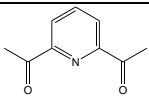
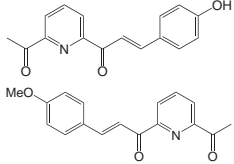
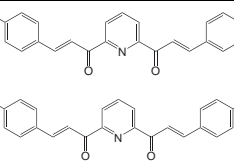
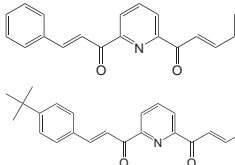
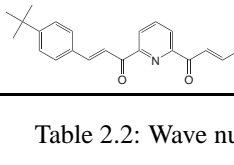
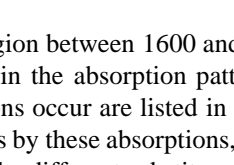
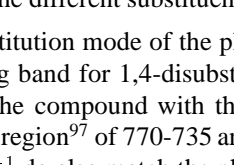
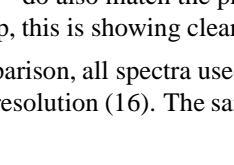
compound	pyridine(C=O)CH ₃	pyridine(C=O)CH=CH-
	1697	
	1705	1659
	1697	1666
		1651
		1658
		1659
		1650
		1666

Table 2.2: Wave numbers for C = O of the chalcones and 2,6-diacetylpyridine.

In the region between 1600 and 1400, of C = C and C = N pyridine ring stretching, there are small differences in the absorption patterns of the strong absorption bands. The wavenumbers at which the absorptions occur are listed in Table 2.3. The mono-chalcones can not be distinguished from the bis-chalcones by these absorptions, and there is no visible trend of slight change in wavenumber that would point to the different substituents.

The substitution mode of the phenyl substituent is visible at the low wave numbers. At 802-810cm⁻¹ the strong band for 1,4-disubstituted phenyl is seen as expected (theoretical range of 840-800cm⁻¹), and for the compound with the pure phenyl substituent, two additional bands show. One is in the expected region⁹⁷ of 770-735 and the other slightly outside 710-685. The patterns in the region of 2000-1600cm⁻¹ do also match the phenyl ring substitution pattern (para- and mono-). In the species with an OH group, this is showing clearly in the expected region, confirming the structure, see Table 2.4.

For comparison, all spectra used in the tables 2.2, 2.3, and 2.4 were measured as solids only (no KBr), in equal resolution (16). The sample of 2,6-Diacetylpyridine was provided by a colleague (Dr. Diane R. Smith).

X-ray

2-Acetyl-6-[3-(4-methoxyphenyl)-1-oxoprop-2-enyl]pyridine This mono-chalcone was obtained as slightly yellowish crystals from a fraction that was eluted off a silica column with hexane : ethyl acetate : diethylamine in a 50 : 10 : 1 ratio, see appendix C on page 201.

2,6-di-[3-(*tert*-Butylphenyl)-1-oxoprop-2-enyl]pyridine This bis-chalcone was obtained as colourless crystals as a byproduct in the synthesis of 2-[3-(4-*tert*-butylphenyl)-1-oxoprop-2-enyl]-6-[3-(4-hydroxyphenyl)-1-oxoprop-2-enyl]pyridine. The crystals were grown by recrystallisation from methanol, see appendix D on page 213.

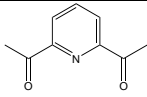
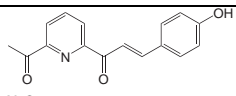
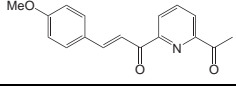
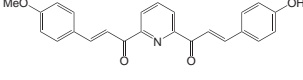
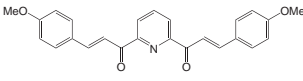
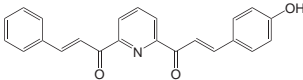
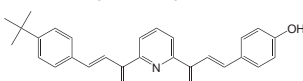
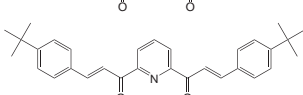
compound	pyridine/phenyl combined $\nu C = C/N$				symmetry
	1610-1600	1590-1580	1520-1470	1460-1440	
monosubstituted benzene (vapour) ⁹⁸	1610-1600	1590-1580	1520-1470	1460-1440	
pyridine (vapour) ⁹⁸	1580	1572	1482	1439	
	1581m			1412m	sym.
	1589sh	1558vs	1512s	1434s	asym.
	1589s	1566s	1512vs	1458w, 1442w, 1420m	asym.
	1589s	1558vs	1504vs	1458m	asym.
	1596s	1566vs	1512s	1466w, 1442w, 1420m	sym.
	1597s	1558vs	1504s	1443m	asym.
	1597vs	1551s	1504s	1453sh, 1412w	asym.
	1604vs	1566sh	1512m	1465m, 1411m	sym.

Table 2.3: Wave numbers for the pyridine- and phenyl-ring stretching modes of the chalcones and 2,6-diacetylpyridine.

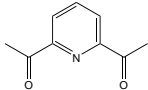
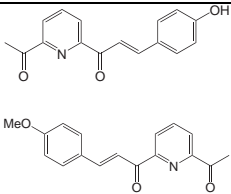
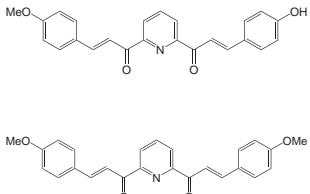
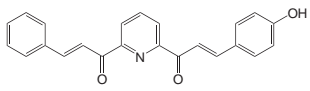
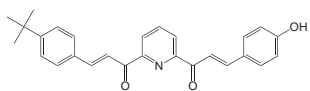
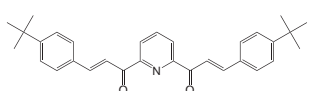
compound	OH-band	1,4-disubstituted phenyl	mono substituted phenyl
			(741m)
	3364b, (3320sh)	810s	(748m)
		810s	(748m)
	3225b	810s	(741w and 694w)
		802s	(740w)
	3356b	810s	741m and 679m
	(3310sh), 3178b	810s	(741w and 710w)
		810s	(748m)

Table 2.4: OH-band and substitution pattern of the phenyl substituents in the of the chalcones and 2,6-diacetylpyridine.

2.4 qnpy derivative ligands: qp, mp and pp

2.4.1 Synthesis

See overview 2.2 on page 17 and Figure 2.3 for labeling. The bis-chalcones described above were the starting material for these syntheses. They already contain pyridine ring C, and the phenyl substituent rings b and d of the target qnpy ligands qp, mp and pp. In the Kröhnke type reaction,⁹² rings B and D are formed, and rings A and E come from the PPI auxiliary reagent. The synthesis of qp was already described in Whall's thesis.⁵¹ The reactants listed in Table 2.5 were added together and refluxed for ~17h. In each case, the products precipitated as a beige solid from a brown solution. After separation and washing with cold methanol, they needed no further purification. In Table 2.5 the different ratios of ingredients for the syntheses of the three qnpy derivatives are listed. Taking an overview over the reactions and their yield, they seem to confirm that a molar ratio of 5 : 1 ammonium acetate : PPI, and a minimum amount of solvent are important. The differing yields also suggest that water disturbs the synthesis, as the driest methanol was used for the qp synthesis, and the least dry methanol for the mp synthesis. The acetic acid was freshly distilled in all cases.

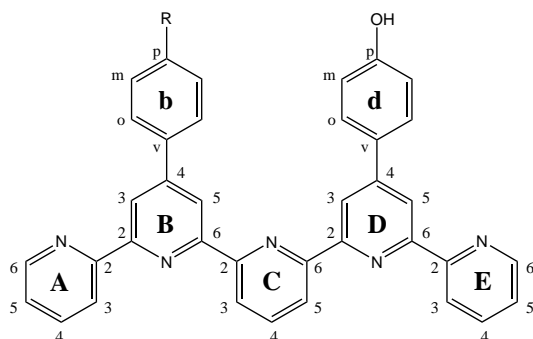


Figure 2.3: General labels of the qnpy derivatives and ligands, R = *tert*-butyl, methoxy and H for qp, mp and pp respectively. For NMR assignment, the H and C were named with the letter of the pyridine or phenyl ring, followed by the number or letter indicating the atom of the ring, e.g. B3 or do can be the proton H_{B3} or H_{do} in the ¹H-NMR or the carbon C_{B3} or C_{do} in the ¹³C-NMR.

	qp	mp	pp
Bis-chalcone/mmol	3.468	3.764	7.398
NH ₄ OAc/mmol	30.4	130	77.6
PPI/mmol	7.070	7.993	14.82
Solvent: methanol/ml	10	10-15	40
Acidic acid/drops	7	4-5	10
yield/%	93.2	48.6	88.6

Table 2.5: Starting materials for the Kröhnke cyclisation reaction to the qnpy derivatives qp, mp and pp.

2.4.2 Characterisation

Since the qp ligand had already been fully characterised by Whall,⁵¹ here this ligand was not characterised again by micro analysis, but the other two were, and fitted well with additional water, see experimental chapter on pages 142, and 148.

Mass spectrometry

With all three qnpy ligands, the mass spectrometric data showed a signal for the molecule M^+ , as well as the mass of the molecule plus water and/or one alkali metal ion of sodium or potassium.

Infrared spectroscopy

The infrared spectrum was recorded of all three of them (qp, mp and pp). The spectra are typical for (oligo)pyridine compounds, with strong signals for heteroaromatic $C=N$ and $C=C$ stretch in the region of $1625-1575\text{cm}^{-1}$, and strong absorption in the area $1525-1475$ typical for $C-C$ in heteroaromatic systems (qp: 1512cm^{-1} , mp: 1574cm^{-1} and 1512cm^{-1} , pp: 1520cm^{-1}). The typical absorption for para-substituted phenyl rings in the area of $860-780\text{cm}^{-1}$ is fulfilled by all the three ligands, with signals at 818cm^{-1} , but the pattern of combinatory vibrations in the area of $2000-1600\text{cm}^{-1}$ is not observed.⁹⁶

UV-Vis spectroscopy

UV-Vis spectra were recorded mainly to emphasize the marked change that occurred when these ligands are complexed e.g. with copper(II/I). These ligands in themselves absorb strongly in the UV region because of the seven aromatic rings per molecule. But as they are almost white in colour, their absorption decreases drastically towards the visible region. For a better view, the results are listed in Table 2.6. The spectrum of pp shows two maxima at 257 and 279nm, while mp and qp only have the one at 280 and 284nm respectively, see Figure 2.4.

qp		mp		pp	
wavelength /nm	extinction coefficient / $M^{-1}\text{cm}^{-1}$	wavelength /nm	extinction coefficient / $M^{-1}\text{cm}^{-1}$	wavelength /nm	extinction coefficient / $M^{-1}\text{cm}^{-1}$
259(sh)	46'100	261(sh)	52'147	257	62'807
280	50'274	284	66'896	279	58'333
308(sh)	24'246	308(sh)	36'147	308(sh)	33'958
318(sh)	18'538	318(sh)	25'734	318(sh)	26'964

Table 2.6: UV-Vis data for the qnpy derivatives qp, mp and pp.

¹H- and ¹³C-NMR study

The NMR spectra of all the qnpy derivatives were recorded on a 600 MHz spectrometer. qp had already been characterised by ¹H-NMR by Whall,⁵¹ with help of a 250 or 300 MHz spectrometer. There are signals in multiplets however, that could be further resolved in the 600 MHz spectrum, and the assignment is described in detail below. Then the other two ligand characterisations follow in the same way. As an example for the ¹H-NMR of these ligands, the spectrum of mp is shown in Figure 2.5. The ¹H-NMR chemical shifts of qp, mp and pp are listed in Table 2.10 on page 31.

All the ¹³C-NMR spectra are new. Because of limited solubility, the carbon spectra had unsatisfactory signal to noise ratio, but the chemical shifts for most carbon atoms could be assigned with HSQC and HMBC. They are listed in Table 2.11 on page 32.

¹H-NMR of qp δ For labeling, compare with Figure 7.7 on page 135. Comparison with Whall's assignment of this ligand⁵¹ gave the chemical shifts of the protons B5, D3, C4, bo, do, bm, dm and *tert*-butyl. It also gave A6, E6, B3, C3, C5, D5, A3 and E3 in one multiplet, one multiplet for A4 and

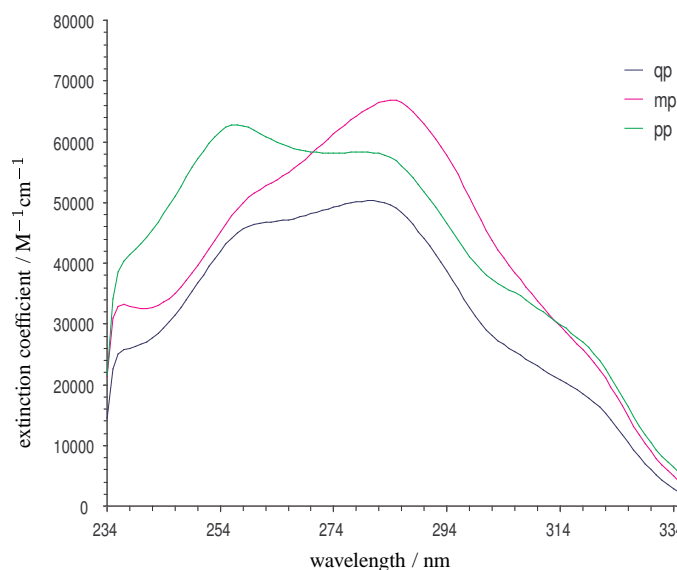


Figure 2.4: The UV absorption spectra of the three qnpy derivatives qp, mp and pp.

E4 and finally the multiplet for A5 and E5. With the 600 MHz, the multiplets split up into three: A6, E6 and B3, C3, C5 and D5, A3, E3. COSY, ROESY and HSQC measurement confirmed this assignment, and when taking into account the trend in up- and downfield shifts within the qnpy ligand, the exact chemical shifts of every proton in qp (except for A5 and E5) could be deduced.

The COSY helped to single out A6/E6, B3, C3/C5, D5 and A3/E3, with some of the cross peaks listed below. It also showed a diagonal trace in the cross peaks between A5/E5 with A6/E6, A3/E3 and A4/E4 that means, that what is shifted low-field, in the 5 position, is low-field as well in the positions 3,4 and 6. This finding fits well with the trend between the B/b and D/d rings derived from the values listed in Table 2.7, where B and b are shifted low-field, with respect to D and d. Because of this general trend, A6 and E6 can be separated and assigned, and so can A4 and E4. For C3 and C5 two separate chemical shifts can be seen, but they could not be assigned separately. The cross peaks seen in the COSY also show which of the protons belong to the same ring.

- B5 and B3
- D3 with D5
- A6/E6 with A3/E3, A4/E4 and A5/E5
- C3/C5 with C4
- bo with bm
- do with dm

The ROESY showed a cross peak of

- bm with CH₃ and with bo.
- bo with B5, B3 and bm
- do with D3, D5 and dm
- A5/E5 with A4/E4 and A6/E6, and a weak one with A3/E3

- A3/E3 show a strong cross peak to A4
- C4 with C3 and C5
- D3 with D5, as these protons come close in an all-trans conformation of the pyridine rings

With the help of HSQC some signals inside the multiplets could be singled out and assigned:

- B3 at 8.73 and D5 at 8.68. The C3 and C5 have the two signals at 8.70 and 8.72.
- Because of a general trend, where the B side of the ligand is low-field shifted compared to the shifted compared to the D side (see table 2.7), A3 may be at 8.68 and E3 at 8.67

δ on <i>t</i> -Bu side		δ on hydroxy side		Δ_{B-D}
B5	9.01	D3	8.95	0.06
B3	8.73	D5	8.68	0.05
bo	7.97	do	7.89	0.08
bm	7.64	dm	6.99	0.65

Table 2.7: Unsymmetrical chemical shifts in the proton-NMR of qp (for labeling see fig. 7.7 on page 135).

$^{13}\text{C-NMR}$ of qp δ For labeling, compare with Figure 7.7 on page 135. The sample was too dilute to get a nice carbon spectrum. However, with help of the HSQC, the following assignments could be made: 149.3 (A6,E6), 139.0 (C4), 137.6 (A4, E4), 128.2 (do), 126.8 (bo), 126.2 (bm), 124.4 (A5, E5), 118.3 (B5), 117.8 (B3, C3 and/or C5), 117.4 (D3), 117.1 (A3, E3 and/or D5), 116.1 (dm).

The HMBC then gave the missing: 34.5 (C(CH₃)₃) and 31.0 (CH₃). Further cross peaks occurred:

- bm gives a cross peak with C(CH₃)₃, but also with two more carbon environments giving signals at 126.5 (bo) and 135.0 (bv).
- dm shows a cross peaks with do and with two other carbons at 159.3 and 116.1 Comparison with a ChemDraw Ultra simulation suggests them to be dp and dm on the other side of the ring respectively
- *tert*-butyl shows a cross peak to 152.3, which could then be bp
- do gives a cross peak with 159.3 (dp), 149.7 and 128.6
- bo shows a cross peak with 127.0 (bo on the other side of the ring), 149.7 and 152.3 (bp)
- a cross peak is seen between C4 and 155.0
- A4/E4 show cross peaks with 149.7 and 155.3
- A6 and E6 give a cross peak at 155.3
- B3 gives cross peaks at 118.6 and 135.0
- the multiplet containing C3 and C5 give cross peaks at 121.4 and 135.0
- the multiplet containing A3, E3 and D5 give cross peaks at 118.0, 124.8, 128.3 155.4
- D3 gives cross peaks at 117.4, 128.2 and 155.0
- B5 gives cross peaks at 118.3 and 135.0

The assignment of the quarternary carbon atoms A2, B2, B4, B6, C2, C6, D2. D4, D6, E2, bv and dv are ambiguous and so left out in Table 2.11. In the experimental chapter, all the chemical shifts are listed.

$^1\text{H-NMR}$ of mp δ For labeling, compare with Figure 7.7, and the spectrum is shown as an example in Figure 2.5. The assignment of the proton signals in mp is consistent with qp, except for the visible OH group at 9.94. The same low-field shift of the B side compared to the D side in the molecule is visible (see table 2.8) and allows the separate assignment of A4 and E4.

The COSY singles out the individual signals in the multiplets at 8.72-8.69 and 8.69-8.66: C3 or C5 are at 8.708, B3 and C3 or C5 are at 8.705, A3 and E3 are at 8.682 and 8.675 and D5 is at 8.680. Because of the trend shown in table 2.8 A3 is at 8.682 and E3 at 8.675.

In the ROESY a cross peak is seen between OH and dm, and one between OMe and bm. This assigns the b to the B and d to the D ring.

δ on the methoxy side		δ on hydroxy side		Δ_{B-D}
B5	8.97	D3	8.95	0.02
B3	8.705	D5	8.680	0.025
bo	8.00	do	7.89	0.11
bm	7.17	dm	7.01	0.16

Table 2.8: Unsymmetrical chemical shifts in the proton-NMR of mp (for different see fig. 7.13).

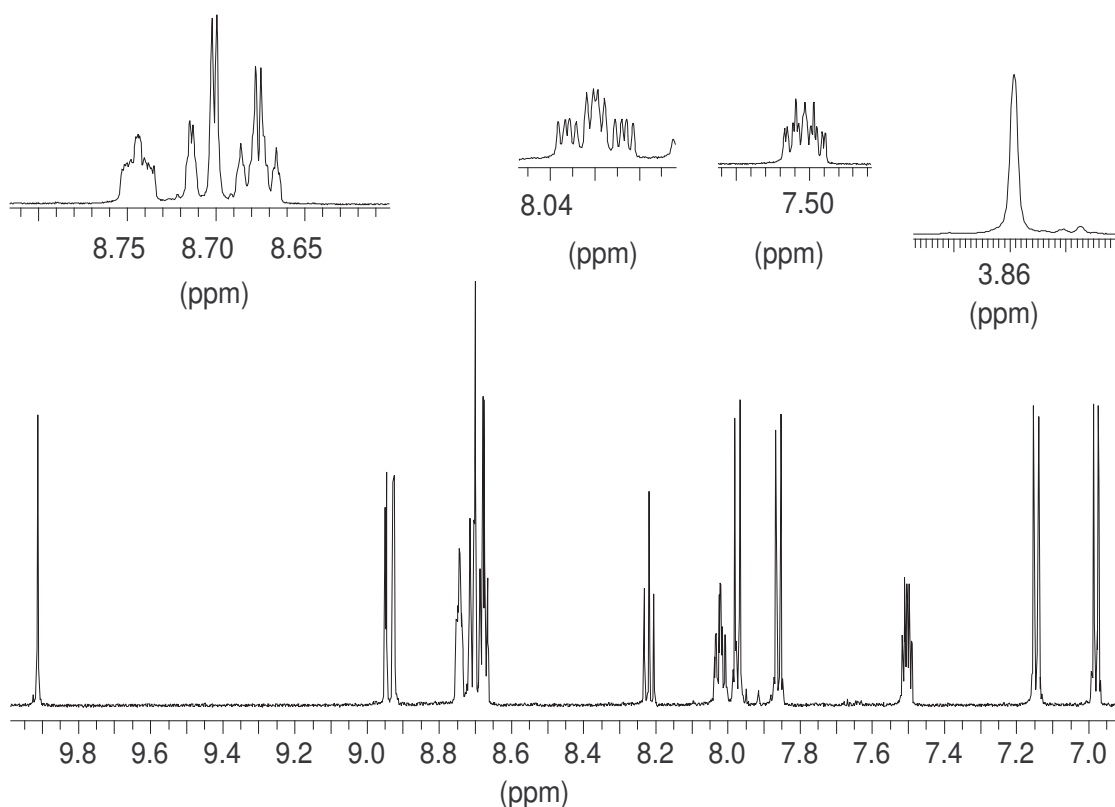


Figure 2.5: 600 MHz $^1\text{H-NMR}$ spectrum of mp.

$^{13}\text{C-NMR}$ of mp δ For labeling, compare with Figure 7.13. The sample was too dilute to get a nice carbon spectrum. However, with help of the HSQC the carbon atoms adjacent to a proton could be assigned as follows: 149.3 (A6, E6), 138.2 (C4), 137.3 (A4, E4), 128.2 (bo, do), 124.5 (A5, E5), 121.5 (B3, C3 and/or C5), 121.0 (A3, E3 and/or D5), 118.3 (B5), 118.0 (D3), 117.8 (B3, C3 and/or C5), 117.4 (A3, E3 and/or D5), 116.2 (dm), 114.9 (bm).

The HMBC gave the coupling of OCH₃ with bm, and the coupling of OH with dm. This distinguished the b and d rings once more, and gave the chemical shifts for OCH₃ and bp of 56.0 and 161.0 respectively, and of dp at 159.1.

Further cross coupling occurred:

- dm show cross peaks with 116.2 (dm on the other side of the ring), 128.2 (do) and 159.1 (dp)
- bm shows cross peaks with 114.9 (bm on the other side of the ring), 129.8 and 161.0 (bp)
- A5, E5 show one cross peak at 120.9
- do show cross peaks at 128.2 (do on the other side of the ring), 149.4 and 159.1 (dp)
- bo show cross peaks at 128.2 (bo on the other side of the ring), 149.0 and 161.0 (bp)
- A4, E4 show cross peaks at 194.4 and 155.1
- C4 shows a cross peak at 154.9
- the multiplet containing D5, A3 and E3 gives cross peaks at 117.9, 124.5 (A5, E5), 128.0 and 155.1
- the multiplet containing B3, C3 and C5 gives cross peaks at 118.2, 121.5, 124.5 (A5, E5), 130.0 and 155.1
- the multiplet containing A6 and E6 gives cross peaks at 124.5 (A5, E5), 137.9 and 155.1
- D3 gives cross peaks at 117.5, 128.0 and 149.0
- B5 gives cross peaks at 117.8 (B3, C3 and/or C5) and 130.0

The assignment of the carbon atoms A2, B2, B4, B6, C2, C6, D2, D4, D6, E2, bv and dv are ambiguous and so left out in Table 2.11

¹H-NMR of pp δ For labeling, compare with Figure 7.16. The assignment of the signals in pp is consistent with the assignment of qp and mp. The same low-field shift of the B side compared to the D side in the molecule is visible (see table 2.9) but the separation of A4 versus E4, A5 versus E5 and A6 versus E6 is not possible directly from the proton-NMR, since they are all multiplets.

Like in mp, the OH group is visible at 9.93, and there is the additional bp proton at 7.59.

In the COSY

- B3 gives a cross peak to B5 and can be placed at 8.77, while D5 can be placed at 8.69.
- The cross peaks of A3, A6, E3, E6 give four equal cross peak signals with A4/E4 and with A5/E5. Since A3 and E3 should give strong interaction with A4/E4 and weaker with A5/E5, this is interpreted to mean that there are only two cross peaks instead of four, but with some uncompensated coupling. The same is true for A6 and E6 the other way round, with stronger interaction with A5/E5 than A4/E4. Since the intensity of the cross peaks are equal with both, and a general trend of low-field shifted B side compared to D side of the molecule, A3 and A6 may possibly be at 8.76 while E3 and E6 may be at 8.70.
- The multiplet with A4, E4 and bo, give cross peaks among other with bm and with A3, A6, E3, E6. They show that A4 and E4 are at 8.04 and bo at 8.02.

In the ROESY, there is

- an exchange peak of the phenol group with water as well as a relayed ROE signal

δ on the methoxy side	δ on the hydroxy side	Δ_{B-D}
B5	9.04	D3 8.98 0.06
B3	8.77	D5 8.69 0.08
bo	8.02	do 7.89 0.13
bm	7.64	dm 7.00 0.64

Table 2.9: Unsymmetrical chemical shifts in the proton-NMR of pp (for different see Figure 7.16).

- interaction between B5 and D3, as these protons come close in an all-trans conformation of the pyridine rings
- a possible cross peaks between A3 with C3, and E3 with C5, that are both drowned in the multiplet where all these signals lay close together.

$^{13}\text{C-NMR}$ of pp δ : The solubility of pp was so poor, that no HSQC or HMBC were measured. At the time, I hadn't yet realised that the pp in the sample was still protonated in the presence of sodium carbonate. These ligands need to be treated thoroughly with sodium hydroxide solution in order to become neutral. NMR probes of the linked ligands described in the next chapter could be obtained in higher concentrations after such treatment.

¹ H-NMR chemical shifts of the qnpy ligands in DMSO-d ₆					
qp		mp		pp	
		OH	9.94	OH	9.93
B5	9.01	B5	8.97	B5	9.04
D3	8.95	D3	8.95	D3	8.98
A6	8.78	A6, E6	8.78-8.76	A6, E6, A3, E3	8.78-8.67
E6	8.77	C3/C5	8.708	C3, C5	8.75, 8.72
B3	8.73	B3, C3/C5	8.705	B3	8.77
C3, C5	8.72, 8.70	A3	8.682	A6, A3	8.76
D5	8.68	D5	8.680	E6, E3	8.70
A3	8.68	E3	8.675		
E3	8.67			D5	8.69
C4	8.25	C4	8.24	C4	8.27
A4	8.06	A4	8.05	A4, E4	8.04
E4	8.04	E4	8.04		
bo	7.97	bo	8.00	bo	8.02
do	7.89	do	7.89	do	7.89
bm	7.64	A5, E5	7.55-7.51	bm	7.64
A5, E5	7.55-7.52	bm	7.17	bp	7.59
dm	6.99	dm	7.01	A5, E5	7.56-7.52
<i>t</i> -butyl	1.38	MeO	3.89	dm	7.00

Table 2.10: ¹H-NMR data for the qnpy derivatives qp, mp and pp.

¹³ C-NMR chemical shifts of the qnpy ligands qp and mp in DMSO-d ₆			
qp		mp	
dp	159.3	bp	161.0
bp	152.3	dp	159.1
A6,E6	149.3	A6,E6	149.3
C4	139.0	C4	138.2
A4,E4	137.6	A4,E4	137.3
do	128.2	do, bo	128.2
bo	126.8		
bm	126.2		
A5,E5	124.4	A5,E5	124.5
B5	118.3	B3, C3 and/or C5	121.5
B3,C3 or C5	117.8	A3, E3 and/or D5	121.1
D3	117.4	B5	118.3
D5,A3 or E3	117.1	D3	118.0
		B3, C3 and/or C5	117.8
		A3, E3 and/or D5	117.4
dm	116.1	dm	116.2
		bm	114.9
C(CH ₃) ₃	34.5	MeO	56.0
CH ₃	31.0		

Table 2.11: ¹³C-NMR data for the qnpy derivatives qp and mp.

Chapter 3

Unsymmetrically linked quinquepyridine ligands

3.1 Overview

3.1.1 Expected features of the linked ligands comprising two qnpy domains

The ligand qcq had been originally designed to form a hairpin-like supramolecular structure, similar to the linked tris-bipy strands connected by a chiral template,^{62,99} see Figure 3.1. The compound qcq had already been synthesised by Whall,⁵¹ but no complexes had been fully characterised. In this thesis the ligands qcq, mcm and pcp were synthesised in an approach to make unsymmetrical double helical complexes of qnpy derivatives with appropriate transition metal ions, where the two qnpy domains of the dinuclear complex are linked together, and if possible get the first ever crystal structure of one of these intriguing structures.

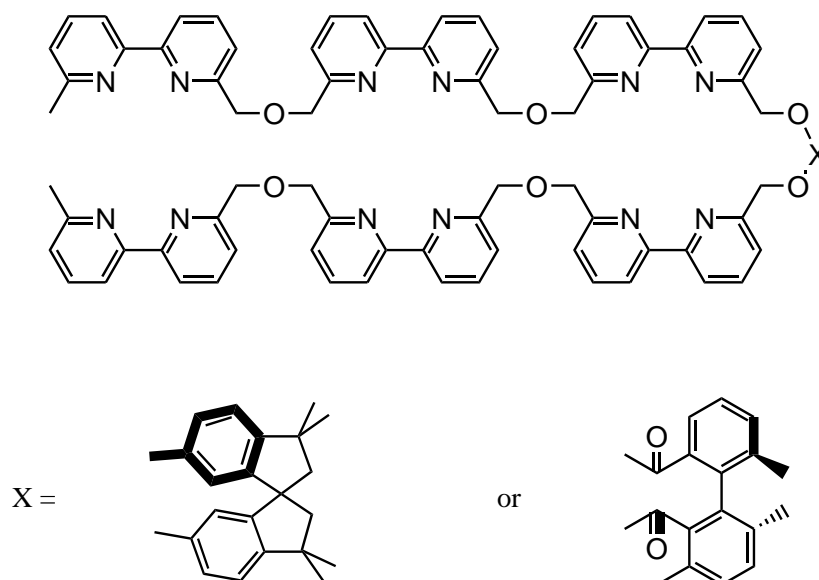


Figure 3.1: Tris-bipy with chiral template

The longest commercially available pure oligo ethyleneglycol (hexaethylene glycol) was chosen as a linking group, because of its flexibility and well understood chemistry, and because it should not in-

terfere with the helicate formation.⁵¹ Because of the hard donor properties of the oxygen atom known from crown ethers (binding hard Li^+ , Na^+ , K^+ etc.), the oxygen atoms of the linker were not expected to compete with the nitrogen-transition metal coordination.

The ligand names are derived from qcq. As Whall made only this one linked qnpy derivative, she called it after the first letters in quinquepyridine-chain-quinquepyridine).⁵¹ The mcm ligand then got the name because of the methoxyphenyl substituent, and the pcq ligands because of the plain phenyl substituent. The ligand names qp, mp and pp for the qnpy units were derived from these names.

3.1.2 Synthetic route to the qnpy derivatives qcq, mcm and pcq

Since qcq had already been synthesised by Whall⁵¹ using literature methods,¹⁰⁰⁻¹⁰³ the same synthetic pathway, that was successful then, was followed for qcq as well as for the new ligands mcm and pcq. Figure 3.2 shows the reaction pathway that was followed in order to obtain qcq, mcm and pcq.

The first step was the tosylation of hexaethylene glycol. A test reaction on the cheaper tetraethylene glycol was successful, and so hexaethylene glycol was tosylated under the same conditions, following the literature method¹⁰⁰ on a scale of $\frac{1}{30}$ of that reported. An aqueous solution of sodium hydroxide was cooled in an ice-water bath, and a solution of hexaethylene glycol in THF was added. A THF solution of tosyl chloride was added dropwise, while the temperature of the reaction mixture was kept at 2-4 °C. Then the product was extracted with DCM, and obtained in good quality in a yield of 95%.

For the formation of the ether bond between the linker, an inorganic base should be present. As Cs_2CO_3 proved superior to other inorganic bases, first in macrocycle ring closures with ester bonds,¹⁰⁴ and later in the reaction of tosylated ethylene glycol derivatives with phenol derivatives, to form crown-ether like compounds,^{101,102} this was assigned to a template effect that was termed the 'cesium effect'. Cs_2CO_3 also outstripped K_2CO_3 and other inorganic bases, in assisting the reaction of tosylated ethylene glycol compounds with 2,3-naphthalene diol to form linear molecules (as opposed to cycles),¹⁰³ giving around 80% yield instead of 5%, it seemed clear that this was the base of choice for the etherification.

The tosylate being such a good leaving group, the coupling of the tosylated linker with the OH group of the qnpy derivatives, in the presence of Cs_2CO_3 , was quite successful. This way two qp units were linked together to form qcq, two mp units to form mcm, and two pp moieties to form pcq.

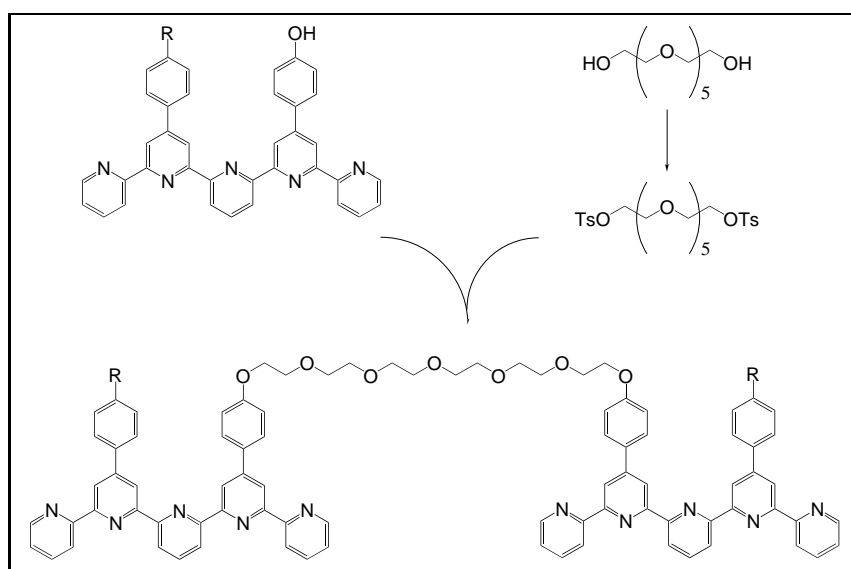


Figure 3.2: Overview of the synthesis of the linked qnpy derivatives and ligands qcq, mcm and pcq, R = *tert*-butyl, methoxy and H for qcq, mcm and pcq respectively.

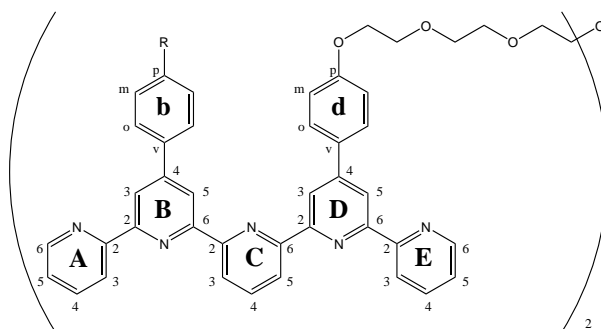


Figure 3.3: General labels of the qnpy derivatives and ligands, R = *tert*-occur, methoxy and H for qcq, mcm and pcp respectively. For NMR assignment, the H and C were named with the letter of the pyridine or phenyl ring, followed by the number or letter indicating the atom of the ring, e.g. B3 of do can be the proton H_{B3} or H_{do} in the $^1\text{H-NMR}$ or the carbon C_{B3} or C_{do} in the $^{13}\text{C-NMR}$.

	qcq	mcm	pcp
qnpy derivative/ μmol	163	603	574
tos ₂ heg/ μmol	84.6	291	286
Cs ₂ CO ₃ / μmol	90	307	328
Solvent: DMF/ml	12	13	12
yield/%	49	53	50

Table 3.1: Starting materials for the reaction of the qnpy derivatives qp, mp and pp to qcq, mcm and pcp.

3.2 Linked qnpy ligands: qcq, mcm and pcp

3.2.1 Synthesis

The procedures of Whall and Weber was followed.^{51,101–103} The qnpy derivative, Cs₂CO₃ and tos₂heg were dried and heated in dry DMF at 80–110 °C for at least 17h. After cooling to room temperature, the crude product was filtered off and dried *in vacuo*. Then it was purified from monosubstituted byproduct by column chromatography, using alox and varying eluents: chloroform : diethylamine (25 : 1) for qcq, DCM : MeOH : Et₂NH (200 : 10 : 0.1) for mcm and chloroform : Et₂NH (42 : 1) for pcp. The reaction to pcp was conducted with just a CaCl₂ tube, instead of an argon atmosphere to protect against water. This did not affect the yield, see Table 3.1.

3.2.2 Crucial point

Drying the product *in vacuo* over P₂O₅ resulted in protonated ligand and markedly reduced solubility, that prevented e.g. NMR characterisation. Treatment with dilute sodium hydroxide solution, by sonicating the ligand in suspension for 15min, followed by extraction with chloroform, gave the neutral ligand and stopped the solubility problem.

3.2.3 Characterisation

Micro analysis

The three linked ligands qcq, mcm and pcp were successfully characterised by micro analysis, each sample containing some water.

Mass spectrometry

Although qcq had been characterised before by Whall,⁵¹ all three of them were characterised by Maldi-Tof methods: qcq and pcp gave signals for M^+ and M plus assortments of Na^+ , K^+ and/or water; mcm gave no M^+ signal, only for $(M+K+H_2O)^+$ and $(M+Na)^+$.

Infrared spectroscopy

The infrared spectra were recorded of the three ligands. In comparison with the unlinked ligands, the linker is visible with pronounced C-H stretch signals at $2955-2862\text{cm}^{-1}$ and C-O-C stretch signals around 1041cm^{-1} .

UV-Vis spectroscopy

UV-Vis spectra were recorded mainly to emphasize the marked changes that occur when these ligands are complexed e.g with copper(II/I). These ligands in themselves absorb strongly in the UV region because of the fourteen aromatic rings per molecule. But as they are almost white in colour, their absorption decreases drastically towards the visible region. The spectra of ligand solutions in chloroform showed absorptions that are not lower in magnitude than the corresponding copper complex in the UV region (compare with page 83. For a better view, the results are listed in Table ???. The spectrum of pcp shows two maxima, while mcm and qcq only have one, and the other listed absorptions are shoulders to this maximum (see Table 3.2 and Figure 3.4). The high absorption of mcm at 284nm, may originate from the fact, that both substituents (at 4' and 4''' on the qnpy backbone), are electronically almost identical. The absorptions from both sides of the molecule add up at this wavelength and this results in a more intense absorption.

qcq		mcm		pcp	
wavelength /nm	extinction coefficient / $M^{-1}\text{cm}^{-1}$	wavelength /nm	extinction coefficient / $M^{-1}\text{cm}^{-1}$	wavelength /nm	extinction coefficient / $M^{-1}\text{cm}^{-1}$
260(sh)	78'773	260(sh)	99'874	257	101'501
281	87'070	284	133'405	280(sh)	97'618
307(sh)	43'562	310(sh)	67'034	307(sh)	57'538
318(sh)	31'917	320(sh)	45'501	316(sh)	46'282

Table 3.2: UV-Vis data for the linked qnpy derivatives qcq, mcm and pcp.

X-ray

Samples of all ligand molecules were set up for crystallisation. But the crystals were of poor quality, and no crystal structure could be solved. From a solution of mcm in a mixture of chloroform acetone, after standing for seven months, a square crystal had grown. It did not diffract well enough, but a tiny

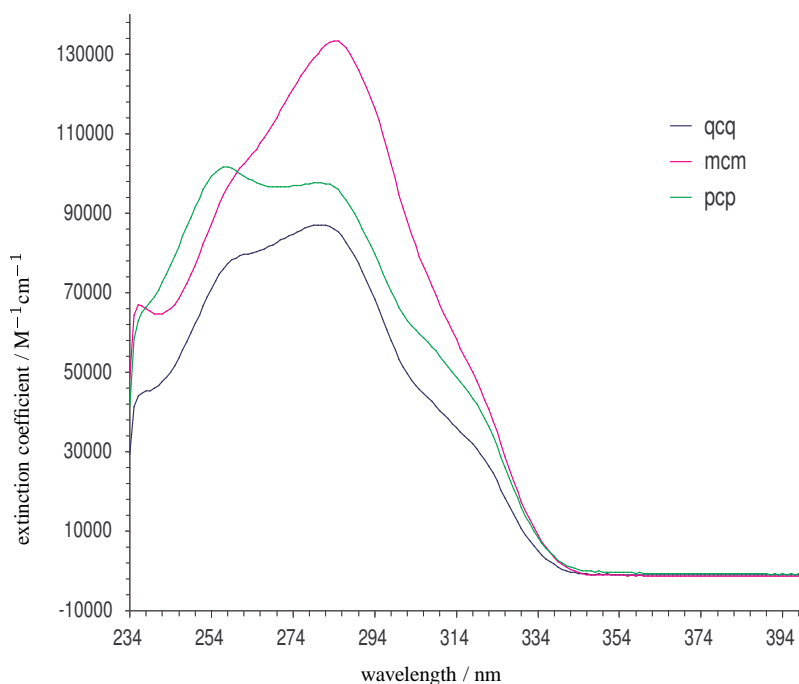


Figure 3.4: The UV absorption spectra of the three linked qnpy derivatives qcq, mcm and pcp.

crystal in the same sample diffracted well enough to give the connectivity of the molecule, that built the structure. It was dibenzo-18-crown-6, see appendix D on page 214, and may be an impurity, a side- or degradation-product.

NMR study of the linked qnpy's qcq, mcm and pcp

All the linked qnpy type ligands qcq, mcm and pcp were recorded on a 600 MHz spectrometer. qcq had already been characterised by $^1\text{H-NMR}$ by Whall,⁵¹ with help of a 250 or 300 MHz spectrometer. There are signals in multiplets however, that could be further resolved in the 600 MHz spectrum, and the assignment is described in detail below. Then the characterisations of mcm and pcp follow in the same way. As an example for the $^1\text{H-NMR}$ spectra of these ligands, that of qcq is shown in Figure 3.5. The $^1\text{H-NMR}$ chemical shifts of qp, mp and pp are listed in Table 2.10 on page 31.

All the $^{13}\text{C-NMR}$ spectra are new. Because of some limited solubility, the carbon spectra had unsatisfactory signal to noise ratio in mcm and pcp, but the chemical shifts of most carbon atoms could be assigned with HSQC and HMBC. They are listed in Table 2.11 on page 32.

$^1\text{H-NMR}$ of qcq δ : Comparison with the spectrum of qp gives B5 at 8.92 and D3 at 8.87, a multiplet (8.72-8.61) for B3, A3, E3, C3, C5, D5, A6 and E6, C4 at 7.99, a multiplet (7.88-7.81) for A4, E4, bo and do, bm at 7.52, A5 and E5 at 7.33 and at 7.31, dm at 7.03, f at 4.18, e at 3.89, a multiplet (3.77-3.74) for d, a multiplet (3.72-3.69) for c, a and b together at 3.68 and finally *tert*-butyl at 1.39. See Figure 2.3 for therefore and Figure 3.5.

In the ROESY:

- the *t*-butyl protons show a cross peak with the bm protons
- and the f-protons from the linker show a cross peak with the dm-protons

δ on <i>t</i> -Bu side		δ on the linker side		Δ_{B-D}
B5	8.92	D3	8.87	0.05
B3	8.71	D5	8.65	0.06
bo	low field of 7.88-7.81	do	high field of 7.88-7.81	positive value
bm	7.52	dm	7.03	0.49

Table 3.3: Unsymmetrical chemical shifts in the proton-NMR of qcq (for therefore see fig. 7.9)

- a weak cross peak is seen between B5 and D3, as these protons come close in an all-trans conformation of the pyridine rings

Because A3, E3, C3 and C5 are very close together in chemical shift, the ROESY contacts of A3-C3 and C5-E3 are not seen. Any cross-couplings are drowned in the diagonal trace.

In the COSY:

- the neighbouring protons of the glycol bridge f and e, and d and c are seen coupling together, localising d at 3.75 and c at 3.70
- the dm protons, assigned by ROESY, couple with do at 7.82
- the bm protons, assigned by ROESY, couple with bo at 7.83
- B5 couples with B3 and localises it at 8.71
- D3 couples with D5 and localises it at 8.65
- A5/E5 cross-couples strongly into the multiplet (8.71-8.61) at 8.70, that localises A6/E6
- A4/E4 inside 7.88-7.81 couple with A3/E3 and thus localise A3/E3 at 8.64, and themselves at 7.85
- C4 couples with C3 and C5 on the high field side of the multiplet 8.72-8.61, and localises C3/C5 at 8.63

Because of the general trend showing rings on the B side more electron rich than the rings on the D side (see table 3.3), it is assumed, that A3, A4, A5 and A6 are slightly shifted towards low field in comparison to E3, E4, E5 and E6. In consequence, the ddd of A5 is at 7.33 and the ddd of E5 is at 7.31.

The HSQC:

- takes the A6/E6 apart into 8.70 and 8.68. Because of the general trend shown in Table 3.3, A6 is expected to be 8.70, and A6 to be 8.68

^{13}C -NMR of qcq δ : With help from the HSQC, the C — H resonances could be assigned as follows: 149.27 (A6), 149.21 (E6), 137.81 (C4), 137.01 (A4, E4), 128.60 (do), 127.17 (bo), 126.11 (bm), 123.92 (A5 or E5), 123.90 (A5 or E5), 121.56, 121.54, 121.41 and 121.39 (C3 or C5 or A3 or E3), 119.11 (B5), 118.84 (B3), 118.55 (D3), 118.36 (D5), 115.17 (dm), 71.08 (d), 70.86 (a or c), 70.85 (a or c), 70.81 (b), 69.91 (e), 67.7 (f), 34.92 (C(CH₃)₃), 31.55(CH₃). See Figure 2.3 for therefore.

- The signals 121.56, 121.54, 121.41, 121.39 belong to C3, C5, A3, E3. Since the other A and E signals in the carbon spectrum coincide, it is assumed that A3 and E3 belong either to 121.56, 121.54 or to 121.41, 121.39.
- A5 and E5 give two signals close to each other at 123.92 and 123.90.
- A4 and E4 coincide.

In the HMBC:

- there is a cross peak for CH₃ to C(CH₃)₃ and from bm to C(CH₃)₃ as well.
- A cross peak is further seen between f and e, e and d, d and c. The remaining assignment for the bridging hexaethyleneglycol carbons is exchange: c at 70.86 or 70.85. Because of the alternating trend with the f, e, d, 'rest', it is assumed, that a is close to c and the chemical shift is either 70.86 or 70.85, while b is at 70.81.
- A5, E5 show a cross peak with A3, E3 and a "weaker" one with A6, E6.
- Further cross coupling is seen between B5 and B3, C3 and C5, D3 and D5.

The HMBC also shows to which ring the quarternary carbons belong:

- 159.89 shows a strong cross peak with the multiplet containing A4, E4, bo and bm, and a weaker one with dm and one to f. It is therefore dp
- 156.52 shows a cross peak into both sides of the multiplet where on the low field side there are A6, E6 and B3, and on the high field side there is D5, A3, E3, C3 and C5
- 156.49 shows a cross peak to the far low field end of the multiplet containing B3, A6 and E6
- 156.10 and 156.09 both couple into the high field side of the multiplet containing D5, C3, C5, A3 and E3
- 155.94 and 155.89 for some reason show no cross peaks in the HMBC.
- 155.58 shows a cross peak to D3, and stronger one to C4. It may be C6
- 155.53 shows a cross peak with B5, and a stronger one to C4. It may be C2
- 152.38 shows a cross peak with CH₃ and the multiplet containing bo and A4. It is therefore bp
- 149.96 shows a cross peak with A4/E4
- 149.52 shows a cross peak with the multiplet on the side of bo and do and a cross peak to one to B5 or D3
- 135.92 shows a cross peak to B5, the multiplet containing B3, A6 and E6, and a strong one with bm. It is probably C_{bv} or C_{B4}
- 131.20 shows a cross peak with D3, with the multiplet containing D5, C3, C5, A3 and E3 and a very strong one with dm. It is probably C_{dv} or C_{D4}

¹⁵N-NMR of qcq δ: In the ¹N-¹⁵H HMBC: five different nitrogen resonances are seen. -14.46 couples, among other with D3 and is therefore assigned as N_D, -13.91 couples among other with B5 and is therefore assigned to N_B, -9.57 couples, among other with E5 and is therefore assigned to N_E, -9.35 couples, among other with A5 and is therefore assigned as N_A, and -11.75 is the one left and is assigned to N_C, although the only coupling seen is with a signal from the multiplet containing D5, A3, E3, C3, and C5. See the spectrum in Figure 3.6, and Figure 2.3 for labelling.

δ on the methoxy side		δ on the linker side		Δ_{B-D}
B5	8.853/8.848	D3	8.853/8.848	unknown
B3	8.65/8.62	D5	8.65/8.62	unknown
bo	7.84	do	7.82	0.02
bm	7.00	dm	7.01	-0.01

Table 3.4: Unsymmetrical chemical shifts in the proton-NMR of mcm (for labelling see fig. 7.14)

¹H-NMR of mcm δ : assignment with Comparison with mp and qcq gave the following assignments. Notable is the much smaller difference in the chemical shifts in the B and D side of this molecule compared to qcq.

A multiplet for B5 and D3 at 8.86-8.84, a multiplet for some of the B3, A6, E6 or D5, C3, C5, A3, E3 protons at 8.72-8.68, a multiplet for some of the same protons at 8.67-8.62, C4 at 7.98, and a multiplet for A4, E4, bo and do at 7.87-7.80, 7.32 and 7.31 for A5 and E5, either bm and dm at 7.01 or 7.00, f at 4.18, e at 3.92-3.89, OCH₃ at 3.88, d at 3.78-3.75, c at 3.73-3.70 and finally a and b at 3.69. See Figure 2.3 for labelling.

In the ROESY:

- OCH₃ shows cross peaks with the bm protons, which assign bm as the signal at 7.00
- the f protons shows a cross peak with the dm protons, which assigns dm as the signal at 7.01
- bm shows a cross peak with bo and localises bo at 7.84
- dm shows a cross peak with do and localises do at 7.82
- B5 and D3 shows cross peaks into the multiplet containing B3 and D5, localising B5 and D3 at 8.853 and 8.848, and B3 and D5 at 8.65 and 8.62
- C4 shows a cross peak with C3/C5 and localises them at 8.64 and 8.63
- A5/E5 shows cross peaks with A4/E4 and A6/E6 and localises these signals at 7.32 and 7.31 for A5/E5, 8.71 and 8.69 for A6/E6, 8.65 and 8.63 for A3/E3 and 7.85 and 7.83 for A4/E4

The COSY gives no additional information.

In Table 3.4 there is shown that there is no trend in different chemical shift in the A and E side of the qnpy parts. Therefore A3, A4, A5 and E6 can not be distinguished from E3, E4, E5 and E6, and neither can C3 from C5.

The HSQC helped to single out the e, d and c protons of the linker.

¹³C-NMR of mcm δ : With help from the HSQC, the C — H resonances could be assigned as follows: 149.30 for A6,E6, 138.00 for C4, 137.10 and 128.70 are A4/E4 or bo/do, 121.50 contains some of B3, D5, A3, E3, C3, C5, 118.70 are B5 and D3, 118.40 contains the other part of the B3/D5/A3/E3/C3/C5, 115.10 and 114.50 are bm and dm, 71.30 is d, 71.10 is c, 71.00 is a,b, 70.0 is e, 67.9 is f and finally 55.8 is MeO. See Figure 2.3 for labelling.

In the HMBC:

- 161 shows cross peaks to the protons of MeO, bm, and the multiplet containing A4, E4, bo and do, it may therefore be bp
- 160 shows cross peaks with dm, and the multiplet containing A4, E4, bo and do, and may therefore be dp
- 157 shows cross peaks with the multiplet containing A4, E4, bo and do, and the multiplet containing B3, D5, A3, E3, C3 and C5

- 156.2 shows a cross peak with the multiplet containing B3, D5, A3, E3, C3 and C5
- 155.7 shows a cross peak with B5/D3 and C4
- 149.3 shows a cross peak with the multiplet containing A4, E4, bo and do
- 131.2 shows cross peaks with bm/dm, the multiplet containing B3, D5, A3, E3, C3 and C5 and B5/D3, it may therefore be bv and dv
- 129 shows a cross peak with the multiplet A4, E4, bo and do
- 124.0 shows cross peaks with the multiplet containing B3, D5, A3, E3, C3, and weakly with A6/E6
- 122 shows a cross peak with A6/E6
- 121 shows a cross peak with the multiplet containing B3, D5, A3, E3, C3
- 118.7 shows cross peaks with the multiplet containing B3, D5, A3, E3, C3, with A6/E6 and with B5/D3
- 115 shows a cross peak with bm/dm
- 71.5 shows a cross peak with proton a/b

¹H-NMR of pcp δ: assignment with Comparison with the spectrum of pp gives B5 at 8.92, D3 at 8.87, a multiplet containing B3, C3, C5, D5, A3, E3, A6 and E6 at 8.73-8.62, C4 at 8.00, a multiplet containing A4, E4, bo and do at 7.91-7.81, a multiplet containing bm and bp at 7.53-7.46, A5 and E5 at 7.34 and 7.31, dm at 7.01, f at 4.19, e at 3.91 d at 3.78-3.75, c at 3.74-3.71 and finally a and b at 3.69. See Figure 2.3 for labelling.

In the ROESY:

- the f-protons show cross peaks with dm
- B5 shows cross peaks with D3 and into the multiplet containing bo, do, A4 and E4, singling out the position for bo at 7.89
- D3 shows cross peaks with B5 and into the multiplet containing bo, do, A4 and E4, singling out the position for do at 7.84
- C4 shows cross peaks with C3/C5 in the multiplet at 8.73-8.62, and singles out C3 and C5 at 8.67 and 8.65
- A5/E5 shows cross peaks with A6/E6 in the 8.73-8.62 multiplet and A4/E4 in the multiplet 7.91-7.81, localising A6/E6 at 8.72 and 8.70, and A4/E4 at 7.87 and 7.85
- A4/E4 shows cross peaks with A5/E5 and A3/E3, localising the latter at 8.67 and 8.64
- bo shows cross peaks with B5, B3 and bm/bp and localises B3 at 8.71 and bm/bp at 7.50 and 7.48
- do shows cross peaks with D3, D5 and dm, localising D5 at 8.63

The COSY gives no new information after the analysis of the ROESY, but it confirms the assignments.

The HSQC then localises d at 3.77 and c at 3.72.

Because of the general trend showing rings on the B side more electron rich than the rings on the D side (see table 3.5), it is assumed, that A3, A4, A5 and A6 are slightly shifted towards low field in comparison to E3, E4, E5 and E6. In consequence, the A6 is at 8.72 and E6 at 8.70, A3 at 8.67 and E3 at 8.64, A4 at 7.87 and E4 at 7.85 and finally A5 at 7.34 and E5 at 7.31.

δ on the phenyl side		δ on the linker side		Δ_{B-D}
B5	8.92	D3	8.87	0.05
B3	8.71	D5	8.63	0.08
bo	7.89	do	7.84	0.05
bm	7.50 or 7.48	dm	7.01	0.49 or 0.47

Table 3.5: Unsymmetrical chemical shifts in the proton-NMR of pcp (for labelling see fig. 7.17)

$^{13}\text{C-NMR}$ of mcm δ : With help from the HSQC, the C — H resonances could be assigned as follows: 149.4 (A6, E6), 138.1 (C4), 137.2 (A4, E4), 129.3 (bm, bp), 128.7 (do), 127.4 (bo), 124.0 (A5, E5), 121.6 (C3, C5, A3 and E3), 119.3 (B5), 119.1 (B3), aa8.7 (D3), 118.4 (D5), 115.0 (dm), 71.2 (d), 70.9 (a, b and c), 69.9 (e), 67.7 (f). See Figure 2.3 for labelling.

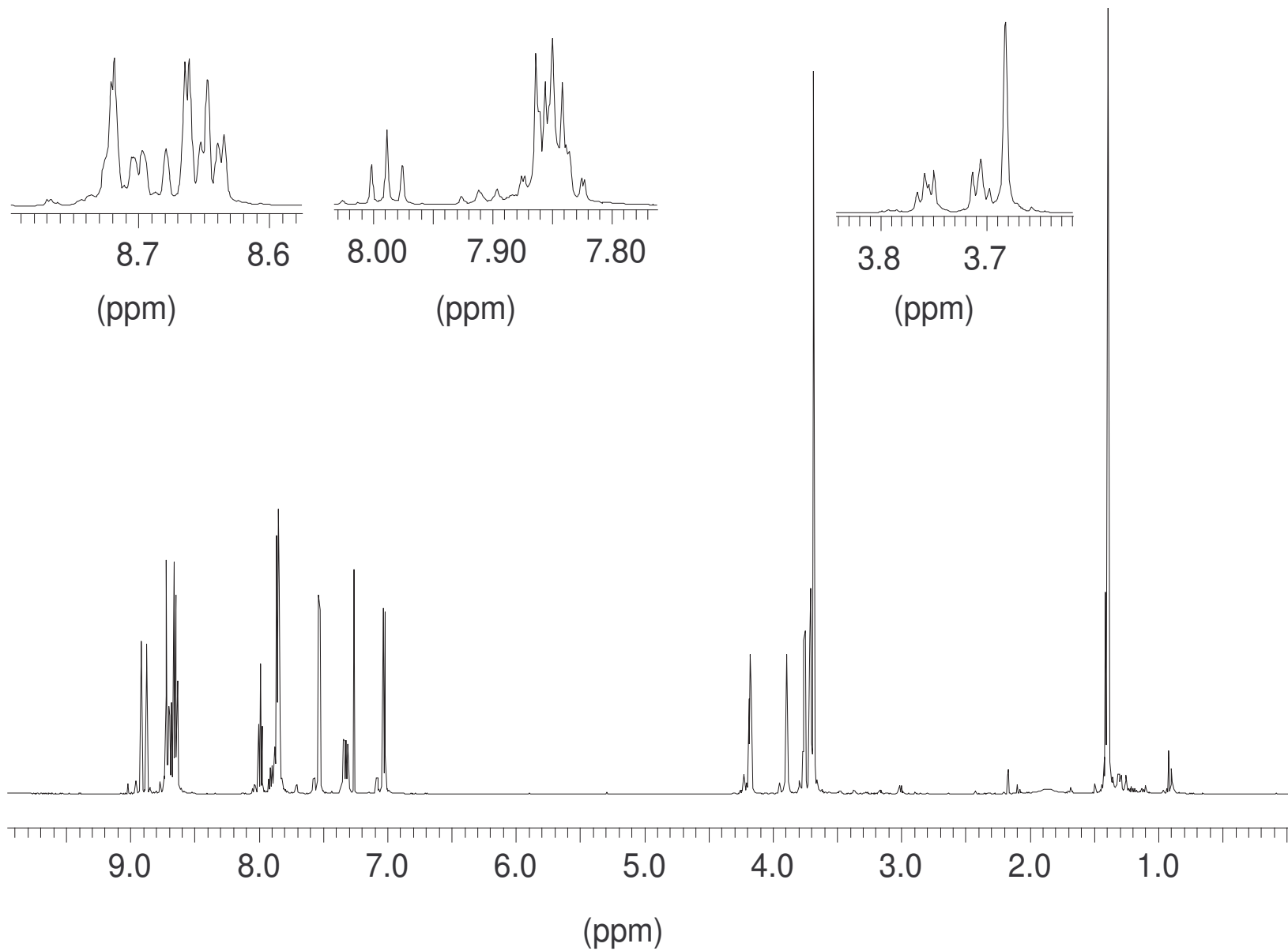
The HMBC shows the same couplings as in the other two samples, but this is was a very dilute sample and it is only possible to assign dp at 160.0.

¹ H-NMR chemical shifts of the linked qnpy ligands in CDCl ₃					
qcq		mcm		pcp	
B5	8.92	B5,D3	8.853	B5	8.92
D3	8.87	B5,D3	8.848	D3	8.87
B3	8.71	A6/E6	8.71	A6	8.72
A6	8.70	A6/E6	8.69	E6	8.70
E6	8.68	A3/E3	8.65	B3	8.71
D5	8.65	A3/E3	8.63	C3/C5	8.67
A3, E3	8.64	B3/D5	8.65	C3/C5	8.65
C3, C5	8.63	B3/D5	8.62	A3	8.67
		C3/C5	8.64	E3	8.64
		C3/C5	8.63	D5	8.63
C4	7.99	C4	7.98	C4	8.00
A4, E4	7.85	A4, E4	7.85	A4	7.87
bo	7.83	bo	7.84	E4	7.85
do	7.82	A4, E4	7.83	bo	7.89
bm	7.52	do	7.82	do	7.84
A5	7.33	A5/E5	7.32	bm/bp	7.50
E5	7.31	A5/E5	7.31	bm/bp	7.48
dm	7.03	dm	7.01	A5	7.34
		bm	7.00	A5	7.31
f	4.18	f	4.18	dm	7.01
e	3.89	e	3.91	f	4.19
d	3.75	OMe	3.88	e	3.91
c	3.70	d	3.77	d	3.77
a,b	3.68	c	3.71	c	3.72
<i>t</i> -butyl	1.39	a, b	3.69	a, b	3.69

Table 3.6: ¹H-NMR data for the linked qnpy derivatives qcq, mcm and pcp.

¹³ C-NMR chemical shifts of the linked qnpy ligands in CDCl ₃					
qcq		mcm		pcp	
dp	159.89	bp	161.0	dp	160.0
bp	152.38	dp	160.0		
A6	149.27	A6, E6	149.3	A6, E6	149.4
E6	149.21				
C4	137.81	C4	138.0	C4	138.1
A4/E4	137.01	A4/E4/bo/do	137.1	A4, E4	137.2
bv or B4	135.92	A4/E4/bo/do	128.7	bm, bp	129.3
dv or D4	131.20			do	128.7
do	128.60			bo	127.4
bo	127.17				
bm	126.11				
A5 or E5	123.92	A5, E5	124.0	A5, E5	124.0
A5 or E5	123.90				
C3 or C5 or A3 or E3	121.56	B3/D5/A3/E3/C3/C5	121.0	C3, C5, A3, E3	121.6
C3 or C5 or A3 or E3	121.54	B5,D3	118.7	B5	119.3
C3 or C5 or A3 or E3	121.41	B3/D5/A3/E3/C3/C5	118.4	B3	119.1
C3 or C5 or A3 or E3	121.39			D3	118.7
B5	119.11			D5	118.4
B3	118.84				
D3	118.55				
D5	118.36				
dm	115.17	bm/dm	115.1		
d	71.08	bm/dm	114.5	dm	115.0
a, b or c	70.86	d	71.3	d	71.2
a, b or c	70.85	c	71.1	a, b and c	70.9
a, b or c	70.81	a,b	71.0		
E6	69.91	e	70.0	e	69.9
f	67.70	f	67.9	f	67.7
<u>C</u> (CH ₃) ₃	34.92	MeO	55.8		
<u>CH</u> ₃	31.55				

Table 3.7: ¹H-NMR data for the linked qnpy derivatives qcq, mcm and pcp.



45

Figure 3.5: 600 MHz ¹H-NMR spectrum of qcq.

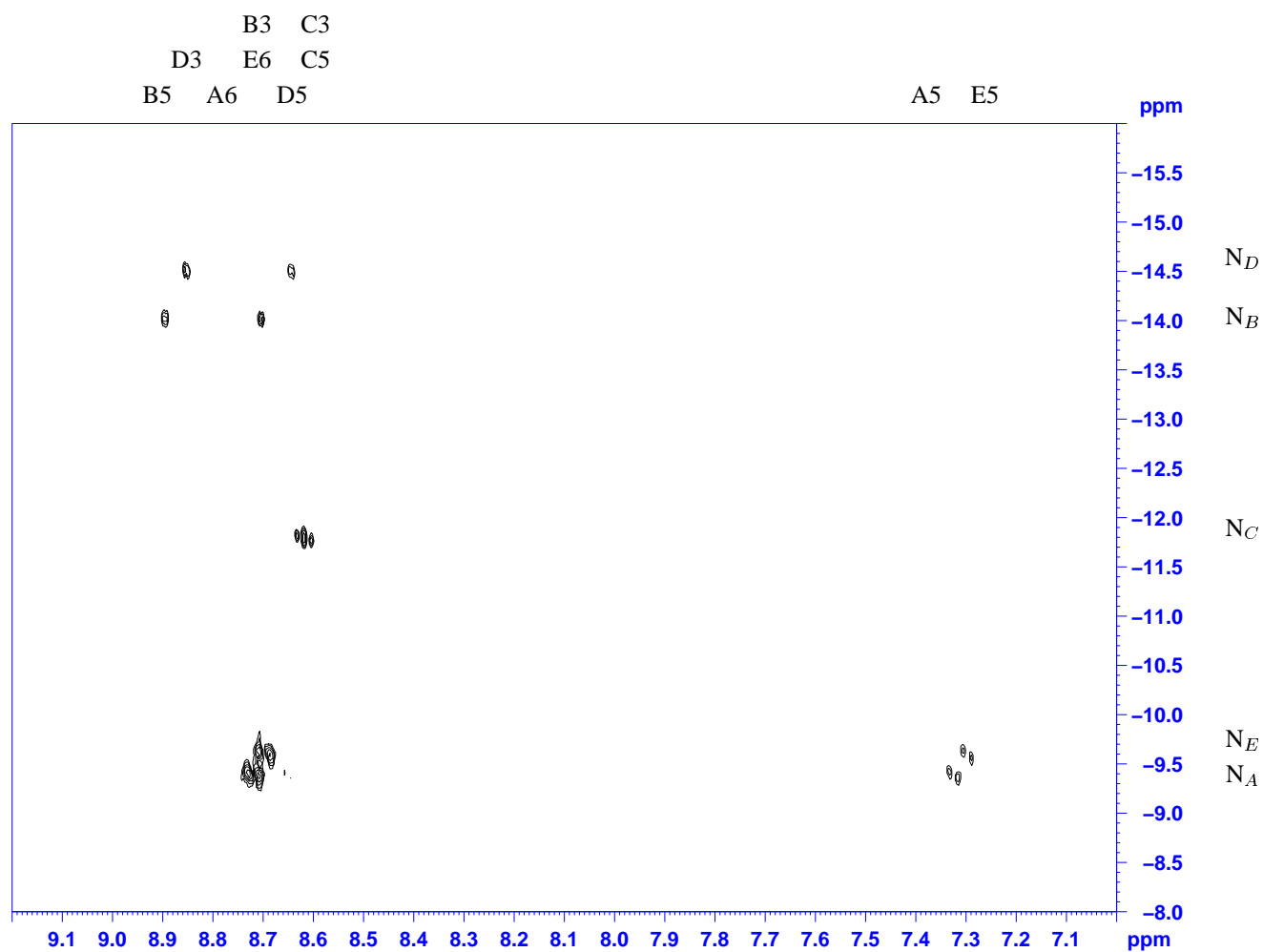


Figure 3.6: $^1\text{H}^{15}\text{N}$ -HMBC NMR spectrum of the unsymmetrically linked qnp derivative qcq. The chemical shifts of the proton resonances are given in the x-axis, and the chemical shifts of the nitrogen resonances are given in the y-axis.

Chapter 4

Complexes of unsymmetrically substituted quinquepyridine and linked quinquepyridine type ligands with copper(II), copper(I), cobalt(II) and nickel(II)

4.1 Tools for the characterisation of the coordination compounds

For the structure in the solid, crystal structure analysis and infrared spectroscopy were applied. Crystal structures give evidence of the connectivity in the crystallised compound and serve as proof for the existence of the compound. Infrared spectroscopy was applied in the region $4000\text{-}400\text{cm}^{-1}$, the N—Cu and N—Co coordination bonds are outside this window, but strong P—F absorptions from the counterions, as well as the ligand vibrations are observable. Solution structures were examined mainly by ^1H -NMR spectroscopy, and in the case of the copper complexes, with UV-Vis measurements. ^1H -NMR spectroscopy is a very common tool in chemistry. When applied to paramagnetic compounds however, parameters had to be changed to accommodate the much increased chemical shift range. There are also other aspects that change, as explained below. With UV-Vis, standard measurements showed the absorption bands of interest. Ligand centred absorptions showed in the UV region, while MLCT bands could be observed in the visible. The metal centred d-d transitions (compare with orbitals of e_g and t_{2g} symmetry, at different energy levels, in Figure 1.1), would also be in the visible region. Mass spectrometry was used to gain information about molecular mass and compound compositions. A Maldi-TOF instrument was used for most of the compounds described.

4.1.1 ^1H -NMR method for paramagnetic compounds

NMR stands for nuclear magnetic resonance, and this method gives information about the structure in solution. In an applied magnetic field, the different spin states of the nucleus divide up into states of different energies. This is called the nuclear Zeeman effect. In the thermal equilibrium the different states are occupied according to the Boltzmann distribution. By adding energy to the system in the form of radio waves, all spin states of different energy become occupied equally. This energy has to match the energy difference of the states in order to gain resonance, and it is the resonance frequency that is characteristic for the kind of nucleus and for the chemical environment of it.

The stronger the magnetic field is, the bigger is the difference between the energy levels of the states of different spin. The following equation illustrates this dependency. γ is the magnetogyric factor. This is

a constant value and characteristic for the nucleus type and controls the size in energetic splitting for the spin states. B_0 is the applied, homogeneous and static magnetic field at the measured nucleus:

$$h\nu = \Delta E = \gamma \frac{h}{2\pi} \cdot B_0$$

As it is technically easier to control a variation of the magnetic field at a constant frequency than control the variation of the frequency at a constant magnetic field, this is how the experiment is done.

The NMR spectrum is plotted as the absorption at the 'chemical shift' δ or 'parts per million' ppm. The reference is TMS and δ of TMS is zero.

$$\delta = \frac{\nu_{\text{substance}} - \nu_{\text{reference}}}{\nu_{\text{reference}}} \cdot 10^6$$

After an absorption, the system needs time to relax back to the Boltzmann distribution. This is called the relaxation time T , and it consists of T_1 and T_2 . T_1 is called the longitudinal relaxation time as it affects the relaxation in the direction of the field. It is dependent on the spin-lattice coupling in a system, and it is for example affected by paramagnetism. T_2 is called the transverse relaxation time, as it affects the relaxation in the direction perpendicular to the field, and it depends on spin-spin coupling. It is influenced, for example, by the viscosity of the measured solution.

In the beginning of the NMR method only magnetic fields as high as 1.4 T and radiowaves of $\lambda=5\text{m}$ corresponding 60 MHz were used. Now ten times stronger magnets are in common use: 14T and 600 MHz. In δ the $\Delta\nu$ is divided by the frequency used for the measurement (e.g. 600 MHz), the δ values stay the same for measurements conducted on instruments with different magnetic fields and δ stays characteristic for the measured substance for all magnetic fields. There is another source of information than δ in the NMR-spectrum. It is the coupling constant J , measured in Hz. It has its origin in the dependency of the effect of spin states chosen by neighbouring nuclei. These spin states are either parallel or antiparallel to the applied magnetic field and thus add or lessen the local magnetic field at the measured nucleus. With e.g. one neighbour nucleus, both spin levels that the measured nucleus may adopt are split up and more transitions become possible. The magnitude of splitting in Hz between the resonance frequencies is characteristic of the nucleus type, and it is independent of the applied magnetic field. It is an advantage to use a strong magnetic field, because the energetic splitting of the spin states and the shifts in $\Delta\nu/\text{Hz}$ become larger, while the splitting J/Hz of the signal stays the same. As long as $\Delta\nu/J > 10$, the spectrum is first order. Otherwise it becomes of higher order, and that is hard to interpret. With stronger magnets, signals close to each other, that would give spectra of higher order with weak magnets, give spectra of first order.^{97,105} (In general is a spectrum first order, when two magnetically equivalent nuclei A and X with spin I_A and I_X in a spin system of n A nuclei and m X nuclei (A_nX_m), are in such different chemical environment, that the absolute value of the difference in chemical shifts is at least 10 times bigger than the splitting of either. When this is the case, the multiplicity of a signal (the number of lines one signal is split into) for A is $(m \cdot 2 \cdot I_X + 1)$ and for X is $(n \cdot 2 \cdot I_A + 1)$. The average in chemical shift of split signals is where the non-split signal would be and the intensity of the split signals follow strict rules.) For the ^1H nuclei measured of the copper, cobalt and nickel complexes in this chapter, $I_H = \frac{1}{2}$, and the multiplicity of each signal would in a first order spectrum be the number of neighbour ($^1\text{H} + 1$), and the relative intensities of split signals follow the Pascal triangle.

Diamagnetic compounds are repelled by a magnetic field, and paramagnetic compounds are drawn into the magnetic field to where the flux is strongest. Diamagnetism is effected by paired electrons in a compound, and paramagnetism by unpaired electrons. Although the complexes discussed here have more paired than unpaired electrons, they are overall paramagnetic, as the paramagnetic contribution to the magnetic properties of a compound is much stronger than all the diamagnetic contributions by the paired electrons. Paramagnetic substances give very different NMR spectra than pure diamagnetic substances, because for instance they cause bigger spin-orbit coupling for the activated proton nucleus close to the paramagnetic metal centre, and this decreases the relaxation time T_1 . The result for the measurement is a line broadening that limits the possibility for interpretations of the spectrum as it overrules the splitting.

As the relaxation becomes faster, the lifetime τ_m/s and relaxation rate $\frac{1}{\tau_m}$ of the excited state grows smaller. The Heisenberg uncertainty principle says that either the energy E/J or the time can be certain, but not both with accuracy at the same time.

$$\delta E \cdot \tau_m \geq \hbar$$

While the uncertainty about the time grows smaller, the uncertainty about the measured energy (frequency) grows bigger. In the experiment, this is observed as broader signals. Possible coupling is not resolved, and thus the information in these spectra become poorer.

The broadest signals are those that are shifted furthest to low field (higher ppm). These belong to the nuclei closest to, and most affected by the paramagnetic ion. Because the signals become so broad, integration does not give the correct number of protons, and it is only possible to count the number of resolved signals.

Another effect of a paramagnetic environment on the measured nuclei, is the bigger range of chemical shifts. It is caused by a large variation of the actual magnetic field B_{eff} experienced by the measured nuclei. In this work, the largest effect is seen in the $^1\text{H-NMR}$ spectra of 'octahedral' high spin d^7 Co(II) found in the dinuclear complexes of qnpy-type ligands, with chemical shifts of 0-270ppm, see page 97. But it is also apparent in seven coordinate Co(II) mononuclear complexes of the same ligands with chemical shifts of 0-140ppm, see page 93. Octahedral d^8 Ni(II) found in the dinuclear complexes of qnpy-type ligands, still give chemical shifts from 0-80ppm, see page 117, and to a certain extent also the proton signals of the ligands coordinated to Cu(II) d^9 . They are shifted 0-25ppm, see page 51.

4.2 Copper complexes

4.2.1 Synthesis

General The general approach of Whall was followed,⁵¹ see Figure 4.1: An equimolar amount of the qnpy-type ligand (qp, mp, pp) and copper(II) acetate monohydrate were suspended in methanol. First a blue solution over a beige precipitate formed, which was methanolic copper(II) acetate and undissolved ligand. By sonicating and heating the mixture, the complex formed in solution. With qp and mp, first the solution was green. This suggests all copper ions to be in oxidation state II.³⁵ After standing, both solutions turned brown. With pp a brown solution was obtained directly. The brown colour is typical for mixed oxidation state (Cu(II)Cu(I) species and of Cu(I) complexes,³⁵ see also the UV-Vis spectra on page 83. For the linked ligands (qcq, mcm and pcp), a two to one ratio of metal to ligand was used. All three complex solutions gave green colours first and turned brown upon standing. To all six brown complex solutions, an excess of ammonium hexafluorophosphate in methanol was added, and a precipitate formed instantly. It was green for qp, pp and pcp, brown for mp, and somewhere in between for mcm and pcp. When the precipitates were separated and dried *in vacuo*, they all turned into brown powders.

Differences and crucial points The yields varied from 31% to 74%: qp 31%, mp 34%, mcm 54%, qcq 60%, pp 74%, pcp 74%. Different amounts of solvent were used, so these percentages are not entirely reliable, but the best yields were obtained with the complexes of which the ligands (pp and pcp) do not bear any group that enhances solubility. We know that the green colour in the complex comes from the complexed Cu(II) ion. We also know that the brown colour comes from the complexed Cu(I) ion, and that the brown colour will override the green as overall colour seen by the eye, as the eye makes brown from red + green. So when e.g. half the compound is the mixed oxidation state (Cu(II)Cu(I))

and half in the oxidised state (2Cu(II)), the green Cu(II) cannot be seen anymore. As the metal salt used as starting material contains only Cu(II), obviously, the redox process of at least one copper ion in the dinuclear complex, that is formed, is at a potential accessible when standing under air.

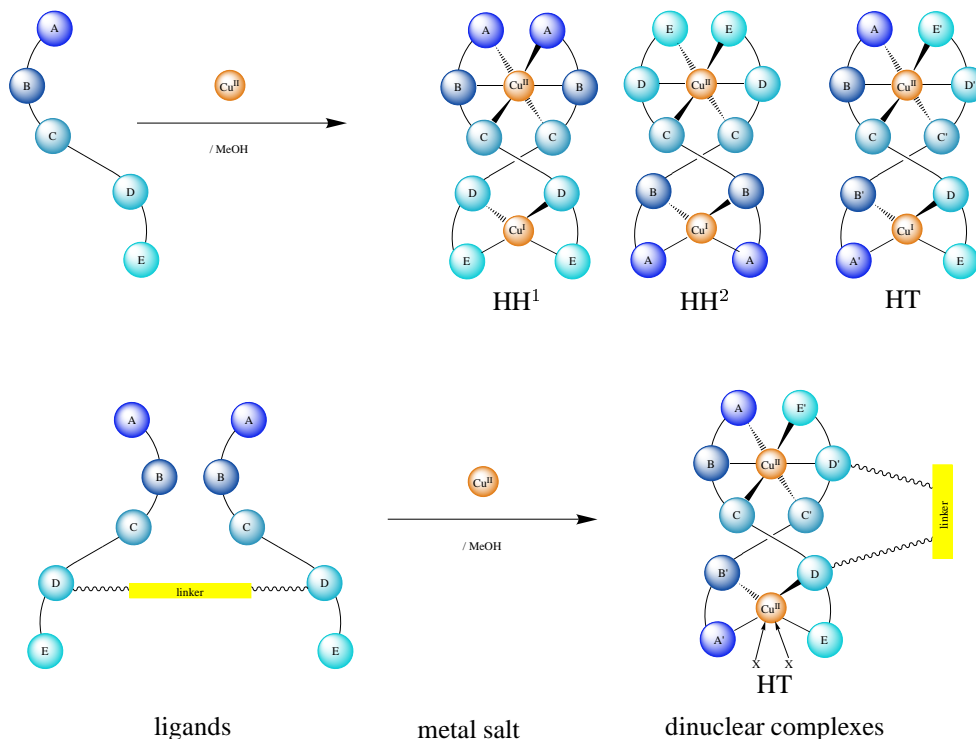


Figure 4.1: Formation of dinuclear complexes with an unsymmetrical qnpy derivative and with an unsymmetrically linked qnpy derivative. With the former, two head-to-head (HH) and one head-to-tail (HT) isomer are possible. With the latter, probably only the HT isomer exists. Other possibilities for oxidation states exist (Cu(II)/(II) for complexes of non-linked and Cu(II)/(I) for complexes of linked ligands), but have not been characterised in this work.

Characterisation

Micro analysis Whall⁵¹ has reported and fully characterised a complex of qp, formulated as $[\text{Cu}_2(\text{qp})_2][\text{PF}_6]_4$. The microanalysis for this compound is also compatible with the mixed oxidation state formula $[\text{Cu}_2(\text{qp})_2][\text{PF}_6]_3 \cdot 7\text{H}_2\text{O}$. The complex of mp fitted a formula $[\text{Cu}_2(\text{mp})_2][\text{PF}_6]_3 \cdot 6\text{H}_2\text{O}$, and the complex of pp also fitted a formula with 6 water molecules per complex $[\text{Cu}_2(\text{pp})_2][\text{PF}_6]_3 \cdot 6\text{H}_2\text{O}$. The complex of qcq fitted a formula that suggests that some of the complex contains two Cu(II) centres so it needed 3.3 PF_6^- counter ions instead of three. The complex of mcm fitted a formula with two Cu(II), as it had 4 PF_6^- counter ions. The sample was brown, and the colour may come from a minor amount of Cu(II)Cu(I) compound in the sample. The complex of pcp contained more of the complex with two Cu(II) than mixed oxidation state Cu(II)Cu(I), because the sample fitted a formula with 3.7 PF_6^- counter ions. The second Cu(II) centre may complete its coordination sphere with two water molecules. Only the non-linked ligands formed pure Cu(II)Cu(I) mixed oxidation state complexes.

Mass spectrometry MalDI-TOF, and in the case of $[\text{Cu}_2(\text{mp})_2][\text{PF}_6]_3$ electrospray MS, suggested a 2 : 2 composition of metal ion : ligand for the complexes of non-linked ligands and a ratio of 2 : 1 for the complexes with linked ligands. For the complex with qp this composition was supported by the mass

signal fitting $(M-2PF_6+K)^+$. For the complex of mp, it was $(M+3PF_6)^{3+}/3$, and for the complex with pp, it was $(M-3PF_6)^+$. Mass spectrometry for the qcq complex gave $(M-2PF_6)^+$ and $(M-3PF_6)^+$, the mcm complex gave $(M-2PF_6)^+$ and $(M-3PF_6)$ and the pcp complex gave $(M-2PF_6)^+$ and $(M-3PF_6)^+$. For all samples, mass spectrometry supported the proposal that the complexes are all dinuclear.

Infrared spectroscopy The infrared spectra of the copper complexes of mp and pp show the OH group at 2641 and 3518 cm^{-1} , and the complex of qp at 3634 and 3510 cm^{-1} . All three show absorptions assigned to the aromatic C—H stretch at 3091 cm^{-1} and the qp complex has additional aliphatic C—H stretch at 2962 cm^{-1} . They all show strong absorptions at 1596 or 1589 cm^{-1} for aromatic C—C and aromatic C—N. Then there are two signals at 1242 cm^{-1} and 1180 cm^{-1} for all three of them, which is typical for C—O stretch vibrations of e.g. aromatic C—OH. The most prominent absorption arises from the counterion PF_6^- at 818 cm^{-1} . An absorption due to $\nu(Cu—N)$ would be expected in the far infrared region $\approx 300 - 200cm^{-1}$ for copper(II) and $\approx 200 - 100cm^{-1}$ for copper(I).¹⁰⁶⁻¹⁰⁸

The infrared spectra of the copper complexes of pcp, mcm and qcq differ from the complexes of non-linked ligands by the hexaethylene glycol chain, that shows an absorption assigned to the C—H stretch at 2870 cm^{-1} . The C—O stretch are still show as two signals, but less pronounced, with absorptions at 1242 and 1188 cm^{-1} .

¹H-NMR spectroscopy The ¹H-NMR spectrum of $[Cu_2(mp)_2][PF_6]_3$ in deuterated acetonitrile is presented in Figure 4.2, and the part of the spectra with the most pyridine and the phenyl signals of $[Cu_2(pp)_2][PF_6]_3$, $[Cu_2(mp)_2][PF_6]_3$ and $[Cu_2(qp)_2][PF_6]_3$ is given in Figure 4.3. In the region of 6-7ppm there are two doublets for the pp and qp complexes and in the mp complex these doublets are much closer together. They are also those signals, together with the substituents CH_3O- and *tert*-butyl, that are least shifted. It is therefore assumed, that these are phenyl signals.

When integrating the spectrum of $[Cu_2(mp)_2][PF_6]_3$, the CH_3O- signals were set to 6H. The phenyl signals at 6.45ppm are not significantly broadened, and the integral of 8H suggests them only to be the phenyl protons in the meta positions (compare with the spectrum of the free ligand). Thus in the rest of the spectrum, which is shifted considerably low field, 38 protons should be found. Unfortunately the multiplets around 7.8 and 9.1ppm, together with the broad signals at 13, 17 and 25ppm, of which the signals at 13 and 17 are barely visible, the integral only adds up to 14H. The explanation for this must be the extreme broadening of some signals, which make them poorly resolved. The CH_3O signals show two distinct chemical shifts.

There can be various explanations for this. The crystal structure (compare with the crystallographic section starting on page 55) shows that in the solid, there are two distinct environments for the CH_3O , due to different oxidation state of the copper ion (I or II), that the pyridine ring, bearing the substituted phenyl, coordinates to, and because the methoxyphenyl may sit on a “Cu(bipy)₂” or a “Cu(terpy)₂” unit of the qnpy ligand. Both effects lead to a total of four environments for the CH_3O protons. As there are only two signals distinguishable in the spectrum, either not all possible arrangements are adopted in solution, or two possibilities give the same chemical shift. But the NMR method is for monitoring solution structures, and they may be different in solid. It is possible that there is one main structure in solution, but there may be several. Also fluctuations within the double helicate would be plausible, and there is no evidence for the absence of other types of structures like e.g. mononuclear ones. The fluctuation theory is not supported by the crystal structure. At least in solid, the difference in distance from the middle pyridine rings to the two copper ions are the same for both the $[Cu_2(mp)_2]^{3+}$ (0.7 and 0.9Å) and $[Cu_2pcp]^{3+}$ (0.7-0.9Å).

All the ¹H-NMR spectra of the six copper complexes are similar to each other. Two main differences are seen between the spectra of the complexes with non-linked ligands qp, mp and pp, and the spectra of the complexes with linked ligands qcq, mcm and pcp. The signals in the former rare split into doublets, where they are only singlets in the latter. Additionally signals for the linker protons are of course only seen in the linked species (at 4.1 – 3.5ppm). The spectra of the mp- and mcm-complex are also different from the other. Signals at 7.0 and 6.4ppm, probably originating from the phenyl substituents, have merged for the mp- to a dd at 6.5ppm, and for the mcm-complex to a broad signal also at 6.5ppm.

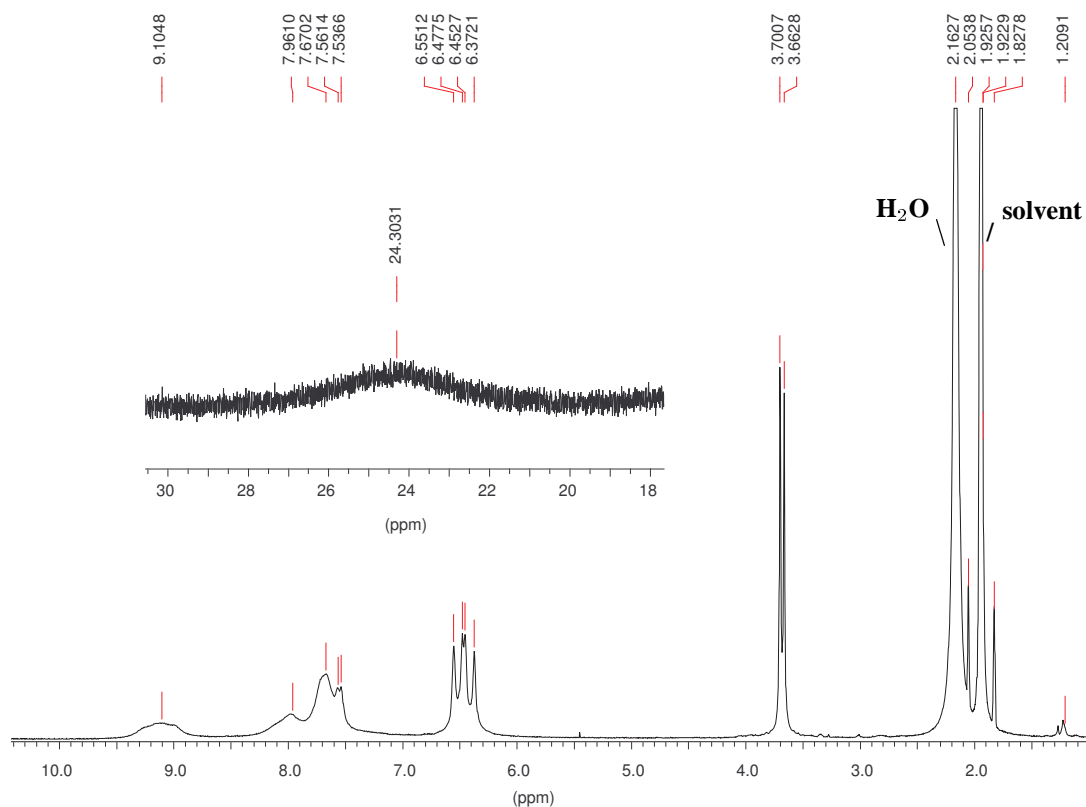


Figure 4.2: 600 MHz ^1H -NMR spectrum of $[\text{Cu}_2(\text{mp})_2][\text{PF}_6]_3$ acetonitrile- d_3 solution.

The most interesting part of the $[\text{Cu}_2(\text{pp})_2][\text{PF}_6]_3$ spectrum is plotted topmost in Figure 4.3. If the doublets at 6.3 and 6.9 ppm are indeed the meta phenyl protons (bm and dm) (compare with the chemical shifts of the free ligand listed in Table 2.10 on page 31 and Figure 2.3 or 7.16 for labelling), they may be set to 8H. The protons remaining are the 30 pyridine, 8 ortho-phenyl (bo and do) and 2 para phenyl protons (bp). Instead of 40, the multiplets around 8 and 9 ppm together with the broad signals at 10.5, 13, 17 and 25 ppm add only up to 19H, which is almost half of what is needed. Again this may be explained by such a strong broadening of some signals, that they are not detectable any more.

The most interesting part of the $[\text{Cu}_2(\text{qp})_2][\text{PF}_6]_3$ spectrum is plotted in the bottom of Figure 4.3. Again it is assumed that the signals at 7.0 and 6.4 ppm are the meta phenyl signals (because of the comparison with the spectra of the copper(II) complexes with pp and mp, and because the chemical shifts are so similar to the ones in the spectra of the free ligand). The integrals are therefore set to 8H for the two of them together. The integral over the *t*-Bu protons at 1.2 ppm is 17H (\approx 18H) and therefore fits well. Again the residual peaks add only up to 13H instead of the required 38H, and the explanation that can be offered is still a strong broadening of most pyridine proton signals.

The spectra of the copper(II) complexes of the linked ligands pcp, mcm and qcq, where recorded and processed under the same conditions and using the same parameters as the spectra of the copper(II) complexes of qnpq ligands discussed above. The signals of the complexes with linked ligands are all broader than the signals above. The most interesting part of the spectra are plotted in Figure 4.4. Apart from this, what is different to Figure 4.3, are the signals of the proton from the linking hexaethylene glycol around 3.6 ppm. Assuming again that the signal at 6.5 and 7.0 ppm for $[\text{Cu}_2\text{pcp}]^{3+}$ and $[\text{Cu}_2\text{qcq}]^{3+}$, and at 6.5 ppm for $[\text{Cu}_2\text{mcm}]^{3+}$, are the meta phenyl protons, gives 24-25H for the linker protons with the pcp and qcq complex and 34H, which is pretty close to the expected 30H for the linker protons plus the methoxy protons in the mcm complex. For the *tert*-butyl group the integral is far too big, 27H instead of 18H. The electronic effects of the methoxy group and the *tert*-butyl group are different (the

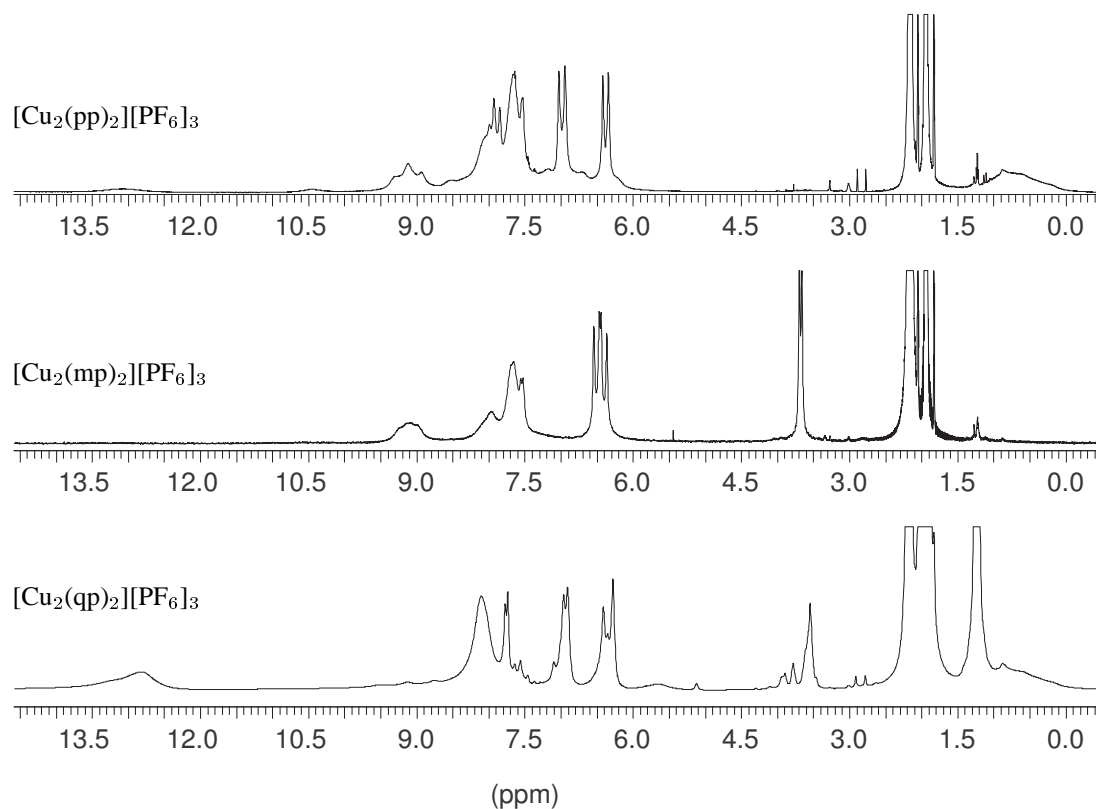


Figure 4.3: A cut of the 600 MHz $^1\text{H-NMR}$ spectra of $[\text{Cu}_2(\text{pp})_2][\text{PF}_6]_3$, $[\text{Cu}_2(\text{mp})_2][\text{PF}_6]_3$ and $[\text{Cu}_2(\text{qp})_2][\text{PF}_6]_3$ acetonitrile- d_3 solution.

not *tert*-butyl acting only inductive), and possibly this is why the integral exceeds the expected integral value even more than the methoxy protons did. The pyridine and ortho-phenyl protons in the mcm and qcq complexes give only values of 11-12H instead of the required 38, and in the pcp complex the integral over the pyridine, ortho- and para-phenyl signals give 18H instead of the required 40. (In this last example, the integral was set over the whole area from 7.5ppm down field to 33 ppm. This is why the integral points to 18H rather than the lower values of 10-15H found when the integrals were only set over the visible signals.) It confirms the theory, that more protons are present, but give too broad signals for being detected as such.

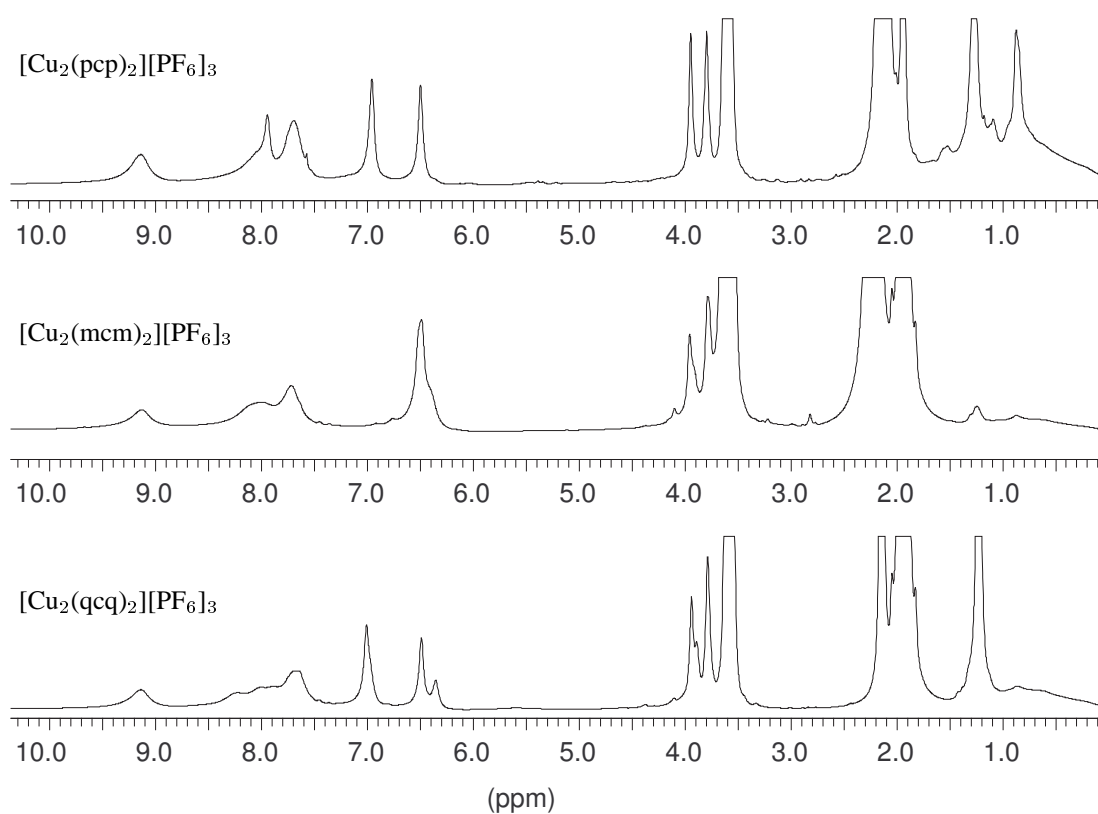


Figure 4.4: A cut of the 600 MHz $^1\text{H-NMR}$ spectra of $[\text{Cu}_2\text{pcp}][\text{PF}_6]_3$, $[\text{Cu}_2\text{mcm}][\text{PF}_6]_3$ and $[\text{Cu}_2\text{qcq}][\text{PF}_6]_3$ acetonitrile- d_3 solution.

4.2.2 Crystallographic analysis

Crystals were obtained of quality that allowed an X-ray diffraction study. Studies of the mixed oxidation state helical complexes of copper(II/I) with two strands of mp and pcp respectively, were made using crystals obtained by slow diffusion of diethyl ether vapour into solutions of the complex in acetone.

$[\text{Cu}_2(\text{mp})_2][\text{PF}_6]_3$ was obtained as small brown crystals by diffusion of diethyl ether vapour into an acetone solution of the complex. The crystal structure was solved in the triclinic space group $P\bar{1}$ with two enantiomeric complex cations per unit cell: $\text{C}_{76}\text{H}_{54}\text{N}_{10}\text{O}_4\text{Cu}_2\text{P}_3\text{F}_{18} \cdot 1.5 \text{C}_3\text{H}_6\text{O}$, $M=1820.43$, see also appendix A on page 175.

$[\text{Cu}_2\text{pcp}][\text{PF}_6]_3$ was also obtained as small brown crystals by diffusion of diethyl ether vapour into an acetone solution of the complex. The crystal structure was solved in the triclinic space group $P\bar{1}$ with two enantiomeric complex cations (see Figure 1.12) per unit cell: $\text{C}_{86}\text{H}_{72}\text{N}_{10}\text{O}_7\text{Cu}_2\text{P}_3\text{F}_{18} \cdot 2.5 \text{C}_3\text{H}_6\text{O}$, $M=2064.76$, see also appendix A on page 186.

General description of the complex cation structures Two views of the complex cation of $[\text{Cu}_2(\text{mp})_2][\text{PF}_6]_3$ are given in Figures 4.5 and 4.6, and of the cation of $[\text{Cu}_2\text{pcp}][\text{PF}_6]_3$ in Figures 4.7 and 4.8. In both cases the crystal structure shows a 2 : 2 system with two metal ions and two ligand strands forming a dinuclear complex, as already indicated by mass spectrometry (see pages 143 and 150). The sideways views in Figures 4.5 and 4.7 show best that one copper centre is coordinated by six, and the other with four nitrogen donor atoms. As the ligand and the lattice-acetone are neutral, counting the counter ions PF_6^- , gives the charge of the of the two complex cations. As the overall charge is three, the copper ions are of different oxidation states. The preferred coordination number of Cu^{II} with these kind of oligopyridine ligands is six, and that of Cu^{I} is four, so the oxidation states are assigned in these complexes accordingly.

The quinquepyridine ligand strands are separated into a “terpy” and a “bipy” domain, by the coordination behaviour. Three nitrogen atoms from one end of the strand coordinate to the copper(II) ion, and the remaining two coordinate to the copper(I). This is shown in Figures 4.9 and 4.10 for the complexed mp ligands and in Figures 4.11 and 4.12 for the complexed pcp ligands.

Between each of the planes formed by a pyridine ring, there is a torsion angle. The planes turn in the same direction throughout the ligand strand, thus forming a helix. In the complex cation, both ligand strands twist in the same direction. Two twisted ligand strands form a double helix. With the metal ion holding the ligand strands together, this is a metallo-supramolecular assembly and is called a double helicate.⁵⁴ The helical axis is defined by the metal ions. As there are two possible directions for this twist in the ligand strands, and two enantiomers are possible. The Δ , P or right handed helicate forms, when both ligand strands turn right when looked at along the axis and progressing from the near to the far end. The Λ , M or left handed helicate forms, when both ligand strands turn left when looked at along the axis progressing from the near to the far end, see Figure 1.12 on page 13. In the crystal structures, both forms are present in a 1 : 1 ratio.

As the two ligand strands are unsymmetrical, more isomeric structures are possible (see Figure 1.9 on page 11, and also Kulke³⁰ and Whall⁵¹). The labelling of the pyridine rings of the ligands displayed in Figures 2.3 and 3.3 on pages 24 and 35 is maintained during the discussion of the crystallographic analysis, but as these homoleptic complex cations contain two ligand strands, I will distinguish between them, using the ‘prime’ sign, and so the ligand strands are called ‘ligand strand’ and ‘ligand strand’’. In both crystal structures, the complex cations consist of head-to-tail arranged ligand strands. Randomly, the pyridine rings coordinating in an octahedral fashion were named A, B and C of ligand strand, and C’, D’ and E’ of ligand strand’. (I could just as well have picked A’, B’ and C’ of ligand strand’ and C, D and E of ligand strand.) One ligand strand thus coordinates with a “terpy”-unit with Ring B carrying substituent b, while the other ligand strand coordinates with a “terpy” unit Ring D carrying substituent d, on the same copper(II) ion.

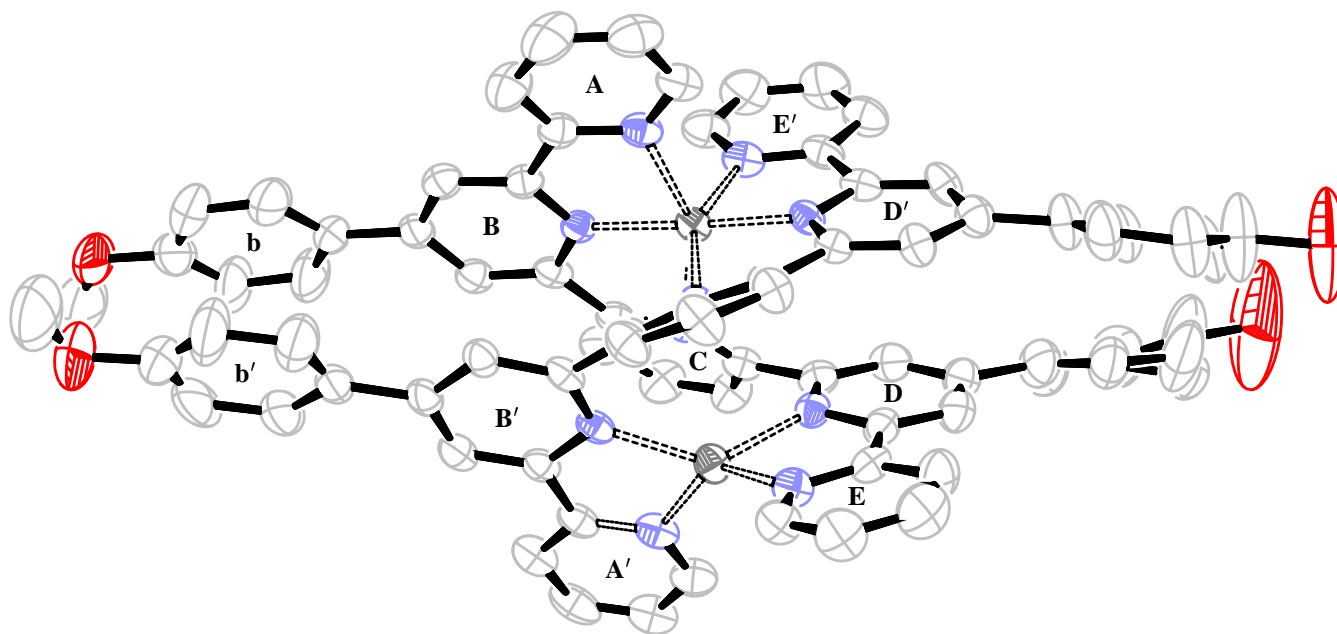


Figure 4.5: Crystal structure of the cation in $[\text{Cu}_2(\text{mp})_2][\text{PF}_6]_3 \cdot 1.5 \text{ acetone}$: sideways view. Atom numbering is given in Figures 4.9 and 4.10.

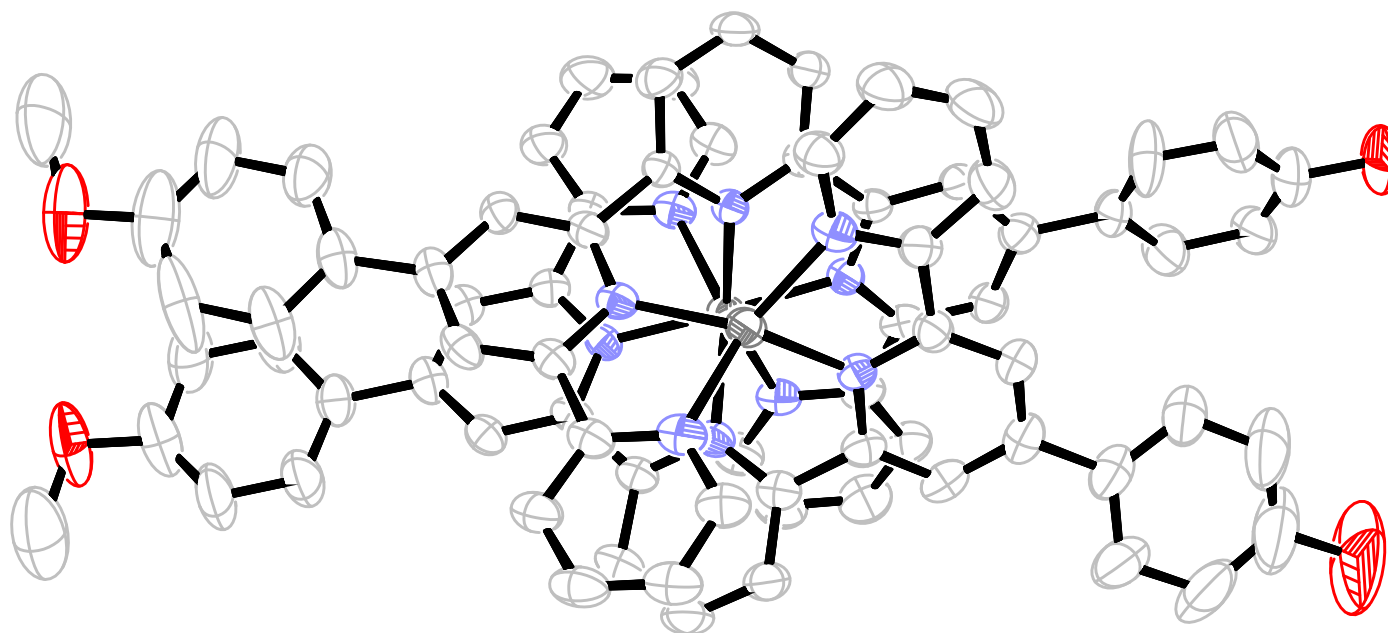


Figure 4.6: Crystal structure of the cation in $[\text{Cu}_2(\text{mp})_2][\text{PF}_6]_3 \cdot 1.5$ acetone: view along the Cu-Cu axis. Atom numbering is given in Figures 4.9 and 4.10.

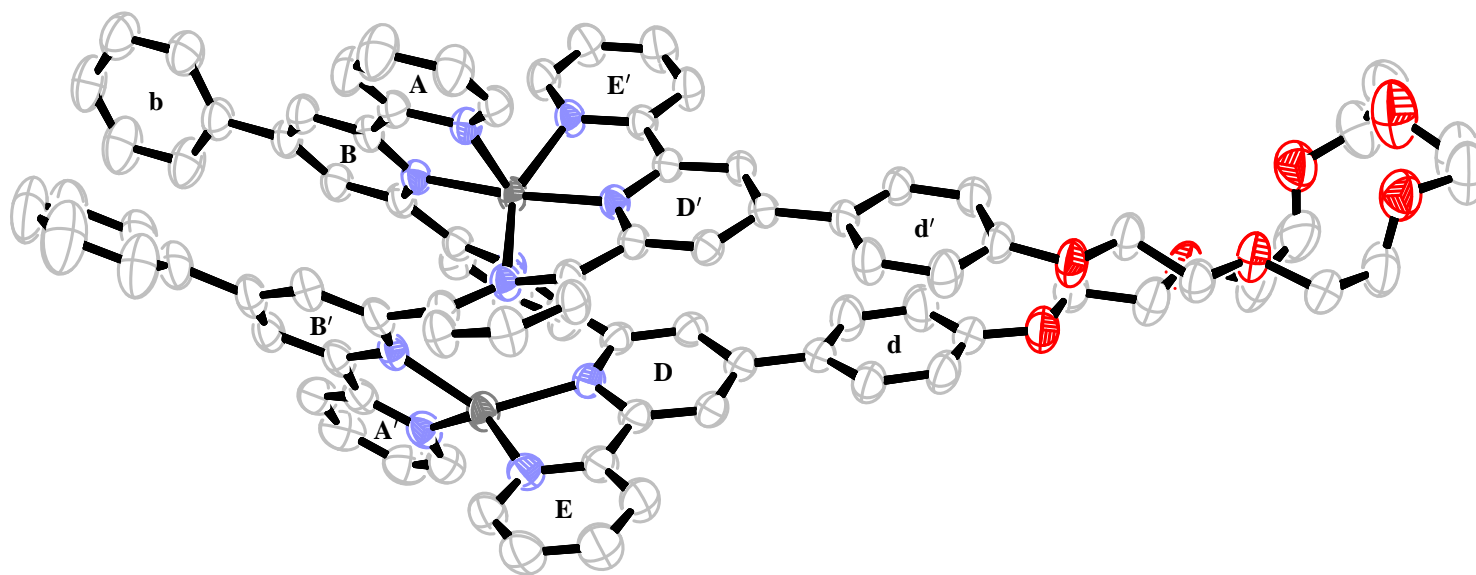


Figure 4.7: Crystal structure of the cation in $[\text{Cu}_2\text{pcp}][\text{PF}_6]_3 \cdot 2.5 \text{ acetone}$: sideways view. Atom numbering is given in Figures 4.11 and 4.12.

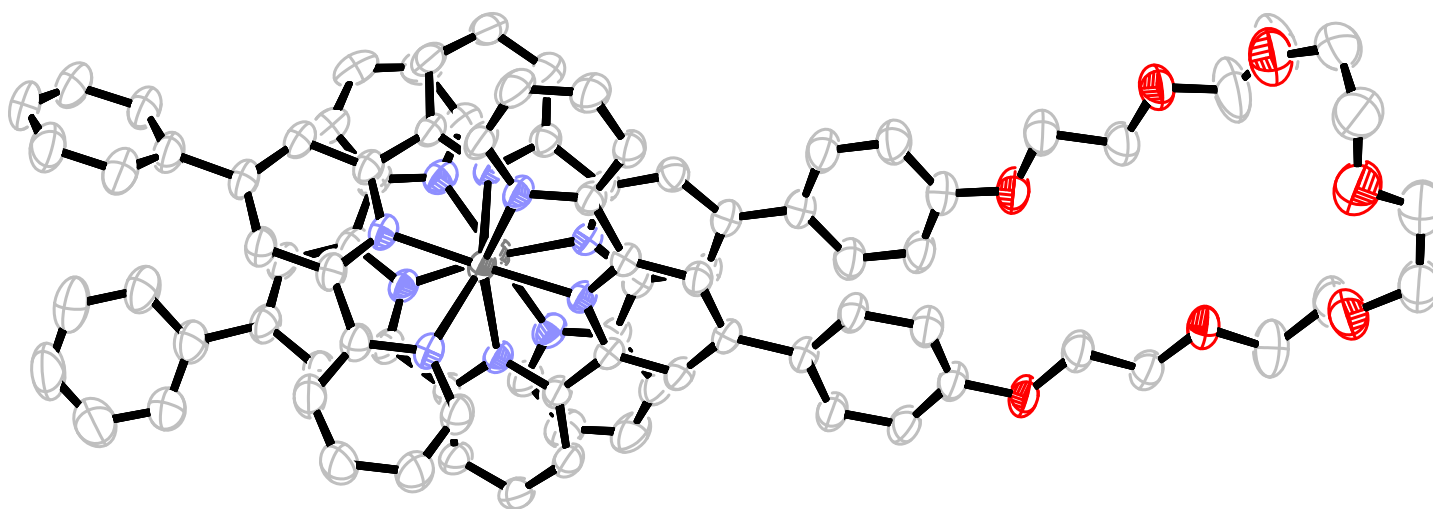


Figure 4.8: Crystal structure of the cation in $[\text{Cu}_2\text{pcp}][\text{PF}_6]_3 \cdot 2.5$ acetone: view along the Cu-Cu axis. Atom numbering is given in Figures 4.11 and 4.12.

Ligand geometry

Ligand conformation in the complex: The ligand strands in the complex cations form a double helicate and this is evident in the twist of each separate ligand strand. The torsion angles between each pyridine ring, progressing through the ligand strands, turn in the same direction. The biggest torsion angle in both ligand strands in both complex cations occur between the second and third ring. For $[\text{Cu}_2(\text{mp})_2]^{3+}$ it is 48.9° and 53.4° respectively for each ligand strand and for $[\text{Cu}_2\text{pcp}]^{3+}$ it is 57.2° and 51.7° . This main twist divides the quinquepyridine ligand strand, like the coordination behaviour, into a “terpy” and a “bipy” unit. There is also a substantial torsion between the third and the fourth ring, $18.6^\circ/23.9^\circ$ in $[\text{Cu}_2(\text{mp})_2]^{3+}$, and $13.0^\circ/19.6^\circ$ in $[\text{Cu}_2\text{pcp}]^{3+}$ (see Table 4.1). The torsion angles in the two ligand strands forming one complex cation are not equivalent, but the torsion angles of C5-C6, C10-C11, C15-C16, C20-C21 in ligand strand, and C105-C106, C110-C111, C115-C116, C120-C121 and C60-C61, C65-C66, C70-C71, C75-C76 respectively in ligand strand', add up to control the pitch of the double helix (see Figures 4.9 to 4.12. In $[\text{Cu}_2(\text{mp})_2]^{3+}$, the torsion angles inside one ligand strand are distributed more evenly than in the other. This other ligand strand' has a more pronounced planar “bipy”- and (close to) planar “terpy”-unit with a bigger twist between these units, and a bigger overall twist. The same difference between the ligand strands can also be seen in $[\text{Cu}_2\text{pcp}]^{3+}$, with a planar “bipy” and “terpy” unit and a bigger dihedral angle between the units in one ligand strand than in the other ligand strand'. Both species are head to tail complexes, so ring B of one ligand strand coordinates trans to ring D' of the other ligand strand' (to the same octahedral copper centre). Ring B' of the ligand strand' is coordinated to the tetrahedral copper centre along with ring D of the other ligand strand.

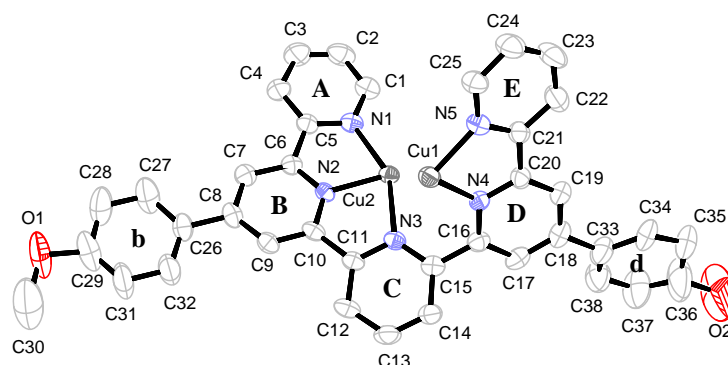


Figure 4.9: Crystal structure: one coordinated ligand strand of $[\text{Cu}_2\text{mp}_2][\text{PF}_6]_3$, emphasizing the terpy and bipy domains.

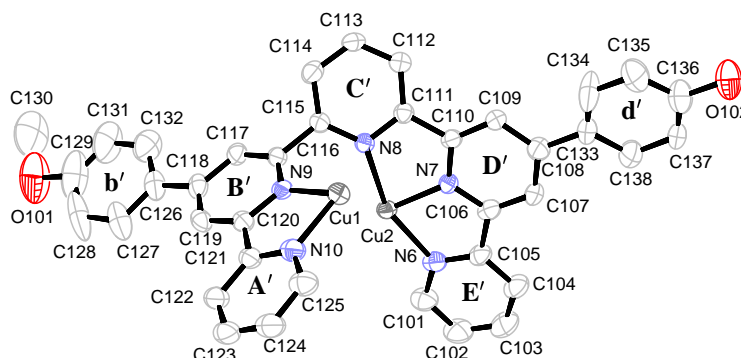


Figure 4.10: Crystal structure: one coordinated ligand strand' of $[\text{Cu}_2\text{mp}_2][\text{PF}_6]_3$, emphasizing the terpy and bipy domains.

[Cu ₂ (mp) ₂][PF ₆] ₃				[Cu ₂ pcp][PF ₆] ₃			
rings	ligand: torsion/degree	ligand': torsion/degree	rings	ring	ligand: torsion/degree	ligand': torsion/degree	rings
A–B	9.0	5.75	E'–D'	A–B	9.6	7.4	E'–D'
B–C	18.6	23.8	D'–C'	B–C	13.0	19.6	D'–C'
C–D	48.9	53.4	C'–B'	C–D	57.2	51.7	C'–B'
D–E	10.1	6.3	B'–A'	D–E	6.85	12.4	B'–A'
sum	86.5	89.2	sum'	sum	86.5	91.1	sum'
Cu–Cu–distance	3.944				4.002		Cu–Cu–distance

Table 4.1: Torsion angles of the ligand strands in [Cu₂mp₂][PF₆]₃ · 1.5 acetone and [Cu₂pcp][PF₆]₃ · 2.5 acetone. Esd values for angles in both structures were given invariable as (3) for the first space after comma. Depending on the torsion angle, the esd for it will vary up to (6). This means that the overall torsion angles of the ligands strands in [Cu₂(mp)₂]³⁺ may be identical, but the ligand strands in [Cu₂pcp]³⁺ are not.

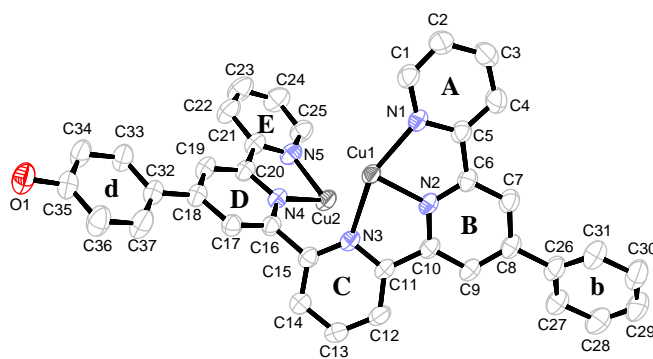


Figure 4.11: Crystal structure: one coordinated ligand strand of $[\text{Cu}_2\text{pcp}][\text{PF}_6]_3$, emphasizing the terpy and bipy domains.

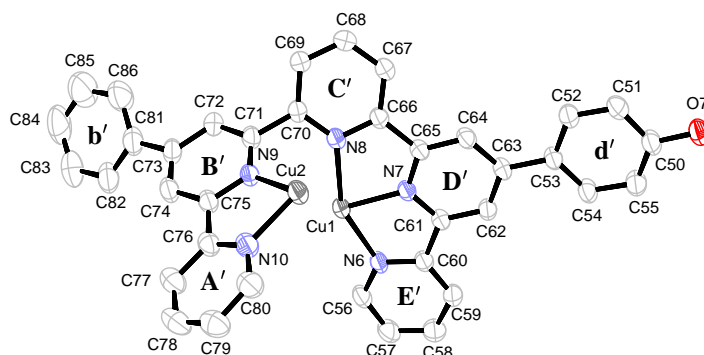


Figure 4.12: Crystal structure: one coordinated ligand strand' of $[\text{Cu}_2\text{pcp}][\text{PF}_6]_3$, emphasizing the terpy and bipy domains.

Bond lengths and angles within the ligand strands In $[\text{Cu}_2(\text{mp})_2]^{3+}$, the bond distances connecting adjacent pyridine rings like C5-C6, C10-C11 etc. are all about identical, depending on the quality of the crystal, bond lengths vary between a minimum of 1.455Å and 1.509Å ($\Delta=0.054\text{\AA}$) when taking the esd into account. In $[\text{Cu}_2\text{pcp}]^{3+}$, these bonds vary between 1.460Å and 1.504Å ($\Delta=0.044\text{\AA}$), compare with Table 4.2.

In $[\text{Cu}_2(\text{mp})_2]^{3+}$, the C-C-N angles like N1-C5-C6 and C5-C6-N2 etc. are not all the same. They vary between 113.2(3)° and 117.9(3)°. The smallest angle is found in ligand strand' between the middle ring of the “terpy” unit leading to the terminal pyridine ring (113°). The biggest angle (118°) is found between the “terpy” and “bipy” unit, on the “terpy” side. All other C-C-N angles vary between 114(3)° and 117(3)°. In $[\text{Cu}_2\text{pcp}]^{3+}$, the C-C-N angles vary only between 114.2(3)° and 117.5(3)°. While all these angles are somewhere between 114(2)° and 115.6(3)°, one of the angles between the “terpy” and the “bipy” unit is slightly bigger (117.5(3)°) see Table 4.3.

Dividing the structures into a $\text{Cu}(\text{“terpy”})_2$ and a $\text{Cu}(\text{“bipy”})_2$ unit, comparison with complexes of terpy-type ligands becomes possible. The interannular bond lengths in the $\text{Cu}(\text{“terpy”})_2$ -unit of $\text{Cu}_2(\text{mp})_2^{3+}$ is an average of 1.480(3)Å and in $\text{Cu}_2\text{pcp}^{3+}$ it is in average 1.482(3)Å see Table 4.2. This is very similar to the copper(II) complexes of 4'-(2,2-biphen-4-yl)-2,2':6',2''-terpyridine¹⁰⁹ (1.488Å) and 4'-(3,4-dimethoxyphenyl)-terpyridine (1.489Å).¹¹⁰ In the free terpy ligand the interannular bonds are 1.490Å, but they are 1.445Å in $\text{Cu}(\text{terpy})_2^{2+}$! Concluding from the difference between terpy type complexes, the phenyl substituents at the 4'-position cause an elongated interannular bond in the coordinated ligand on Cu(II). This effect is preserved in both $[\text{Cu}_2(\text{mp})_2]^{3+}$ and $[\text{Cu}_2\text{pcp}]^{3+}$.

	[Cu ₂ (mp ₂) ³⁺		[Cu ₂ pcp] ³⁺	
“terpy” unit	C5-C6	1.479(5)Å	C5-C6	1.475(5)Å
	C10-C11	1.484(5)Å	C10-C11	1.480(5)Å
	C105-C106	1.476(6)Å	C60-C61	1.483(5)Å
	C110-C111	1.482(5)Å	C65-C66	1.490(5)Å
average		1.480(3)Å±0.004Å		1.482(3)±0.006
between the units	C15-C16	1.473(6)Å	C15-C16	1.490(5)Å
	C115-C116	1.494(5)Å	C70-C71	1.492(4)Å
		1.484(4)Å±0.015Å		1.491(3)±0.001Å
“bipy” unit	C20-C21	1.478(6)Å	C20-C21	1.486(5)Å
	C120-C121	1.482(6)Å	C75-C76	1.487(6)Å
		1.480(4)±0.003		1.487(4)±0.001

Table 4.2: Interannular bonds between the pyridine rings in the ligand strands of [Cu₂(mp₂)³⁺ and [Cu₂pcp]³⁺.

The C-C-N angles of the free terpy ligand are 116° and those for the Cu(II) complex are 115°. ¹¹¹ This decrease of the C-C-N angles is accompanied by an increase in the dihedral angles between the pyridine rings. ¹¹² The C-C-N average also 115° in the complexed 4'-(3,4-dimethoxyphenyl)-terpyridine ¹¹⁰ and 114° in the complexed 4'-(2,2-biphen-4-yl)-2,2':6',2''-terpyridine. ¹⁰⁹ The phenyl substituents seem not to have an effect on the C-C-N angles. In the Cu(“terpy”)₂ unit of both the new structures, these angles average 115°.

The Cu(“bipy”)₂ unit of the new complex cations, have an interannular bond of 1.480(4)Å for [Cu₂(mp₂)³⁺ and 1.487(4) for [Cu₂pcp]³⁺. But the interannular bond in plain bipy is 1.491Å, ¹¹³ while it is only 1.440Å in the Cu(I) complex. ¹¹⁴ No structures of 4-phenyl substituted bipy ligands could be found, so it is not possible to say anything about a possible substituent effect on the interannular bond length. But in the new structures these bonds stay long upon complexation of the ligands.

The C-C-N angles are 116° in the free ligand bipy and the angles do not change upon complexation with Cu(I). In the Cu(“bipy”)₂-unit of both the two new structures, the C-C-N angles average 115°. As with the interannular bonds, no crystal structures of complexed phenyl-substituted bipy is known, and thus it is not possible to know if the substituents play a role here, but judging from terpy, these 4-phenyl substituents do not affect C-C-N angles.

After having discussed the conditions inside the units, where “terpy”- and “bipy”-units are close to planar, the conditions between these units must also be considered. While the interannular bonds between the units are not so different from the other, they average: 1.489Å in Cu₂(mp₂)³⁺ and 1.481Å in Cu₂pcp³⁺, the C-C-N angles between the units average 116° in both complex cations. The extreme C-C-N angles in the complexed ligand strands are found at this place.

π-stacking inside the complex cations In [Cu₂(mp₂)³⁺, π-stacking distances occur between the co-planar rings B and B' at distances of 3.236-3.476Å and between rings D and D' at distances of 3.250-3.549Å. The slightly tilted rings C and A' with a distance of 3.141-3.953Å and rings E to C' with a distance of 2.900-3.623Å have also close enough contact. The other terminal pyridine ring to central pyridine ring interactions are at a bigger angle, and only the side of the nitrogen show close enough contact for some orbital overlap (see Figure 4.5). Ring b and b' are co-planar and have a distance between the planes of 3.426-3.494Å. The d and d' rings are disordered. While C33 and C36 of the ligand strand and C133 and C136 of the ligand strand' have full occupancy at the position shown in Figures 4.9 and 4.10, the other members of ring d and ring d' have only half occupancy. The closest distance found between these two rings is 2.759Å.

	$[\text{Cu}_2(\text{mp})_2]^{3+}$		$[\text{Cu}_2\text{pcp}]^{3+}$		
ligand strand	N1C5C6	114.5(3)	N1C5C6	114.6(3)	"terpy"
	C5C6N2	115.5(3)	C5C6N2	114.2(3)	
	N2C10C11	116.1(3)	N2C10C11	114.2(3)	
	C10C11N3	115.5(3)	C10C11N3	115.2(3)	
	N3C15C16	117.9(3)	N3C15C16	117.5(3)	"bipy"
	C15C16N4	115.2(3)	C15C16N4	115.0(3)	
	N4C20C21	114.1(3)	N4C20C21	114.7(3)	
	C20C21N5	116.4(3)	C20C21N5	115.3(3)	
ligand strand'	N6C105C106	114.7(3)	N6C60C61	115.1(3)	"terpy"
	C105C106N7	113.1(3)	C60C61N7	115.5(3)	
	N7C110C111	114.0(3)	N7C65C66	114.8(3)	
	C110C111N8	114.0(3)	C65C66N8	115.5(3)	
	N8C115C116	116.6(3)	N8C70C71	115.3(3)	"bipy"
	C115C116N9	113.2(3)	C70C71N9	114.9(3)	
	N9C120C121	114.5(3)	N9C75C76	114.6(3)	
	C120C121N10	114.8(3)	N75C76N10	115.6(3)	

Table 4.3: C-C-N angles in the cations $[\text{Cu}_2(\text{mp})_2]^{3+}$ and $[\text{Cu}_2\text{pcp}]^{3+}$.

In $[\text{Cu}_2\text{pcp}]^{3+}$, π -stacking distances occur between the co-planar rings B and B' at distances of 3.307-3.823Å and rings D and D' at distances of 3.196-3.514 Å, the slightly tilted rings C and A' with a distance of 3.232-3.841Å and rings E to C' at a distance of 3.072-3.835Å. The other terminal pyridine ring to central pyridine ring interactions are at a bigger angle, and only the side of the nitrogen show close enough contact (see Figure 4.7). The b and b' rings are at an angle of 65° to each other, the closest distance is 3.515Å. The d and d' rings are not distorted in this case. They are co-planar at a distance of 3.177 to 3.541Å (see table 4.4).

Hydrogen bonds Potential sites where hydrogen bonds may occur in the new structures is at the phenol group of the mp ligand in $[\text{Cu}_2\text{mp}_2][\text{PF}_6]_3 \cdot 1.5$ acetone. However, no hydrogen bond can be seen between the ligand strands inside the complex cation, nor between adjacent cations. The distance between the phenol-oxygen atoms inside one cation is 6.093Å. Curiously, the methoxy groups of the ligand strands, at the other side of the complex are closer together, the distance between the oxygen atoms is 4.198Å. The only hydrogen bond was found between the phenol group of ring d' and an acetone oxygen atom. In the crystal formed by $[\text{Cu}_2\text{pcp}][\text{PF}_6]_3 \cdot 2.5$ acetone there are no sites where hydrogen bonds could occur.

		[Cu ₂ mp ₂][PF ₆] ₃ · 1.5 acetone		[Cu ₂ pcp][PF ₆] ₃ · 2.5 acetone	
ring	ring'	distance /Å	angle between the rings	distance /Å	angle between the rings
A	C'	2.563-4.387	46°	2.243-4.168	49°
B	B'	3.236-3.476	5°	3.307-3.823	11°
C	A'	3.141-3.953	18°	3.232-3.841	11°
C	E'	2.341-4.443	59°	2.478-4.609	57°
D	D'	3.250-3.549	6°	3.196-3.514	7°
E	C'	2.900-3.623	17°	3.072-3.835	17°
b	b'	3.426-3.980	2°	3.515-5.969	65°
d	d'	disordered		3.177-3.541	8°

Table 4.4: π -stacking interaction distances in [Cu₂mp₂][PF₆]₃ · 1.5 acetone and [Cu₂pcp][PF₆]₃ · 2.5 acetone.

Coordination geometry

Head to head versus head to tail Since the two metal ions in these two complex cations are in different oxidation states, it could be expected, that they direct to a head-to-head complex, where pyridine rings with the same substituent prefer the same metal ion for coordination. Actually the head-to-tail complex is formed in both crystal structures. In the case of the linked ligand pcp, the linker would be strained in a head-to-head isomer, so this may explain why the head-to-tail complex is formed. Here the linker is relaxed and folds similarly to a hair-pin. It is however difficult to understand, why also the non-linked double helical complex of mp with copper(II/I) gives the head-to-tail complex. Possibly the packing in the crystal is more favorable for this complex isomer, while in solution both head-to-head and head-to-tail exist.

Metal induced distortion The Jahn-Teller distortion of copper(II) with six equivalent donor atoms would lead one to expect an elongated Cu(II) sphere, where the energy of $d_{x^2-y^2}$ is higher than d_{z^2} , (or more seldomly a squashed sphere, where the energy of d_{z^2} is higher than of $d_{x^2-y^2}$). In these two new structures, the donor atoms are not equal, nor can they distribute evenly around the metal, so the ligand already dictates a lower symmetry, and it becomes hard to tell to which degree the geometry preferences of the metal ion affect the actual symmetry adopted by the complex.

The preferred coordination geometry of copper(I), which has a full d-shell, with four equal donor atoms is tetrahedral for a maximum distance between the electron clouds from the donor atoms. No distortion of the tetrahedron is expected.

Ligand induced distortion The N_B -Cu and $N_{D'}$ -Cu bond lengths involving the middle pyridine rings in the “terpy”-subunits that coordinate octahedrally are the shortest bonds of all in both complex cations (see values for ‘B/D’ or D/B’ versus the values for ‘A/E’ or E/A’ and ‘C/C’ in Table 4.10). It would have to elongate the interannular bonds or the C-N bonds of the pyridine rings and reduce the C-C-N angles in order to give a 90° angle around the Cu(II). In the tetrahedron around Cu(I), a N-Cu-N angle of 109° would be the ideal geometry. Since this angle is bigger than the 90° in the octahedron, an even stronger deformation of the ligand would be necessary to oblige this geometry: A stronger elongation of the interannular bond and a more reduced C-C-N angle would then be expected. This is however not what happens, see page 62.

N_i -Cu- N_j bite angles The discussed interannular bonds, CCN angles, Cu-N bond lengths and torsion angles together with the C-N bond lengths in the ligand, culminate in the N-Cu-N bite angles. They are listed in Table 4.12. As copper is a heavier atom than carbon and nitrogen, the esd values of the angles are smaller. For $[\text{Cu}_2(\text{mp})_2]^{3+}$ they are (in the “Cu(terpy)₂” unit) $\angle N_{A/E'}\text{Cu}N_{B/D'} = 78.3(1)^\circ$, $\angle N_{B/D'}\text{Cu}N_{C/C'} = 76.3(1)^\circ$ and (in the “Cu(bipy)₂” unit) $\angle N_{D/B'}\text{Cu}N_{E/A'} = 81.1(1)^\circ$. For $[\text{Cu}_2\text{pcp}]^{3+}$ they are (in the “Cu(terpy)₂” unit) $\angle N_{A/E'}\text{Cu}N_{B/D'} = 78.8(1)^\circ$, $\angle N_{B/D'}\text{Cu}N_{C/C'} = 76.1(1)^\circ$ and (in the “Cu(bipy)₂” unit) $\angle N_{D/B'}\text{Cu}N_{E/A'} = 81.6(1)^\circ$. The bite angles are thus identical for both new complexes.

Relative size of the two copper centres When treating the measured bond lengths between copper and nitrogen of both new species statistically and calculating a confidence interval at a 99% level, the interval for the Cu(II)—N bonds is completely separated from the interval for the Cu(I)—N bonds. This means that, with an error probability of less than 1%, the true average of a bond length of Cu I — N differs from the true average of Cu2 — N. (A student’s t-test failed however, because only the bond lengths could be taken as input values. These are not enough data to give narrow enough intervals.) Curiously enough, as can be viewed in tables 4.5 and 4.6, the octahedral Cu(II), has a longer bond to the nitrogen than the tetrahedral Cu(I). Comparing the shortest bonds in the “Cu(terpy)₂” and “Cu(bipy)₂” unit, it becomes clear that Cu(II) must be the smaller ion of the two after all. The reason for the other two long bonds in the “Cu(terpy)₂” unit is caused by the limited flexibility of 2,6:2'-terpy and higher

oligopyridines to wrap around such small metal ions. These bond lengths may therefore not be used to determine the relative size of the copper ions.

The average of the shortest Cu-N bonds in the “Cu(terpy)” units of $[\text{Cu}_2(\text{mp})_2]^{3+}$ is 1.948(2)Å and the average for those of $[\text{Cu}_2\text{qcp}]^{3+}$ is 1.962Å, see Table 4.7. This is a significant difference. The nitrogen atoms concerned are at $\sim 180^\circ$ angles to each other via the copper centre, and carrying a different substituent in the 4' and 4''' position respectively. This may be the arrangement that allows the substituents to show their differing effect most pronouncedly. It would be interesting to know the actual electron distribution within the complex.

Symmetry inside the “Cu(terpy)₂”- and “Cu(bipy)₂”-units of the double helicate Both complex cations are slightly more open at the tetrahedral-end than in the octahedral end. This can be viewed as N — N distances between the two stands, across the double helix. The difference in the distance of the terminal nitrogen atoms of both ends of the double helicate ($N_A - N_{E'} - N_E - N_{A'}$) is 0.30Å for $\text{Cu}_2(\text{mp})_2^{3+}$, and 0.34Å for $\text{Cu}_2\text{pcp}^{3+}$ (see Table 4.7). Neglecting the N-N distances in the interior of the complexes, they may approximately be considered having shape similar to a cone.

Dividing the complexes again into a “Cu(terpy)₂” and a “Cu(bipy)₂” unit, in the “Cu(terpy)₂” unit of both new species, the bond lengths of Cu(II) to the terminal pyridine rings (ring A and E') are shorter than to the other relatively long bonds from the C- and C'-rings to Cu(II). It is a difference of $\Delta_{(Cu-N_{middle})-(Cu-N_{terminal})}=0.155\text{Å}$ in $[\text{Cu}_2(\text{mp})_2]^{3+}$, and 0.138Å in $[\text{Cu}_2\text{pcp}]^{3+}$. This fits well with the beforementioned conical form.

In the “Cu(bipy)₂” unit the bond lengths of the Cu(I) to the terminal pyridine rings A' and E are shorter than to the neighbouring rings B'- and D-rings (see Tables 4.7 and 4.10). But this is a smaller difference than in the “Cu(terpy)₂” unit, $\Delta_{(Cu-N_{secondlast})-(Cu-N_{terminal})}=0.026\text{Å}$ in $[\text{Cu}_2(\text{mp})_2]^{3+}$, and 0.028 in $[\text{Cu}_2\text{pcp}]^{3+}$.

Comparing again with the other two similar complexes, the same is seen for $[\text{Cu}_2(\text{qnp})_2]^{3+}$: $\Delta_{(Cu-N_{middle})-(Cu-N_{terminal})}=0.143\text{Å}$ in the “Cu(terpy)₂”, and 0.101Å in the “Cu(bipy)₂”. For $[\text{Cu}_2(\text{ms}_2\text{qnp})_2]^{3+}$ it is 0.144Å in the “Cu(terpy)₂” and 0.032Å in the “Cu(bipy)₂” part.

Because of ligand induced distortion, in the “Cu(terpy)₂” unit only the angles from central nitrogen (N_B) to copper centre to central nitrogen ($N_{D'}$) are approximately 180° , with $\angle N_A\text{Cu}N_C = 153^\circ \neq 180^\circ$, $\angle N_B\text{Cu}N_{D'} = 177^\circ \approx 180^\circ$ and $\angle N_{E'}\text{Cu}N_{C'} = 155^\circ \neq 180^\circ$ for $[\text{Cu}_2(\text{mp})_2]^{3+}$, and $\angle N_A\text{Cu}N_C = 156^\circ \neq 180^\circ$, $\angle N_B\text{Cu}N_{D'} = 176^\circ \approx 180^\circ$ and $\angle N_{E'}\text{Cu}N_{C'} = 154^\circ \neq 180^\circ$ for $[\text{Cu}_2\text{pcp}]^{3+}$.

In Figure 4.13, the angles of the Cu-N bonds around the ‘octahedral’ Cu(II) in the “Cu(terpy)₂” unit of $\text{Cu}_2(\text{mp})_2^{3+}$ are shown without the ligand backbone. With the angles listed above, and with the differing bond lengths ($\text{Cu}-N_{C'}/\text{Cu}-N_{C'} > \text{Cu}-N_A/\text{Cu}-N_{E'} > \text{Cu}-N_B/\text{Cu}-N_{D'}$), the symmetry of the geometric arrangement of the nitrogen atoms and the copper ion is reduced to C_2 . The ligand backbone being unsymmetrical finally removes even the C_2 -axis.

In Figure 4.13, the angles of the Cu-N bonds around the ‘tetrahedral’ Cu(I) in the “Cu(bipy)₂” unit are shown. The bond lengths $\text{Cu}-N_{A'}$ and $\text{Cu}-N_E$ are shorter than $\text{Cu}-N_{B'}$ and $\text{Cu}-N_D$. This reduces the symmetry from D_{2d} to C_{2v} , but the angle between the planes formed by $N_{B'}\text{Cu}N_D$ and $N_{A'}\text{Cu}N_E$ are far from 90° , and so the σ_v are removed. When taking the backbone of the ligand into account as well, the remaining C_2 axis is also gone, and the symmetry is again removed completely.

The situation for $[\text{Cu}_2\text{pcp}]^{3+}$ is practically identical to the one discussed for $[\text{Cu}_2(\text{mp})_2]^{3+}$. The angles of the Cu-N bonds around the ‘octahedral’ Cu(II) in the “Cu(terpy)₂” unit are shown in Figure 4.14 and those in the “Cu(bipy)₂” unit are shown in Figure 4.14).

Despite the lack of symmetry discussed in this section, the metal centres are centred well in their ‘octahedral’ and ‘tetrahedral’ environment. In order to make this visible, in Figures 4.15 and 4.16, the nitrogen atoms across the helix and diagonally across each coordination sphere were connected by turquoise lines. The fact, that the copper ions lie where these lines cross may give an idea of how centred the copper centres are.

[Cu ₂ (mp) ₂][PF ₆] ₃						
	six-coordinate			four-coordinate		
	ring	bonds of Cu2	length / Å	ring	bonds of Cu1	length / Å
	A	Cu2 N1	2.186(3)	E	Cu1 N5	1.986(3)
B	Cu2 N2	1.963(3)	D	Cu1 N4	2.037(3)	
C	Cu2 N3	2.356(3)	A'	Cu1 N10	2.011(3)	
E'	Cu2 N6	2.104(3)	B'	Cu1 N9	2.011(3)	
D'	Cu2 N7	1.933(3)				
C'	Cu2 N8	2.243(3)				
standard deviation σ_x		0.009			0.009	
average \bar{x}		2.1308			2.0113	
standard deviation of the average $\sigma_{\bar{x}}$		0.0037			0.0045	
confidence interval, level 99% CI ₉₉	2.121–2.140			2.000–2.023		

Table 4.5: Bond lengths of the coordinative bonds in [Cu₂mp₂][PF₆]₃.

[Cu ₂ pcp][PF ₆] ₃						
	six-coordinate			four-coordinate		
	ring	bonds of Cu1	length / Å	ring	bonds of Cu2	length / Å
	A	Cu1 N1	2.117(3)	E	Cu2 N5	2.006(3)
B	Cu1 N2	1.950(3)	D	Cu2 N4	2.027(3)	
C	Cu1 N3	2.240(3)	A'	Cu2 N10	2.001(3)	
E'	Cu1 N6	2.201(3)	B'	Cu2 N9	2.035(3)	
D'	Cu1 N7	1.973(3)				
C'	Cu1 N8	2.354(3)				
standard deviation σ_x		0.009			0.009	
average \bar{x}		2.1392			2.0173	
standard deviation of the average $\sigma_{\bar{x}}$		0.0037			0.0045	
confidence interval, level 99% CI ₉₉	2.124–2.155			2.010–2.025		

Table 4.6: Bond lengths of the coordinative bonds in [Cu₂pcp][PF₆]₃.)

		“terpy”			“bipy”	
		outer	middle	inner	inner	outer
		$N_A - N_{E'}$	$N_B - N_{D'}$	$N_C - N_{C'}$	$N_D - N_{B'}$	$N_E - N_{A'}$
Cu₂(mp)³⁺	distances across the inner side of the double helix: $N_i - N_j / \text{Å}$	3.391	3.894	3.533	3.725	3.688
	Cu-N bond length average: $\bar{x} = \frac{Cu-N_i + Cu-N_j}{2}$	2.145(2)	1.948(2)	2.300(2)	2.024(2)	1.999(2)
	$\angle N_i Cu N_j$	104°	177°	100°	134°	135°
Cu₂pcp³⁺	distances across the inner side of the double helix: $N_i - N_j / \text{Å}$	3.393	3.917	3.343	3.682	3.729
	Cu-N bond length average: $\bar{x} = \frac{Cu-N_i + Cu-N_j}{2}$	2.159(2)	1.962(2)	2.297(2)	2.031(2)	2.004(2)
	$\angle N_i Cu N_j$	104°	174°	102°	130°	137°

Table 4.7: Symmetry in the “Cu(terpy)₂” and “Cu(bipy)₂” units. By forming the average over two bond lengths, the original esd values of (3) were reduced to (2) by the formula $\frac{3}{\sqrt{2}}$.

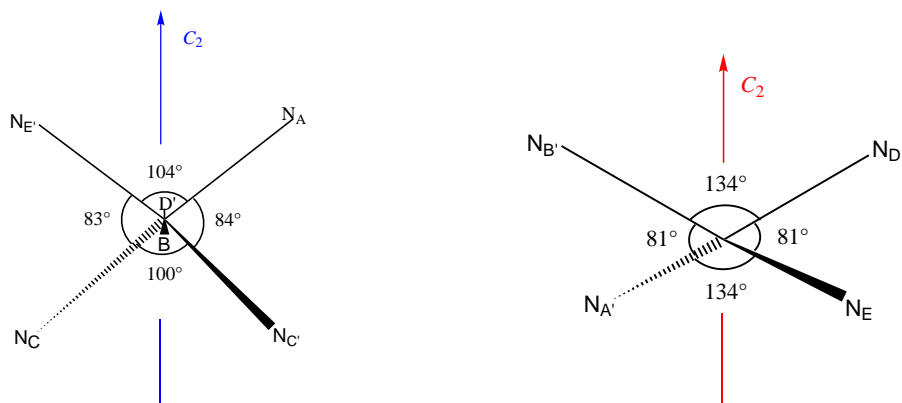


Figure 4.13: N-Cu-N angles of the octahedrally coordinated Cu(II) and the tetrahedrally coordinated Cu(I) in $Cu_2(mp)_2^{3+}$.

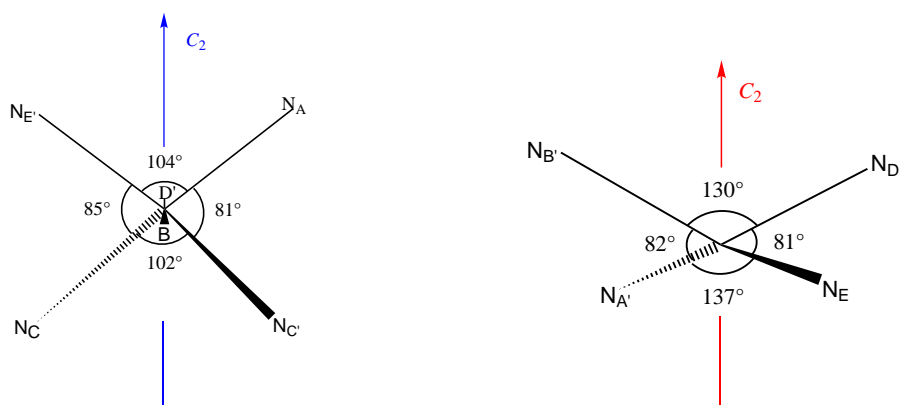


Figure 4.14: N-Cu-N angles of the octahedrally coordinated Cu(II) and the tetrahedrally coordinated Cu(I) in Cu_2pcp^{3+} .

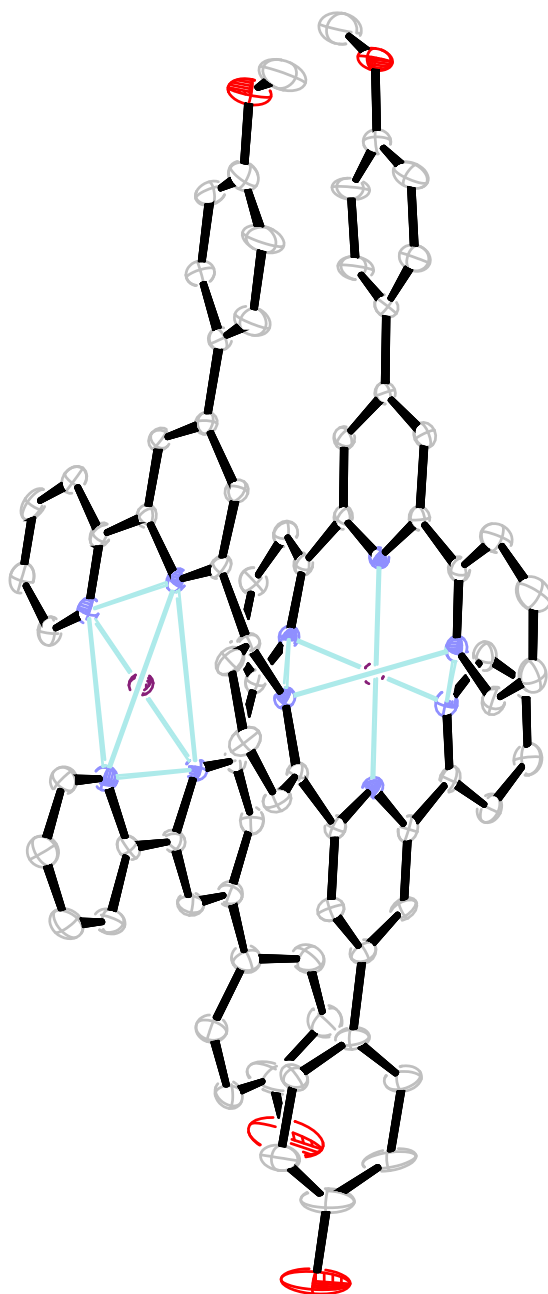


Figure 4.15: Well centred copper(II) and copper(I) in the complex $[\text{Cu}_2(\text{mp})_2]^{3+}$. Coordination polyhedra are drawn as turquoise lines, connecting the nitrogen atoms of each coordination sphere.

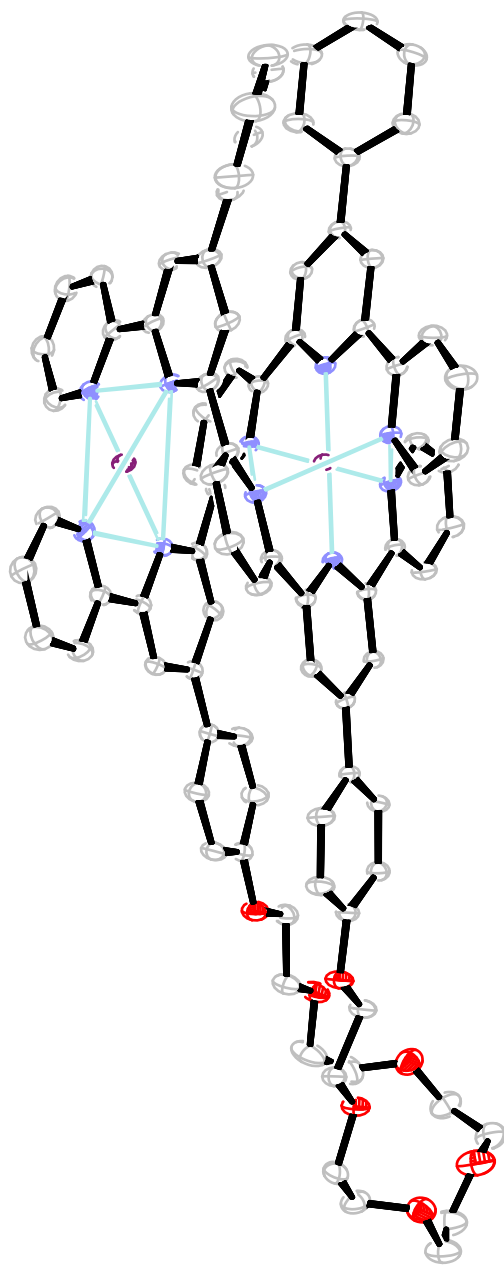


Figure 4.16: Well centred copper(II) and copper(I) in the complex $[\text{Cu}_2\text{pcp}]^{3+}$. Coordination polyhedra are drawn as turquoise lines, connecting the nitrogen atoms of each coordination sphere.

4.2.3 Comparison with other substituted quinquepyridine complexes

In Tables 4.11, 4.10 and 4.9 the two new structures are compared with similar, already published structures retrieved from the Cambridge Database.^{37,40,41,43,64} These structures are all symmetrical, as opposed to the new structures, which means that there is no head-to-head / head-to-tail isomerism.

Ligand geometry

Ligand conformation in the complex: In all of the copper complexes of qnpy type ligands,^{37,40,41,43,64} the torsion along the strands are similar. Direct comparison makes most sense with the mixed oxidation state complex of the unsubstituted qnpy ligand⁴¹ and the symmetrically substituted ms_2qnpy ³⁷ that have no substituents that could sterically interfere with the formation of the helicate. In the case of $\text{Cu}_2(\text{qnpy})_2^{3+}$, the torsion between the “bipy” and “terpy” unit (49° and 48°) is very similar to the new complexes, but the planarity of the units themselves is lower, and the torsion angles per ligand strand add up to 92° and 95° respectively, which is more than in the new complexes. In $\text{Cu}_2(\text{ms}_2\text{-qnpy})_2^{3+}$, the situation is the other way round, the torsion between the units (63° and 70°) being stronger, and the planarity within the units being more distinct. Total torsion of the ligand strands in $\text{Cu}_2(\text{mp})_2^{3+}$ is 89° , and of $\text{Cu}_2\text{pcp}^{3+}$, $\text{Cu}_2(\text{qnpy})_2^{3+}$ is 90° and $\text{Cu}_2(\text{ms}_2\text{qnpy})_2^{3+}$ it is 90° (see Table 4.9).

Bond lengths and angles within the ligand strands As mentioned before, in the Cu(II) complex of terpy $[\text{Cu}(\text{terpy})_2][\text{PF}_6]_2$,¹¹¹ the bonds connecting adjacent pyridine rings are shorter (1.445\AA) than in the free ligand (1.490\AA).¹¹⁵ If Δ is defined as the interannular bond in the complex minus the interannular bonds in the ligand, then Δ for terpy becomes $\Delta = 1.445\text{\AA} - 1.490\text{\AA} = -0.045\text{\AA}$. In the complex Cu(I) complex of bipy $[\text{Cu}(\text{bipy})_2][\text{ClO}_4]$, the bonds connection adjacent pyridine rings are also shorter (1.440\AA)¹¹⁴ than in the free ligand (1.491\AA),¹¹³ and Δ becomes $\Delta = -0.051\text{\AA}$. In the copper(II) complex of 4'-substituted terpy $[\text{Cu}(4'-(3,4\text{-dimethoxyphenyl})\text{-terpy})_2]^{2+}$, the interannular bonds average 1.489\AA and in $[\text{Cu}(4'-(4\text{-biphenyl})\text{-2,2':6',2''-terpy})_2]^{2+}$, they average 1.488\AA . Both these values (1.489\AA and 1.488\AA) are closer to the interannular bonds of the free terpy (1.490\AA) than the complexed terpy (1.445\AA). Complexation may have a shortening effect, while the electron withdrawing phenyl substituents in the 4' positions may have the effect of elongating these bonds. However, if the esd values for the interannular bonds in these structures are as high as in those for the interannular bonds in the new structures, these differences are not significant.

When qtpy is complexed with copper(I) in $[\text{Cu}_2(\text{qtpy})_2][\text{PF}_6]$, not only new coordinative bonds are formed, but also a metallo-supramolecular double helix. In this double helicate, the interannular bonds average 1.500\AA , while they are 1.484\AA in the free ligand.⁸³ This gives a positive difference between the interannular bond in the complex minus the interannular bond in the ligand $\Delta = 0.016\text{\AA}$. So it seems that though complexation with Cu(II) as well as Cu(I) leads to a shorter interannular bond in the mononuclear complex, helication leads to elongated interannular bonds (in case the differences are significant).

There is no known structure of the neutral qnpy ligand, but when assuming that the interannular bonds average somewhere between 1.484 and 1.491 like in the lower 2,6-oligopyridines, then $\text{Cu}_2(\text{qnpy})_2^{3+}$ resembles the mononuclear complexes as the interannular bonds average 1.424\AA , which give $\Delta = -0.064\text{\AA}$. The arrangement of the pyridine rings is very different from the previously discussed complexes, as 2×5 pyridine rings (two qnpy) arrange themselves around an octahedral and a tetrahedral copper ion, than when 2×4 pyridine rings (two qtpy) arrange themselves around two tetrahedral copper ions. Also interactions like π -stacking may play a role. The interannular bond lengths in the complexes $[\text{Cu}_2(\text{ms}_2\text{qnpy})_2]^{3+}$, $[\text{Cu}_2(\text{mp})_2]^{3+}$ and $\text{Cu}_2\text{pcp}^{3+}$ are 1.484\AA , $1.480(4)\text{\AA}$ and $1.486(4)\text{\AA}$ respectively.

In the copper(II/I) complex of the basic ligand qnpy the interannular bond lengths vary over a wider range ($1.309\text{-}1.608\text{\AA}$ $\Delta=0.299\text{\AA}$), while the corresponding bond lengths in the copper(II/I) complex of the 4',4'''-substituted qnpy type ligands vary less: $\text{Cu}_2(\text{ms}_2\text{-qnpy})_2^{3+}$ (1.466\AA to 1.504\AA), $\text{Cu}_2(\text{mp})_2^{3+}$: $1.473(6)\text{\AA}$ to $1.494(5)\text{\AA}$ and $\text{Cu}_2\text{pcp}^{3+}$ ($1.475(5)\text{\AA}$ to $1.492(4)\text{\AA}$). At least for the last two complexes, of which esd values are known, the differences are not significant.

	A-C'	B-B'	C-A'	C-E'	D-D'	E-C'	b-b'	d-d'
$\text{Cu}_2(\text{qnp})_2^{3+}$	48°	10°	20°	49°	10°	19°		
$\text{Cu}_2(\text{ms}_2\text{qnp})_2^{3+}$	60°	6°	3°	75°	2°	12°		
$\text{Cu}_2(\text{mp})_2^{3+}$	46°	5°	18°	59°	6°	17°	2°	
$\text{Cu}_2\text{pcp}^{3+}$	49°	11°	11°	57°	7°	17°	65°	8°

Table 4.8: π -stacking angles in mixed oxidation state copper(II/I) complexes of qnp-type ligands.

For the C-C-N angles of 4'-phenyl type terpy, no substituent effect could be seen, as these angles vary even less on complexation than the interannular bonds. Comparing C-C-N angles in $[\text{Cu}_2(\text{qtpy})_2]^{2+}$ (112°-119°, $\Delta=7^\circ$) with those of the free ligand qtpy (116-117°, $\Delta=1^\circ$), upon complexation and helicate formation, the C-C-N angles just seem to vary more strongly. The C-C-N angles in $[\text{Cu}_2(\text{qnp})_2]^{3+}$ vary also very strongly (104°-123°, $\Delta=19^\circ$). In one ligand strand, the smallest angle is at the terminal ring in the "bipy"-unit (107°), and the biggest angle in the joint between the "bipy" and the "terpy" unit, on the "bipy" side (123°). In the other strand the smallest angle is in the joint between the "bipy" and the "terpy" unit, also on the side of the "bipy" (104°), and the biggest angle towards the terminal ring in the "terpy" unit (124°). The remaining angles vary between 110° and 120°. This irregularity is in contrast to the structures of $[\text{Cu}_2(\text{mp})_2]^{3+}$ and $[\text{Cu}_2\text{pcp}]^{3+}$ which only vary $\Delta=5^\circ$ and $\Delta=3^\circ$. Also in the complex $[\text{Cu}_2(\text{ms}_2\text{qnp})_2]^{3+}$ the C-C-N angles vary only between 113° and 117° ($\Delta=4^\circ$) (see table 4.9). Substitution in the 4' and 4'''-position of the qnp ligand seem to even out the C-C-N angles. It might be an effect of the π - π -stacking interactions of the phenyl substituents in the new compounds and a van-der-Waals interaction between the sulfur atoms of the substituents in ms_2qnp (see below).

π -stacking The differences in the torsion and the interannular bond lengths effects the π -stacking in the complex cation. As the qnp-type ligand strands have the same length, difference in total torsion gives the difference in the helical pitch and thus also the difference in the distances between π -stacking pyridine ring planes. In both the new structures, the substituents add additional π -stacking interactions of the b-, b'- and d-, d'-ring compared to the previously known structures. The co-planarity between the "bipy" unit of one ligand strand with the "terpy" unit of the other is distinct. The terminal pyridine rings in the "terpy" unit stick out at an angle of over 60°, but all the other rings have π -stacking partners of the other ligand strand. Table 4.8 shows the angles of the π -stacking planes, keeping the numbering from the asymmetric head-to-tail complexes for the symmetrical ones as well.

This is in contrast to the unsubstituted $\text{Cu}_2(\text{qnp})_2^{3+}$ complex, where the pyridine rings are less coplanar than in the Cu(II/I) complexes of mp, pcp and ms_2qnp . Another difference exists between the ms_2qnp complex and the other ones. While one terminal pyridine ring sticks out of the complex cation of ms_2qnp at an angle of 60° and above, in the complex cation of qnp, all four terminal pyridine rings are integrated in the π -stacking, and so the C- and C'-rings, are sandwiched between two other. In the new structures, the angles of the terminal pyridine rings are in between the previously known structures (compare also with Table 4.4).

As the torsion angles, interannular bond lengths and C-C-N angles are more even in all three substituted qnp Cu(II/I) double helicates than in plain $\text{Cu}_2(\text{qnp})_2^{3+}$, it is assumed that π -stacking of the phenyl substituents and the van der Waals interaction with sulfur-sulfur distances of 3.942 and 3.998 Å in $[\text{Cu}_2(\text{ms}_2\text{qnp})_2]^{3+}$ have the effect of evening out the double helicate.

Coordination geometry

Ligand induced distortion Previously published structures of double helical complexes with copper ions containing qnpy-type ligands do also have a three- and a two-dentate domain. The N_B -Cu and $N_{D'}$ -Cu bond lengths involving the middle pyridine rings in the “terpy”-subunits that coordinate octahedrally are the shortest bonds of all in all complex cations (see values for ‘B/D’ or D/B’ versus the values for ‘A/E’ or E/A’ and ‘C/C’ in Table 4.10). As mentioned above, this is because a 2,6-oligopyridine cannot bend the C-C-N angle nor stretch the bond connecting adjacent pyridine rings far enough to oblige the preferred coordination sphere of the copper(II) ion. In the complex with terpy,¹¹¹ the “terpy” units are positioned symmetrical around the central pyridine ring, the Cu-N bonds to the outer rings being 2.179Å and to the middle ring 1.978Å, these bond lengths are found with only small variation in all the qnpy derived, double helical copper complexes.

Symmetry inside the “Cu(terpy)₂”- and “Cu(bipy)₂”-units of the double helicate All qnpy type complexes $[\text{Cu}_2(\text{qnpy})_2]^{3+}$, $[\text{Cu}_2(\text{ms}_2\text{qnpy})_2]^{3+}$ and the new ones, are more open in the “Cu(bipy)₂” end than in the “Cu(terpy)₂” end. The N_E - $N_{A'}$ distance is longer than the $N_{E'}$ - N_A distance. In the non substituted copper complex qnpy complex, this difference in N-N distance between one end and the other is 0.43Å, and in the symmetrically substituted copper complex of ms_2qnpy it is 0.36Å and as already stated it is 0.30Å for $[\text{Cu}_2(\text{mp})_2]^{3+}$ and 0.34Å for $[\text{Cu}_2\text{qcq}]^{3+}$, see also Table 4.7.

It has to do with the narrower bite angles at the six coordinate Cu(II) and the bigger bite angles at the four coordinate Cu(I). Consequently, the symmetrical copper(II) complex of sixpy $[\text{Cu}_2(\text{ms}_2\text{sixpy})_2]^{4+}$ has almost the same N-N distance in both ends (3.450 and 3.454Å ($\Delta=0.004\text{\AA}$)). But surprisingly, the Cu(I) complex of qtpy $[\text{Cu}_2(\text{qtpy})_2]^{2+}$ forms a double helicate, that is slightly narrower in one end than the other (3.874Å and 3.792Å $\Delta=0.082\text{\AA}$), despite for that both copper ions are approximately tetrahedral and have the same oxidation state.

The same asymmetry in the “Cu(terpy)₂”- and “Cu(bipy)₂”-units, where the N-Cu bonds to the terminal rings are shorter than to the inner ones is seen in earlier published structures listed in table 4.10. The one exception is of the ligand strands in $[\text{Cu}_2(6,6''''\text{-dimethyl-4',4''''-diphenyl-qnpy})_2]^{3+}$, where the $N_{C'}$ -Cu(2) bond is shorter than the N'_E -Cu(2) bond (2.308 < 2.331), but in this special case, there is a sterically hindering methyl group positioned at the 6- and 6''''-position, apart from the peripheral substituents in the 4'- and 4''''-positions. This influences the overall structure sterically. But when comparing the average of the $N_{A/A'}$ -Cu with the average of the $N_{C/C'}$ -Cu bond length in this structure, the bond length of Cu to $N_{A/A'}$ (2.285Å) and $N_{C/C'}$ (2.290Å) are about the same.

N_i -Cu- N_j bite angles The bite angles of the new complexes were identical $[\text{Cu}_2(\text{mp})_2]^{3+}/[\text{Cu}_2\text{qcq}]^{3+}$: 78.3(1)/78.8(1)° and 76.3(1)/76.1(1)° for the “Cu(terpy)₂” unit and 81.1(1)/81.6(1)° for the “Cu(bipy)₂” unit. Comparing with mononuclear copper(II) complex of terpy and copper(I) complex of bipy shows that in $[\text{Cu}(\text{terpy})_2]^{2+}$ these angles are 76.9° inside the ligand strand, and in $[\text{Cu}(\text{bipy})_2]^+$ they are 81.5°, which gives 79.2° in average. These are identical angles as in the new complexes. An overview including $\text{Cu}_2(\text{qnpy})_2^{3+}$ and $\text{Cu}_2(\text{ms}_2\text{qnpy})_2^{3+}$ is given in Table 4.12. Also these have the same bite angles: 77.9°, 78.2° and 81.1° for $[\text{Cu}_2(\text{qnpy})_2]^{3+}$ and 77.8°, 75.4° and 80.3° for $[\text{Cu}_2(\text{ms}_2\text{qnpy})_2]^{3+}$. And so the new complexes have quite ordinary bite angles.

Cu-Cu distances As the discussion so far suggests, the copper-copper distances in the new complexes do not differ much from the similar, already published structures of qnpy type ligands (see Table 4.11). The Cu-Cu distance in $\text{Cu}_2(\text{qnpy})_2^{3+}$ is 3.957Å and in $\text{Cu}_2(\text{qnpy})_2^{3+}$ it is 4.250Å. Arranging the ligands after the copper-copper distance in the mixed oxidation state complexes, gives the order of the ligands: mp (3.94Å) < qnpy (3.96Å) < pcp (4.00Å) < ms_2qnpy (4.25Å). The latter has a longer Cu-Cu distance than the other. It is a special complex because of the sulfur substituents. The neighbouring sulfur atoms are at a distance (3.942 and 3.998Å) close to the sum of the van-der-Waal radii of 4.80Å, and this interaction may be causing the long pitch and also the long copper-copper distance of the complex.

Inter-ligand interactions: 4' - and 4'''-substituents					
parameters	$\text{Cu}_2(\text{qnp})_2^{3+}$	$\text{Cu}_2(\text{mp})_2^{3+}$	$\text{Cu}_2(\text{pcp})_2^{3+}$	$\text{Cu}_2(\text{ms}_2\text{qnp})_2^{3+}$	substituent effect
	none	b-b' π -stacking (and d-d' dis- torted π -stacking? distance $\geq 3.4\text{\AA}$)	b-b' and d-d'- π - stacking	weak sulfur-sulfur van der Waals inter- action (3.998\AA B- B' and at D-D')	
torsion _{total} of the pyridine ring planes	88°	87°	87°	92°	the helical pitch of the two ligand strands in the cation become more equal
torsion' _{total} of the pyridine ring planes'	91°	89°	91°	89°	
Δ_{torsion} (ligand-ligand')	3°	3°	5°	3°	
\angle C-C-N	107°-123°	114°-118°	114°-118°	113°-117°	the C-C-N angles vary less within each of the ligand strands
$\Delta_{\text{max-min}}$	16°	4°	3°	4°	
\angle C'-C'-N'	104°-124°	113°-117°	115°-116°	114°-115°	
$\Delta'_{\text{max-min}}$	20°	4°	1°	1°	
interannular bonds / \AA	1.407-1.567	1.473(6)-1.484(6)	1.475(5)-1.490(5)	1.471-1.482	the inter annular bonds become more equal in both ligand strands
$\Delta_{\text{highest-lowest}}$ / \AA	0.160	0.011	0.015	0.011	
interannular bonds' / \AA	1.309-1.608	1.476(6)-1.494(5)	1.483(5)-1.492(4)	1.466-1.504	
$\Delta'_{\text{highest-lowest}}$ / \AA	0.299	0.018	0.009	0.038	

Table 4.9: Inter-ligand strand interactions of the substituents at the 4' - and 4'''-position.)

	octahedral Cu-N bond/Å			tetrahedral Cu-N bond/Å	
	A/E'	B/D'	C/C'	D/B'	E/A'
[Cu ₂ (mp) ₂][PF ₆] ₃	2.186(3)/2.104(3)	1.963(3)/1.933(3)	2.356(3)/2.243(3)	2.037(3)/2.011(3)	1.986(3)/2.011(3)
[Cu ₂ pcp][PF ₆] ₃	2.117(3)/2.201(3)	1.950(3)/1.973(3)	2.240(3)/2.354(3)	2.027(3)/2.035(3)	2.006(3)/2.001(3)
[Cu ₂ (qnp) ₂][PF ₆] ₃	2.168/2.179	1.971/1.968	2.325/2.308	2.156/2.099	2.043/2.011
[Cu ₂ (4',4'''-di-methylthio-qnp) ₂][PF ₆] ₃	2.145/2.170	1.975/1.974	2.296/2.307	2.031/2.064	2.021/2.010
[Cu ₂ (6,6''''-dimethyl-4',4'''-diphenyl-qnp) ₂][OAc] ₃	2.238/2.331	1.950/1.966	2.271/2.308	2.055/2.061	2.029/2.011
	octahedral Cu-N bond			five coordinate Cu-N bond	
[Cu ₂ (qnp) ₂ (OAc)][PF ₆] ₃	2.162/2.160	2.018/1.964	2.319/2.378	2.214/2.078	1.994/1.996
	octahedral			six coordinate	
[Cu ₂ (4',4'''-di-methylthio-qnp) ₂ (OAc)][PF ₆] ₃	2.170	1.949	2.349	2.145	1.981
	octahedral nickel ion			tetrahedral	
[Cu ^(I) ,Ni ^(II)](4',4'''-di-methylthio-qnp) ₂][PF ₆] ₃	(2.133)	(2.011)	(2.222)	2.005	1.998

Table 4.10: Octahedral and tetrahedral coordinated copper ions: comparing bond lengths (labelling according to the NMR-labelling, see Figures 7.13, and 7.17).

	octahedral	tetrahedral	Cu-Cu distance/Å
average for [Cu ₂ (mp) ₂][PF ₆] ₃ (interval _{99%})	2.131(2) (2.121–2.140)	2.011(2) (2.000–2.023)	3.944
average for [Cu ₂ pcp][PF ₆] ₃ (interval _{99%})	2.139(2) (2.124–2.155)	2.017(2) (2.010–2.025)	4.002
average for [Cu ₂ (qnp) ₂][PF ₆] ₃	2.153	2.077	3.957
average for [Cu ₂ (ms ₂ qnp) ₂][PF ₆] ₃	2.145	2.032	4.250
average for [Cu ₂ (6,6''''-dimethyl-4',4'''-diphenyl-qnp) ₂][OAc] ₃	2.177	2.039	3.953
	octahedral	five coordinate	Cu-Cu distance/Å
average for [Cu ₂ (qnp) ₂ (OAc)][PF ₆] ₃	2.167	2.071	4.504
	octahedral (N ₆)	six coordinate (N ₄ O ₂)	Cu-Cu distance/Å
average for [Cu ₂ (ms ₂ qnp) ₂ (OAc)][PF ₆] ₃	2.156	2.063	4.438
	octahedral nickel ion	tetrahedral	Ni-Cu distance/Å
average for [Cu ^(I) ,Ni ^(II)](4',4'''-di-methylthio-qnp) ₂ [PF ₆] ₃	(2.122)	2.002	(4.701)

Table 4.11: Octahedral and tetrahedral coordinated copper ions: comparing bond lengths. Forming the average over n values reduces the esd values by the formula $\frac{esd}{\sqrt{n}} = \frac{3}{\sqrt{3}}$ for the octahedral, and $\frac{3}{\sqrt{2}}$ for the tetrahedral).

	bite angle	$[\text{Cu}_2(\text{mp})_2]^{3+}$		$[\text{Cu}_2\text{pcp}]^{3+}$		$[\text{Cu}_2(\text{qnp})_2]^{3+}$		$[\text{Cu}_2(\text{ms}_2\text{qnp})_2]^{3+}$	
		strand	strand'	strand	strand'	strand	strand'	strand	strand'
“terpy” unit	$\text{N}_A\text{CuN}_B / \text{N}_{E'}\text{CuC}_{D'}$	77.94(12)	78.66(13)	79.28(11)	78.30(10)	75.65	80.23	78.03	77.65
	$\text{N}_B\text{CuN}_C / \text{N}_{D'}\text{CuC}_{C'}$	75.65(12)	76.89(11)	77.07(11)	75.20(10)	81.50	74.83	75.48	75.28
“bipy” unit	$\text{N}_D\text{CuN}_E / \text{N}_{B'}\text{CuC}_{A'}$	81.37(13)	80.74(13)	81.43(12)	81.86(13)	77.23	85.00	80.27	80.37

Table 4.12: $\angle\text{N}_i\text{CuN}_j$ bite angles in the qnp-type ligands strands of the mixed oxidation state Cu complexes. Taking the esd values into account, $\angle\text{N}_A\text{CuN}_B$ and $\angle\text{N}_{E'}\text{CuN}_{D'}$ are identical for all these complexes, as are $\angle\text{N}_B\text{CuN}_C$ and $\angle\text{N}_{D'}\text{CuN}_{C'}$ and $\angle\text{N}_D\text{CuN}_E$ and $\angle\text{N}_{B'}\text{CuN}_{A'}$.

4.2.4 Electrochemistry

The electrochemical behaviour of the two species characterised by X-ray diffraction ($[\text{Cu}_2(\text{mp})_2][\text{PF}_6]_3$ and $[\text{Cu}_2\text{pcp}][\text{PF}_6]_3$) was studied under conditions described on page 173.

The exact potentials were obtained by differential pulse voltammetry. In both complexes the values for the Cu(II/I) processes are 0.14V and -0.43V versus ferrocene. The cyclovoltammograms of both complexes were recorded between -1.250V and +1.250V to show metal and ligand oxidations and reductions. Ligand reductions could not be resolved well. In $[\text{Cu}_2(\text{mp})_2][\text{PF}_6]_3$, there is a decrease in the current intensity from the first to the second scan of the cyclovoltammogram. But the third scan is identical to the second. In $[\text{Cu}_2\text{pcp}][\text{PF}_6]_3$, there is a decrease in the current intensity from the first to the second and from the second to the third scan. The current maxima are not resolved well, and peak splitting ΔE_p at the scan rate of 0.1V/s can only be estimated. They are above 59mV and this suggests non-reversibility of the redox process in the molecules at this scan rate, or uncompensated solution resistance and/or non-ideal cell geometry.¹¹⁶ For $[\text{Cu}_2(\text{mp})_2][\text{PF}_6]_3$, $E=0.14\text{V}$ has an estimated $\Delta E_p \approx 360\text{mV}$, and the ΔE_p for $E=-0.43\text{V}$ cannot be estimated. For $[\text{Cu}_2\text{pcp}][\text{PF}_6]_3$, $E=0.14\text{V}$ has an $\Delta E_p \approx 350\text{mV}$, and $E=-0.43\text{V}$ has an $\Delta E_p \approx 210\text{mV}$. These peak splittings are much larger than that of ferrocene $\Delta E_p \approx 110\text{mV}$ (ideally, when diffusion controlled =90.6mv). But as return waves are seen for both substances, their redox processes may be called quasi-reversible. In Table 4.13, some redox potentials of related complexes^{35,37,40,41,51,67,91} are listed, ordered after increasing first reduction potential.

For comparison of the new complexes with asymmetric ligands, it would have been interesting if the complex of hp_2qnp_y , would have been measured. This has not been successful yet, perhaps because of deprotonation of the phenol group.⁵¹ So only the complexes without the phenol group, like of the new asymmetric ligand pcp and of the known asymmetric ligand tbpcpqnp_y , can be compared directly with the complexes of the symmetric parent ligands: in pcp , both substituents are most similar to 4-methoxyphenyl. Indeed, as shown in Table 4.13, each of the potentials for dinuclear copper complexes differ only by 30mV from the parent complex, which is not significant. The complex of tbpcpqnp_y can best be compared with the complexes of symmetrically substituted qnp_y with 4-chlorophenyl and 4-*tert*-butylphenyl. Both potentials of the dinuclear copper complex of tbpcpqnp_y are close to the cp_2qnp_y complex, and far from the tbp_2qnp_y complex. In fact, both potentials are influenced mainly by the 4-chlorophenyl. This may mean that the complex of tbpcpqnp_y is head-to-tail, like the new complexes, and so the 4-chlorophenyl substituent is relatively close to both of the metals. Or if it is head-to-head, there must be strong communication through the complex in order to explain the influence of 4-chlorophenyl also on the second metal based reduction.

An example of a complex with electron donating substituents is the dinuclear copper complex with ms_2qnp_y . Three redox potentials have been reported by Potts *et al.*³⁷ There are two potentials at 0.32V, and -0.24V (converted vs ferrocene). Comparing these two potentials with the average of the two potentials in the table, a shift of +0.14V is seen for the first and +0.18V for the second process, so this complex is reduced more easily than the complexes of 4-R-phenyl substituted qnp_y ligands. The difference between the two potentials 0.29V and -0.24V is 0.53V, and this value fits in well with the ones in the right hand column of Table 4.13.

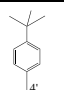
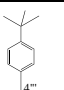
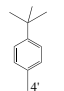
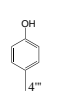
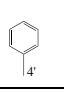
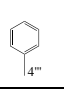
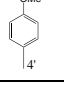
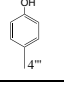
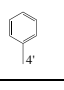
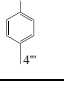
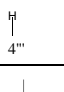
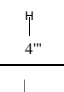
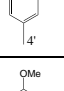
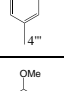
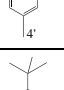
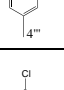
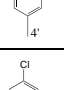
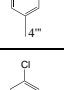

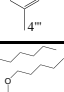
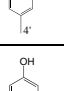
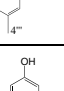
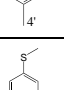
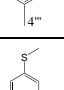
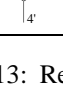
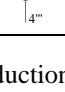
Cu ₂ (4'-R ¹ ,4'''-R ² -qnpy) ₂				
R ¹	R ²	first metal based reduction in Volt versus ferrocene (± 20mV)	second metal based reduction in Volt versus ferrocene (± 20mV)	Difference between the two reduction potentials
		0.11	-0.45	0.56
		0.12	-0.40	0.52
		0.12	-0.43	0.55
		0.14	-0.43	0.57
		0.14	-0.43	0.57
		0.15	-0.37	0.52
		0.15	-0.40	0.55
		0.16	-0.45	0.61
		0.17	-0.40	0.57
		0.18	-0.41	0.59
		0.19	-0.40	0.59
		-	-	-
		0.29	-0.24	0.53

Table 4.13: Reduction potentials (versus ferrocene) of dinuclear copper complexes of qnpy-type ligands^{35,37,40,41,51,67,91}.

4.2.5 UV-Vis spectra and spectroelectrochemistry

UV-Vis spectroscopy All copper complexes obtained of qp, mp, pp, qcq, mcm and pcp are brown. The colour is assumed to be coming from the complexed Cu(I), as Cu(I) complexes of oligopyridines are typically brown, due to the Cu(I)-Ligand(π^*) charge transfer band where the electron is transferred via a π -type overlap of the d orbital from the copper with the ligand π^* LUMO.³⁵

The highest ϵ values in the visible region are $2.50 - 6.44 \cdot 10^3 \text{ M}^{-1}\text{cm}^{-1}$ at 467 – 473nm, while there is a shoulder with ϵ values of $1.02 - 2.24 \cdot 10^3 \text{ M}^{-1}\text{cm}^{-1}$ at 572 – 585nm, see Table 4.14. The former is an absorption of blue light and it makes the species appear orange, while the latter is an absorption of yellow light and makes the species look blue. This generally makes the eye see a brown colour. The absorption of red light at 690nm (seen as a maximum in the fully oxidised complex $[\text{Cu}_2(\text{qnp})_2]^{4+}$ ³⁵) which makes the species look green, have in the case for the complexes studied here, only weak ϵ values of $3.09 - 4.64 \cdot 10^3 \text{ M}^{-1}\text{cm}^{-1}$. So the magnitude in the molar absorption coefficient around 470nm, 579nm and 690nm are in the ratio of $\sim 20 : 10 : 1$.

Of each compound, two acetonitrile solutions of different concentrations were made. The weak absorptions in the Vis region were measured with the more concentrated solutions, and the strong absorption in the UV-region were measured with the diluted solutions.

Concentrations of the complex solutions in acetonitrile:

$[\text{Cu}_2(\text{pp})_2][\text{PF}_6]_3$:	$c_1=1.04 \cdot 10^{-4}\text{M}$,	$c_2=9.32 \cdot 10^{-6}\text{M}$
$[\text{Cu}_2(\text{mp})_2][\text{PF}_6]_3$:	$c_1=1.14 \cdot 10^{-4}\text{M}$,	$c_2=1.14 \cdot 10^{-5}\text{M}$
$[\text{Cu}_2(\text{qp})_2][\text{PF}_6]_3$:	$c_1=1.19 \cdot 10^{-4}\text{M}$,	$c_2=1.19 \cdot 10^{-5}\text{M}$
$[\text{Cu}_2(\text{pcp})][\text{PF}_6]_3$:	$c_1=1.22 \cdot 10^{-4}\text{M}$,	$c_2=1.22 \cdot 10^{-5}\text{M}$
$[\text{Cu}_2(\text{mcm})][\text{PF}_6]_3$:	$c_1=1.05 \cdot 10^{-4}\text{M}$,	$c_2=1.05 \cdot 10^{-5}\text{M}$
$[\text{Cu}_2(\text{qcq})][\text{PF}_6]_3$:	$c_1=1.15 \cdot 10^{-4}\text{M}$,	$c_2=1.15 \cdot 10^{-5}\text{M}$

The solvent acetonitrile, leaves a window for measurement above wavelength 210nm. Therefore, the shoulder at 222-226nm is already relevant. Then there is a maximum at 288-292nm, that is most probably an intraligand π - π^* transition, as in the $\text{Cu}_2(\text{qtpy})_2^{2+}$ complex.^{37,117} Going to higher wavelengths, the absorption in all complexes except $[\text{Cu}_2(\text{mp})_2][\text{PF}_6]_3$ stays relatively high (see figure 4.17). There is another shoulder at 316-320nm, most distinct in the complexes of mp, mcm and qcq, and another one at 347-351nm. The maximum at 467-473nm and the shoulder at around 572-585nm (see figure 4.18) are much weaker. They are attributed to MLCT transitions, but d-d transitions would also be expected around 600nm.^{37,117,118} The maxima and shoulders in the UV-Vis spectra are listed in Table 4.14.

Figure 4.19 illustrates the change that takes place, when a qnpy type ligand complexes into a double helicate. Here the UV-spectra of qp, mp and pp and their copper(II/I) double helical complex are shown. For comparison, the y-axis is the extinction coefficient rather than the measured absorption. In the complex, the double amount of aromatic rings are present per mol, compared to the pure ligands. The maximum absorption is shifted towards lower energy, and it is not reduced as quickly, when going towards bigger wavelength either. This finding suggests that by complexation, part of the original chromophoric system is expanded. Figure 4.20 shows the same kind of changes in the linked qnpy type ligands qcq, mcm and pcp and their complexes with copper(II/I).

All spectra of the six coordination compounds exhibit similar absorption pattern. The molar extinction coefficients at $\sim 280\text{nm}$, are higher for the complexes of linked ligand than the corresponding non-linked ligand. $\epsilon_{qcq} > \epsilon_{qp}$ and $\epsilon_{pcp} > \epsilon_{pp}$ the mp-complex and mcm-complex show extinction coefficients very close to each other, but also here, $\epsilon_{mcm} > \epsilon_{mp}$. The decrease in absorption towards higher wavelength is most distinct with the pp-complex.

The molar extinction coefficients for the absorption maximum at $\sim 470\text{nm}$, have the opposite intensities. $\epsilon_{qp} > \epsilon_{qcq}$, $\epsilon_{mp} > \epsilon_{mcm}$ and $\epsilon_{pp} > \epsilon_{pcp}$. The difference of ϵ are $1600\text{M}^{-1}\text{cm}^{-1}$ for the qp/qcq pair, $1770\text{M}^{-1}\text{cm}^{-1}$ for the mc/mcm pair and $1650\text{M}^{-1}\text{cm}^{-1}$ for the pp/pcp pair and thus all similar. This is an effect of the different ratios of mixed valence (Cu(II)Cu(I) helicates and Cu(II)Cu(II) helicates in the samples. The helicates of non-linked ligands occur in mixed valence, and the helicates of the linked ligands mainly as Cu(II)Cu(II) valence. As the complexed Cu(I) is responsible for the absorption at this wavelength, the amount of Cu(I) present in the helicates accounts for the intensity of the absorption.

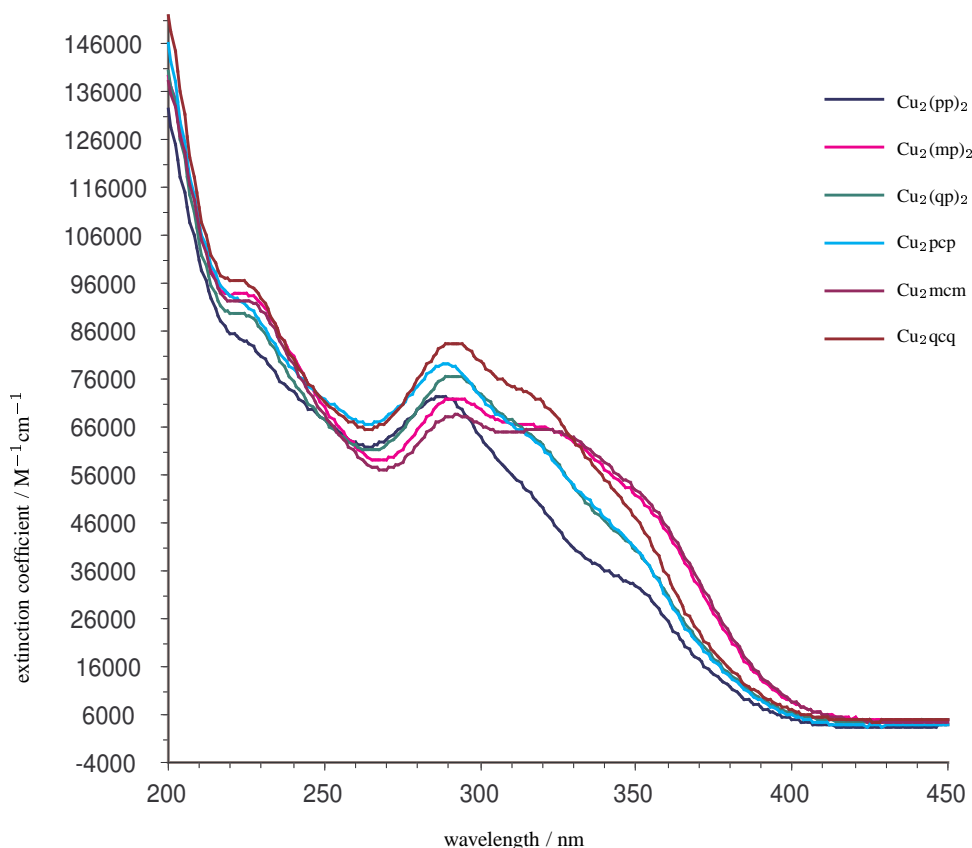


Figure 4.17: UV spectra of the qnpy-type copper complexes in the region 200nm-450nm in acetonitrile.

It would be interesting to compare the intensity and position of the maxima and shoulders in the visible spectra of these compounds with those of $[\text{Cu}(\text{bipy})_2]^+$, $[\text{Cu}(\text{terpy})_2]^{2+}$, $[\text{Cu}_2(\text{qtpy})_2]^{2+}$ and $[\text{Cu}_2(\text{qnpy})_2]^{3+}$. The only published data found, however, was on $[\text{Cu}(\text{terpy})_2]^{2+}$,¹¹⁹ and trinuclear copper(I) double helicate of two tris-bipy ligands¹²⁰ (see Figure 4.21). The former is a green compound, formed in water, and the green colour is due to a weak absorption maximum at $\sim 640\text{nm}$ and a molar extinction coefficient of $77\text{M}^{-1}\text{cm}^{-1}$. It shows a d-d absorption typical for d-block complexes, and would be easily overruled by the intensity of an MLCT absorption band from a Cu(I) complex described above or in the literature example below.

The latter was a red compound with λ_{max} at 500nm and an extinction coefficient ϵ of $26000\text{M}^{-1}\text{cm}^{-1}$. The maximum is red-shifted compared to the new species and has a much higher absorption coefficient. The higher absorption is partly due to three copper(I) metal centres per complex cation. But as the absorption at around 470nm in the new compounds times three: $3 \times 6500\text{M}^{-1}\text{cm}^{-1}$ do not reach $26000\text{M}^{-1}\text{cm}^{-1}$, the profound difference of the ligands, and the way they complex, also must play a role. It is plausible, as the absorption band 500nm ($26000\text{M}^{-1}\text{cm}^{-1}$) is assigned to a metal-to-ligand charge transfer (MLCT).

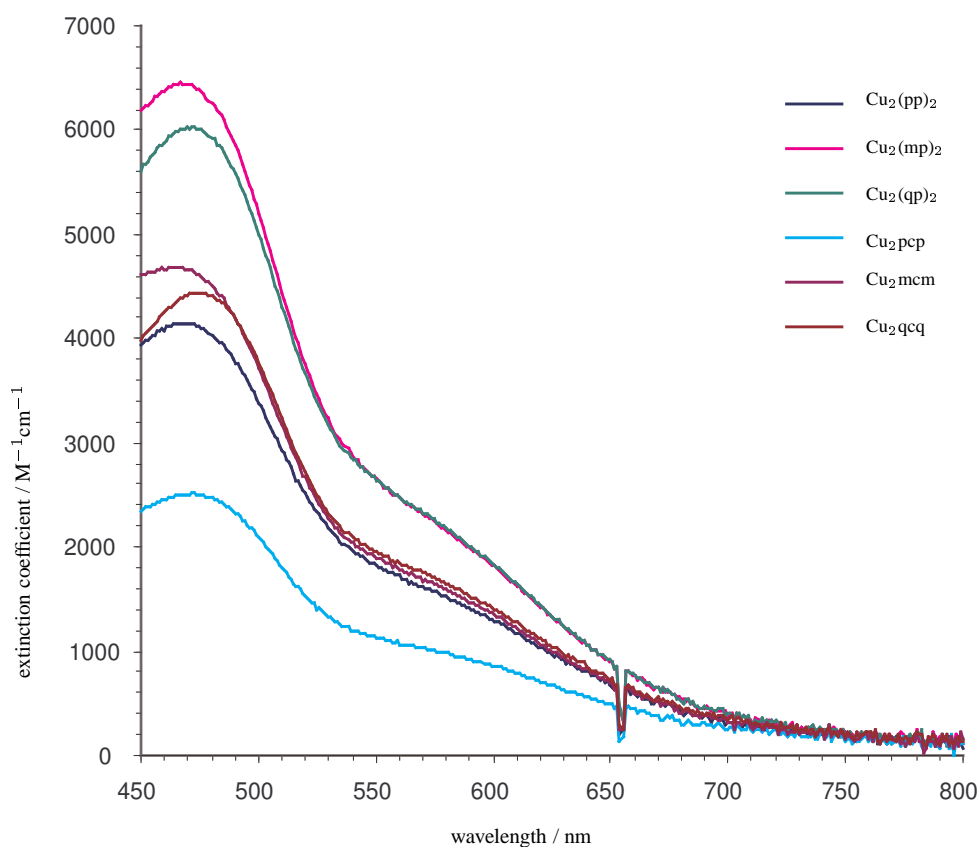


Figure 4.18: Vis spectra of the qnpy-type copper complexes in the region 450nm-800nm in acetonitrile (change of the lamp at ~ 650 nm).

[Cu₂(pp)₂][PF₆]₃		[Cu₂(mp)₂][PF₆]₃		[Cu₂(qp)₂][PF₆]₃	
λ / nm	$\epsilon / \text{M}^{-1}\text{cm}^{-1}$	λ / nm	$\epsilon / \text{M}^{-1}\text{cm}^{-1}$	λ / nm	$\epsilon / \text{M}^{-1}\text{cm}^{-1}$
222	$8.50 \cdot 10^4$	226	$9.36 \cdot 10^4$	224	$8.99 \cdot 10^4$
288	$7.24 \cdot 10^4$	292	$7.20 \cdot 10^4$	292	$7.70 \cdot 10^4$
319	$4.99 \cdot 10^4$	317	$6.63 \cdot 10^4$	318	$6.36 \cdot 10^4$
351	$3.24 \cdot 10^4$	351	$5.12 \cdot 10^4$	348	$4.21 \cdot 10^4$
467	$4.15 \cdot 10^3$	467	$6.44 \cdot 10^3$	470	$6.05 \cdot 10^3$
572	$1.60 \cdot 10^3$	581	$2.14 \cdot 10^3$	577	$2.24 \cdot 10^3$
[Cu₂pcp][PF₆]₃		[Cu₂mcm][PF₆]₃		[Cu₂qcq][PF₆]₃	
λ / nm	$\epsilon / \text{M}^{-1}\text{cm}^{-1}$	λ / nm	$\epsilon / \text{M}^{-1}\text{cm}^{-1}$	λ / nm	$\epsilon / \text{M}^{-1}\text{cm}^{-1}$
224	$9.16 \cdot 10^4$	225	$9.25 \cdot 10^4$	224	$9.68 \cdot 10^4$
289	$7.89 \cdot 10^4$	292	$6.84 \cdot 10^4$	291	$8.39 \cdot 10^4$
316	$6.38 \cdot 10^4$	320	$6.55 \cdot 10^4$	316	$7.30 \cdot 10^4$
351	$3.97 \cdot 10^4$	348	$5.43 \cdot 10^4$	347	$4.98 \cdot 10^4$
473	$2.50 \cdot 10^3$	468	$4.67 \cdot 10^3$	473	$4.45 \cdot 10^3$
574	$1.02 \cdot 10^3$	576	$1.63 \cdot 10^3$	585	$1.60 \cdot 10^3$

Table 4.14: UV-Vis wavelengths and extinction coefficients for maxima and shoulders of the acetonitrile solutions of the complexes. Measured on two separate solutions for the UV-region and the Vis-region.

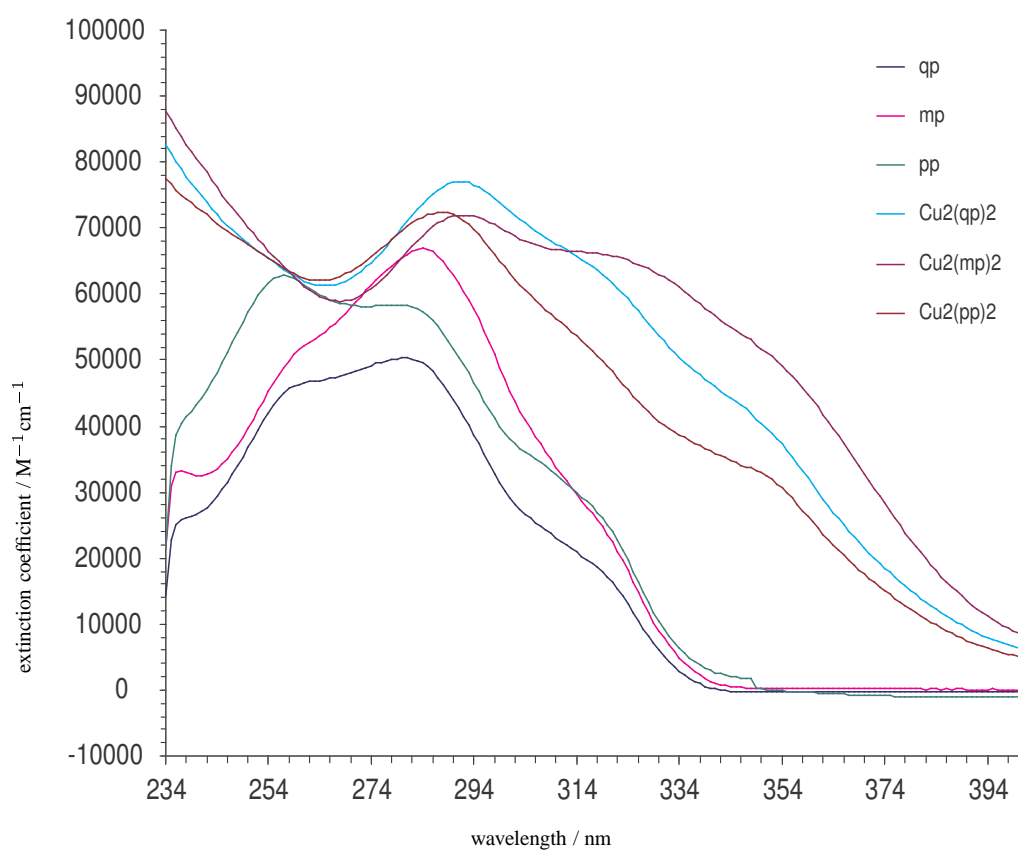


Figure 4.19: The UV absorption spectra of the three qnpy derivatives qp, mp and pp in chloroform and their copper(II/I) helicate complexes in acetonitrile solutions.

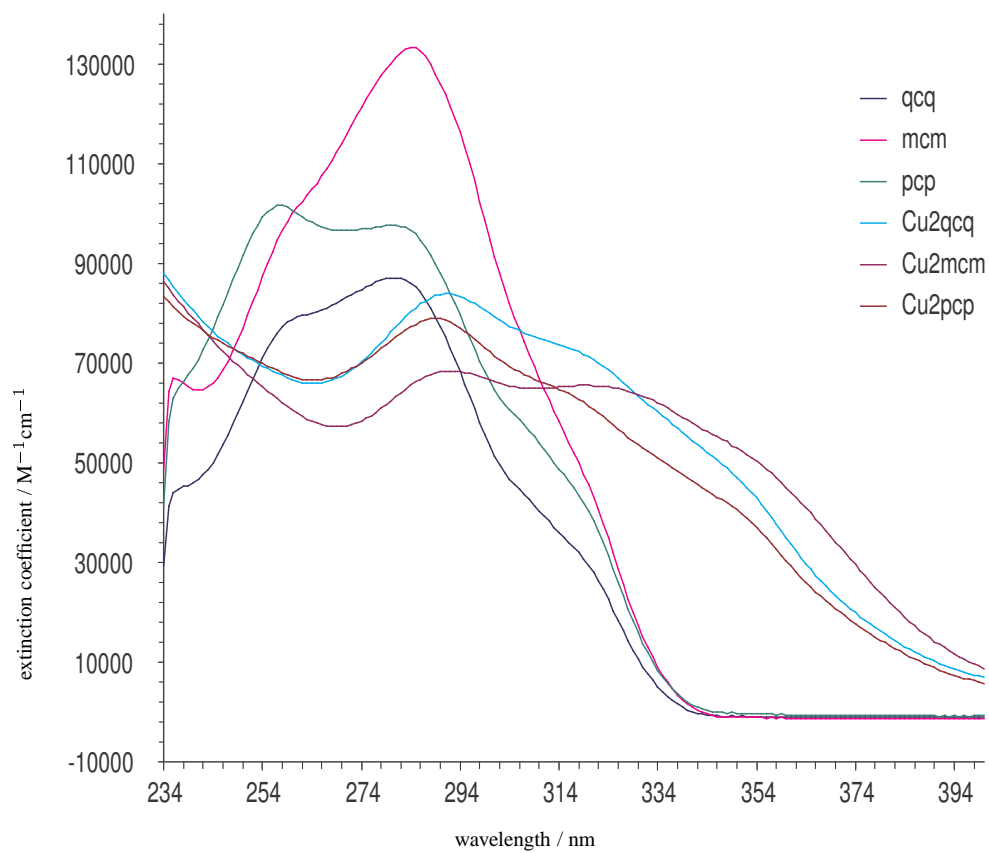


Figure 4.20: The UV absorption spectra of the three linked qnpy derivatives qcq, mcm and pcp in chloroform and their copper(II/I) helicate complexes in acetonitrile solutions.

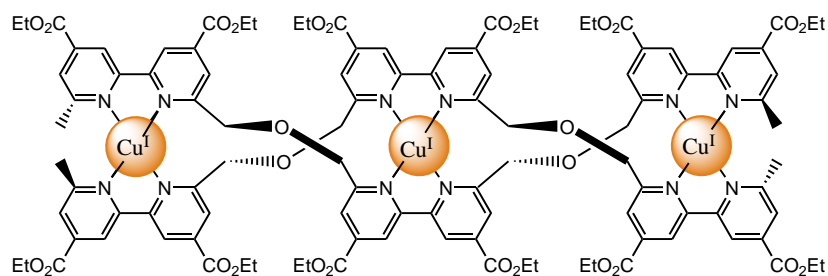


Figure 4.21: A copper(I) trinuclear tris-bipy double helicate, synthesised and characterised by Lehn *et al.*¹²⁰

The spectroelectrochemistry was conducted in absolute acetonitrile. The absorption in the visible region was measured as it changed over time, while a constant potential was applied. The acquisition range was from 190 nm to 1100 nm and the cycle time was 15 s. In the oxidative scan, the mixed valence compound would oxidise: $\text{Cu(II)Cu(I)} \rightarrow \text{Cu(II)Cu(II)}$, and in the reductive scan, it would be reduced: $\text{Cu(II)Cu(I)} \rightarrow \text{Cu(I)Cu(I)}$. The absorption at this wavelength was assigned to an MLCT band of coordinated Cu(I). Thus the absorption was expected to diminish upon oxidation, and increase upon reduction.

For $[\text{Cu}_2(\text{mp})_2][\text{PF}_6]_3$, at a constant potential of +800mV the typical absorption at $\sim 480\text{nm}$ and the shoulder at $\sim 570\text{nm}$ vanishes completely over time, see Figure 4.22. At this potential the Cu(I) is oxidised to Cu(II). When a potential of -400mV is applied, these absorptions grow over time, see Figure 4.23. The increase and decrease were measured at 480nm and could be plotted as saturation curves.

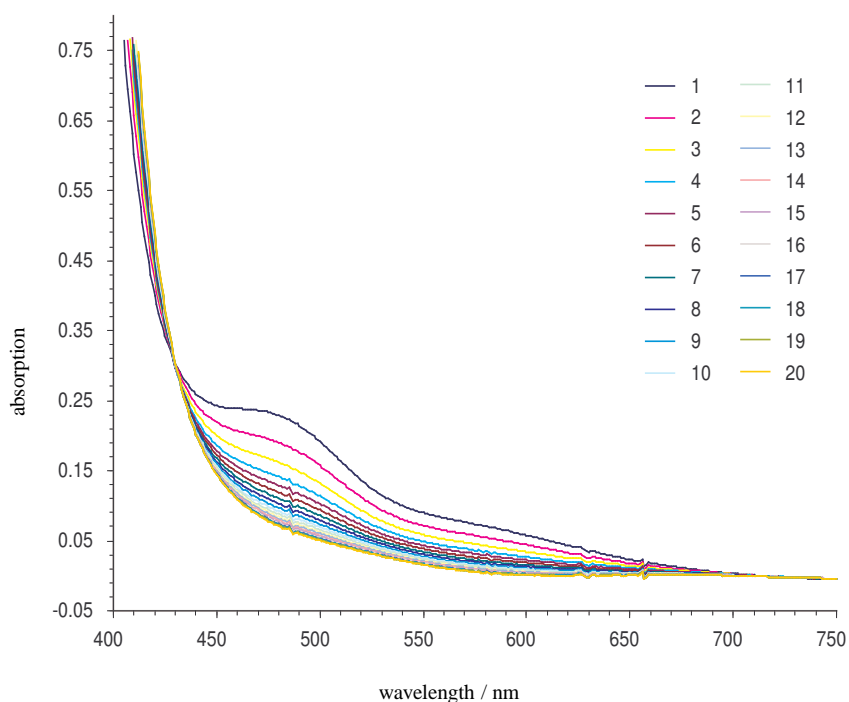


Figure 4.22: Spectroelectrochemistry of $[\text{Cu}_2(\text{mp})_2][\text{PF}_6]_3$ in acetonitrile, applied potential of +800mV: the absorption decreases with time.

For $[\text{Cu}_2\text{pcp}][\text{PF}_6]_3$ at a constant potential of +1100mV the typical absorption at $\sim 480\text{nm}$ and the shoulder at $\sim 570\text{nm}$ of the complexed Cu(I) vanishes completely over time too, see Figure 4.24. At this potential the Cu(I) is oxidised to Cu(II). And when a potential of -100mV is applied, these absorptions grow over time, see Figure 4.25. The increase and decrease were measured at 480nm and could be plotted as saturation curves.

4.2.6 Summary and conclusions

The ligands qp, mp, pp, qcq, mcm and pcp were complexed with copper(II) acetate. Mass spectrometry confirmed a ratio of 2 : 2 metal to ligand, and crystallographic studies of $[\text{Cu}_2(\text{mp})_2]^{3+}$ and $[\text{Cu}_2\text{pcp}]^{3+}$ show a dinuclear, double helical structure, with mixed oxidation states Cu(II)Cu(I). Cu(II) is coordinated by two “terpy” domains of two ligand strands, and Cu(I) by two “bipy” domains of the same two ligand strand. In both structures, the ligand strands are arranged in a head-to-tail (HT) fashion based on the metal-metal axis, which makes the identical substituents come close enough for π - π -stacking.

Micro analysis suggests mixed oxidation state complexes with the ligands qp, mp and pp, and mainly

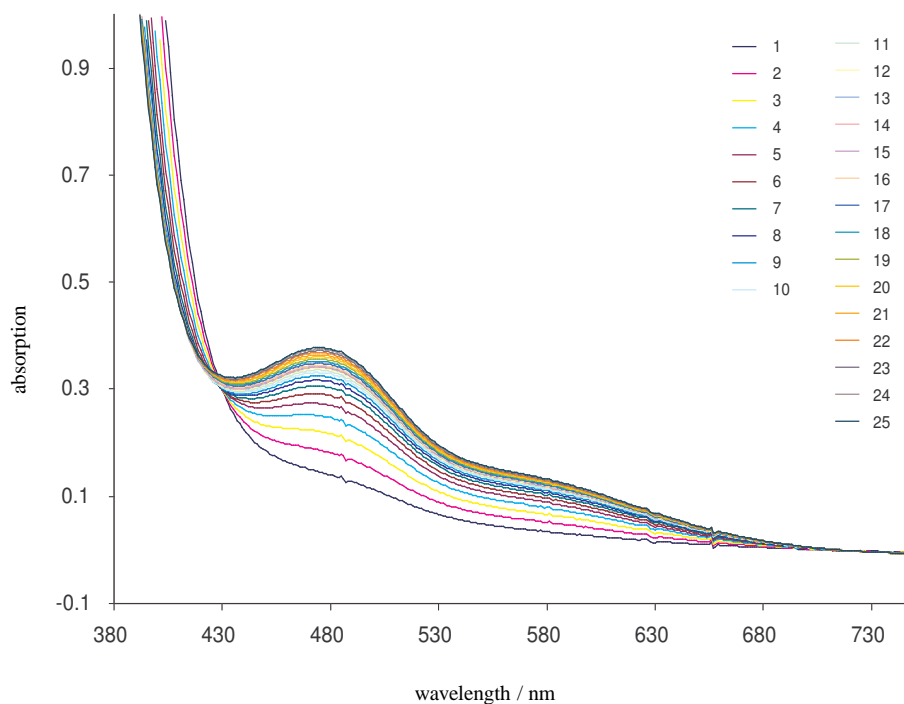
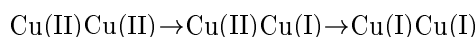


Figure 4.23: Spectroelectrochemistry of $[\text{Cu}_2(\text{mp})_2][\text{PF}_6]_3$ in acetonitrile, applied potential of -400mV : the absorption increases with time.

$\text{Cu}(\text{II})\text{Cu}(\text{II})$ complexes with the ligands qcq, mcm and pcp, which is in contrast to the crystal structure of $[\text{Cu}_2\text{pcp}]^{3+}$. Often when the complexes were synthesised they were green at first, which is typical for the $\text{Cu}(\text{II})\text{Cu}(\text{II})$ species, but turned brown upon standing and upon drying *in vacuo*. Differential pulse voltammetry showed metal centred reductions at 0.14V and -0.43V vs ferrocene, of which the first potential is accessible for the copper centres when the samples are standing unprotected from air.



The UV spectra of all six ligands were recorded. Upon complexation with copper(II), the absorption maxima were red-shifted, and the absorption stayed high to 80nm higher wavelength, instead of decreasing rapidly over the range of the next higher 40nm . This indicates an extended chromophore system. When comparing the spectra of the complexes with each other, an interesting effect was seen at the absorption maximum of $\sim 470\text{nm}$. This absorption was assigned the $\text{Cu}^{\text{I}}(\text{bipy})_2$ chromophore. The molar extinction coefficient of the complexes with non-linked ligands were always smaller by $1600\text{--}1800\text{M}^{-1}\text{cm}^{-1}$. This reflected the amount of reduced copper ($\text{Cu}(\text{I})$), that is present in the helicates.

With spectroelectrochemical measurements, the increase and decrease of the absorption in the visible region was observed. By applying a constant potential of $+800\text{mV}$ and then of -400mV for $[\text{Cu}_2(\text{mp})_2][\text{PF}_6]_3$, and $+1100\text{mV}$ and -100mV for $[\text{Cu}_2\text{pcp}][\text{PF}_6]_3$, full oxidation and full reduction of the mixed valence compounds were reached: $\text{Cu}(\text{II})\text{Cu}(\text{I}) \rightarrow \text{Cu}(\text{II})\text{Cu}(\text{II})$, and $\text{Cu}(\text{II})\text{Cu}(\text{I}) \rightarrow \text{Cu}(\text{I})\text{Cu}(\text{I})$. The loss of absorption when oxidising, and the gain in absorption when reducing the compounds confirmed the assignment to complexed $\text{Cu}(\text{I})$, and it also confirmed the state of mixed oxidation that the complexes of the non-linked ligands adopted in ambient conditions, and in absence of any applied electrical field.

The $^1\text{H-NMR}$ spectra suggest very similar solution structures for all six complexes, but they are simpler for the complexes of linked ligands. These results may be interpreted as follows: Because of the result of the crystal structures and the spectroelectrochemistry, one may assume that the mixed valence

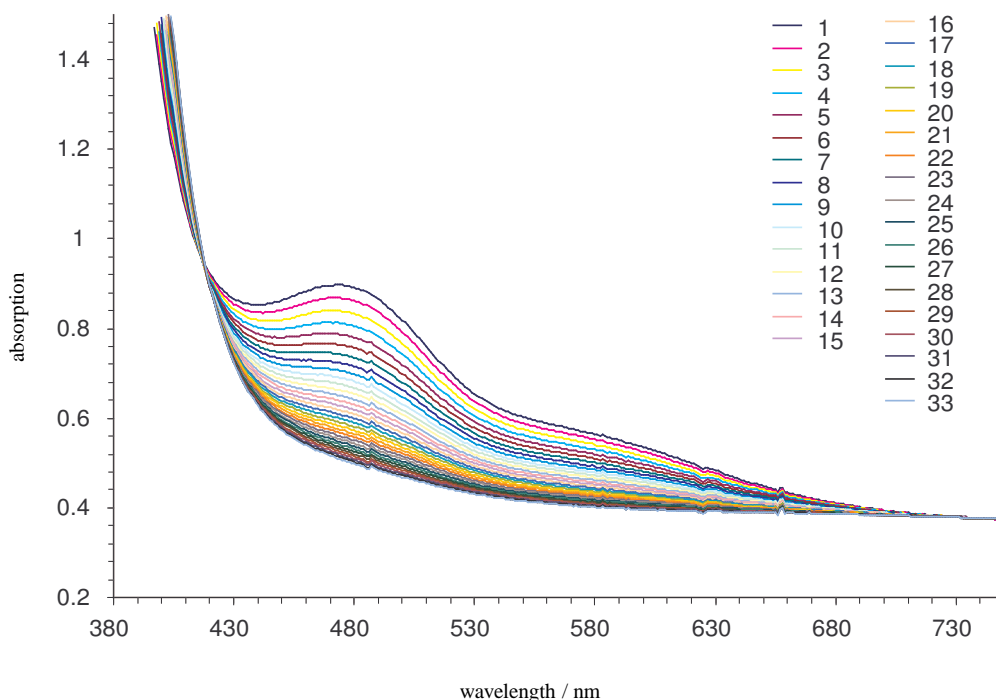


Figure 4.24: Spectroelectrochemistry of $[\text{Cu}_2\text{pcp}](\text{PF}_6)_3$ in acetonitrile, applied potential of +1100mV: the absorption decreases with time.

dinuclear helical structure is preserved in solution. From the crystal structures it is clear, that the coordinative bond of the middle pyridine ring (C and C') to the octahedral copper(II) centre are the longest, and thus weakest. These nitrogen donor atoms N_C and N' are not extremely far from to the tetrahedrally bound copper(I), the distance to the tetrahedral centre being 3.132/2.973 Å, and to the octahedral centre 2.243(3)/2.356(3) Å in the solid for $[\text{Cu}_2(\text{mp})_2]^{3+}$. For $[\text{Cu}_2\text{pcp}]^{3+}$ the distances for the central pyridine nitrogen to the tetrahedral metal centre are 3.150/3.101 Å, and to the octahedral 2.240(3)/3.101(3) Å. In solution, maybe the middle nitrogen donor atoms of $[\text{Cu}_2\text{pcp}]^{3+}$ fluctuate between bonding the two copper centres, or switch the metal they coordinate to, in the time scale of vibration in the molecule. This would reinstate the symmetry of the complex by making the metal centres equal, at least on NMR timescale, and it would reduce the number of signals in the $^1\text{H-NMR}$ spectra. However it is not clear why this should only happen in the complex of the linked ligand. A second explanation suggests that the number of isomers in solution is limited by the steric requirements of the linker. In a head-to-head (HH) arrangement of a dinuclear double helicate, the linker would be stretched, and unflexible, while in the head-to-tail (HT) isomer, the linker would be much more free. It is thus possible, that in solution, complexes of the *non-linked* ligands occur as a mixture of HH^1 , HH^2 and HT (see Figure 1.9) of dinuclear double-helical isomers, while complexes of the *linked* ligands occur predominantly as the HT dinuclear double-helical isomer. Both alternative explanations would fit with the experimental findings. The crystal structures of $[\text{Cu}_2(\text{mp})_2]^{3+}$ and $[\text{Cu}_2\text{pcp}]^{3+}$ were considered a great success, because the structure of a double helicate, in which the oligopyridine ligand strands are inter-connected, is unique, and the crystal structure proves their existence in a proposed dinuclear, double helical arrangement.

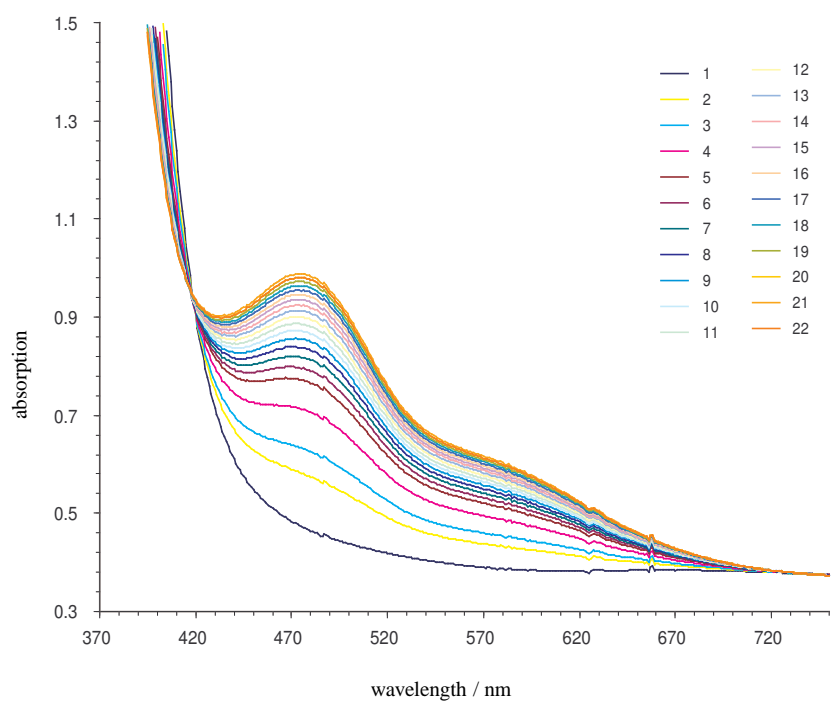


Figure 4.25: Spectroelectrochemistry of [Cu₂pcp][PF₆]₃ in acetonitrile, applied potential of -100mV: the absorption increases with time.

4.3 Cobalt complexes

4.3.1 Synthesis and characterisation of mononuclear complexes

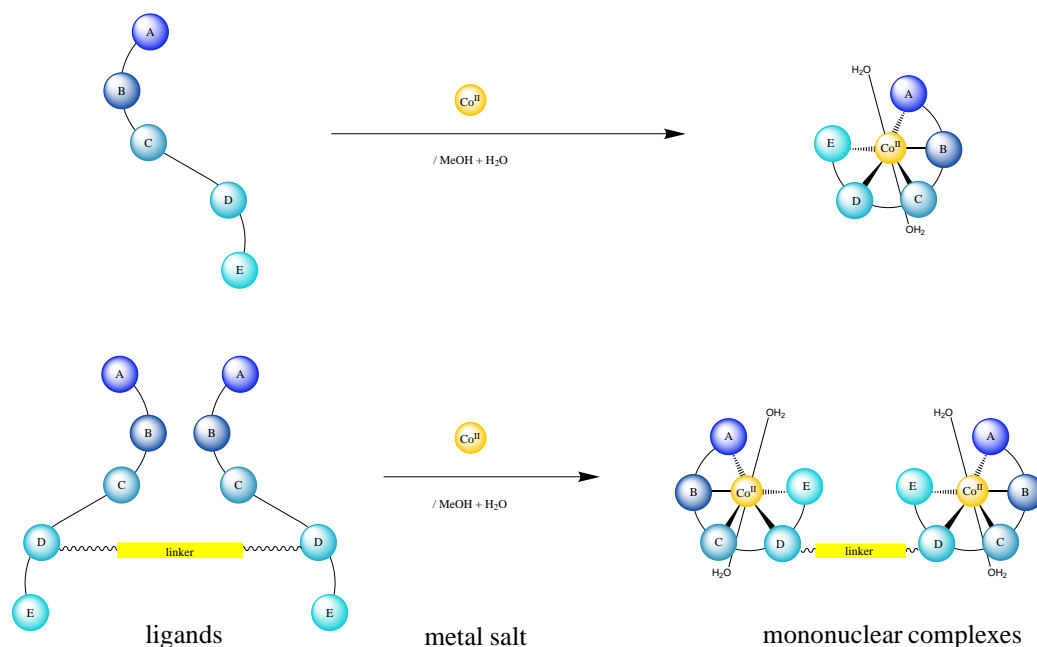


Figure 4.26: Formation of mononuclear complexes with an unsymmetrical qnpy derivative and with an unsymmetrically linked qnpy derivative.

$[\text{Co}(\text{mp})(\text{OH}_2)_2][\text{PF}_6]_2$

The procedure of Whall⁵¹ was followed. Cobalt(II) acetate tetrahydrate and ligand (mp) were mixed in methanol, metal to ligand were in a ratio of 1 : 1, to give an orange solution. Ammonium hexafluorophosphate was added in excess as a solution in methanol, and a golden precipitate formed. It was filtered off, washed with ice-cold methanol and dried *in vacuo* to give an orange powder, contaminated with ammonium hexafluorophosphate. ¹H-NMR and electrospray MS were measured. The ¹H-NMR spectrum was very characteristic for mononuclear qnpy cobalt(II) complexes (see Figure 4.27, 4.28 and the discussion in the next section). The mass spectrum showed signals for (M+Na)⁺, (M-PF₆-2H₂O)⁺, (M-2PF₆)⁺ and (M-H₂O-2PF₆)⁺. Infrared spectroscopy gave a spectrum that was very similar to the spectrum of the dinuclear compound. The main absorptions were located at equal wavenumbers. A microanalysis confirmed excess nitrogen. In order to purify the sample, it was washed with methanol, but this only diminished the yield to 1.7mg.

$[\text{Co}_2(\text{qcq})(\text{OH}_2)_2(\text{MeOH})_2][\text{PF}_6]_4$

The procedure of Whall⁵¹ was followed. Cobalt(II) acetate tetrahydrate and linked ligand (qcq) were mixed in methanol, metal to ligand were in a ratio of 2 : 1, to give an orange-brown solution. Ammonium hexafluorophosphate was added in excess as a solution in methanol, and a golden precipitate formed. It was filtered off, washed with ice-cold methanol and dried *in vacuo* to give an orange powder in 69% yield. Micro analysis, ¹H-NMR and Electrospray MS were measured. The microanalysis fitted a formula: [Co₂(qcq)(OH₂)₂(MeOH)₂][OAc][PF₆]₃ · H₂O · $\frac{1}{4}$ PF₆ and the ¹H-NMR spectrum was very characteristic for mononuclear qnpy cobalt(II) complexes (see Figure 4.29 and the discussion in the next section). The mass spectrum showed signals for (Co₂(qcq)+K+PF₆)⁺, (Co₂qcq(MeOH)₂+2PF₆)⁺,

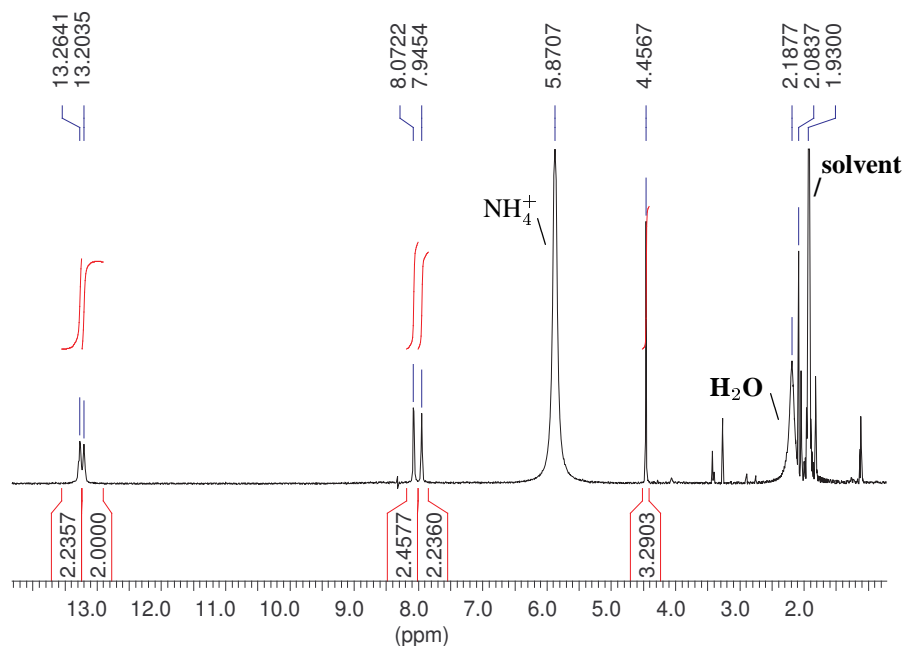


Figure 4.27: 600 MHz $^1\text{H-NMR}$ spectrum of $[\text{Co}(\text{mp})(\text{OH})_2][\text{PF}_6]_2$ in acetonitrile- d_3 , the region of least shifted protons.

$(\text{M}-3\text{PF}_6+\text{H}_2\text{O})^{2+}/2$, $710 (\text{Co}_2\text{qcq}(\text{MeOH})+2\text{Na}+3\text{PF}_6)^{3+}/3$. Infrared spectroscopy gave the typical spectrum for the ligand qcq (C-H bands at $2955\text{-}2870\text{cm}^{-1}$) and the mononuclear mp-complex (absorptions between 1099 and 1362 , the two bands at 1202 and 1013cm^{-1} , plus a very intense absorption band for the P—F bond of the counter ion at 827cm^{-1} . But there is also a medium strong, relatively broad band at 1115cm^{-1} typical for C-N and C-O stretch bonds, only present in this spectrum.

$^1\text{H-NMR}$ chemical shifts of mononuclear complexes Potts *et al.* displayed the region 0-140ppm for illustration of the spectrum of the mononuclear species $[\text{Co}(\text{ps}_2\text{qnp})\text{X}_2][\text{PF}_6]_2$.⁶⁸ The same pattern is seen for the mononuclear complexes of cp_2qnp , tpb_2qnp , and similar ones for the unsymmetrical qp^{51} and qcq and new ligand mp , see Figures 4.27, 4.28, 4.29 and Table 4.15. A $^1\text{H-NMR}$ study of $[\text{Co}(\text{qnp})\text{X}_2][\text{PF}_6]_2$, $[\text{Co}(\text{cp}_2\text{qnp})\text{X}_2][\text{PF}_6]_2$, $[\text{Co}(\text{ph}_2\text{qnp})\text{X}_2][\text{PF}_6]_2$ and $[\text{Co}(\text{ps}_2\text{qnp})\text{X}_2][\text{PF}_6]_2$ (X is Cl^- or a solvent molecule) show the characteristic pattern with a broad signal shifted low field to $\sim 133\text{ppm}$, and a group of four signals at δ 81.3, 77.9, 75.6 and 69.9. Then there is one signal at 22-25 ppm, the $4''$ signal at $\sim 20\text{ppm}$ and the substituent signals. In the case of $\text{Co}(\text{qnp})$ there is the $4'$ -H signal at $\sim 21\text{ppm}$ as well.^{66, 68, 121}

Whall compared $^1\text{H-NMR}$ spectra of a series of mononuclear cobalt(II) complexes of qnp ligands with planar cobalt(II) complexes of qtpy .^{51, 72, 73, 122} As a result of this, it was possible to distinguish between the signals originating from pyridine and from phenyl in the complexes and tentative assignments could be made to which pyridine ring the resonances belonged, for the complexes with the symmetrically substituted qnp ligands tpb_2qnp , cp_2qnp and hp_2qnp as well as with the unsymmetrically substituted qnp ligands tbpcqnp and qp . $\text{H}_{\text{C}4}$ could be assigned on the basis of it being only half the intensity of the other pyridine signals.

The spectra for the complexes with the unsymmetrically substituted showed a splitting of the signals for B3/B5 and D3/D5 centred at 75ppm and 73ppm. In the mononuclear complexes of mp and qcq , this splitting is also seen. But the overall pattern is identical for all the measured complexes, see Figures 4.27, 4.28 and 4.29, and Table 4.15.

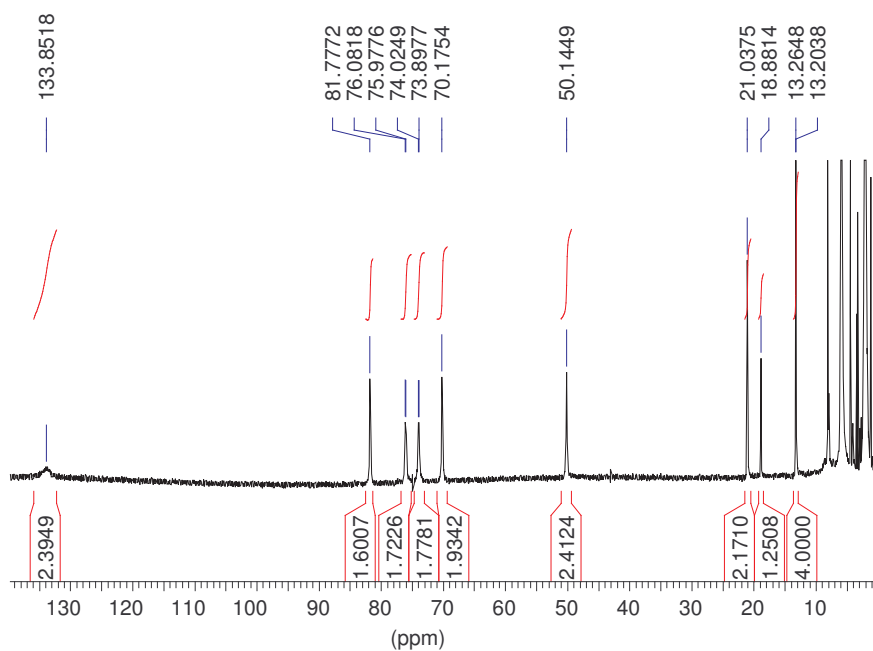


Figure 4.28: 600 MHz $^1\text{H-NMR}$ spectrum of $[\text{Co}(\text{mp})(\text{OH}_2)_2][\text{PF}_6]_2$ in acetonitrile- d_3 , the farthest low-field shifted signal still detectable is at $\sim 140\text{ppm}$.

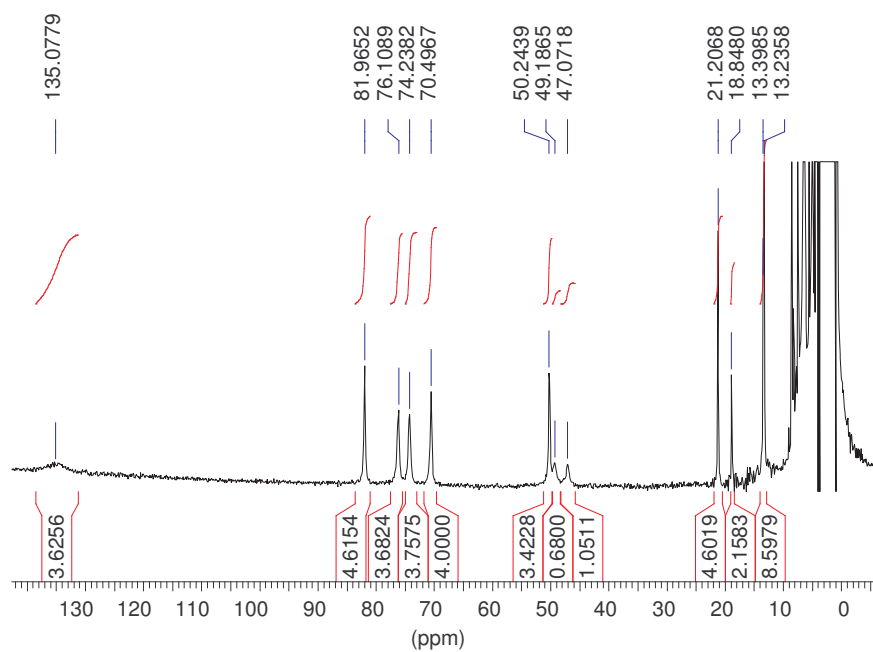


Figure 4.29: 250 MHz $^1\text{H-NMR}$ spectrum of $[\text{Co}_2(\text{qcq})(\text{OH}_2)_2][\text{PF}_6]_4$ in acetonitrile- d_3 , the farthest low-field shifted signal still detectable is at $\sim 140\text{ppm}$.

Ligand	Pyridine ring protons, 7 x 2H / 4H intensity for qnpy / linked qnpy							1H / 2H	Phenyl protons 8H/16H		Substituent / H _{B4,D4}
qnpy	135	80.8	76.6	75.0	69.6	49.9	21.5	19.0	-	-	20.1
cp ₂ qnpy	134	80.5	74.1	72.5	69.4	49.4	20.8	18.7	13.1	8.5	-
tbp ₂ qnpy	134	80.8	75.4	73.6	69.9	49.9	21.0	18.8	13.1	8.6	2.1
hp ₂ qnpy	133	81	76	74	69	50	21	19	14	8	-
tbpcpqnpy	134	81.3	75.6 74.7	73.8 72.9	70.0	50.1	21.1	18.9	13.1	8.5	1.8
qp	133	81.4	75.8 75.5	73.8 73.5	69.6	49.9	21.0	18.9	13.2	8.5 7.9	2.1
qcq	135	82.1	76.3	74.4	70.7	50.4 47.5	21.2	18.9	13.4 13.2	8.5 8.1	7.5-0.8 (m)
dop ₂ qnpy	133	81.4	75.7	73.7	69.9	49.9	21.0	18.9	13.2	8.1	9.2-0.9 (m)
mp	134	81.8	76.1 76.0	74.0 73.9	70.2	50.1	21.0	18.9	13.3 13.2	8.1 7.9	4.5
Assignment	A/E ring	A/C/E ring	B/D ring		A/C/E ring	A/E ring	A/E ring	C4	phenyl ortho	phenyl meta	Substituent / H _{B4,D4}

Table 4.15: Seven coordinate cobalt(II) complexes with pentadentate qnpy ligands, and two water or solvent molecules coordinated in axial positions.^{51,67}

4.3.2 Synthesis and characterisation of dinuclear complexes

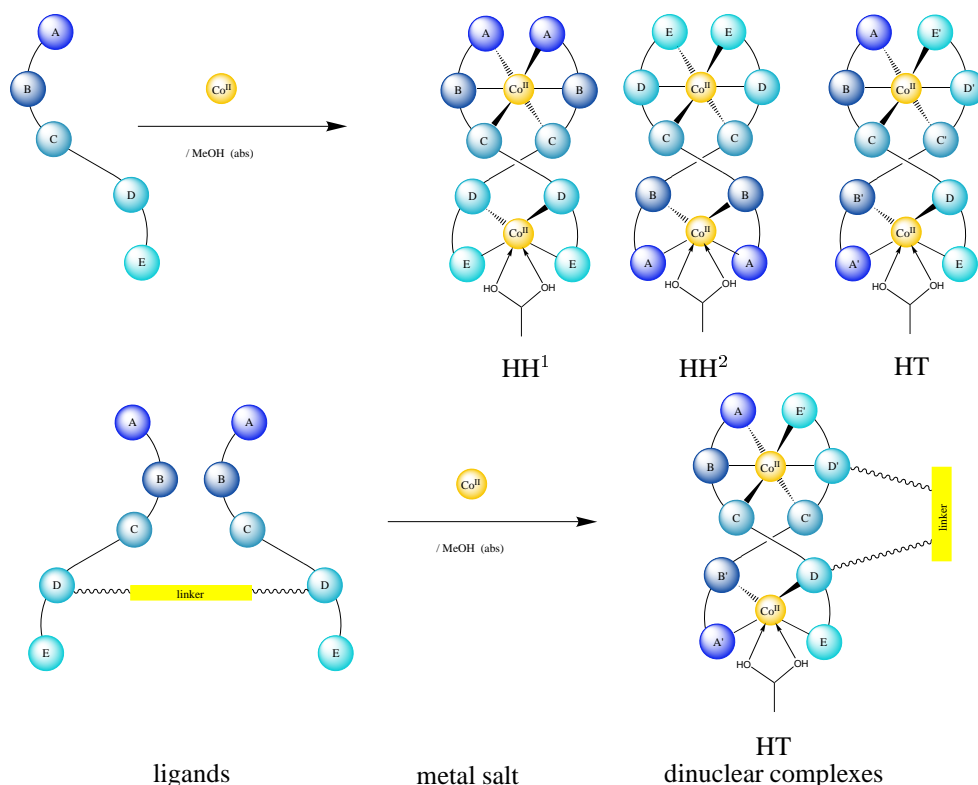


Figure 4.30: Formation of dinuclear complexes with an unsymmetrical qnpy derivative and with an unsymmetrically linked qnpy derivative. With the former, two head-to-head (HH) and one head-to-tail (HT) isomer are possible. With the latter, probably only the HT isomer exists.

$[\text{Co}_2(\text{qcq})(\text{OAc})][\text{PF}_6]_3$

Complex formation was attempted under anhydrous conditions in dry methanol, following Wards⁵¹ procedure. As it was not yet known how very sensitive the complex formation react on water, the complex of qcq was made with pink tetrahydrate metal salt. $\text{Co}(\text{II})$ acetate $\cdot 4\text{H}_2\text{O}$ and ligand were mixed in dry methanol in a ratio of 2 : 1. A brown-orange solution formed. Excess ammonium hexafluorophosphate was added, and a brown precipitate formed. It could be filtered off, washed with methanol and dried *in vacuo* to give 66% product. It was characterised with ^1H -NMR spectroscopy. The spectrum was typical for dinuclear cobalt(II) complexes of qnpy, but showed that also the mononuclear species, that was discussed above, was present, see Figure 4.31 and the discussion in the next section). Instead of adding ammonium hexafluorophosphate, once sodium tetraphenylborate was added instead, in the hope of growing crystals for X-ray diffraction measurements. This gave also a brown powder, and it was characterised by ^1H -NMR and Maldi-TOF mass spectrometry. It showed the core of $[\text{Co}_2\text{qcq}(\text{OAc})]'$ with different additional molecules and ions: $(\text{Co}_2\text{qcq}(\text{OAc})_2 + \text{MeOH})^+$, $(\text{Co}_2\text{qcq}(\text{OAc}) + (\text{H}_2\text{O}))^+$, $(\text{Co}_2\text{qcq}(\text{OAc}))^+$.

$[\text{Co}_2(\text{mp})_2(\text{OAc})][\text{PF}_6]_3$

When the dinuclear cobalt(II) complex with mp was synthesised, it had become clear how very sensitive the complex formation was to the presence of water, and not only the methanol and ligand were dried prior to reaction, also the crystal water from the metal salt was removed. It was dried during three hours at 60°C *in vacuo*, the colour changed from pink to blue, and the IR spectrum confirmed that it was water

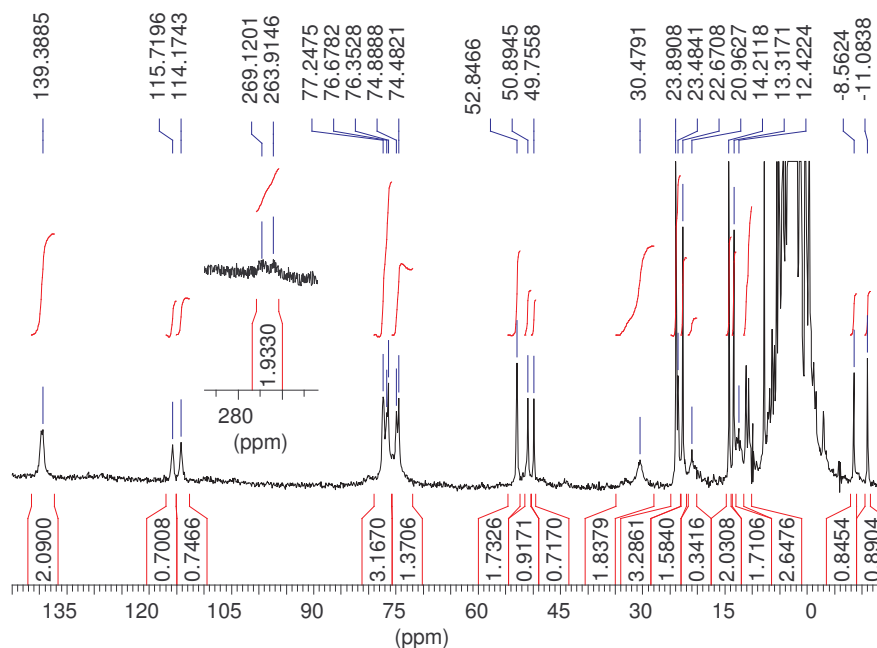


Figure 4.31: 250 MHz ^1H -NMR spectrum of the dinuclear double helicate $[\text{Co}_2(\text{qcq})(\text{OAc})][\text{PF}_6]_3$ in acetonitrile- d_3 , the farthest low-field shifted signal still detectable is at ~ 270 ppm. Additionally, mononuclear compound is present in this sample.

free. The metal salt and ligand were mixed in the dry methanol in a ratio of 1 : 1 under inert atmosphere. A brown solution formed, and dry ammonium hexafluorophosphate was added in excess. A brown precipitate formed and could be filtered off and dried *in vacuo* to give the product as a brown powder in 61% yield. It was characterised by ^1H -NMR, IR spectroscopy, cyclic voltammetry and differential pulse voltammetry. The ^1H -NMR spectrum was typical for dinuclear cobalt(II) qnpy complex, see Figure 4.32 and the discussion in the next section). When the solution in the plastic capped NMR tube was measured again two days later, the signals in the regions of 142-132 and 67-82 ppm showed mononuclear compound in similar intensity to original dinuclear compound. In the IR, the acetato auxiliary ligand would show by the ν_{asym} at 1597cm^{-1} , but coincides with 4-substituted pyridine ring signals,⁹⁸ and PF_6^- shows at 825cm^{-1} , see Nakamoto,¹²³ volume B, chapter III-8 on pages 60 and 271. The electrochemical measurements gave similar results to those of dinuclear cobalt(II) double helicate of ms_2qnpy (see discussion of electrochemical measurements on page 113).

^1H -NMR chemical shifts of dinuclear complexes: A plot of the spectrum of the $[\text{Co}_2(\text{ph}_2\text{qnpy})_2(\text{Solv})_2][\text{PF}_6]_4$ with a trace of the mononuclear complex was reported by Walker.⁹¹ The chemical shifts of this compound is listed in Table 4.16. The resonance shifted furthest to low field at 262ppm is very broad. The lower symmetry of the dinuclear helicate compared with the mononuclear, gives rise to double the number of proton signals that are expected for the mononuclear species. Whall compared the double helical complexes of the symmetric ligands cp_2qnpy , tbp_2qnpy and and unsymmetric ligand tbpcpqnpy . Some signals from the symmetrical ligands are split up in the complexes of the unsymmetrical. The same is happening with the dinuclear cobalt(II) complex of the new qnpy ligand mp:

- The two complexes of symmetrical ligands tbp_2qnpy and cp_2qnpy gave only one signal at 268.5 and 263.0ppm respectively. In the complex of the unsymmetrically substituted ligand tbpcpqnpy , it is split into four signals at 275.3, 268.7, 264.8 and 259.0ppm. In the complex of the new unsymmetrically substituted ligand mp, they are also split into four signals: 266, 162, 261 and 256ppm.

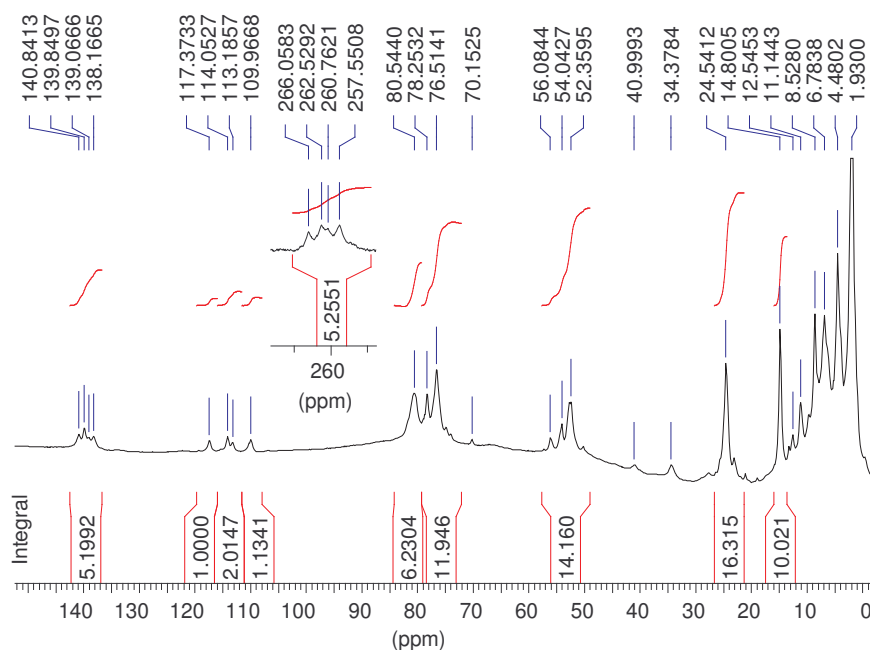


Figure 4.32: 600 MHz ^1H -NMR spectrum of $[\text{Co}_2(\text{mp})_2(\text{OAc})][\text{PF}_6]_3$ in acetonitrile- d_3 , the farthest low-field shifted signal still detectable is at $\sim 270\text{ppm}$.

- The complexes of the symmetrically substituted ligands give only one signal at 141.0 and 138.6ppm respectively. In the complex of the unsymmetrically substituted ligand *tbcpqnp*, it is split up into three signals at 140.0, 139.1 and 137.9ppm with a 1:1:2 ratio of intensities. In the complex of the new unsymmetrically substituted ligand *mp*, they are split into four signals at 141, 140, 139 and 138ppm with similar intensities.
- The signals at: 117.1 and 117.4ppm are split into 121.9, 116.1, 115.7 and 111.1ppm in the complex of *tbcpqnp*, and 117, 114, 113 and 110ppm for the new complex of *mp*.
- The signals at 80.8 and 90.8 for the complex of the symmetrically substituted ligands becomes a multiplet for both complexes of unsymmetrically substituted ligands *tbcpqnp* and *mp*.
- Then there are two signals, that only occur in the complexes of symmetrically substituted ligands: 78.1 and 76.1ppm for *tbp₂qnp* and 83.7 and 74.1ppm for *cp₂qnp*.
- The signals at 71.3 and 51.5ppm respectively give a signal at 69.9 for the complex of *tbcpqnp* and a signal at 70.2 for the complex of *mp*. The signals at 53.5 and 52.8ppm respectively give a multiplet for both complexes of unsymmetrically substituted ligands.
- Then there is a signal again, which is unique for the complexes of symmetrically substituted ligands at 52.1 and 51.7 ppm respectively.
- The signals at 30.1 and 27.7ppm are split up for the complex of *tbcpqnp* into the four signals 32.2, 30.7, 28.2, 27.1ppm. The spectrum of the *mp*-complex however shows only one small, broad signal at 34.4.

In the region to high field of 27ppm signals for phenyl and pyridine protons are found, and some are overlapping:

- The two complexes of the symmetrically substituted ligands *tbp₂qnp*/*cp₂qnp* show pyridine signals at: 25.9/20.8, 13.7/18.7, 7.7/7.3, -1.7/-2.7 and -8.5/-9.5ppm. Corresponding to this, the

complex of tbpcqnpny show signals centred at similar chemical shifts, but split up: 25.9, 25.5, 25.2ppm (in a ratio of 1H : 1H : 2H), 14.4, 14.1ppm (in a ratio of 2x2H), 7.1, 6.9, 6.6, 6.4ppm (in a ratio of 4x1H), 1.3, 1.1, 1.0ppm (in a ratio of 1H : 2H : 1H), and -7.4, -8.1, -8.4, -9.5ppm (in a ratio of 4x1H). The complex of mp show only a signal at 34.4ppm, and it may contain pyridine and also phenyl protons, two signals 14.8 and 12.5ppm, that may correspond to the two pyridine signals of the tbpcqnpny complex of 2H intensity each centred at 14ppm. Then there is only a multiplet from 11.1 to 0.0ppm.

- Of the complexes of tbp_2qnpny , cp_2qnp and tbpcqnpny , phenyl signals were assigned: For the complexes of the symmetrical ligands they were at 24.9/24.7, 15.8/15.7, 6.7/7.3, 5.9/5.3ppm and for tbp_2qnpny the *tert*-butyl group gave signals at 5.9 and 1.2ppm (with 9H intensity each). The complex of the asymmetrically substituted ligand tbpcqnpny gave again signals that were split up: 24.3, 24.0 and 23.7 (in a ratio of 2H : 4H : 2H), 15.8, 15.5 and 15.1 (in a ratio of 2H : 2H : 4H), 8.5 and 8.4 (in a ratio of 4H : 4H), 5.9 and 5.8 (in a ratio of 4H : 4H), and finally 2.1ppm for the substituent.

Also in the complexes with cobalt(II), at least two alternatives explain the splitting in the mononuclear, that disappears for the dinuclear. It may be that fluctuation occurs, or it may be the different number of isomers. The distance from the nitrogen donor atom of the central rings in $[\text{Co}_2(\text{qnp})_2(\text{OAc})]^{3+}$,⁴² is 1.3Å, but this distance may of course be less in the acetonitrile solutions of the complexes with linked ligand qcq , that was measured.

In the case of HH isomers, the arrangement of the two ligands in the complex ion is symmetrical, and the protons are in equal environment. In the case of double helical HT complexes however, each proton is in a unique environment. Cobalt(II) double helicates of the 4',4'''-disubstituted qnpny ligands compared with each other by Whall⁵¹ gave 30 (HT) and 15 (HH) pyridine signals, respectively. The ¹H-NMR of $[\text{Co}_2(\text{tbpcqnpny})_2(\text{Solv})_2][\text{PF}_6]_4$ in acetonitrile solution contained 60 pyridine protons which were present in 34 separate environments, 32 phenyl protons in 10 separate environments, and 36 substituent protons as a singlet. A maximum for one pure HT isomer would be 30 separate pyridine protons, 16 phenyl protons and 18 protons from the *t*-Bu substituent. It was concluded that a statistical 1:1:2 mixture of double helical $\text{HH}^1:\text{HH}^2:\text{HT}$ isomers of $[\text{Co}_2(\text{tbpcqnpny})_2(\text{Solv})_2]^{4+}$ was present in the measured acetonitrile solution. Four distinct ligand environments in these isomers gave rise to four sets of signals, one each for the HH isomers and two for the HT isomer. The same conclusion that $\text{HH}^1 : \text{HH}^2 : \text{HH}$ are present in a statistical mixture, giving the ratio 1 : 1 : 2, can then be made for the new complex cation $[\text{Co}_2(\text{mp})_2(\text{OAc})]^{4+}$.

Comparing the two spectra of complexes with unsymmetrically substituted ligands tbpcqnpny and mp with the spectrum of the complex of the unsymmetrically linked ligand qcq ($[\text{Co}_2(\text{qcq})(\text{OAc})]^{3+}$), it is apparent that in the complex of the linked ligand, the signals split up differently, see Figure 4.31 and Table 4.16.

- Where there were four signals for the complexes of $\text{tbpcqnpny}/\text{mp}$ centred at 266/262ppm there are only two at 269 and 264ppm.
- Where there were four signals centred at 139/140ppm there are only two at 140 and 139ppm.
- Where there were four signals centred at 116/114ppm, there are only two at 116 and 114ppm.
- The multiplet in the complexes of $\text{tbpcqnpny}/\text{mp}$ centred at 78/78ppm is split up into into four individual signals at 77.2, 76.4, 74.9 and 74.5ppm.
- The signals at 69.9/70.2ppm is missing in the complex of qcq
- The multiplet centred at 54/53ppm is split up into three signals 52.8, 50.9 and 49.8ppm with intensities of (2H : 1H : 1H).
- Like in the complex of mp (34.4ppm) there is only one signal at 30.5ppm, opposed to four signals in the complex of tbpcqnpny .

- The resolution is not so high in the spectra of the new complexes with mp and qcq, but by comparison with the complex of tbpcqnpq and mp, the signals of the qcq-complex at 23.9, 23.4 and 22.7 may be assigned as phenyl proton resonances and 14.2, 13.3 and 12.4 as pyridine proton resonances. But of course, with all the protons of the linker, there is a multiplet from 10.0-(-5.0)ppm.
- Like in the complex of tbpcqnpq, the spectrum of the qcq-complex show resonances in the negative ppm area. Two signals of equal intensity at -8.6 and -11.0ppm.

As the signals, although with different splitting, are centred at the same chemical shifts for all the discussed dinuclear complexes, they are most likely all double helical like the complex of the parent ligand qnpq. Some of the split up signals are reduced again from four to two in the linked ligand complex compared to the non linked, unsymmetrical ligand complexes (see the first three points discussed above). There are two possible explanations for this. Either there exists a mixture of the HH¹ and HH² isomers in the solution, or there is only the HT isomer present. Both possibilities would explain the resolution of the multiplets discussed in points 4, 6 and 8. When drawing a three-dimensional model of the double helical complex, the head-to-tail isomer has more possibilities to arrange the linker in a relaxed conformation, while the linker becomes stretched in the head-to-head isomers. It is therefore likely, that the latter explanation is more realistic, and that complex cation [Co₂(qcq)(OAc)]³⁺ exists solely as the HT isomer.

The four signals at lowest field (around 270ppm) in the beforementioned complexes are similar to shift to those observed in cobalt(II) complexes of sexipyridine ligands. It may therefore be assumed, that these signals from the qnpq derivative complexes belong to the “Co(terpy)₂” end of the double helicates.^{51,124} It is also likely that they belong to the A6/E6-position of the rings, due to the juxtaposition with the paramagnetic Co centre. The four signals at 266, 262, 261 and 256ppm in the spectrum of [Co₂(mp)₂(OAc)₂][PF₆]₃ thus may represent the protons A6, A6' of HH¹, E6, E6' of HH² and A6, E6' of the HT isomer. The two signals at 269 and 264ppm in the spectrum of [Co₂(qcq)(OAc)₂][PF₆]₃ may represent the protons A6 and E6' or the HT isomer, see ligand diagrams for labelling in Figure 2.3 and 3.3 and Table of chemical shifts 4.16.

Conclusion The ¹H-NMR spectra of the mononuclear and dinuclear complexes are very different and significant for the different solution structures. Comparison of the spectra of *mononuclear complexes* with varying substituents in the 4',4'''- position, including the new ligand mp and the linked ligand qcq, show almost no differences. The signals are not split up for complexes of unsymmetrically substituted ligands compared to symmetrically substituted ligands.

The ¹H-NMR spectra of *dinuclear complexes* with varying substituents in the 4',4'''- position, including the new ligand mp, are also very similar to each other. But the spectra of the complexes that are unsymmetrically substituted give rise to splitting of the signals possible, depending on the number of isomers present in solution. In the spectra of complexes with non-linked ligands, a statistical mixture is present, while the spectrum of the complex of the linked ligand qcq show that there may be fluctuation going on or that the number of isomers is reduced to the HT (or possibly to two HH) isomer.

[Co ₂ qcq(OAc)][PF ₆] ₃	[Co ₂ (mp) ₂ (OAc)][PF ₆] ₃	[Co ₂ (tbpcqnpq) ₂ (OAc)][PF ₆] ₃		
pyridine		pyridine	intensity	
269, 264	266, 162, 261, 256	275, 269, 265, 259	4 x 1H	60 H
140, 139	141, 140, 139, 138	140, 139, 138	1H 1H 2H	
116, 114	117, 114, 113, 110	122, 116.1, 115.7, 111	4 x 1H	
77.2, 76.4, 74.9, 74.5	80.6-74.0 (m)	83.0-72.7 (m)	12H	
	70.2	69.9	4H	
52.8, 50.9, 49.8	56.1-50.0 (m)	55.3-52.6 (m)	8H	
30.5	34.4	32.2, 30.7, 28.2, 27.1	4 x 1H	
mixed pyridine and phenyl signals				
23.9, 23.4, 22.7	24.5 (phenyl)	25.9, 25.5, 25.2	1H 1H 2H	
14.2, 13.3, 12.4	14.8, 12.5 (pyridine)	14.4, 14.1	2 x 2H	
10-(-5) (m)	11.1-0.0 (m)	7.1, 6.9, 6.6, 6.4	4 x 1H	
		1.3, 1.1, 1.0	1H 2H 1H	
-8.6, -11.0		-7.4, -8.1, -8.4, -9.5	4 x 1H	
		phenyl		32 H
		24.3, 24.0, 23.7	2H 4H 2H	
		15.8, 15.5, 15.1	2H 2H 4H	
		8.5, 8.4	4H 4H	
		5.9, 5.8	4H 4H	
		substituent		36H
		2.1	36H	

Table 4.16: Pattern of the chemical shift in the ¹H-NMR spectra of dinuclear cobalt(II) complexes with unsymmetrical qnpq ligands. The pattern consists of well resolved peaks between 270ppm and 30pp: In this region the pattern for the complex with qcq is simpler than the pattern of the complex with mp and with tbpcqnpq. Between 30ppm and 0ppm there is overlap of the pyridine ring signals with the phenyl ring signals. The spectra of the qcq- and tbpcqnpq-complexes were recorded well below 0, and there are only two signals for the qcq complex whereas there are four signals for the tbpcqnpq complex.

Interconversion between the di- and mononuclear complexes

The difference in synthesis of mononuclear and dinuclear cobalt(II) complexes discussed above, shows that the presence or absence of water is crucial to which of the complexes is formed.

Whall already did two experiments to show interconversion from the dinuclear complex $\text{Co}_2(\text{tp}_2\text{qnp}_2)(\text{OAc})^{3+}$ to the mononuclear complex $\text{Co}(\text{tp}_2\text{qnp}_2)\text{X}_2^{2+}$. In the first experiment, she synthesised the dinuclear complex, but before precipitating it, she doubled the solution volume with water. After that she precipitated and characterised what turned out to be exclusively the mononuclear complex. In a second experiment she observed and recorded by $^1\text{H-NMR}$ spectroscopy, the change that occurred in the structure of the same dinuclear complex, by adding a drop of D_2O to a solution in acetonitrile- d_3 , and recording spectra at regular intervals.⁵¹

When one drop of D_2O was added to a solution of the dinuclear complex $\text{Co}(\text{tp}_2\text{qnp}_2)_2\text{X}_2^{2+}$ in acetonitrile- d_3 the solution composition changed from an initial ratio of 4:1 dinuclear : mononuclear complex to a ratio of 1:4 dinuclear : mononuclear species over a period of an hour. Additionally a new double helical species seemed to form, because a change in chemical shift for the signals originating from the dinuclear complex was observed. Most of the signals shifted downfield, but the signal at 269 was shifted upfield to 266 ppm and the signals at 53.5 and 52.1 ppm were shifted upfield too, to 50.2 and 46.9 ppm. Possibly the new dinuclear complex had replaced the bidentate auxiliary acetato ligand with acetonitrile- d_3 or water molecules. This new dinuclear species may act as an intermediate in the pathway from the original double helical dinuclear form to the mononuclear form, but it also appeared to be an independently stable solution species.

The result of this NMR experiment demonstrated that water need not be present in huge excess to effect the transition from dinuclear to mononuclear forms. This explained why the dinuclear form is often hard to obtain without at least traces of the mononuclear species. When Whall recorded the $^1\text{H-NMR}$ spectrum of the cobalt(II) complexes of tbpcqnp_2 and tbphpqnp_2 , the dinuclear form was even harder to obtain, and the purest dinuclear form she got with tbpcqnp_2 was a 6 : 1 mixture of dinuclear : mononuclear, and for tbphpqnp_2 a 1 : 1 mixture of the dinuclear : mononuclear complex.

When the dinuclear complex changes into two mononuclear complexes, for the individual ligand strands two things change. Judging by the crystal structure of the double helicate⁶⁵ and monohelicate⁶⁷ complex of cp_2qnp_2 (and the other published crystal structures of cobalt(II) qnp_2 type helicates), inside one enantiomer, the torsion angles in any dinuclear double helicates and mononuclear helicates of qnp_2 derivatives most probably all turn in the same direction. But in the latter structural type the overall torsion is less, and the helical pitch of each ligand is reduced upon the transformation from dinuclear double helicate to mononuclear (and slightly helical). The other change is the coordination number of the metal centre from six to seven. A possible mechanism for the transformation from dinuclear double helicate to two mononuclear complexes is the exchange of the acetato ligand with two water molecules and possibly the coordination of one water molecule to the other cobalt centre, followed by separation of the ligand strands, 'relaxation' of the helical twist by reduction of the pitch, while the according nitrogen donor atoms switch the metal they are binding to (see Figure 4.33).

Based on these findings, the new dinuclear complexes of $\text{mp} [\text{Co}_2(\text{mp})_2(\text{OAc})]^{3+}$ and $\text{qcq} [\text{Co}_2(\text{qcq})(\text{OAc})]^{3+}$ were also tested in a $^1\text{H-NMR}$ titration with D_2O . 1-4mg of complex were used and $3\mu\text{L}$ to $50\mu\text{L}$ D_2O . In molar ratio, this means $6 \cdot 10^{-7} - 2 \cdot 10^{-6}$ mol of complex were treated with $1.6 \cdot 10^{-4} - 2.8 \cdot 10^{-3}$ mol D_2O . After addition, the structure of the dinuclear starting compound adjusted rapidly. The main change had taken place before the first measurement could be made, that was started about half a minute after addition and going on for about 2 minutes. Both complexes were obtained once as pure double helical complexes and several times as mixtures with mononuclear complexes, because of the water sensitivity. The titration of both complexes (with mp and qcq), were carried out twice. In each case once with the pure dinuclear complex and once with adding D_2O to the mixed dinuclear/mononuclear complex.

In order to estimate the ratio of dinuclear : mononuclear compound, the integral was taken over the four signals centred at 139ppm for the dinuclear compound and divided by four (for 4H), and the broad signal at 134ppm for the mononuclear compound and divided by two (for 2H, as they probably belong to the A6 and E6 protons).

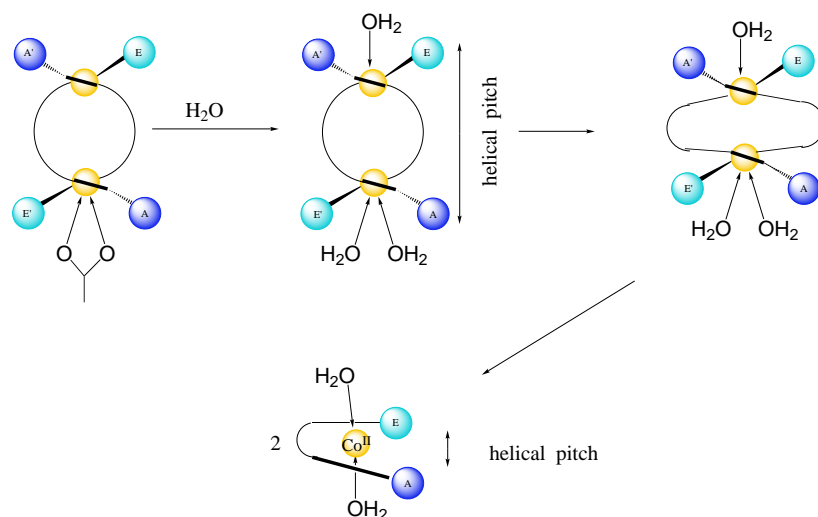


Figure 4.33: A possible mechanism for the transition from dinuclear double helicate to mononuclear helicate.

Experiment 1: NMR-titration of mixed dinuclear/mononuclear complex $[\text{Co}_2(\text{mp})_2(\text{OAc})][\text{PF}_6]_3$ / $[\text{Co}(\text{mp})(\text{OH}_2)_2][\text{PF}_6]_2$ with D_2O : A sample of the dinuclear $[\text{Co}_2(\text{mp})_2(\text{OAc})][\text{PF}_6]_3$ (~1mg, also containing some mononuclear complex) was dissolved in dry acetonitrile- d_3 in an NMR tube. After running the spectrum, one drop of D_2O ($3\mu\text{L}$) was added, and the spectrum between 0 and 150ppm recorded at regular intervals. Now this means that the molar ratio of complex to water was approximately 250:1, although not all complex dissolved. Because of the wide spread signals, the spectra were divided up in four Figures to display four regions of the spectra, see Figures 4.34, 4.35, 4.36 and 4.37. All of these Figures contain the same four spectra. The farthest down-field shifted region displayed in Figure 4.34 are discussed first, followed by the other. The chemical shifts of the original dinuclear species, new (dinuclear) species and mononuclear species are listed in Table 4.17 on page 109.

The first spectrum shown in the Figures was taken before addition of D_2O , and it shows that quite an amount of mononuclear complex is present (signal at 134ppm) along with the dinuclear complex that was to be studied. The second spectrum was recorded 4 min after D_2O addition, and it showed a profound broadening and a down-field shift of the protons corresponding to the dinuclear species in the 150-110ppm region. The four signals around 140ppm were so broad they even merged into a broad doublet. The signals of the mononuclear species at 133ppm seemed undisturbed. The broadness of the peaks may origin from the changing of structure taking place in the same time scale.

After 7 minutes, the signals became sharper and the broad doublet at 143ppm divided again into four signals, but grouped into pairs. The conversion was nearly complete after this, as indicated by the spectrum taken one day after D_2O addition, where no further changes were visible. See Figure 4.34.

Figure 4.35 shows the changes that occur within the spectral window of the second region of 90-45ppm in the ^1H -NMR spectrum on addition of D_2O . In the first recorded spectrum, the signals from 82 to 70ppm originate from dinuclear and mononuclear complex, the signals from 56 to 51ppm originate from dinuclear complex and the signal at 50ppm from mononuclear compound. 4min after the addition, a new set of signals emerged from 93 to 86ppm. The signals were extremely broad, even after 7 minutes, but they became sharper during the 4-5 hours after the addition. After 1 day they had sharpened considerably, and no further change was evident even after several more days. They had been shifted from under the overlapping signals at 82 to 70 ppm, as integral comparison with the purely mononuclear signal at 70ppm showed. The signals, originally from 82 to 70ppm originated now mainly from the mononuclear species. They had shifted slightly up-field to 81-69ppm, and so had the signal at 49, that had been at 50ppm before. The signals originating from the dinuclear complex at 56 to 51ppm shifted up-field to 54-50ppm. They were poorly resolved after 4 minutes, but became better resolved over time.

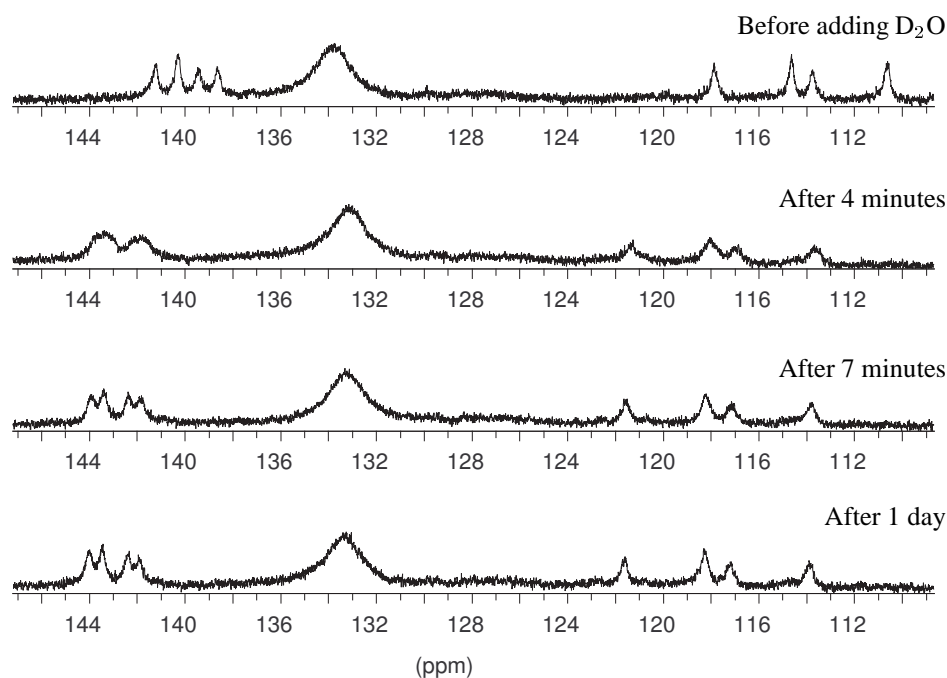


Figure 4.34: 600 MHz ^1H -NMR titration of $[\text{Co}_2(\text{mp})_2(\text{OAc})][\text{PF}_6]_3$ in acetonitrile- d_3 with D_2O , the area of most shifted protons.

Figure 4.36 shows the region from 27.5 to 14.5ppm. The first spectrum shows a group of signals from 26 to 23ppm that originate from the dinuclear species. They moved down-field upon D_2O addition to 27-24ppm and broadened notably. After 1 day, these signals were still as broad. The signals at 21.0ppm and 18.9ppm origin both from the mononuclear species, and only the latter is shifted slightly up-field to 18.6. The split signal centred originally at 14.9ppm belonged to the dinuclear species and experienced a downfield shift to 18.8ppm and broadening.

Figure 4.37 shows the region from 13.5 to 1.5ppm. The signal at 13.3ppm originating from the mononuclear species was almost unaffected and shifted to 13.4ppm. A multiplet that was originally centred at 8.6ppm and originated from the dinuclear complex broadened and shifted down-field to 9.1ppm. The two mononuclear signals at 8.1 and 7.9ppm shifted slightly down-field to 8.2 and 8.0ppm. The signal at 4.5ppm seemed unaffected, as did the signal at 3.5ppm. As expected, the intensity of the D_2O signal became large after the addition, compared to the signal of acetonitrile- d_3 .

In this experiment the ratio of mononuclear to dinuclear compound was constant during the first day it stayed 3 : 1. 12 days later, the spectrum was measured again, and the ratio had turned to 4 : 1. But then the conversion from dinuclear to the mononuclear complex did not, as shown by Whall with $[\text{Co}_2(\text{tbp}_2\text{qnp}_2)(\text{Sol}_2)_2]^{4+} / [\text{Co}(\text{tbp}_2\text{qnp}_2)(\text{Sol}_2)_2]^{2+}$, proceed to completion in acetonitrile solution either, but ended at 4 : 1 18h after D_2O addition. Depending on the amount of water added, the stability of the dinuclear form over the mononuclear or vice versa may also depend somewhat on the solvent. After all, the mononuclear complex was always obtained from the synthesis in moist methanol, as opposed to acetonitrile- d_3 , in which the titration was carried out.

In order to see which difference the amount of added water makes, at a later date, 50 μL of D_2O was added to this probe, and recorded further with only one scan at 6 min after addition, then with more scans 20min, 30min and 2h 45min later. The ratio of added D_2O to original dinuclear complex was now in the range of 5000 : 1. The main change in the spectrum had occurred immediately after addition, and no further change could be made out upon standing. The initial ratio (before the addition of 50 μL D_2O) of mononuclear to dinuclear complex changed from 6 : 1 changed to 8 : 1, and thus there was still some dinuclear compound left.

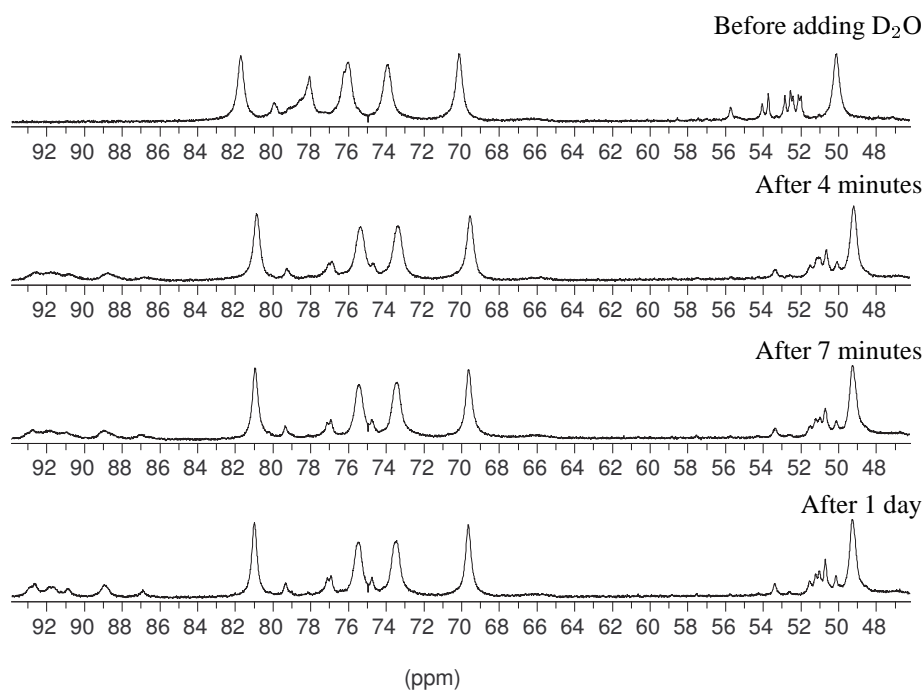


Figure 4.35: 600 MHz ¹H-NMR titration of [Co₂(mp)₂(OAc)][PF₆]₃ in acetonitrile-d₃ with D₂O, the area of next most shifted protons.

Experiment 2: NMR-titration of the dinuclear complex [Co₂(mp)₂(OAc)][PF₆]₃ with D₂O: The NMR sample of pure dinuclear compound [Co₂(mp)₂(OAc)][PF₆]₃ was obtained by transferring the sample, prepared according to the description in the experimental chapter on page 144, to the NMR-tube inside the glove box, using acetonitrile-d₃ (abs) from an ampulle. The ¹H-NMR spectrum is showed in Figure 4.32 on page 98. After standing with just the plastic cap to protect from moisture for five weeks, mononuclear compound had formed in the sample. The ratio was then approximately 2 : 1 for mononuclear to dinuclear complex. At a later date, the ratio had changed further to 5 : 1, and after addition of 50 μL D₂O, the ratio changed at once to 6 : 1, but then stayed stable.

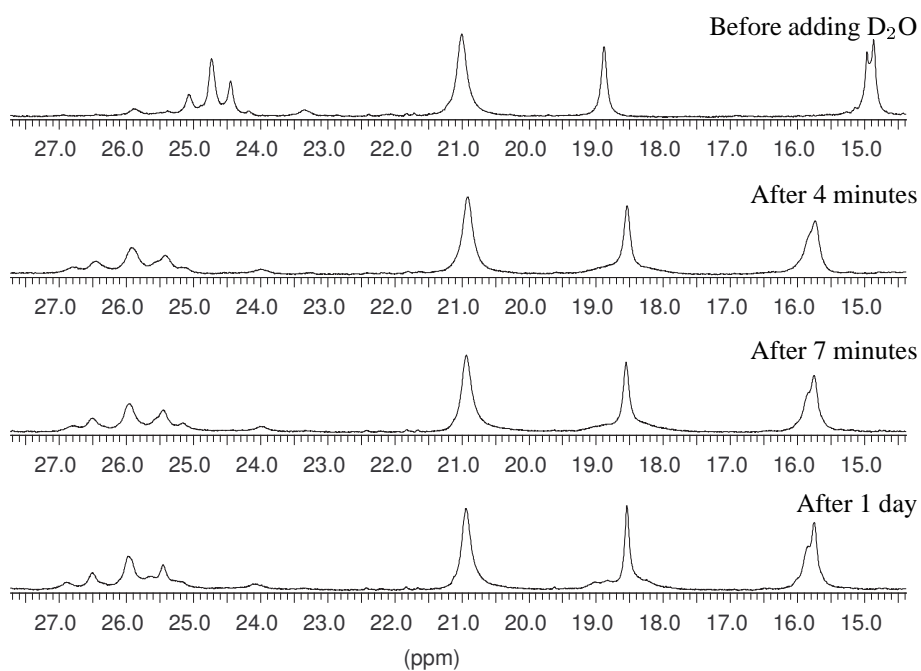


Figure 4.36: 600 MHz ^1H -NMR titration of $[\text{Co}_2(\text{mp})_2(\text{OAc})][\text{PF}_6]_3$ in acetonitrile- d_3 with D_2O , the area of next least shifted protons.

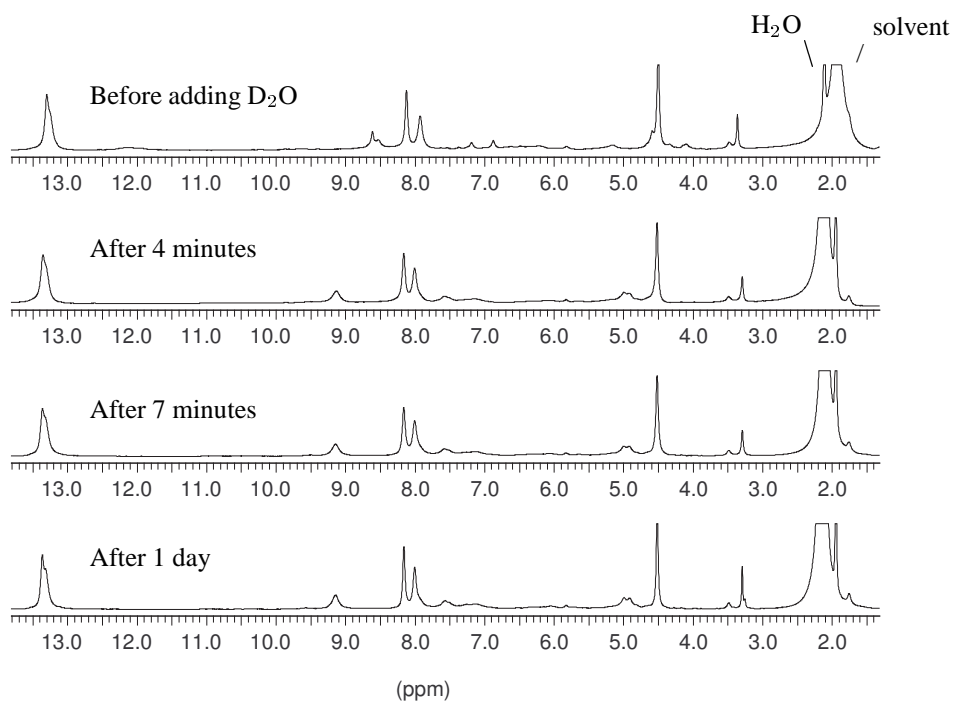


Figure 4.37: 600 MHz ^1H -NMR titration of $[\text{Co}_2(\text{mp})_2(\text{OAc})][\text{PF}_6]_3$ in acetonitrile- d_3 with D_2O , the area of least shifted protons.

Experiment 3: NMR-titration of the dinuclear complex $[\text{Co}_2(\text{qcq})(\text{OAc})][\text{PF}_6]_3$ with D_2O : A sample of the dinuclear $[\text{Co}_2(\text{qcq})(\text{OAc})][\text{PF}_6]_3$ (4.2mg) in acetonitrile- d_3 (predried over molecular sieves (3\AA)) was prepared in an NMR tube. The probe was very dark, and it was hard to see if any precipitate formed. Solely the dinuclear complex was present. After running the probe, D_2O ($64\mu\text{L}$) was added and the spectrum recorded again. The signals had shifted slightly, but no mononuclear compound seemed to have formed. More D_2O was added, so the total amount was 164, 264, 314, 441 and $514\mu\text{L}$. The ratio of added D_2O to original dinuclear complex was 14'000 : 1 in the end. There were shifting of signals, but no evidence of any mononuclear species. Between the last two spectra, no further changes were visible.

Experiment 4: NMR-titration of mixed dinuclear/mononuclear complex $[\text{Co}_2(\text{qcq})(\text{OAc})][\text{PF}_6]_3 / [\text{Co}_2(\text{qcq})(\text{OH}_2)_2(\text{MeOH})_2][\text{PF}_6]_2$ with D_2O : The titration of a mixed dinuclear/mononuclear sample was then carried out (see Figures 4.38, 4.39 and 4.40. The chemical shifts before and after the addition are listed in Table 4.17. A sample of the dinuclear $[\text{Co}_2(\text{qcq})(\text{OAc})][\text{PF}_6]_3$ (5mg) in dry acetonitrile- d_3 was prepared in an NMR tube. Not everything dissolved. After running the probe, 1 drop of D_2O ($50\mu\text{L}$, excess) was added, and the spectrum between 0 and 150ppm recorded 2, 12 and 22min after addition. The ratio of added D_2O to complex was approximately 2000 : 1.

Because of the wide spread signals, the spectra were divided up again, this time only into three regions, as only multiplets were seen in the region from 8.5 – 1.5ppm after the addition of D_2O .

The first spectrum shown in the Figures was taken before addition of D_2O , and it showed that quite an amount of mononuclear complex was present (e.g. signal at 134ppm) along with the dinuclear complex that was to be studied. The second spectrum was recorded 2 min after the addition of D_2O . It showed only extremely broad peaks, which may origin from the change, that was taking place. The signal to noise ratio had become much smaller.

The signals for the dinuclear species from 141 to 139ppm became one broad bulk, the signal from the mononuclear did not shift, and the signals between 118 and 111ppm that originated from the dinuclear complex had become one broad bulk too. After 10 more minutes the next spectrum was recorded. The signals were sharper now. (But the last two spectra in these Figures were recorded with 512 scans instead of 32.) Otherwise no changes were observed to the previous spectrum. 22 minutes after addition, the region at lowest field showed no signals of any dinuclear form anymore.

Figure 4.39 shows the region from 90 to 30ppm. Neither in this experiment nor in the one above, did any new signals emerge in the 82 – 70ppm region (that had been observed for the dinuclear cobalt(II) complex of mp). But the signals at 78 and 52, originating both from a dinuclear form and the mononuclear form had lost the contribution of the dinuclear ones. The signals at 56 – 51ppm, originating from dinuclear compound had already vanished completely 2min after addition. The signal at 49.5 from the mononuclear form was unperturbed. The spectrum recorded 12min after addition was indistinguishable from the former, but 22min after addition, the signals of the mononuclear, that were the only ones left, had all shifted up-field for 0.5 – 0.7ppm.

Finally Figure 4.40 shows the region from 30 to 0ppm. In the first spectrum, a dinuclear and a mononuclear species were visible. 2min after the D_2O addition, the signals of the dinuclear species had broadened and seemed much smaller. No new dinuclear species appeared like it did with the former probe or the mp analogue, but some other new signals appeared. Apart from the worse signal to noise ratio, the resonances originating from the mononuclear species seemed unperturbed.

After 10 more minutes the next spectrum was recorded. The signals were sharper now. (But as already mentioned, the last two spectra in these Figures were recorded with 512 scans instead of 32.) Otherwise no changes were observed compared to the former spectrum. 22 minutes after addition, this region at lowest field showed only very weak traces of a dinuclear form. A control measurement was made after one day. It is shown in Figure 4.41 and, although not pure, the sample now contained mainly mononuclear complex.

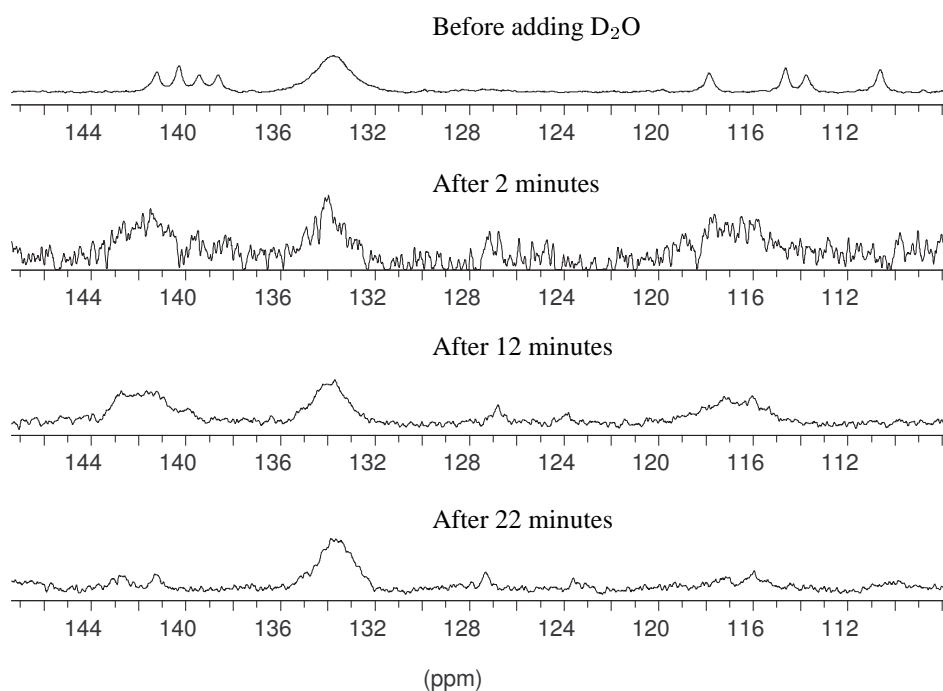


Figure 4.38: 600 MHz ^1H -NMR titration of $[\text{Co}_2\text{qc}(\text{OAc})][\text{PF}_6]_3$ in acetonitrile- d_3 with D_2O , the area of the most shifted protons. The spectra were processed with the same line broadening, in order to make them directly comparable. The first and second spectrum were recorded with 32 scans. Because of the decreased signal to noise ratio, the proceeding spectra were recorded with 512 scans.

Table 4.17: Overview of the proton signals in the NMR-titrations of $[\text{Co}_2(\text{mp})_2(\text{OAc})][\text{PF}_6]_3$ and $[\text{Co}_2(\text{qc})_2(\text{OAc})][\text{PF}_6]_3$ with D_2O .

Titration of $[\text{Co}_2(\text{mp})_2(\text{OAc})][\text{PF}_6]_3$ with D_2O				Titration of $[\text{Co}_2(\text{qc})_2(\text{OAc})][\text{PF}_6]_3$ with D_2O			
original dinuclear	new after 12 days dinuclear	original mononuclear	new after 12 days mononuclear	original dinuclear	original mononuclear	new after 1 day mononuclear	new after 1 day unknown
141.2	143.9			141.2			147.2
140.3	143.4			140.3			142.6
139.5	142.3			139.4			141.2
138.7	141.8			138.7			
		133.7	133.4		133.7	133.6	127.3
117.9	121.5			117.9			
114.6	118.1			114.6			
113.7	117.0			113.7			
110.6	113.8			110.6			
	92.45						95.1
	92.13						92.3
	91.42						
	91.18						
	90.47						
	88.60						
	86.52	81.71	81.05		81.7	81.1	
		76.01	75.53		76.0	75.3	
79.93	79.39	73.89	73.50	79.9	73.9	73.4	

Table 4.17: Overview of the proton signals in the NMR-titrations of $[\text{Co}_2(\text{mp})_2(\text{OAc})][\text{PF}_6]_3$ and $[\text{Co}_2(\text{qcq})_2(\text{OAc})][\text{PF}_6]_3$ with D_2O .

Titration of $[\text{Co}_2(\text{mp})_2(\text{OAc})][\text{PF}_6]_3$ with D_2O				Titration of $[\text{Co}_2(\text{qcq})_2(\text{OAc})][\text{PF}_6]_3$ with D_2O			
original dinuclear	new after 12 days dinuclear	original mononuclear	new after 12 days mononuclear	original dinuclear	original mononuclear	new after 1 day mononuclear	new after 1 day unknown
78.07	77.20	70.14	69.69	78.1	70.1	69.8	66.9
	76.99						
	74.82						
55.7	53.42			55.7			
54.00	51.59			54.0			
53.69	51.07			53.7			
52.81	50.75			52.8			
52.51	50.19			52.5			
52.38				52.4			
52.10				52.1			51.4
51.96		50.07	49.31	52.0	50.1	49.5	42.5
							37.1
25.07	26.48			25.9			27.4
24.73	25.93			25.1			26.9
24.44	25.42	21.00		24.7			26.2
		18.87		24.5			25.1
				23.3			24.5
							23.9
			20.95		21.0	21.0	
			18.56		18.9	18.6	
							17.1
							16.6
							16.5
							16.3
							15.9
14.95	15.78			15			15.4
14.85	15.71			14.9			14.8
							14.6
							14.1
		13.30	13.36	12.10	13.3	13.4	
						13.2	
						13.1	
							10.4
8.61	9.12			8.61			9.42
8.53		8.12	8.15	8.53	8.13	8.16	9.02
7.18	7.54	7.92		7.19	7.93	8.00	8.54
6.87	7.16		7.99	6.88			7.92
							7.47
				6.75-5.00			6.97-3.37
	4.97						
	4.89						
4.49	4.50	4.49	4.50	4.50			
				3.48			
				3.36			
				2.11	2.11	2.09	3.26

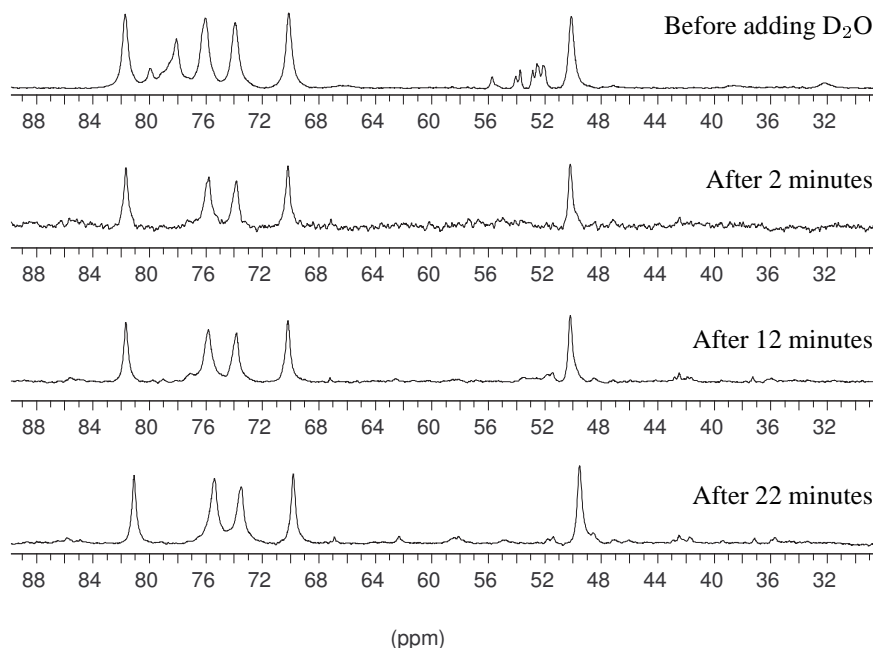


Figure 4.39: 600 MHz $^1\text{H-NMR}$ titration of $[\text{Co}_2\text{qcq}(\text{OAc})][\text{PF}_6]_3$ in acetonitrile- d_3 with D_2O , the area of the medium shifted protons. The spectra were processed with the same line broadening, in order to make them directly comparable. The first and second spectrum were recorded with 32 scans. Because of the decreased signal to noise ratio, the proceeding spectra were recorded with 512 scans.

Summary and discussion The only sample of pure dinuclear complex that was treated with an excess of water after dissolution in acetonitrile- d_3 was the first of the experiments with the qcq-complex $[\text{Co}_2(\text{qcq})(\text{OAc})][\text{PF}_6]_3$. D_2O was added in portions, and it caused a shift of the signals originating from the dinuclear species, but there was no evidence for the mononuclear complex to form, even with a large excess D_2O present. It was the first of these experiments (described as ‘experiment 3’), and it was considered, if the dinuclear complex was more stable than the mononuclear complex in an acetonitrile solution as opposed to methanol, in which it had been synthesised. The sample, with mixed dinuclear/mononuclear species, ‘experiment 4’ showed a change to mononuclear that was very fast. This finding seems to contradict the findings of the ‘experiment 3’. Possibly the mononuclear species somehow catalysed its own formation. It was also considered, whether methanol could have an influence, possibly there was some present in the mixed sample, as a remnant from synthesis.

‘Experiment 1’ was done with the complexes of non linked ligand mp. The sample contained a mixture of dinuclear and mononuclear compound. First D_2O was added in a molar ratio of D_2O to complex 250 : 1 (if all complex cations were dinuclear). A shifting of the signals originating from the dinuclear species were observed. Adding more D_2O (ratio 5000 : 1) then did change the ratio of the complexes in favour of the mononuclear. Possibly the signals for the dinuclear were so small because of interconversion of several similar dinuclear species, broadening the signals so they appeared smaller. The signals of the dinuclear complex were in fact only seen in the regions of 144ppm and 270ppm, after the last addition. A possible effect of methanol was checked on the sample with mp-complex. After completion of this experiment, 0.5mg of methanol- d_4 was added to see if this had any effect on the complex ratio. But the addition did not show any effect on the $^1\text{H-NMR}$ signals.

In ‘experiment 2’, a sample of pure dinuclear mp-complex, was left standing without protection from moisture. The ratio of the dinuclear to mononuclear species changed, but water did not show in the $^1\text{H-NMR}$ beside acetonitrile, as the signals were very broad here (also when the spectrum was processed without line extra broadening).

Not all the dinuclear compound of the mp-complexes vanished, and the signals in the spectrum of the

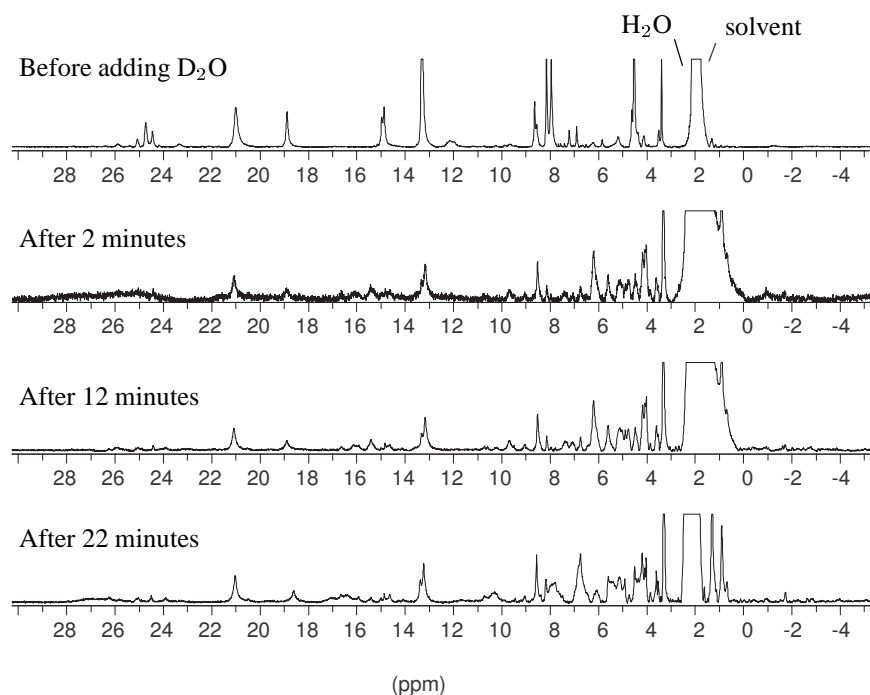


Figure 4.40: 600 MHz ^1H -NMR titration of $[\text{Co}_2\text{qcq}(\text{OAc})][\text{PF}_6]_3$ in acetonitrile- d_3 with D_2O , the area of the least shifted protons. The spectra were processed with the same line broadening, in order to make them directly comparable. The first and second spectrum were recorded with 32 scans. Because of the decreased signal to noise ratio, the proceeding spectra were recorded with 512 scans.

dinuclear cobalt(II)-qcq complex became very broad after addition, and stayed so broad that only some of them were still detectable. Also new, hitherto un-assignable signals occurred. It may be speculated that there is an equilibrium present in both systems, but that the linker has the effect to slow down conversion rates. There was unfortunately a solubility problem with the complex(es) of mp, and also to some extent with the complex(es) of qcq, which made the determination of the ratio D_2O : dissolved complex difficult. It may be concluded that D_2O addition in both species caused the dinuclear species to unravel. If there was no mononuclear complex present at the start, the reaction was very slow and seemed inhibited. Further titrations, conducted under equal conditions would be necessary to make any conclusions, about possible substituent and linker effects on the rate of conversion and of the ratio reached when excess D_2O is present.

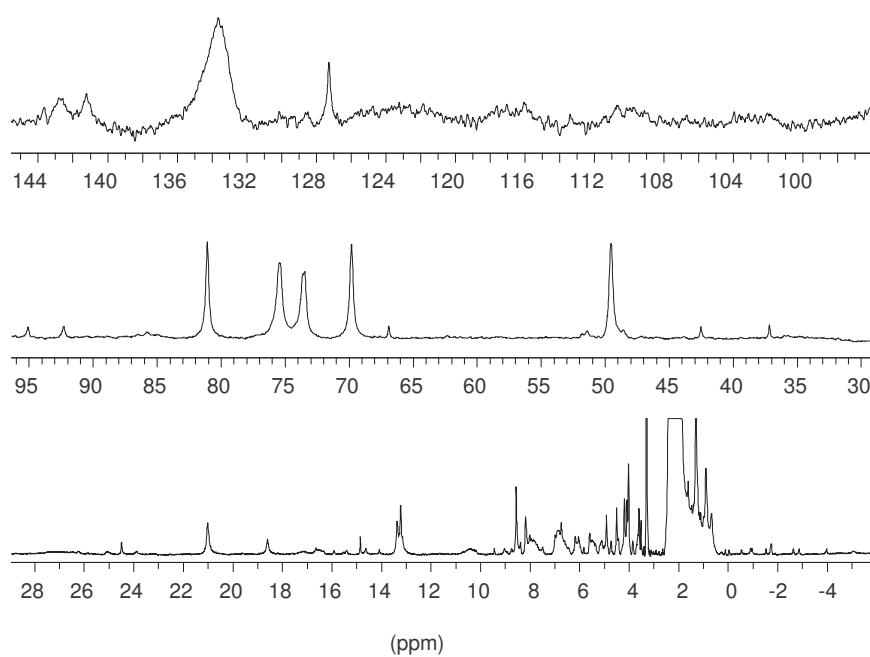


Figure 4.41: 600 MHz $^1\text{H-NMR}$ of $[\text{Co}_2\text{qcq}(\text{H}_2\text{O})_2][\text{PF}_6]_4$ in acetonitrile-d_3 after 2 days, area from 145 to 0 ppm.

4.3.3 Electrochemistry

The cobalt(II) complex of mp $[\text{Co}_2(\text{mp})_2(\text{OAc})][\text{PF}_6]_3$ was studied. The sample showed only the dinuclear double helicate when it was measured with proton-NMR as an acetonitrile- d_3 solution. The electrochemical behaviour was studied by two kinds of measurements: differential pulse voltammetry and cyclic voltammetry (see Figures 4.42 and 4.43). The former gives the potentials accurately, while the latter gives information about the reproducibility. In both methods, the potential is varied linearly over time. The measurements were conducted in absolute acetonitrile. In order to see if the electrolyte (3mg dry tetrabutylammonium hexafluorophosphate into 0.7ml NMR probe) had any effect on the solution structure, a ^1H -NMR was recorded before and after addition. There was no effect on the signals. In the cyclic voltammogram, recorded at a scan rate of 200mV/s, three rather broad reduction peaks are seen, but only two large return waves so the process does not seem to be electrochemically reversible. The differential pulse voltammetry was recorded with ferrocene as reference. It showed a first reduction potential at -1.04V, then a weak one at -1.50V, one at -1.72V, and three subsequent ligand reductions at $>2\text{V}$. The oxidative scan of $\text{Co}_2(\text{mp})_2^{2+}$ show no signal at a higher potential (except for the [ferrocenium] $^+$ + e \rightleftharpoons ferrocene), and this means there is no Co^{III} species up to a potential of 0.83V vs ferrocene, that is up to 1.23V vs standard hydrogen.

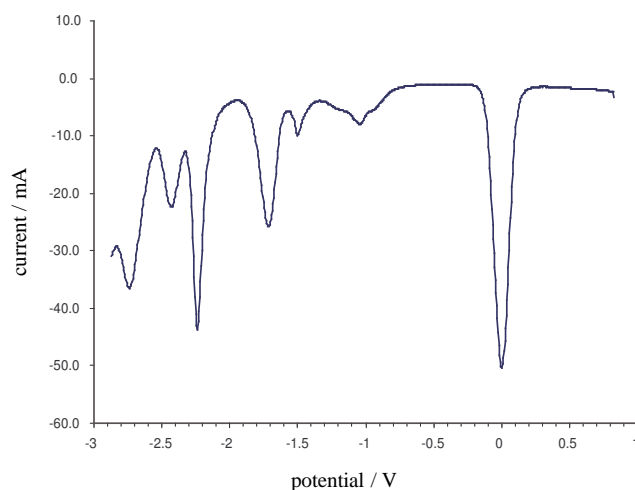


Figure 4.42: Redox potentials of $[\text{Co}_2(\text{mp})_2(\text{OAc})][\text{PF}_6]_3$ versus ferrocene: differential pulse voltammetry in acetonitrile (abs), with tetrabutylammonium hexafluorophosphate (0.1M) as electrolyte.

A double helical qnpy complex may be sectioned into a “ $\text{Co}(\text{terpy})_2^{2+}$ ”- and a “ $\text{Co}(\text{bipy})_2^{2+}$ ”-unit and the electrochemical potentials compared with the redox potentials of $[\text{Co}(\text{terpy})_2]^{2+}$ and $[\text{Co}(\text{bipy})_2]^{2+}$.¹²⁵ The potentials taken from the literature were the 3+/2+ and 2+/1+ reduction potentials and they were converted from vs SCE to vs ferrocene with the help of the electrochemical series, see Handbook¹²⁶ page D-151. For the $\text{Co}(\text{terpy})_2^{n+}$, these potentials are -0.176V and -1.199V vs ferrocene. The second one would correspond to the Co(II)-Co(I) reduction in the new complex with mp. It does not tally well with it however, but then the Co(II) complex of terpy is low spin, as opposed to the $[\text{Co}_2(\text{mp})_2(\text{OAc})]_2^{3+}$. For the $\text{Co}(\text{bipy})_2^{n+}$ the potentials are -0.170V and -1.420V vs ferrocene. Again it is the second value that corresponds to the Co(II)-Co(I) reduction. But the comparison is not so simple, since two “bipy” units in the mp ligand coordinate alongside an acetate ion or two solvent molecules. And indeed also this potential is remote from any potential measured for the new complex.

Data for comparison with the parent complex of qnpy, the symmetrically and aliphatically substituted ms_2qnpy , and the symmetrically and aromatically substituted mop_2qnpy and tbp_2qnpy , and finally for the unsymmetrically substituted tbpcqnpy are presented in table 4.18. To complete the picture, the mononuclear complex of Co(II) with cp_2qnpy , confirmed by the crystal structure, and the mononuclear complex of qnpy are included in the table as well.^{35,66-68,91,127}

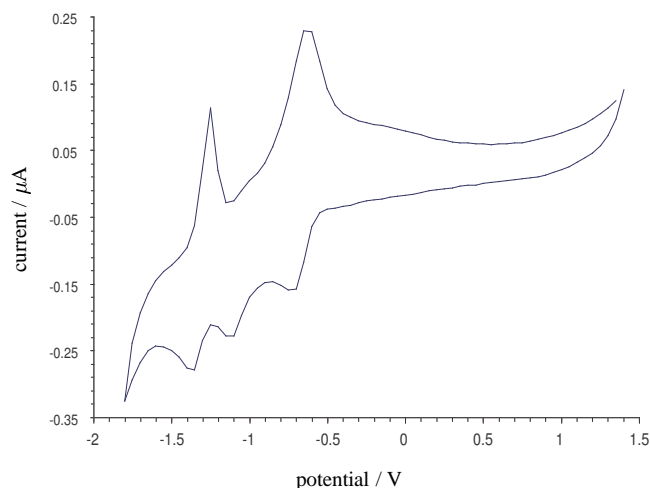


Figure 4.43: Cyclic voltammogram of $[\text{Co}_2(\text{mp})_2(\text{OAc})][\text{PF}_6]_3$ in acetonitrile with tetrabutylammonium hexafluorophosphate (0.1M) as electrolyte. The cycle, started at 1.4V, and the scan rate was 0.20Vs^{-1} .

Both values associated with the metal based Co(II)-Co(I) reductions in the new dinuclear mp complex, -1.04V and -1.72V, tally well with those found for $[\text{Co}_2(\text{ms}_2\text{qnp})_2(\text{OAc})][\text{PF}_6]_3$.⁹¹ Although the structure of the two ligands mp and mop₂qnp, and in consequence their dinuclear complexes would be more closely related, only the first reduction potentials are actually close to each other. The values found for the complex of mop₂qnp along with most of the literature values assigned for dinuclear complexes, fit better to the values of recently measured mononuclear complexes, listed on the right hand side in Table 4.18). At the time the electrochemistry of these complexes was recorded, nothing about the water sensitivity of the dinuclear cobalt(II) complex of qnp derivatives was known yet. This was only recognised a few years ago.⁵¹ It is therefore assumed that in all the samples made and measured previously, at least some mononuclear compound was present, even though this was neither known nor stated at the time.

4.3.4 Summary

Mononuclear, seven coordinate cobalt(II) complexes and dinuclear double helical cobalt(II) complexes were synthesised of the unsymmetrically substituted non-linked ligand mp, and of the unsymmetrically linked ligand qcq. Mass spectrometry confirmed the mononuclear structures. For the double helicate of qcq, an envelope of peak corresponding to the mass of the dinuclear core could be seen in the Maldi-TOF spectrum, but it was not considered very reliable and the dinuclear mp-complex was not measured, as it would require putting solution on a gold plate, and ¹H-NMR studies had shown the structure to be unstable in moist conditions. Infrared spectroscopy was done on the dinuclear mp-complex, but the only indication for the complex was the very strong absorption band at 825cm^{-1} . The acetato vibrations were obscured by the aromatic ones present also in the copper(II/I) helicates of qp, mp and pp. A spectrum of the qcq-complex, was not measured, as it was considered not to include any more information. The spectra of mononuclear cobalt(II) complex of mp and qcq gave very similar spectra to the one for dinuclear copper and nickel complex (see below), and did not help to distinguish between mono and dinuclear complexes. The coordinative bond, absorbing outside the range measurable by the available instrument.

The redox-potentials of the dinuclear complexes could not be fitted with other qnp-derivative complexes of cobalt. Because the instability of these compounds was only recognised recently, many potentials from the literature, thought to belong to dinuclear compounds, belonged to mononuclear compounds, or for all that is known, to even a different solution structure. ¹H-NMR spectroscopy gives the most information about different solution structures, as the spectra could be compared with those of

complex potentials in Volt	mother complex	complexes of sym. subst. ligands			complexes of unsym. subst. ligands		mononuclear complexes	
	$[\text{Co}_2(\text{qnpv})_2(\text{OAc})][\text{PF}_6]_3$	$[\text{Co}_2(\text{ms}_2\text{qnpv})_2(\text{OAc})][\text{PF}_6]_3$	$[\text{Co}_2(\text{mop}_2\text{qnpv})_2(\text{OAc})][\text{PF}_6]_3$	$[\text{Co}_2(\text{tbp}_2\text{qnpv})_2(\text{OAc})][\text{PF}_6]_3$	$[\text{Co}_2(\text{tbpcpnpv})_2(\text{OAc})][\text{PF}_6]_3$	$[\text{Co}_2(\text{mp})_2(\text{OAc})][\text{PF}_6]_3$	$[\text{Co}(\text{cp}_2\text{qnpv})](\text{Solv})[\text{PF}_6]_2$	$[\text{Co}(\text{qnpv})](\text{Solv})[\text{PF}_6]_2$
oxidative scan	0.74			0.9				
	0.53			0.5				
	0.32			0.3				
reductive scan	-1.10	-1.02	-1.00	-0.97	-0.95	-1.04	-0.89	-0.76
	-1.19			-1.11	-1.14			-1.06
	-1.37		-1.31	-1.32	-1.31		-1.29	-1.36
						-1.50 (weak)	-1.60	-1.55
	-1.71	-1.68	-1.60	-1.65	-1.66	-1.72		
	-1.93		1.94	-1.89	-1.98		-1.89	-1.89
	-2.11	-2.13		-2.06	-2.03		-2.00	
	-2.30					-2.24		
						-2.43		
					-2.74			

Table 4.18: Comparing redox potentials of dinuclear quinquepyridine type complexes of Co(II) in Volt. The experiments were conducted in acetonitrile, against ferrocene.^{35,66,67,91} Potts *et al.* also measured dinuclear cobalt(II) ms_2qnpv complexes once in acetonitrile, once in DMF vs SSCE. Converted vs ferrocene the potentials were -0.82, -1.13, -1.44, -1.86 and -2.10V in acetonitrile, and -1.06, -1.29, -1.47, 1.72V, and -1.95V in DMF. The difference in the first potential being biggest, and because it was the first reduction potential, it was assigned to the $\text{Co(II)} \rightarrow \text{Co(I)}$ reduction of the cobalt centre with an acetato / acetonitrile ligand(s).^{68,127}

substructures in samples containing mixtures of different structures, of which some had been solved by X-ray, like for example the mononuclear $[\text{Co}(\text{cp}_2\text{qnp}_y)(\text{OH}_2)_2][\text{PF}_6]_2$, and other mixtures of dinuclear and mononuclear complexes. NMR-titration in acetonitrile- d_3 of dinuclear species with D_2O give the impression that at least two dinuclear species and a mononuclear species may interconvert with each other, and that the mononuclear species is favoured more, the more D_2O is present.

4.4 Nickel complexes

4.4.1 Synthesis and characterisation

The nickel(II) complex of mp was synthesised according to Whall,⁵¹ using a 1 : 1 ratio of metal salt to ligand. The turquoise nickel acetate · tetrahydrate and beige ligand were dissolved in a minimum amount of hot methanol to give a brown solution. A precipitate formed upon cooling and could be separated. The microanalysis fit a formulation of the dinuclear complex with one auxiliary acetate ligand $[\text{Ni}_2(\text{mp})_2(\text{OAc})][\text{PF}_6]_3 \cdot 3.5\text{H}_2\text{O}$. The mass spectrum confirm a 2 : 2 ratio of metal to ligand by the signals at 1637 and 450 which correspond to $(\text{M}-\text{PF}_6)^+$ and $(\text{M}-3\text{PF}_6)^{3+}$ respectively. Infrared spectroscopy was practically indistinguishable from the dinuclear spectra of copper and cobalt complexes.

Because the compound is paramagnetic, broad signals were expected in the ^1H -NMR spectrum. It was recorded on a 600 MHz spectrometer, and the signals were resolved from zero downfield to 160ppm, see Figure 4.44. In published nickel complexes of cp_2qnp and ms_2qnp ,⁶⁷ the ortho-phenyl protons give signals at lower field than the meta phenyl protons. The shifts are very similar to the shifts in the cobalt complexes, and therefore one may assume, that the shift at $\sim 13\text{ppm}$ belongs to the ortho-phenyl proton, and the signal at $\sim 8\text{ppm}$ belongs to the meta phenyl proton.

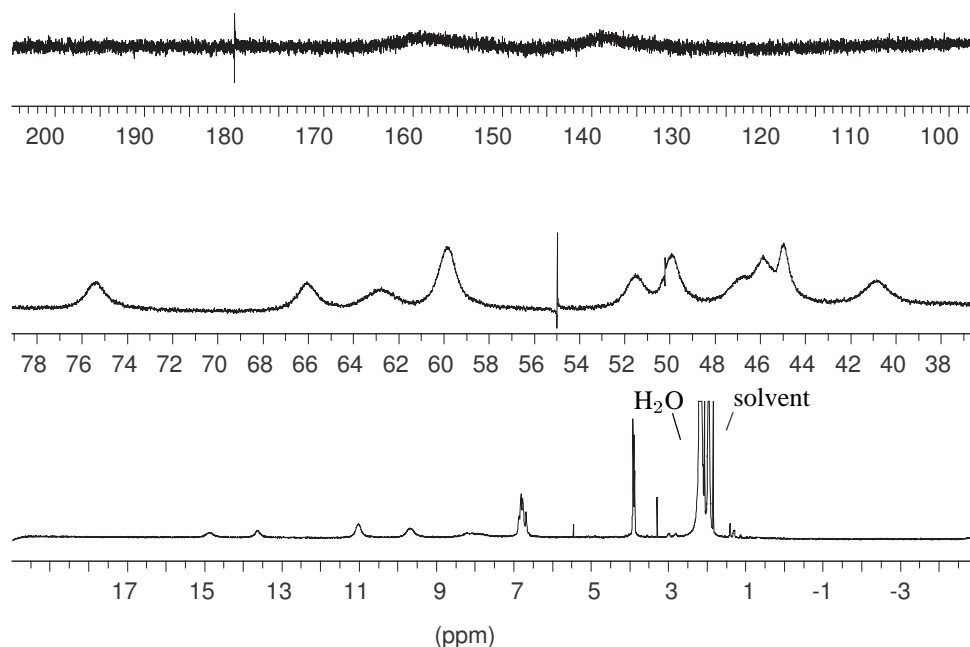


Figure 4.44: 600 MHz ^1H -NMR of $[\text{Ni}_2(\text{mp})_2(\text{OAc})][\text{PF}_6]_3$ in acetonitrile- d_3 at ambient temperature.

Assuming the three signals at 3.9ppm to belong to the CH_3O - group, the integral of 6H suggests that the 8H signal at 6.8ppm are the phenyl protons. All the other signals must thus come from pyridine protons or acetate, if not replaced by solvent molecules. There are 15 environments up to 80ppm plus the two very broad signals at 159 and 139ppm. 15 signals of 2H intensity would be expected of a head-to-head isomer. However, because the two metal ions are not coordinated to equivalently, two head-to-head isomers and one head-to-tail isomer are possible. In the case of head-to-tail, all pyridine protons would be in unique environments and 30 signals of 1H intensity might be expected. But the chemical shift would not differ much for the different isomers, as the main structural feature is the double helical arrangement. With signals for pyridine and acetate protons at 17 different shifts and varying intensity (see experimental part, page 143), it is hard to assign the different signals. What is definite, however, is that more than just one head-to-head isomer is present in solution. It can not be ruled out, that additionally a completely different structure is present, e.g. a mononuclear form, like in the cobalt(II) complexes discussed above.

Chapter 5

Synthesis of a quaterpyridine to be linked at the 4-position of the terminal ring

5.1 Overview

Led by the desire to make a real hair-pin complex, where the linker lies in the direction of the metal-metal axis of the complex, an attempt was made to prepare a 2,6-quater- or quinquepyridine ligand, with a substituent on a terminal ring. These ligands would be able to form dinuclear complexes. The substituent would have to be chosen so that it would be able to react with a linker molecule, to form a linked ligand similar to qcq, mcm or pcp, with the linker attached to the last ring, instead of the second last. The phenol group had proven convenient for attaching a linker, and a synthesis was planned that would result in a 4-methoxyphenyl substituent. During the synthesis of the quaterpyridine ligand, a methoxy group would protect the hydroxy group, and prevent it from disturbing early reaction steps. The protection group would then be eliminated in the very last step.

Previously, a route to unsymmetrically substituted quaterpyridines had been published.¹³⁰ This route involved Mannich bases, and as I had found out during my Diploma thesis, some of these are not easy to make.¹³¹ Therefore, a new synthetic route for asymmetrically substituted quaterpyridine ligands was designed, where two asymmetrically substituted bipy units would be coupled in order to get the quaterpyridine type ligand. If successful with the quaterpyridine, the same reaction route would be applied on an unsymmetrically substituted bipy and terpy derivative in order to obtain a quinquepyridine type ligand.

A few test reactions were tried in order to make a 5-substituted qtpy or qnpy, but they were not promising. An overview of the planned pathway is given in Figure 5.2, and the reactions tried, are marked with blue arrows and described in the experimental chapter.

In this thesis, it was possible to find a reaction pathway to a 4-substituted qtpy ligand: 4-(4-methoxyphenyl)-2,2':6',2'':6'',2''':6''',2''''-quaterpyridine. This quaterpyridine derivative was fully characterised. In the overview over all the tried syntheses given in Figure 5.1, the reaction steps of the reaction pathway that gave better overall yield, are marked with blue arrows. The reaction steps of an alternative route, that was more demanding, and also gave a lower overall yield, are marked with pink arrows).

5.2 Reaction steps to 4-(4-methoxyphenyl)-2,2':6',2'':6'', 2'''-quaterpyridine (4MeOphqtpy)

The two unsymmetrically substituted bipy units that were to form the new ligand 4-(4-methoxyphenyl)-2,2':6',2'':6'',2'''-quaterpyridine in a Stille coupling,^{132,133} were 6-tributylstannyl-2,2'-bipyridine and 6-Bromo-4'-(4-methoxyphenyl)-2,2'-bipyridine. The former had already been synthesised by Hanan,¹³⁴ though only the last step of his synthesis was identical to the synthesis described here. The latter compound was synthesised by a Kröhnke cyclisation, with an auxiliary carboxylate group, that was essential in order to obtain a reasonable yield.

The individual steps to 6-tributylstannyl-2,2'-bipyridine are described first, followed by the steps leading to 6-Bromo-4'-(4-methoxyphenyl)-2,2'-bipyridine. Finally the Stille cross coupling reaction giving the unsymmetrically substituted quaterpyridine derivative is described on page 122.

5.2.1 6,6'-Bromo-2,2'-bipyridine

The synthesis was consistent with the literature procedure.⁸² Dry 2,6-dibromopyridine was suspended in dry diethyl ether and cooled in an acetone/dryice bath to under argon. A *n*-BuLi solution in hexane was added slowly. Additional cooling with liquid nitrogen helped to keep the temperature below -75°C. After the addition was complete, the temperature was raised to -50°C, and then kept between -50 and -60°C until everything had dissolved. The yellow solution was cooled to ≤-75°C, and dry copper(II) chloride was added as a solid. It is an efficient coupling agent for lithiopyridine reagents. The suspension was stirred at that temperature for 40min, and then the dipyriddylocuprate was oxidised to the product by bubbling dry air through the mixture. The colour changed from brown to greenish brown, and HCl (6.0M, 50ml) was added to quench the reaction. The mixture was stirred until it reached ambient temperature. The beige precipitate was filtered off and washed with HCl (2.0M) and dried *in vacuo* over P₂O₅ to give pure product in 57.5% yield. It was characterised by ¹H-NMR spectroscopy and melting point (220.3-220.9°C, Literature: 226-227°C⁸² and 220-222°C¹³⁵).

5.2.2 6-Bromo-2,2'-bipyridine

The literature procedure¹³⁵ was modified, because using the exact temperature given there, gave only the starting material back (in good yield), but no product. Raising the reaction temperature above -80°C for the right amount and time, was found to make the reaction work to produce the desired product in reasonable yield: 2,6-Dibromopyridine was suspended in dry THF in an argon-flushed reaction flask. The resulting orange suspension was cooled to -90°C and a phenyllithium solution was added drop wise, while the temperature was allowed to rise to -80°C. After the addition was complete, the temperature was kept between -95°C and -80°C for 15 min., and then between -75°C and -65°C for 45 min. It was crucial to maintain this temperature range very carefully, until the reaction mixture turned into an ink black solution. The time varied considerably for this colour change to occur. The reaction was carried out several times, and the time it took for the reaction mixture to turn into an ink black solution, varied between 20 min and one hour. After the colour change had taken place, the reaction temperature was kept in the range of -75°C to -65°C for about half an hour to ensure complete reaction. The solution was cooled back to -90°C, and then let warm slowly to -70°C. This procedure was repeated, and then, when -70°C were reached the second time, the reaction was quenched by adding methanol, and after two to three minutes, water. After reducing the amount of solvent *in vacuo* the crude product could be obtained by filtration. It was purified by column chromatography to give the pure product as a white solid in 63% yield. It was characterised by ¹H-NMR spectroscopy.

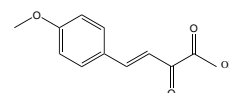
5.2.3 6-Tributylstannyl-2,2'-bipyridine

The procedure of Hanan¹³⁴ was followed. Best results were obtained when the amount of BuLi, that was added, was equivalent to the amount of 6-bromo-2,2'-bipyridine. The BuLi-solution was there-

fore titrated against HCl (0.20M) before use, see 'Organikum'¹³⁶ on pages 746–747: 6-Bromo-2,2'-bipyridine was suspended in diethyl ether and cooled to -100°C under argon, and lithiated by BuLi while the temperature was kept below -100°C . During 40 minutes, the temperature was raised to -80°C . The black suspension turned slowly into a reddish-brown solution. After cooling back to -100°C , tributyltin chloride was added and the solution turned black. The temperature was raised over 4h to -30°C to give an orange solution with white precipitate. The solvent was removed *in vacuo* and the product was obtained as a yellow oil. It was characterised by $^1\text{H-NMR}$ spectroscopy, which showed the relatively pure desired compound. The exact yield was not determined, as the compound was used directly for the next step.

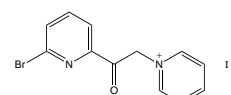
5.2.4 3-(4'-Methoxyphenyl)-1-oxo-2-butenoic acid

The literature procedure for the preparation of 4-bromo-cinnamaldehyde was applied,¹ except for a different ratio of ethanol/water. It was changed in favour of ethanol so that all starting material could be dissolved: Sodium pyruvate was dissolved in water, and 4-methoxy-cinnamaldehyde was added. Ethanol was added in order to obtain a solution. The colourless solution was cooled in an ice-water bath to 4°C , and a 10 per cent potassium hydroxide solution was added slowly, while the temperature was kept at $4 \pm 1^{\circ}\text{C}$. After the first few drops, the solution turned yellow, and later, a precipitate formed. Towards the end of the addition, the quantity of precipitate prevented magnetic stirring, so the suspension was swirled every few minutes. The reaction mixture was acidified to pH 4 with hydrochloric acid, still in the cooling bath, and the colour became more intensely yellow. It was then filtered, and the product was obtained as a yellow solid that was washed with water followed by diethylether and dried *in vacuo* to yield 58.9%. It was characterised by $^1\text{H-NMR}$ spectroscopy.



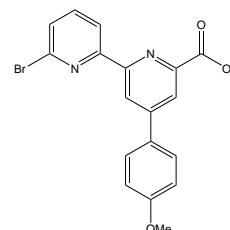
5.2.5 N-[1-Oxo-1-(6-bromo-2-pyridyl)eth-2-yl]pyridinium iodide (Br-PPI)

The synthesis was consistent with the literature procedure of Newkome *et al.*¹³⁷ This approach gave a better yield than the analogue reaction conditions to the PPI synthesis. An equivalent amount of pyridine was used, instead of an excess, and the product was recrystallised from water. It was characterised by infrared spectroscopy, and this confirmed the identity.



5.2.6 6'-Bromo-6-carboxylate-4-(4-methoxyphenyl)-2,2'-bipyridine

The literature procedure for the synthesis of 6'-bromo-4-(4-bromophenyl)-6-carboxylate-2,2'-bipyridine and 6'-bromo-4-(4-methylphenyl)-6-carboxylate-2,2'-bipyridine¹ was slightly altered for this synthesis, by the use of ethanol in addition to water. It is a Kröhnke cyclisation reaction:⁹² 3-(4'-Methoxyphenyl)-1-oxo-2-butenoic acid, Br-PPI and NH_4OAc were suspended in water and heated in the to 80°C . A minimum of ethanol was added in order to dissolve everything. The mixture was then heated to 100°C and left to reflux for 16h. After cooling to room temperature, a cream beige precipitate could be filtered off. It was washed with water and dried *in vacuo* to yield the product as an off-white powder in 96% yield.

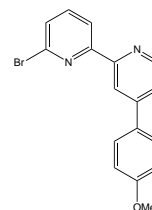


As this is a new compound, it was fully characterised: The micro analysis fitted the formula. The ^1H - and ^{13}C -NMR spectra were recorded on a 250 MHz spectrometer and the signals of the $^1\text{H-NMR}$ could

be assigned. All chemical shifts are listed in the experimental chapter on page 167. The carboxylic-acid group showed a broad signal for COO—H at 2523cm^{-1} and for C=O at 1682cm^{-1} . The C—O asym. stretch of the methoxy group showed at 1258cm^{-1} . EI mass spectrometry showed the molecule peak (M^+), a fragment without the carboxylate group, and fitting isotope patterns for both. Crystals in good quality were obtained from chloroform- d_1 , and X-ray analysis confirmed the structure, see appendix C on page 209.

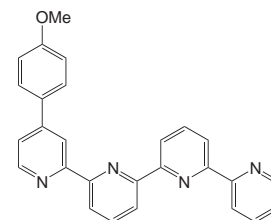
5.2.7 6-Bromo-4'-(4-methoxyphenyl)-2,2'-bipyridine

The synthesis by decarboxylation of the 6'-Bromo-6-carboxylate-4-(4-methoxyphenyl)-2,2'-bipyridine was new. After several attempts by refluxing in various solvents, in the oilbath as well as in the micro wave oven, the approach of Hammarström, Toftlund and Åkermark was used.¹³⁸ Small portions of 6'-bromo-4-(4-methoxyphenyl)-6-carboxylate-2,2'-bipyridine (10-20mg) were heated with a heat gun in a round bottomed flask (10 ml). As soon as the compound melted, it spontaneously decomposed with loss of CO_2 . The brown liquid obtained, was cooled to room temperature, it still contained some carboxylated material and was purified by recrystallisation from hot THF. The carboxylated starting material did not dissolve in this, and was filtered off. Adding some charcoal to the filtrate and renewed filtration gave the product as a brown powder in 51% yield. Micro analysis fitted the formula. It was further characterised by $^1\text{H-NMR}$ - and infrared-spectroscopy. Mass-spectrometry gave signals for the molecule ion and the fragment without brom, with fitting isotope patterns. Crystals in good quality were obtained from THF, and X-ray analysis confirmed the structure, see appendix C on page 204.



5.2.8 4-(4-Methoxyphenyl)-2,2':6',2'':6'',2'''-quaterpyridine

The procedure of a Stille coupling was followed as described by Hanan¹³⁴ for a similar synthesis. Dry DMF was degassed for 50 min, and the catalyst $\text{Pd}(\text{OAc})_2$ was added. This gave an orange-brown solution. Triphenylphosphine was added and the solution then turned lemon yellow. This catalyst solution was kept under argon while a degassed solution of 4'-(4-methoxyphenyl)-6-bromo-2,2'-bipyridine in dry DMF was prepared and added to the catalyst solution via cannula. The colour of the solution turned orange-brown again. The 6-(2,2'-bipyridyl)tributyltin was then added as a degassed solution in dry DMF. This mixture was refluxed for 25 hours and then cooled to room temperature. In the hope of removing the tin as an inorganic salt, a saturated aqueous solution of sodium fluoride was added, and the mixture was stirred at 60°C overnight. The suspension was allowed to cool to room temperature, and some additional water was added. The white precipitate was filtered off and washed with a small amount of DMF-water mixture followed by diethyl ether. The solvent of the filtrate was removed *in vacuo* to give the crude product as a brown powder.



The compound was run over an alox column as a first purification step. This way the product could be freed of starting material, but not from the tin, as the butyl groups could still be observed in the $^1\text{H-NMR}$ spectrum. The following eluents were used for the column: DCM : MeOH : Et_2NH (200:10:1) or (200:50:1). Recrystallisation from ethanol gave an enrichment of product in the solid, but not the pure compound. In a second step, the compound was run over a silica column. Now the tin could be removed from the product, (but 6-brom-4'-(4-methoxyphenyl)-2,2'-bipyridine did not separate from the product very well, if it had not been removed in by alox column first). The following eluents were tried: EtOAc: hexane : Et_2NH (8:20:1), (40:100:1) and CHCl_3 : MeOH, Et_2NH (20:2:1). The latter gave a solubility problem. A chromatotron with silica and EtOAc : hexane : Et_2NH (8:20:1) gave slightly better results

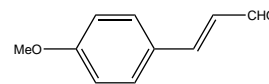
to the column. Very small amounts of crude product could be purified in one just one step. But for bigger quantities, two purification steps were necessary, one column with alox, and a second one with silica. Although the synthesis seemed to give an acceptable result judging by the $^1\text{H-NMR}$ spectrum, it was hard to extract the product from the columns.

This new unsymmetrically substituted quaterpyridine derivative was fully characterised: The micro analysis fitted the formula, $^1\text{H-}$ and $^{13}\text{C-NMR}$ spectra were recorded and the signals assigned with help from COSY, NOESY, HMQC and HMBC hetero spectra (see on page 169 in the experimental chapter). The infrared spectrum showed the C—H of the aromatic rings at 3055 and 3016cm^{-1} , of the methoxy group at 2931 - 2839cm^{-1} , and the strong signals of the asym. stretch of C—O at 1242cm^{-1} . The aromatic C—C and C—N stretch gave signals at 1566cm^{-1} , and the strong signal at 820cm^{-1} is typical for para substituted phenyl groups. The EI mass spectrum showed the protonated molecular signal $(\text{M-H})^+$, $(\text{M})^{2+}/2$ and the fragments $(\text{M-CH}_3)^+$ and (M-OCH_3) , and the FAB-MS showed the $(\text{M+H})^+$. A crystal structure of the compound could be solved, with a crystal that had grown from a fraction off a silica column: The eluent had been EtOAc: hexane : Et₂NH (8:20:1), see appendix B on page 197.

5.3 Alternative reaction steps to 4MeOphqtpy

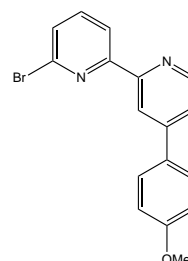
4-Methoxycinnamaldehyde

The general procedure for Wittig reaction described in the literature¹³⁹ was followed, but the work up conditions were altered in order to avoid $\text{Ph}_3\text{P=O}$ impurity in the product. Predried 1,3-dioxolan-2-ylmethyl triphenyl phosphoniumbromide and a solution of MeOLi in methanol were degassed in three pump-freeze cycles and heated to 90°C , before a solution of freshly distilled 4-methoxybenzaldehyde in dry DMF was added slowly. The mixture was refluxed overnight, cooled to room temperature, and quenched with water, upon which the clear solution turned into a white suspension. After extraction with hexane, a slightly yellowish oil was obtained. $^1\text{H-NMR}$ spectroscopy showed it to contain the desired protected product 1-(1,3-dioxolan-2-yl)-2-(4-methoxyphenyl)ethen and some already deprotected product. For deprotection, the oil was dissolved in a mixture of approximately 1 : 1 THF : HCL (10%) and stirred under argon for 2.5h at ambient temperature, upon which the colour became more intensely yellow. The mixture was extracted with hexane, and washed with a sodium hydrogencarbonate solution and brine. The solvent was removed *in vacuo* and the residue dried to give 95% pure product. It was characterised by $^1\text{H-NMR}$ spectroscopy.



6-Bromo-4'-(4-methoxyphenyl)-2,2'-bipyridine via 4-methoxycinnamaldehyde

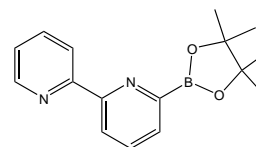
The Method of Kröhnke⁹² was followed. Dry 4-methoxycinnamaldehyde, dry Br-PPI and dry ammonium acetate were suspended in acetic acid under argon and heated to 100° to form a solution. The temperature was raised to 120°C , and the reddish black solution was refluxed at that temperature for 4.5h. The reaction was quenched by addition of dilute HCl solution. A precipitate formed and was filtered off, washed with HCl (2M) and dried *in vacuo* to give the product in 23% yield. It was characterised by $^1\text{H-NMR}$ spectroscopy. This reaction did not work every time.



When cyclising the analogue with a carboxylate group in the 6'-position (that had to be removed in a second step) the yield was improved and the reaction reproducible. The carboxylate group possibly helps to favour the first reaction step of the cyclisation, the Michael addition, see Figure 5.3.

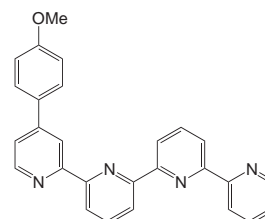
5.3.1 (2,2'-6-bipyridyl)-4,4,5,5-tetramethyl-1,3,2-dioxaborolan

From the literature, the lithiation procedure with PhLi^{135, 141} and the reaction procedure of lithiated bipyridine with boronic esters¹⁴²⁻¹⁵⁰ was followed. 6-Bromo-2,2'-bipyridine was suspended in dry THF and cooled under argon until the internal thermometer showed -85 °C. A solution of PhLi in a mixture of cyclohexane and ether was added slowly, and the reaction mixture turned into a black solution. Slowly the temperature was allowed to rise to -60 °C. After cooling to -80 °C, 2-isopropoxy-4,4,5,5-tetramethyl-1,3,2-dioxaborolan was added dropwise, while the temperature was kept below -70 °C. The solution was stirred in the cooling bath for another 2h. After yet another 45 minutes, the colour became lighter and the reaction was quenched at -70 °C with HCl (2M). The internal temperature raised immediately to 0 °C, and the colour changed to orange. Saturated sodium carbonate was added to neutralise the mixture, that was extracted with diethyl ether. Removing the solvent *in vacuo* gave a yellow oil that slowly turned brown. Characterisation by ¹H-NMR spectroscopy showed both product and starting material. A flash column with alox, and toluene with traces of Et₂NH as eluent, seemed to cause decomposition. The compound was synthesised a second time, and used for the next step (Suzuki coupling, see below) without purification.



5.3.2 4-(4-Methoxyphenyl)-2,2':6',2'':6'',2'''- quaterpyridine

For the Suzuki coupling,^{142, 143, 147, 151} the procedure from the literature¹⁴⁷ was followed. A solution of (2,2'-bipyrid-6-yl)-4,4,5,5-tetramethyl-1,3,2-dioxaborolan in dioxane was degassed in three pump-freeze cycles, and 6-bromo-4'-(4-methoxyphenyl)-2,2'-bipyridine and potassium carbonate were added give a yellow suspension. The freeze-pump cycle was repeated three more times. The catalyst: Pd(Ph₃P)₄ was washed with ethanol and diethyl ether and then added. After refluxing under inert atmosphere for 48h, the colour changed to brown. Water was added to quench the reaction. Extractions with ethyl acetate and removal of the solvent *in vacuo* gave a brown oil. The ¹H-NMR spectrum showed traces of product, but mainly starting material. The MS showed among other signals one matching the product and also one matching 6-bromo-4'-(4-methoxyphenyl)-2,2'-bipyridine. For full characterisation of the pure product, see page 169, and for the crystal structure, see page 197.



5.4 Conclusions about the syntheses

In a first attempt, it was tried whether the step via the 6-carboxylated 6'-Bromo-4-(4-methoxyphenyl)-2,2'-bipyridine could be omitted. The cyclisation step without the carboxylate group proved to give low yields, and a second disadvantage of the direct route was that it required 4-methoxycinnamaldehyde as starting material. Although the yield was high, this reaction needed oxygen and moisture free conditions, whereas the starting material to make the carboxylated 6'-bromo-4-(4-methoxy)-bipy were conducted in an ethanol-water mixture. This made the reaction pathway, that was described first (page 120- 123), easier and more reliable.

The synthesis of the (2,2'-bipyrid-6-yl)-4,4,5,5-tetramethyl-1,3,2-dioxaborolan, that was the starting material for the Suzuki coupling, was not really successful, and/or this compound not very stable. It may be therefore, that the following Suzuki coupling only worked very poorly. Even though the Stille coupling, described before (page 122) had worked better, the purification was not yet working satisfactorily. Like with the qnpy derivatives, described in chapter 2 and 3, it might be better to sonicate the crude ligand with dilute sodium hydroxide, before extracting with chloroform and adding it to a column. This procedure would deprotonate the ligand and preventing it from adsorbing too strongly on the alox or silica.

5.5 Summary and outlook

Two new asymmetrically substituted bipyridine derivatives and one new asymmetric ligand 4-(4-methoxyphenyl)-2,2':6',2'':6'',2''':6''',2''''-quaterpyridine were successfully synthesised and characterised. Although the method for purifying the ligand must still be improved, this opens up a second reaction pathway for other unsymmetrically substituted qtpy ligands. Study of helicate formation with copper(I) and silver(I) would be interesting, especially the investigation into possible effects of the unsymmetrical ligand substitution on head-to-head and head-to-tail isomerism in Ag(I)Cu(I) mixed metal helicates. Also self-assembly studies of this ligand with mixtures of metal ions that direct close-to-planar tetradentate, and metal ions that direct tetrahedral coordination would be of interest.

Then a next step would be to deprotect the hydroxy group and link two qtpy units together. In this new bridged ligand, the linker would connect the terminal rings of the qtpy, and a head-to-head helicate would resemble a hairpin. In a head-to-tail helicate, the linker would not be in the direction of the metal-metal axis, but on the side. The effect of the linker on the helicate self-assembly could easily be different from the effect of a linker positioned on the second last ring, compare Figures 1.13 on page 13 and 4.1 on page 50. By the techniques, used for the qnpy derivative helicates described in the previous chapter, these effects could be studied on the new qtpy-helicates.

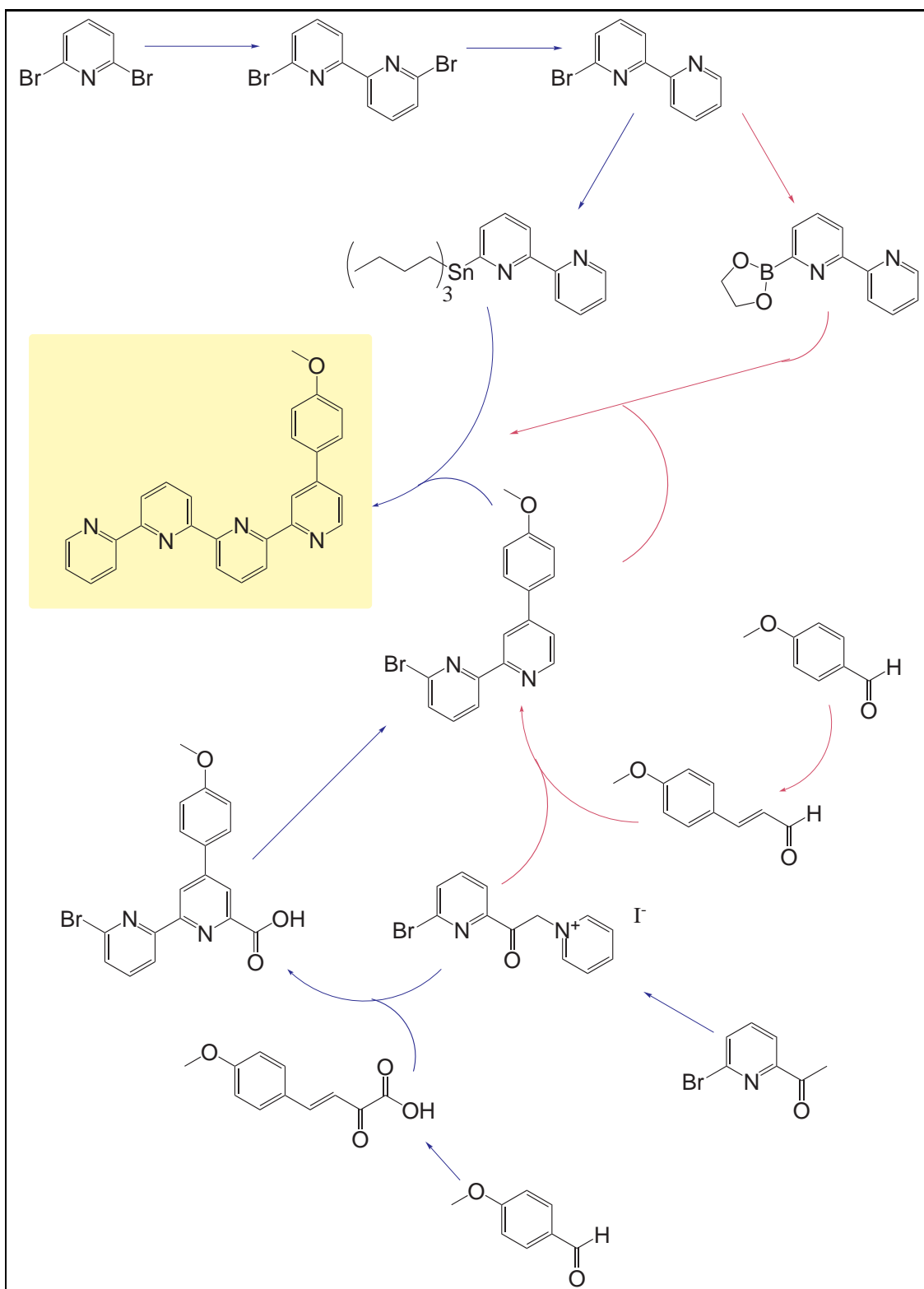


Figure 5.1: Overview over the synthesis of 4-(4-methoxyphenyl)-2,2':6'',2'':6''',2'''-quaterpyridine. The reaction steps of the better route are marked with blue arrows, and those of a route with low yields in the Kröhnke cyclisation are marked with pink arrows.

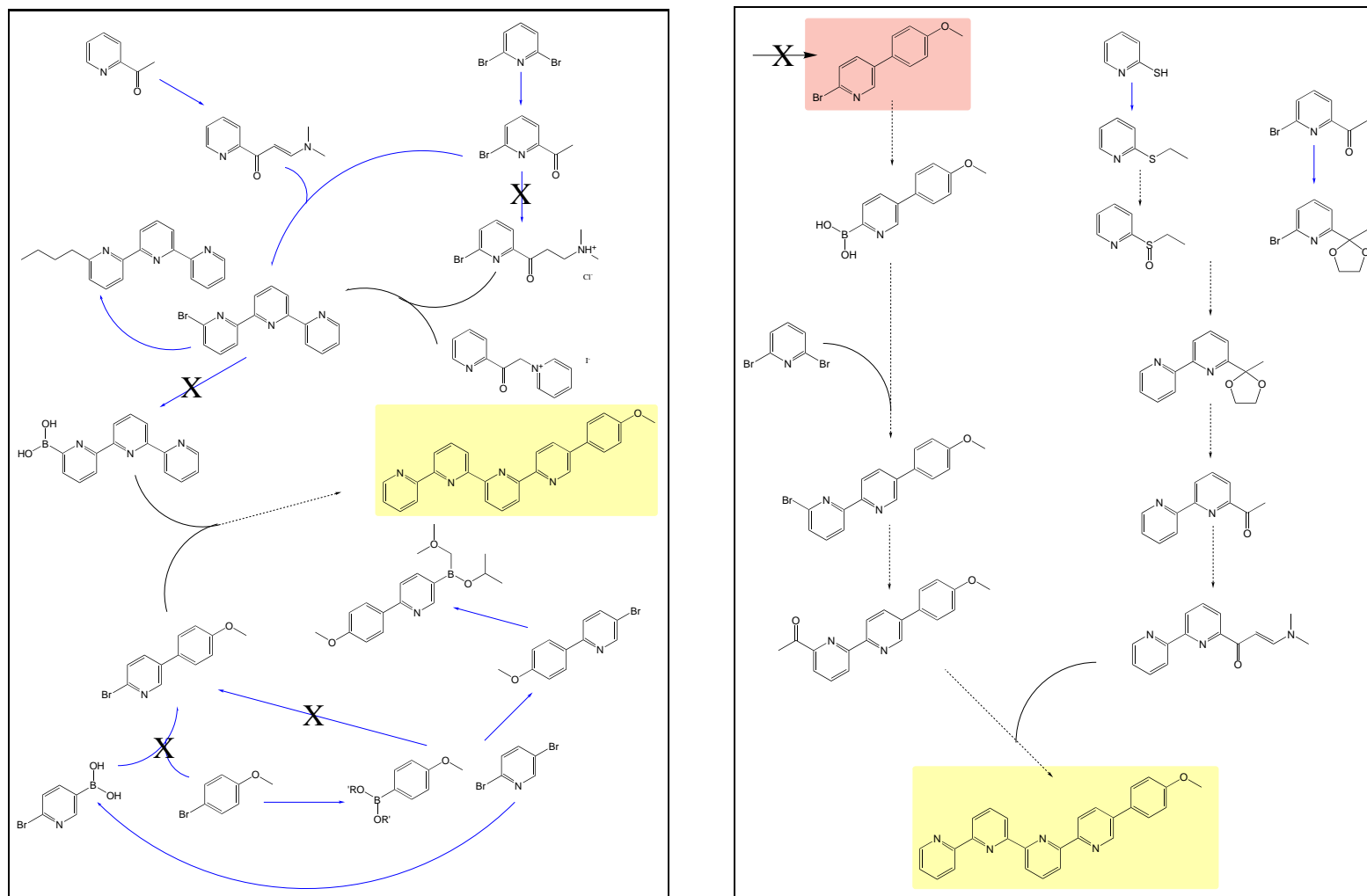


Figure 5.2: Two partially alternative reaction pathways to 5-(4-methoxyphenyl)-2,2':6',2'':6'',2'''-quaterpyridine. The target molecule is highlighted with a yellow background, and the reactions tried are marked in blue arrows. The 2-bromo-5-(4-methoxyphenyl)pyridine (with pink background) was to be obtained as the second last step in both pathways, and it could unfortunately not be synthesised in these attempts.

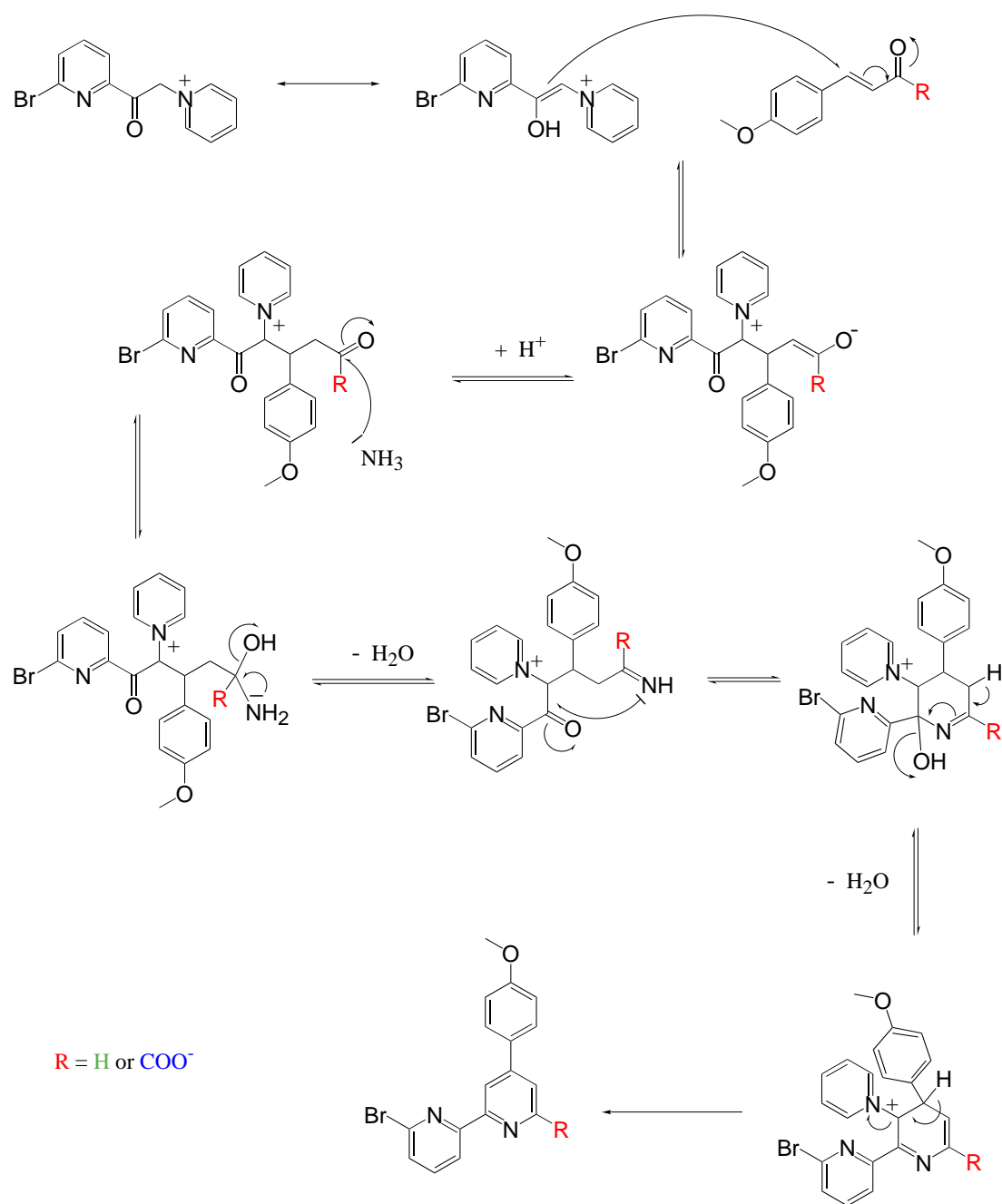


Figure 5.3: A possible Kröhnke cyclisation mechanism^{51,92} to the unsymmetrical bipy derivative with and without a substituent in the 6 position. Another variety is given by Jie Jack Li,¹⁴⁰ but also with a Michael addition as the first reaction step by the enolate attack. $R = \text{COO}^-$: 6'-bromo-6-carboxylate-4-(4-methoxyphenyl)-2,2'-bipyridine, and $R = \text{H}$: 6'-bromo-4-(4-methoxyphenyl)-2,2'-bipyridine.

Chapter 6

Conclusions and perspectives

This thesis is placed in the area of helicate self-assembly. Previous work had already established, that linear oligopyridines strands, like 2,2':6',2'':6'',2''':6'''-quaterpyridine (**qtpy**) and higher, are directed into dinuclear double helicates by certain transition metal ions, see for instance Lehn,^{54,55,152} Constable,^{41,42,121,130,153} Potts.³⁷ Unless prevented, helical structures form as two enantiomers. With unsymmetrical ligand strands, further possible isomer forms are accessible. Derivatives of linear quaterpyridine and quinquepyridine were chosen, as they may form dinuclear double helicates and are small enough to be quite soluble. All ligands synthesised in this thesis were unsymmetrically substituted, and this opened the possibility for the ligand strands inside a helicate to arrange in equal orientation (head-to-head) or in contrary orientation (head-to-tail).

Building on Ward's, Walker's and Whall's work,^{35,51,91} unsymmetrically substituted 2,2':6',2'':6'',2''':6''',2''''-quinquepyridine (**qnpq**) ligand strands were synthesised. In a second step, the ligand strands were linked together via their second pyridine ring, as pairs of identical, moieties. The linker was long and flexible, so that it would not prevent the two interlinked ligand strands forming a single helicate. In total, three **qnpq** derivatives and three interlinked **qnpq** derivatives were synthesised. Helicate formation of both non-linked and linked ligands was studied.

The metal ions used to direct double helicate formation with the **qnpq** derivatives were cobalt(II), nickel(II), copper(II), and in situ formed copper(I). The three first named all prefer octahedral environments, and thus in a (two stranded) double helicate claim three donor atoms per ligand. The copper(I) in the double helicate claims two donor atoms of each ligand strand. This was illustrated by two crystal structures of mixed valence copper(II/I) complexes of one double helicate comprised of two non-linked ligands, and one double helicate comprised of two interlinked ligands. Both helicates are arranged as the 'head-to-tail' isomer, with contrary oriented ligand strands. The likeness between helicates of linked and non-linked ligands in the crystal, did not extend to the general structure in solid nor to solution structures. Microanalysis, ¹H-NMR and UV-Vis measurements showed a difference between the copper-helicates of the non-linked and of the corresponding linked ligands. The helicates of which the crystal structure could be solved, were also measured electrochemically. The two metal based reduction potentials for Cu(II)→Cu(I) were identical for both the helicate with non-linked and with linked ligand strands. It suggests that the structure adapted in solution, although slightly different, is of the same type for the complex with non-linked and with linked ligands.

Double helicates of cobalt(II) and **qnpq** derivatives proved to be very sensitive to moisture. Nevertheless, a double helicate of non-linked and one of linked ligands could be obtained. In the ¹H-NMR spectra of these double helicates, there was seen the same kind of difference between helicates of linked and of non-linked ligands, as in the spectra of copper-double helicates: a double set of signals in the well resolved regions. This suggests that the linker affects the structure of the double helicate.

The structure adapted by the cobalt(II)-**qnpq** derivative system in moist conditions, was a mononuclear, almost planar monohelicate. The monohelicate and double helicate were easily distinguishable

in the $^1\text{H-NMR}$. The structures were assigned by comparison with previously published crystal structures^{42,65-67} and $^1\text{H-NMR}$ spectra^{51,68,91} of mono- and double helicates of the parent **qnp**y and similar **qnp**y derivatives. Also interconversion from the double helical to the monohelical structures were studied.

One complex of nickel(II) was synthesised and characterised. $^1\text{H-NMR}$ spectroscopy was not as conclusive as with cobalt(II) helicates, and the UV-Vis measurements were not expected to be as informative as in the partially mixed valence copper(II)/(I) helicates.

In a second project, one new unsymmetrically substituted **qtp**y derivative was synthesised in eight steps. It is considered an interesting ligand for the study of helicate formation directed by copper(I) and silver(I) metal centres. The substituent on the ligand was placed on the terminal pyridine ring, and it was chosen so that two entities could be linked together. The ligand was fully characterised.

Two new **qnp**y derivatives were synthesised. They were linked together to form two symmetrical ligands, each comprising two identical unsymmetrical moieties. One known non-linked and one known linked ligand were synthesised additionally. Of all six ligands, complexes with copper(II) were formed and characterised. For one double helicate with a new **qnp**y derivative, and with a new linked **qnp**y derivative, crystal structures were solved. They showed a double helical arrangement. Mass spectrometry, pointed to a 2 : 2 metal : ligand ratio for all six species, and all the $^1\text{H-NMR}$ spectra were very similar. This suggests that double helicates were obtained with all six **qnp**y ligands.

Cobalt(II) complexes of one of the non-linked and one of the linked **qnp**y derivative were synthesised. Depending on the conditions, two types of complexes formed with each ligand type. $^1\text{H-NMR}$ study suggested strongly a double helical array for the complexes formed in absolute environment, and a monohelical array for those formed in moist environment. Also interconversion in the direction from dinuclear double helicate to mononuclear monohelicate, triggered by the addition of water, was monitored.

Finally a new reaction pathway was developed for unsymmetrically substituted **qtp**y derivatives. It was used to synthesise a new unsymmetrical **qtp**y ligand. It was characterised by microanalysis, $^1\text{H-}$ and $^{13}\text{C-NMR}$, mass spectrometry, infrared spectroscopy, and the crystal structure was determined.

Further study on the copper-helicates of **qnp**y derivatives would include to establish whether helical isomers may be separated with e.g. HPLC, or if they are in a dynamic equilibrium.

In carefully controlled dry conditions, also the cobalt double helicates of the other four **qnp**y derivative helicands could be formed, and NMR-spectroscopy would reveal if the difference between helicates with non-linked and linked ligands strands seen in the two compounds, studied so far, is extended to the other. NMR-spectroscopy could further be used to monitor interconversion from these other cobalt(II)-double helicates to monohelicates.

The **qtp**y helicand could be complexed with silver(I) and copper(I), and the formation of double helical isomers studied with the same methods.

Chapter 7

Experimental Details

7.1 The synthesis of 4'-(*tert*-butylphenyl)-4'''-(4-hydroxyphenyl)-2,2':6',2'':6'',2''':6''', 2''''-quinquepyridine (qp) and complexes

7.1.1 Diethyl 2,6-dipicolinate

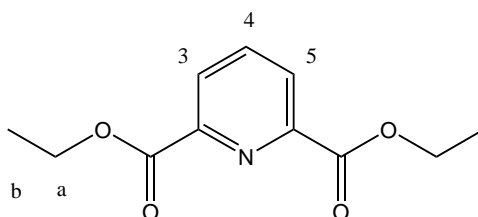


Figure 7.1: Diethyl 2,6-dipicolinat

The procedure of Smith was followed.⁹³ In a literature procedure from 1976, this synthesis step was also described.¹⁵⁴ 2,6-Dipicolinic acid (30.25g, 181.0mmol) and thionyl chloride (150ml, 245.7g, 2.065mol) were kept at reflux for 15h while the white suspension turned into a brown solution. Excess thionyl chloride was removed by distillation and after cooling to room temperature, toluene (abs., 100ml) was added and the mixture cooled to $\sim 0^{\circ}\text{C}$. Ethanol (abs., 63ml) was added dropwise over a period of 1.5h, and then the reaction mixture was refluxed for 17h. After cooling, sodium carbonate solution (20%, 300ml) was added, and the mixture was stirred for 20 minutes before the phases were separated. The aqueous phase was extracted with *t*-butyl methyl ether, the combined organic layers dried over sodium sulfate and filtered. After removing the solvent *in vacuo*, a brown solid was obtained (37.9g, 94%).

¹H-NMR, 250 MHz, CDCl₃ δ : 8.26 (d, H3 and H5, J=7.8Hz, 2H), 7.98 (t, H4, J=7.8Hz, 1H), 4.46 (q, CH₂, J=7.2Hz, 4H), 1.43 (t, CH₃, J=7.1Hz, 6H).

7.1.2 2,6-Diacetylpyridine

The procedure of Smith was followed.⁹³ (The reaction conditions for this step have been improved in 2001 by a chinese group,⁹⁴ using toxic CrO₃. Another synthetic pathway has been patented in 2003.⁹⁵) Under an argon atmosphere, ethanol (abs., 120ml) was added dropwise to sodium (9.74g) at room temperature and the mixture heated at reflux until all sodium had dissolved. Ethyl acetate (40ml, 36g, 0.41mol) was added dropwise under vigorous stirring, followed by diethyl 2,6-dipicolinate (20.79g,

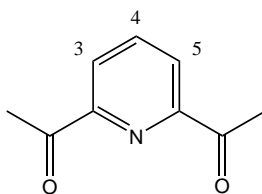


Figure 7.2: 2,6-Diacetylpyridine

93.14mmol) in xylene (60ml). The dropping funnel was then rinsed with more xylene (10ml). The reaction mixture was refluxed under argon for 15h and a colour change from dark brown to light brown occurred with a small amount of precipitate being formed. After cooling to room temperature, HCl (25%, 260ml) was added slowly and the colour changed to yellow. A white precipitate also formed. The two phases were separated, and the aqueous phase extracted twice with xylene. The organic layers were combined and the solvent removed *in vacuo* to give a brown oil (26.00g). It was stored overnight in the dark. The brown oil, and the aqueous phase containing the precipitate were combined and refluxed for 4h. The precipitate dissolved to give a brown solution. After cooling to room temperature, the solution was cooled in ice and neutralised carefully with sodium carbonate, before extracting twice with *tert*-butyl methyl ether. The combined organic layers were dried over sodium sulfate, filtered and the solvent removed *in vacuo* to give the crude product (11.35g).

Recrystallisation from hot hexane : pentane (9 : 1) gave slightly yellowish needles (6.63g, 44%).

¹H-NMR, 250 MHz, CDCl₃ δ: 8.17 (d, H3, H5, J=8.3Hz, 2H), 7.96 (t, H4, J=7.8Hz, 1H), 2.75 (s, CH₃, 6H).

EI-MS, 70eV, 350 °C: m/z= 163 M⁺, 121 (M - CH₃CO + H)⁺, 106 (M - CH₃CO - CH₃ + H)⁺, 93 (pyridine + O)⁺.

7.1.3 2-Acetyl-6-[3-(4-hydroxyphenyl)-1-oxoprop-2-enyl]pyridine

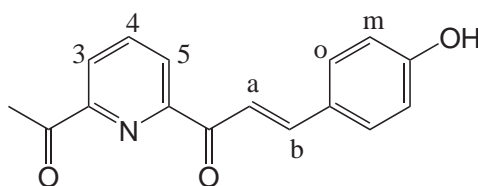


Figure 7.3: 2-Acetyl-6-[3-(4-hydroxyphenyl)-1-oxoprop-2-enyl]pyridine

The synthesis was consistent with that reported by Whall⁵¹ and the product was obtained in 34% yield.

¹H-NMR, 250 MHz, CDCl₃ δ: 8.37 (dd, H5, J_{H5-H4}, J_{H5-H3}=7.70Hz and 1.2Hz, 1H), 8.23 (dd, H3, J_{H3-H4}, J_{H3-H5}=7.9Hz and 1.2Hz, 1H), 8.23 (d, Ha, J_{Ha-Hb}=16Hz, 1H), 8.03 (t, H4, J_{H4-H3}/J_{H4-H5}=7.7Hz, 1H), 7.96 (d, Hb, J_{Hb-Ha}=16Hz, 1H), 7.65 (d, Ho, J_{Ho-Hm}=8.5Hz, 2H), 6.92 (d, Hm, J_{Hm-Ho}=8.5Hz, 2H), 2.88 (s, CH₃, 3H).

IR KBr ($\tilde{\nu}$ / cm⁻¹): 3364m, ~3320sh, 3070w, 3009w, 2021w, 1960w, 1890w, 1705s, 1659s, 1589s, 1558vs, 1512s, 1435s, 1350s, 1303m, 1265s, 1211s, 1164s, 1103w, 1041s, 980vs, 957m, 879w, 810vs, 748s.

7.1.4 2-[3-(4-*tert*-Butylphenyl)-1-oxoprop-2-enyl]-6-[3-(4-hydroxyphenyl)-1-oxoprop-2-enyl]pyridine

The procedure of Whall⁵¹ was used, and a modification of this procedure was equally successful:

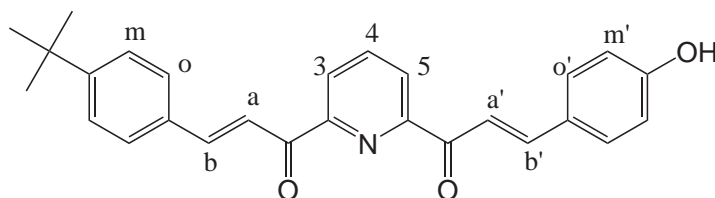


Figure 7.4: 2-[3-(4-*tert*-Butylphenyl)-1-oxoprop-2-enyl]-6-[3-(4-hydroxyphenyl)-1-oxoprop-2-enyl]pyridine

2,6-Diacetylpyridine (1.597g, 9.787mmol), 1-propanol (45ml) and diethylamine (3ml) were heated, using an oil bath at 120 °C; this gave a temperature of 95 °C within the flask. A mixture of 4-hydroxybenzaldehyde (1.071g, 8.770mmol) in 1-propanol (15ml) was added over 30 minutes and then the reaction mixture was heated under reflux for 6.5 hours. A mixture of 4-*tert*-butylbenzaldehyde (1.539g, 9.486mmol) in 1-propanol (15ml) was then added to the boiling solution over a period of 10 minutes followed by more diethylamine (5ml). After a further 18 hours, another 2ml of diethylamine was added; and after a further four hours, the reaction mixture was allowed to cool to room temperature. It was a reddish brown, dark solution. The solvent was removed in *vacuo* to give an oily residue which was shown to contain a mixture of the two precursor aldehydes and the desired product.

The residue was suspended in dichloromethane to afford a yellow solid, which was filtered off and washed with a small amount dichloromethane.

Proton NMR analysis showed that this was the title compound. Yield 0.748mg (21%).

¹H-NMR, 250 MHz, CDCl₃ δ: 8.45-8.30 m (m, H₃, H₅, H_a, H_{a'}, 4H), 8.11-8.00 (m, H₄, H_b, H_{b'}, 3H), 7.73-7.68 (m, H_o, H_{o'}, 4H), 7.48 (d, H_m, J_{m-o}=8.3Hz, 2H), 6.91 (d, H_{m'}, J_{m'-o'}=8.3Hz, 2H), 1.38 (s, H_t, 9H).

IR KBr ($\tilde{\nu}$ / cm⁻¹): ~3310sh, 3178m, 3078w, 3032w, 2962m, 2901w, 2872w, 1982w, 1898w, 1782w, 1650s, 1597s, 1550vs, 1504vs, 1412w, 1350s, 1273m, 1234vs, 1211s, 1165s, 1111w, 1034vs, 980vs, 872w, 833sh, 810vs, 741s, 710m, 663m.

7.1.5 Side product of the synthesis above: 2,6-di[3-(4-*tert*-butylphenyl)-1-oxoprop-2-enyl]pyridine

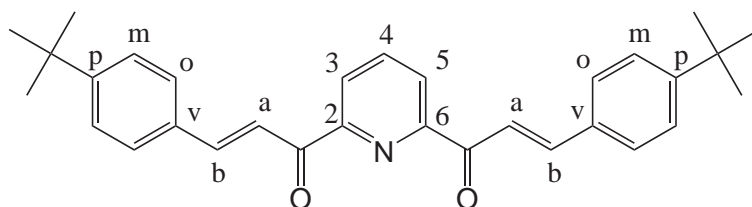


Figure 7.5: 2,6-Bis[3-(4-methoxyphenyl)-1-oxoprop-2-enyl]pyridine

2,6-di[3-*tert*-Butylphenyl)-1-oxoprop-2-enyl]pyridine was obtained as a side product in 14% yield from the synthesis of 2-acetyl-6-[3-(4-methoxyphenyl)-1-oxoprop-2-enyl]pyridine, see page 133 when recrystallising the crude product from methanol.

¹H-NMR, 250 MHz, CDCl₃ δ: 8.48 (d, Ha, J=16.1Hz, 2H), 8.38 (d, H3 and H5, J=7.8Hz, 2H), 8.08 (t, H4, J=7.8Hz, 1H), 8.03 (d, Hb, J=16.1Hz, 2H), 7.74 (d, Ho, J=8.3Hz, 4H), 7.50 (d, Hm, J=8.8Hz, 4H), 1.38 (s, *t*-Bu).

EI-MS, 70eV, ~450°C: m/z= 451 M⁺, 436 (M - CH₃)⁺, 422 (M - 2CH₃)⁺, 408 (M - 3CH₃)⁺, 394 (M - C(CH₃)₃)⁺, 318 (M - phenyl-C(CH₃)₃)⁺, 263 ((M - phenyl-C(CH₃)₃ - C(CH₃)₃)⁺, 211, 129, 57.

IR diamond ($\tilde{\nu}$ / cm⁻¹): 3333w, 3078b, 3032w, 2962s, 2901sh, 2870m, 1666s, 1605vs, 1566sh, 1512m, 1465m 1412m, 1335vs, 1273m, 1211m, 1150w, 1103m, 1026vs, 987vs, 810vs, 748m, 640m.

Melting point 154°C.

7.1.6 *N*-[1-Oxo-1-(2-pyridyl)-eth-2-yl]pyridinium iodide (PPI)

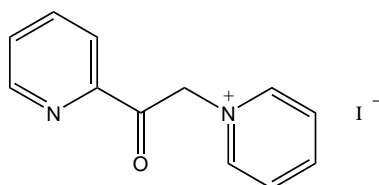


Figure 7.6: *N*-[1-Oxo-1-(2-pyridyl)-eth-2-yl]pyridinium iodide (PPI)

The literature procedure was followed.^{92, 155-157} Iodine (12.75g, 50.22mmol) and pyridine (60ml) were heated at 60°C. 2-Acetylpyridine (5.60ml, 6.05g, 49.9mmol) was added and the temperature raised to 125°C. A black precipitate formed. After 90 minutes the mixture was cooled to room temperature and filtered. The solid was redissolved in a minimum amount of hot ethanol. Charcoal was added and the mixture was stirred under reflux for 15 min. The charcoal was filtered off, and the hot solution cooled to room temperature. Greenish-yellow crystals formed and were filtered off (2.297g). After concentrating the filtrate *in vacuo*, more precipitate was obtained (0.348g). The solids were washed with ethanol and diethyl ether and dried *in vacuo*. Infrared spectroscopy showed both samples to be pure product, so the yield was 2.645g, 16.2%.

IR KBr ($\tilde{\nu}$ / cm⁻¹): 3313(w), 3126(w), 3082(m), 3051(s), 3008(m), 2877(s), 2807(m), 1735(w), 1710(vs), 1630(vs), 1583(s), 1483(vs), 1459(m), 1437(s), 1413(s), 1356(m), 1333(vs), 1292(m), 1264(m), 1227(vs), 1212(vs), 1194(s), 1146(m), 1087(m), 1027(m), 998(vs), 952(m), 849(m), 786(vs), 760(m), 691(vs), 668(vs), 619(m), 569(vs).

7.1.7 4'-(4-*tert*-Butylphenyl)-4'''-(4-hydroxyphenyl)-2,2':6',2'':6'',2''':6''',2''''-quinquepyridine (qp)

The synthesis was consistent with that of Whall,⁵¹ and the product was isolated in 93% yield.

¹H-NMR, 600 MHz, DMSO-d₆ δ: 9.01 (d, B5, J_{B5-B3}=1.6Hz, 1H), 8.95 (d, D3, J_{D3-D5}=1.7Hz, 1H), 8.78 (ddd, A6, J=4.7Hz, 1.8Hz and 0.9Hz, 1H), 8.77 (ddd, E6, J=4.7Hz, 1.7Hz and 1.0Hz, 1H), 8.76-8.72 (m, B3, C3, C5, ~3H) where B3 is at 8.73 and C3, C5 have the signals at 8.72 and 8.70, 8.72-8.69 (m, D5, A3, E3, ~3H) where D5 is at 8.68 and A3 at 8.68 and E3 at 8.67, 8.25 (t, C4, J_{C4-H3, C4-H5}=7.8Hz, 1H), 8.06 (td, A4, J=7.5Hz and 1.7Hz, 1H), 8.04 (td, E4, J=7.5Hz and 1.7Hz,

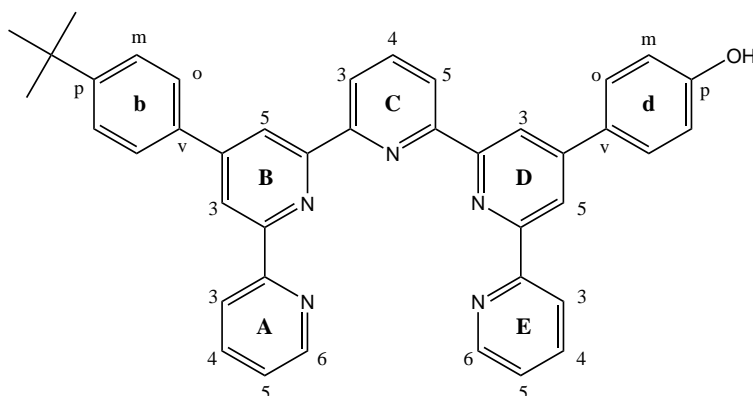


Figure 7.7: 4'-(4-*tert*-butylphenyl)-4'''-(4-hydroxyphenyl)-2,2':6',2'':6'',2''':6''',2''''-quinquepyridine

^1H), 7.97 (d, bo, $J_{bo-bm}=8.5\text{Hz}$, 2H), 7.89 (d, do, $J_{do-dm}=8.6\text{Hz}$, 7.64 (d, bm, $J_{bm-bo}=8.7\text{Hz}$, 2H), 7.55-7.52 (m, A5, E5, 2H), 6.99 (d, dm, $J_{dm-do}=8.7$, 2H), 1.38 (s, ^{tert}Bu , 9H).

^{13}C -NMR, 150 MHz, DMSO- d_6 δ : 159.3 (dp), 155.5, 155.3, 155.1, 152.3 (bp), 149.6, 149.3 (A6, E6 and B4 or bv and D4 or dv), 139.0 (C4), 137.6 (A4, E4), 135.0 (B4 or bv and D4 or dv), 128.2 (d_o), 126.8 (b_o), 126.2 (bm), 124.4 (A5, E5), 121.4 (C3, C5, A3 or E3), 120.9 (C3, C5, A3 or E3), 118.63 (B5), 118.1 (B3), 117.8 (D3), 117.1 (D5), 116.1 (dm), 34.5 ($^{tert}\text{Bu}_{\text{quarternary}}$), 31.0 ($^{tert}\text{Bu}_{\text{primary}}$).

Maldi-TOF MS m/z: 1293, 857, 816, 669 ($\text{M} + \text{K} + \text{H}_2\text{O} + \text{H}$) $^+$, 668 ($\text{M} + \text{H}_2\text{O}$) $^+$, 629, 612 ($\text{M} + \text{H}$) $^+$, 572, 552, 492, 479 ($\text{M} - \text{tert-butylphenyl} + \text{H}$), 430, 404.

IR diamond ($\tilde{\nu}$ / cm^{-1}): 3055w, 2965m, 2901w, 2870w, 1975w, 1790w, 1666w, 1605s, 1574vs, 1512vs, 1466s, 1443sh, 1381vs, 1273vs, 1227s, 1173m, 1111m, 1018vs, 949m, 895m, 818vs, 787vs, 733vs, 663vs.

UV-Vis / chloroform, c=22.9 μM , wavelength/nm (extinction coefficient/ $\text{cm}^{-1}\text{M}^{-1}$): 259 (46,100), 280 (50,300), 308 (24,200), 318 (18,500).

7.1.8 [$\text{Cu}_2(4'-(4\text{-tert-Butylphenyl})-4'''-(4\text{-hydroxyphenyl})-2,2':6',2'':6'',2''':6''',2''''\text{-quinquepyridine})_2][\text{PF}_6]_3$, [$\text{Cu}_2(\text{qp})_2][\text{PF}_6]_3$

The synthesis of Whall was used,⁵¹ and the product was isolated as a brown powder in 31% yield.

^1H -NMR, 600 MHz, acetonitrile- d_3 δ : 33.1 (vb), 24.9 (vb), 12.8 (vb), 9.51 (b), 9.13 (b), 8.76 (b), 8.10 (b), 7.77, 7.73, 7.10 (b), 6.93 (d, $J=33.5\text{Hz}$), 6.41, 6.35, 6.27, 1.22 ($(\text{CH}_3)_3\text{C}$).

Maldi-TOF MS (matrix: α -Cyano-4-hydroxycinnamic acid) m/z: 1536 ($\text{M} - 2\text{PF}_6 + \text{K} + 4\text{H}$) $^+$, 885, 676 ($\text{qp} + \text{Cu} + \text{H}$) $^+$, 637, 613 ($\text{qp} + 2\text{H}$) $^+$.

IR diamond ($\tilde{\nu}$ / cm^{-1}): 3657w, 3634w, 3572w, 3510w, 3186sh, 3094b, 2962w, 2870w, 2284w, 2230w, 2168w, 2021w, 1983w, 1705w, 1589s, 1543m, 1528w, 1481m, 1458m, 1420w, 1358m, 1273sh, 1242m, 1180m, 1119w, 1080m, 1026m, 818vs, 787sh, 741s, 694s, 671m, 648m, 617m.

UV-Vis / acetonitrile, $c_1=11.9\mu\text{M}$ and $c_2=119\mu\text{M}$, wavelength/nm (extinction coefficient/ $\text{cm}^{-1}\text{M}^{-1}$): 224 (89,900)sh, 292 (77,000), 318 (63,600)sh, 348 (42,100)sh, 470 (6,050), 577 (2,240)sh.

7.2 The synthesis of 1,17-di(4-(4'-(4-*tert*-Butylphenyl)-2,2':6',2'':6'', 2''':6''',2''''-quinquepyridyl)-phenoxy)-3,6,9,12,15-pentaoxaheptadecane (qcq) and complexes

7.2.1 Hexaethylene glycol ditosylate (Tos₂Heg)

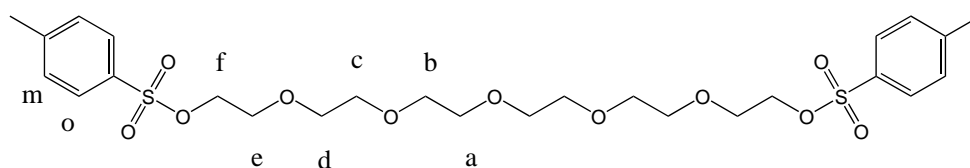


Figure 7.8: Hexaethyleneglycol ditosylate

This compound was synthesised according to the method of Ouichi and Inoue¹⁰⁰ on a scale of $\frac{1}{30}$ of that reported. An aqueous solution of sodium hydroxide (3.15g, 78.8mmol in 15ml H₂O) was cooled in an ice-water bath, and a solution of hexaethylene glycol (6.00ml, 6.76g, 23.9mmol) in THF (15ml) was added. A THF solution of tosyl chloride (8.35g, 43.7mmol in 15ml) was added dropwise, while the temperature of the reaction mixture was kept at 2-4°C. The colourless solution became white and opalescent, and it was left standing in the fridge for one week. After addition of 40ml of ice-cold water, the product was extracted three times with DCM. The combined extracts were dried over magnesium sulfate, and the solvent removed *in vacuo* to give 12.3g of a colourless oil (yield 95%). ¹H-NMR showed the identity, and a TLC-test did not reveal any impurities.

¹H-NMR, 250 MHz, CDCl₃ δ : 7.79 (d, Ho, $J_{Ho-Hm}=8.2\text{Hz}$, 4H), 7.34 (d, Hm, $J_{Hm-Ho}=7.9\text{Hz}$, 4H), 4.17-4.13 (m, Hf, 4H), 3.70-3.58 (m, Ha,b,c,d,e 20H), 2.44 (s, CH₃, 6H).

7.2.2 1,17-di(4-(4'-(4-*tert*-Butylphenyl)-2,2':6',2'':6'', 2''':6''',2''''-quinquepyridyl)phenoxy)-3,6,9,12,15-pentaoxaheptadecane (qcq)

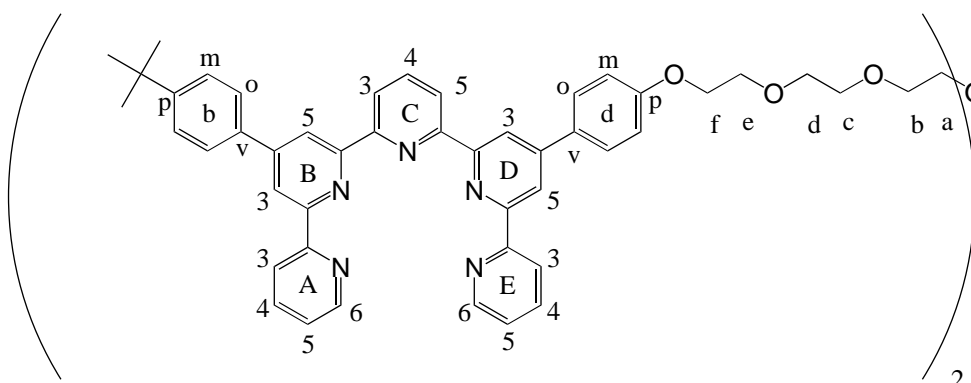


Figure 7.9: 1,17-Bis(4-(4'-(4-*tert*-butylphenyl)-2,2':6',2'':6'', 2''':6''',2''''-quinquepyridyl)phenoxy)-3,6,9,12,15-pentaoxaheptadecane

The synthesis was consistent with that used by Whall,⁵¹ except for the purification; qcq was purified by column chromatography on Alox 90 (Merck), eluting with chloroform : diethylamine (25 : 1), and collected as the first yellow band in 49% yield.

Microanalysis: found (calculated: C₉₄H₈₈N₁₀O₇ · 1½ H₂O) % C: 75.32 (75.43), % H: 6.04 (6.13), % N: 9.29 (9.36).

¹H-NMR, 600 MHz, CDCl₃ δ: 8.92 (d, B5, J=1.6Hz, 2H), 8.87 (d, D3, J=1.6Hz, 2H), 8.71-8.61 (m, A3, E3, B3, C3, C5, D5, A6 and E6, 16H) where B3 comes at 8.71, A6 at 8.70, E6 at 8.68, D5 at 8.65, A3 and E3 at 8.64 and C3 and C5 at 8.63, 7.99 (t, C4, J_{C4-C3/C5}=7.7Hz, 2H), 7.88-7.82 (m, A4, E4, bo and do, 12H) where A4 and E4 are at 7.85, bo at 7.83 and do at 7.82, 7.52 (d, bm, J_{bm-bo}=8.2Hz, 4H), 7.33 (ddd, A5, J=0.8Hz, 7.4Hz and 7.4Hz, 2H), 7.31 (ddd, E5, J=0.7Hz, 7.2Hz and 7.3Hz, 2H), 7.03 (d, dm, J_{dm-do}=8.6Hz, 4H), 4.18 (t, f, J_{f-e}=4.7Hz, 4H), 3.89 (t, e, J_{e-f}=4.8Hz, 4H), 3.75 (m, d, 4H), 3.70 (m, c, 4H), 3.68 (s, a and b, 8H), 1.39 (s, ^tBu, 18H).

¹³C-NMR, 150 MHz, CDCl₃ δ: 159.89 (dp), 156.52, 156.49, 156.10, 156.09, 155.94, 155.89, 155.58, 155.53, 152.38 (bp), 149.96, 149.52, 149.27 (A6), 149.21 (E6), 137.81 (C4), 137.01 (A4, E4), 135.92 (bv or B4), 131.20 (dv or D4), 131.10, 128.60 (do), 127.17 (bo), 126.11 (bm), 123.92 (A5 or E5), 123.90 (A5 or E5), 121.56 (C3 or C5 or A3 or E3), 121.54 (C3 or C5 or A3 or E3), 121.41 (C3 or C5 or A3 or E3), 121.39 (C3 or C5 or A3 or E3), 119.11 (B5), 118.84 (B3), 118.55 (D3), 118.36 (D5), 115.17 (dm), 71.08 (d), 70.86 (a or c), 70.85 (a or c), 70.81 (b), 69.91 (e), 67.70 (f), 34.92 (C(CH₃)₃), 31.55(CH₃).

¹⁵N-NMR, 60.81 MHz, CDCl₃ δ: -14.46 couples (N_D), -13.91 (N_B), -9.57 (N_E), -9.35 (N_A), -11.75 (N_C).

Maldi-TOF MS (matrix: α-Cyano-4-hydroxycinnamic acid) m/z: 1533 (M + K + Na + 3H)⁺, 1527 (M + K + H₂O + 2H)⁺, 1492 (M + Na + H)⁺, 1470 (M + 2H)⁺, 919, 818, 652 (qp + K)⁺, 479, 423

IR diamond (ν̄ / cm⁻¹): 3526(w), 3070(w), 2955(m), 2924(m), 2862(m), 2322(w), 2291(w), 2167(w), 1983(w), 1967(w), 1913(w), 1790(w), 1720(m), 1605(m), 1582(vs), 1543(s), 1512(vs), 1474(m), 1450(m), 1420(m), 1389(vs), 1250(vs), 1180(m), 1111(vs), 1065(s), 1041(s), 987(m), 941(w), 894(m), 818(vs), 787(vs), 733(vs), 663(s), 640(m), 617(s).

UV-Vis / chloroform, c=8.16 μM, wavelength/nm (extinction coefficient/cm⁻¹M⁻¹): 260 (78,800), 281 (87,100), 307 (43,600)sh, 318 (31,900)sh.

7.2.3 [Cu₂(1,17-di-(4-(4'-tert-Butylphenyl)-2,2':6',2'':6'',2''':6''',2''''-quinquepyridyl)-phenoxy)-3,6,9,12,15-pentaoxaheptadecane)][PF₆]₃, [Cu₂qcq]PF₆]₃

Methanol (~3ml) was added to the solid qcq ligand (20.4mg, 13.9 μmol) and Cu(OAc)₂ · H₂O (5.8mg, 29.1 μmol). In the sonicating bath, a green-brown solution was obtained. This solution was filtered, and a solution of NH₄PF₆ (56mg, 344 μmol) in methanol (1ml) was added. The brown precipitate was filtered off and washed with a little ice cold methanol, water, more ice cold methanol and ether, and dried *in vacuo* to yield a brown powder (17mg, 60%).

Microanalysis: found (calculated: C₉₄H₈₈N₁₀O₇Cu₂3.3(PF₆) % C: 52.75 (52.93), % H: 4.16 (4.16), % N: 6.32 (6.57).

¹H-NMR, 250 MHz, CDCl₃ δ: 24.9 (vb), 17.5(vb), 12.7 (d, J=104Hz), 9.13 (b), 8.23-7.30 (m), 7.01, 6.49, 6.35, 3.94, 3.88, 3.78, 3.63, 3.62, 3.60, 3.56, 3.54 (3.94-3.54 linker -CH₂O- protons), 1.22 (s, (CH₃)₃C).

Maldi-TOF MS (matrix: α-Cyano-4-hydroxycinnamic acid) m/z: 1740 (M – 2PF₆ + H)⁺, 1596 (M – 3PF₆ + 2H)⁺, 1546, 1533 (M – 3PF₆ – Cu + 2H)⁺, 1470 (qcq + 2H)⁺, 980, 715.

IR diamond ($\tilde{\nu}$ / cm⁻¹): 3657w, 3587w, 3086b, 2947m, 2870m, 2168w, 1597s, 1573m, 1543m, 1520m, 1481m, 1450m, 1427w, 1358w, 1304sh, 1242s, 1188s, 1111m, 1080m, 1026m, 949w, 818vs, 787s, 741s, 694m, 648m, 617m.

UV-Vis / acetonitrile, c₁=11.5 μM and c₂=115 μM, wavelength/nm (extinction coefficient/cm⁻¹M⁻¹): 224 (96,800)sh, 291 (83,900), 316 (73,000)sh, 347 (49,800)sh, 473 (4,450), 585 (1,600)sh.

7.2.4 [[Co₂(1,17-di-(4-(4'-*tert*-butylphenyl)-2,2':6',2'':6'',2''':6''',2''''-quinquepyridyl)-phenoxy)-3,6,9,12,15-pentaoxaheptadecane)(OAc)][PF₆]₃, [Co₂(qcq)(OAc)][PF₆]₃

The qcq-ligand (30mg, 20 μmol) and Co(OAc)₂ · 4H₂O (10mg, 41 μmol) were suspended in dry methanol (6.0ml) under nitrogen and heated to 85 °C. This temperature was kept for 75 minutes, and a brown-orange solution was obtained. NH₄PF₆ (11mg, 67 μmol) was added, and it dissolved immediately. After two minutes of stirring, the solution was allowed to cool to room temperature. After cooling with ice, a white precipitate was filtered off, using an inverse sinter with nitrogen atmosphere, and celite. The solvent was evaporated *in vacuo*, to give a brown powder (28mg, 66%).

¹H-NMR, 250 MHz, acetonitrile-d₃ δ: 269 (b), 264 (b), 142, 140, 119, 113, 79.5, 78.8, 75.8, 74.9, 64.3 (b), 55.5, 54.4, 52.6, 50.3, 35.0 (b), 28.8 (b), 26.2, 25.6, 24.5, 23.8, 15.8, 14.8, 13.0, 12.3, 9.67, 9.34, 7.06, 6.73, 5.92, 5.44, 4.94, 4.54, 4.42-3.51 (m), -0.50 (b), -6.36, -10.2.

Maldi-TOF MS m/z: 1738 (Co₂qcq(OAc)⁺ + OAc + MeOH + 2H)⁺, 1661 (Co₂qcq(OAc) + (H₂O) – 2H)⁺, 1583 (Co₂qcq(OAc) – 3H)⁺, 1516 (qcq + 2Na + 2H)⁺.

7.2.5 [Co₂(1,17-bis(4-(4'-*tert*-Butyl phenyl)-2,2':6',2'':6'',2''':6''',2''''- quinquepyridyl)phenoxy)-3,6,9,12,15-pentaoxaheptadecane)(H₂O)₂(MeOH)₂][OAc][PF₆]₃, [Co₂(qcq)(OH₂)₂(MeOH)₂][PF₆]₄

For the synthesis, the procedure of Whall⁵¹ to make the cobalt complex of qp was followed. Ligand qcq (24mg, 16 μmol) and cobalt(II) acetate · 4H₂O were suspended in methanol (5ml). The orange suspension was heated to reflux to give an orange-brown solution. A solution of ammonium hexafluorophosphate (9.0mg, 55 μmol) in methanol (1.2ml) was added and upon cooling to room temperature, a golden precipitate formed. It was filtered off, washed with ice-cold methanol and dried *in vacuo* to give an orange powder (25mg, 69%).

Microanalysis: found (calculated: C₉₈H₁₀₃N₁₀O₁₃Co₂P₃F₁₈ · $\frac{1}{4}$ HPF₆) · H₂O % C: 52.44 (52.64), % H: 4.36 (4.74), % N: 6.26 (6.26).

¹H-NMR, 250 MHz, acetonitrile-d₃ δ: 138 (b), 135 (b), 82.1, 76.3, 74.4, 70.67, 50.4, 47.5, 21.2, 18.9, 13.4, 13.2, 8.53, 8.12, 7.47, 7.31, 6.33, 5.56, 2.43, 2.26, 2.10. 1.53, 1.29, 0.88.

Maldi-TOF MS m/z: 1770 (Co₂qcq + K + PF₆)⁺, 1531 (qcq + K + MeOH)⁺, 952 (M - 2PF₆ - Co + O₂H - 5H)²⁺/2 or (Co₂qcq(MeOH)₂ + 2PF₆ - 4H)⁺, 912 (M - 3PF₆ + H₂O + H)²⁺/2, 710 (Co₂qcq(MeOH)₂ + 2Na + 3PF₆)³⁺/3, 670 (qp + Co)⁺.

IR diamond ($\tilde{\nu}$ / cm⁻¹): 3655w, 3084w, 2955m, 2870m, 2164w, 2039w, 1983w, 1599vs, 1574s, 1545s, 1520s, 1479s, 1452s, 1427m, 1402m, 1391sh, 1362w, 1302w, 1242s, 1188s, 1115s, 1080s, 1059sh, 1022s, 1012s, 937w, 876sh, 827vs, 820vs, 790vs, 746sh, 739vs, 692s, 658s.

7.3 The synthesis of the 4'-(methoxyphenyl)-4'''-(4-hydroxyphenyl)-2,2':6',2'':6'',2''':6''',2''''-quinquepyridine (mp) and complexes

7.3.1 2-Acetyl-6-[3-(4-methoxyphenyl)-1-oxoprop-2-enyl]pyridine

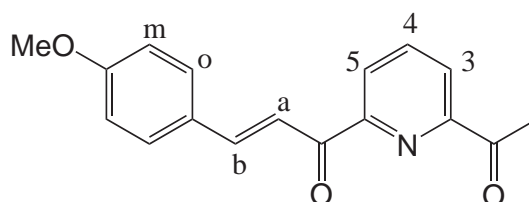


Figure 7.10: 2-Acetyl-6-[3-(4-methoxyphenyl)-1-oxoprop-2-enyl]pyridine (see also crystal structure: figure C.1 on page 201)

2,6-Diacetylpyridine (4.771g, 29.24mmol) and 4-methoxybenzaldehyde (3.55ml, 3.98g, 29.2mmol) were dissolved in 1-propanol (50ml) and heated in the oilbath to 120°C. Diethylamine (2ml) were added and the orange solution was refluxed. During the next 4h, two portions of diethylamine, each of 2ml, were added dropwise, and overnight another 10ml of diethylamine were added dropwise to the hot mixture. This resulted in a beige suspension. After cooling to room temperature, the yellow solid was filtered from the orange solution. ¹H-NMR spectroscopy showed the solid (4.057g) contained a mix of product and 2,6-bis[3-(4-methoxyphenyl)-1-oxoprop-2-enyl]pyridine. The filtrate was collected and the solvent removed *in vacuo*. 4.170g of solid was obtained, containing mainly starting material.

Recrystallisation from hot methanol with a small amount of toluene gave 2,6-bis[3-(4-methoxyphenyl)-1-oxoprop-2-enyl]pyridine. The solvent of the filtrate was removed *in vacuo* and the filtrate redissolved in DCM and toluene. To the hot brown solution, hexane was added slowly and then the mixture was left to cool to room temperature. The desired compound formed a yellow precipitate. It was filtered off and dried *in vacuo* to give 2.063g (25%) of 2-acetyl-6-[3-(4-methoxyphenyl)-1-oxoprop-2-enyl]pyridine.

Alternatively, a silica column with hexane : EtOAc : Et₂NH (50:10:1) as eluent was used for purifying the compound.

Microanalysis: found (calculated: C₁₇H₁₅N₁O₃ · 0.2 H₂O) % C: 71.69 (71.67), % H: 5.57 (5.45), % N: 4.95 (4.92).

¹H-NMR, 250 MHz, CDCl₃ δ: 8.36 (dd, H5, J=7.6Hz and 1.01Hz, 1H), 8.23 (d, Ha, J=16.2Hz, 1H), 8.22 (dd, H3, J=7.6Hz and 1.01Hz 1H), 8.018 (t, H4, J=7.6Hz, 1H), 7.98 (d, Hb, J=16.2Hz, 1H), 7.68 ("dt", H(ortho), J_{om}=9.1Hz, J_{om'}=~2Hz, J_{oo'}=~1Hz, 2H), 6.97 ("dt", H(meta), J_{mo}=9.1Hz, J_{mo'}=~2Hz, J_{mm'}=~1Hz, 2H), 3.87 (s, methoxy, 3H), 2.87 (s, acetyl, 3H).

EI-MS, 70eV, ~250°C: $m/z = 281 M^+$, $252 (M - OCH)^+$, $161 (M - (1-(4-methoxyphenyl)-1-ethen-2-yl) + 2H)^+$, $133 ((2,6-diacetylpyridine) - 2H)^+$, $121 (2-acetylpyridine)^+$.

IR diamond ($\tilde{\nu} \text{ cm}^{-1}$): 3001w, 2970w, 2901w, 2885w, 2839w, 2361w, 2322w, 2191w, 2160w, 2044w, 1983w, 1944w, 1890w, 1697s, 1666s, 1589s, 1566s, 1512s, 1458m, 1442m, 1420m, 1342m, 1304m, 1250s, 1219m, 1204m, 1180s, 1150m, 1103m, 1034vs, 987vs, 949m, 879w, 833w, 810vs, 787s, 748m, 725m, 648m.

7.3.2 Side product of the synthesis above: 2,6-bis[3-(4-methoxyphenyl)-1-oxoprop-2-enyl]pyridine

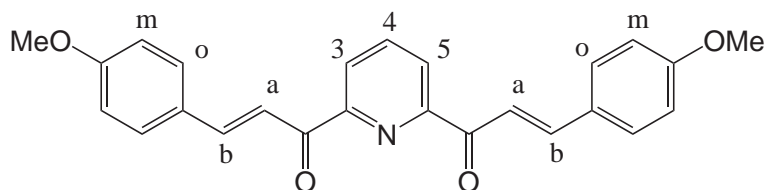


Figure 7.11: 2,6-Bis[3-(4-methoxyphenyl)-1-oxoprop-2-enyl]pyridine

2,6-Bis[3-(4-methoxyphenyl)-1-oxoprop-2-enyl]pyridine was obtained as a side product from the synthesis of 2-acetyl-6-[3-(4-methoxyphenyl)-1-oxoprop-2-enyl]pyridine, see page 139.

Microanalysis: found (calculated: $C_{25}H_{21}N_1O_4 \cdot \frac{1}{4} H_2O$) % C: 74.45 (74.33), % H: 5.33 (5.36), % N: 3.71 (3.47).

$^1\text{H-NMR}$, 250 MHz, CDCl_3 δ : 8.37 (d, H3 and H5, $J=7.7\text{Hz}$, 2H), 8.33 (d, Ha, 16.05Hz , 1H), 8.07 (“t”, H4, $J=7.5\text{Hz}$, 1H), 8.00 (d, Hb, $J=15.7\text{Hz}$, 1H), 7.73 (“dt”, H(ortho), $J_{om} = 8.7\text{Hz}$, $J_{om'} = \sim 2\text{Hz}$, $J_{oo'} = \sim 1\text{Hz}$, 2H), 6.98 (“dt”, H(meta), $J_{om} = 8.7\text{Hz}$, $J_{mo'} = \sim 2\text{Hz}$, $J_{mm'} = \sim 1\text{Hz}$, 2H), 3.89 (s, H(MeO), 5-6H)

EI-MS, 70eV, 350°C: $m/z = 399 M^+$, 370, 342, 292, 237, 210, 161, 133, 90.

IR diamond ($\tilde{\nu} / \text{cm}^{-1}$): 3063w, 2970w, 2924w, 2839w, 2037w, 1982w, 1890w, 1697w, 1659s, 1597vs, 1566vs, 1512vs, 1465w, 1443w, 1420s, 1343s, 1304s, 1258vs, 1204w, 1180vs, 1111w, 1026vs, 987vs, 926sh, 872w, 833w, 802vs, 740w 640w.

7.3.3 2-[3-(4-methoxyphenyl)-1-oxoprop-2-enyl]-6-[3-(4-hydroxyphenyl)-1-oxoprop-2-enyl]pyridine

Route via 2-acetyl-6-[3-(4-methoxyphenyl)-1-oxoprop-2-enyl]pyridine The procedure of Whall⁵¹ (to make 2-[3-(4-*tert*-butylphenyl)-1-oxoprop-2-enyl]-6-[3-(4-hydroxyphenyl)-1-oxoprop-2-enyl]pyridine) was adjusted. 2-Acetyl-6-[3-(4-methoxyphenyl)-1-oxoprop-2-enyl]pyridine (2.047g, 7.277mmol) was dissolved and heated in 1-propanol (40ml) and Et_2NH (4ml) to 120°C then let cool to 70°C . At this temperature a solution of 4-hydroxybenzaldehyde (0.964, 7.89mmol) in 1-propanol (25ml) was added dropwise by syringe, over a period of an hour. When half of the solution containing the aldehyde was added, more Et_2NH (1ml) was added to the hot reaction mixture, before adding the second half of the aldehyde solution. The reaction mixture was refluxed at 120°C for 4.5 h, then cooled to room temperature. The solvent was removed *in vacuo* and a greenish brown solid was obtained (3.28g). Proton-NMR showed a mixture of product and both starting materials in the ratio of about 1:1:1.

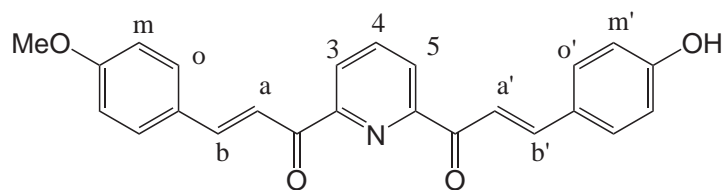


Figure 7.12: 2-[3-(4-Methoxyphenyl)-1-oxoprop-2-enyl]-6-[3-(4-hydroxyphenyl)-1-oxoprop-2-enyl]pyridine

Route via 2-acetyl-6-[3-(4-hydroxyphenyl)-1-oxoprop-2-enyl]pyridine Again, the procedure of Whall⁵¹ was adjusted to this synthesis. 2-Acetyl-6-[3-(4-hydroxyphenyl)-1-oxoprop-2-enyl]pyridine (6.90g, 25.8mmol) and 4-methoxybenzaldehyde (30.0ml, 33.6g, 0.247mol) were heated in 1-propanol (100ml) and Et₂NH (6ml) to 80 °C. After a few minutes, everything dissolved, and the mixture was then refluxed at 120 °C for one hour, before more Et₂NH (4ml) was added. After half an hour more, Et₂NH (4ml) was added and the reaction mixture refluxed for 45 more minutes, before cooling to room temperature. The solvent was removed *in vacuo* to give a brown oil. Proton-NMR showed product and 4-methoxybenzaldehyde.

The oil was added to a silica column and eluted with DCM:MeOH:Et₂NH(20:1:0.1). The third band contained the product. It was obtained as an orange powder (3.6g, 36%).

Microanalysis: found (calculated: C₂₄H₁₉N₁O₄ · H₂O) % C: 71.31 (71.45), % H: 5.22 (5.25), % N: 3.53 (3.47).

¹H-NMR, 400 MHz, CDCl₃ δ: 9.54 (b, OH), 8.36 (d, H3, H5, J_{H3/H5-H4}=7.8Hz, 2H), 8.324 (d, Ha, J_{Ha-Hb}=15.9Hz, 1H), 8.319 (d, Ha', J_{Ha'-Hb'}=15.9Hz, 1H), 8.07 (t, H4, J_{H4-H3/H5}=7.8Hz, 1H), 8.00 (d, Hb, J_{Hb-Ha}=15.9Hz, 1H), 7.99 (d, Hb', J_{Hb'-Ha'}=16.2Hz, 1H), 7.72 (d, Ho, J_{Ho-Hm}=8.8Hz, 2H), 7.68 (d, Ho', J_{Ho'-Hm'}=8.8Hz, 2H), 6.98 (d, Hm, J_{Hm-Ho}=8.8Hz, 2H), 6.92 (d, Hm', J_{Hm'-Ho'}=8.8Hz, 2H), 3.89 (s, methoxy, 3H).

¹³C-NMR, 150 MHz, CDCl₃ δ: ~189 (C = O), ~162 (Cp), ~159 (Cp'), 154 (C2 and C6), 145.66 (Cb, Cb'), ~138 (C4), 131.41 (Co'), 131.22(Co), ~128 (Cv and Cv'), 126.34 (C3 and C5), ~118 (Ca, Ca'), 116.82 (Cm'), 115.19 (Cm), ~57 (MeO).

EI-MS, 70eV, ~450 °C: m/z= 385 M⁺, 292 (M – hydroxyphenyl)⁺, 278 (M – methoxyphenyl)⁺, 161 (2,6-diacetyl pyridine – 2H)⁺, 133 (1-oxo-1-(2-pyridyl)-prop-2-en)⁺.

IR diamond (ν̄ cm⁻¹): 3225w, 2962m, 2824m, 2754m, 2476m, 2384w, 2044w, 1983w, 1875w, 1651s, 1589vs, 1558vs, 1504vs, 1458s, 1389m, 1342s, 1281sh, 1250vs, 1165vs, 1111sh, 1034vs, 987s, 810vs, 740m, 694m, 663m.

7.3.4 4'-(4-Methoxyphenyl)-4'''-(4-hydroxyphenyl)-2,2':6',2'':6'',2''':6''',2''''-quinquepyridine (mp)

The synthesis procedure from Whall's thesis⁵¹ was applied. 2-[3-(4-methoxyphenyl)-1-oxoprop-2-enyl]-6-[3-(4-hydroxyphenyl)-1-oxoprop-2-enyl]pyridine (1.451g, 3.764mmol), PPI (2.607g, 7.993mmol) and dry ammonium acetate (10g, 1.3·10⁻¹mol) were heated to 90 °C in methanol (~12ml) under argon. Almost all dissolved, and 4 drops freshly distilled acetic acid was added. The mixture was refluxed overnight. A beige precipitate had formed. After cooling in the fridge, the precipitate was

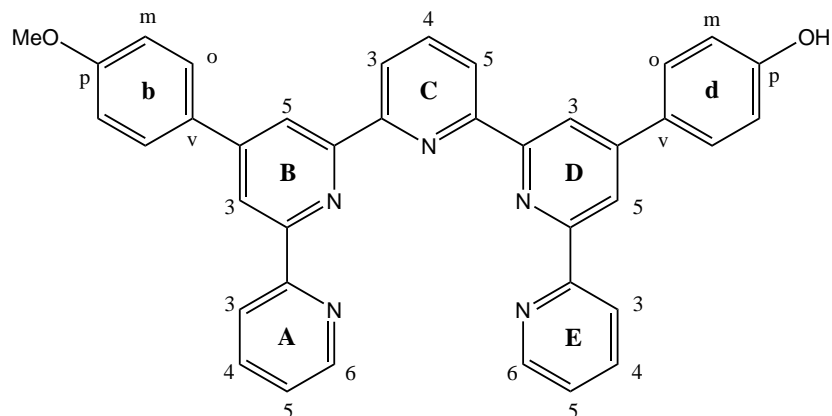


Figure 7.13: 4'-(4-Methoxyphenyl)-4'''-(4-hydroxyphenyl)-2,2':6',2'':6''',2''':6''',2''''-quinquepyridine

filtered off from the brown solution, washed three times with ice cold methanol and dried *in vacuo* to yield 1.072g (49%) of product.

Microanalysis: found (calculated: C₃₈H₂₇N₅O₂ · H₂O) % C: 75.40 (75.61), % H: 4.89 (4.84), % N: 11.67 (11.60).

¹H-NMR, 600 MHz, DMSO-d₆ δ: 9.94 (s, OH, 1H), 8.97 (d, B5, J_{B5-B3}=1.8Hz, 1H), 8.95 (d, D3, J_{D3-D5}=1.7Hz, 1H), 8.78-8.76 (m, A6, E6), 8.72-8.69 (m, B3, C3, C5, ~3H) where C3 or C5 is at 8.708 and B3 and C3 or C5 are at 8.705, 8.69-8.66 (m, D5, A3, E3, ~3H) where A3 is at 8.682, D5 at 8.680 and E3 at 8.675, 8.24 (t, C4, J_{C4-C3, C4-C5}=7.7Hz, 1H), 8.05 (ddd, A4, J=7.6Hz, 3.0Hz and 1.9Hz, 1H), 8.04 (ddd, E4, J=7.7Hz, 3.0Hz and 1.8Hz, 1H), 8.00 (d, bo, J_{bo-bm}=8.7Hz, 2H), 7.89 (d, do, J_{do-dm}=8.6Hz, 2H), 7.55-7.51 (m, A5, E5, 2H), 7.17 (d, bm, J_{bm-bo}=8.8Hz, 2H), 7.01 (d, dm, J_{dm-do}=8.5Hz, 2H), 3.89 (s, MeO, 3H).

¹³C-NMR, 150 MHz, DMSO-d₆ δ: 161.0 (bp), 159.1 (dp), 155.4, 154.9, 149.3 (A6, E6), 149.1, 138.2 (C4), 137.3 (A4, E4), 130.0 (B4 or bv), 128.2 (bo, do), 128.0 (D4 or dv), 124.5 (A5, E5), 121.5 (C3, C5), 121.1 (A3, E3), 118.3 (B5), 118.0 (D3), 117.8 (B3), 117.4 (D5), 116.2 (dm), 114.9 (bm), 56.0 (MeO).

Maldi-TOF MS (matrix: α-Cyano-4-hydroxycinnamic acid) m/z: 664 (M + H + 2K)⁺, 609 (M + Na + H⁺), 587 (M + 2H)⁺, 573, 546, 250.

IR diamond (ν̄ cm⁻¹): 3330b, 3135w, 3055w, 3009w, 2939w, 2901w, 2831w, 2592w, 2492w, 2446w, 2353w, 2291w, 2168w, 2021w, 1983w, 1882w, 1790w, 1659w, 1605sh, 1574s, 1551sh, 1512vs, 1466m, 1450m, 1381s, 1258vs, 1173s, 1103m, 1072m, 1034m, 987m, 887m, 818vs, 787vs, 733vs, 687w, 663m.

UV-Vis / chloroform, c=17.1 μM, wavelength/nm (extinction coefficient/cm⁻¹M⁻¹): 261 (52,200)sh, 284 (66,900), 308 (36,100)sh, 318 (25,700)sh.

7.3.5 [Cu₂(4'-(4-methoxyphenyl)-4'''-(4-hydroxyphenyl)-2,2':6',2'':6''',2''':6''',2''''-quinquepyridine)₂][PF₆]₃, [Cu₂(mp)₂][PF₆]₃

4'-(4-Methoxyphenyl)-4'''-(4-hydroxyphenyl)-2,2':6',2'':6''',2''':6''',2''''-quinquepyridine (19mg, 32.4 μmol) and Cu(OAc)₂ · H₂O (8.2mg, 4.1 · 10⁻⁵ mol) were dissolved in methanol (~3ml). The

brown solution was filtered. A solution of NH_4PF_6 in methanol (1ml) was filtered and added. The brown precipitate was filtered off and washed with ice cold methanol, water, ice cold methanol again, and ether to yield a brown powder (19 mg, 34%).

Microanalysis: found (calculated: $\text{C}_{76}\text{H}_{54}\text{N}_{10}\text{O}_4\text{Cu}_2\text{P}_3\text{F}_{18}\cdot 6\text{H}_2\text{O}$) % C: 49.38 (49.57), % H: 3.29 (3.61), % N: 7.54 (7.61).

$^1\text{H-NMR}$, 600 MHz, acetonitrile- d_3 δ : 24.2 (vb), 17.2 (vb, weak), 13.2 (b), 9.24 (b), 7.97 (b), 7.67 (b), 7.55, 7.52, 6.50 (d, $J=44.2\text{Hz}$), 6.40 (d, $J=48.4\text{Hz}$), 3.69 (CH_3O), 3.65 (CH_3O).

Electrospray MS / acetonitrile, m/z: 649 ($\text{mp} + \text{Cu}$)⁺, 433 ($\text{M} - 3\text{PF}_6$)³⁺/3.

IR diamond ($\tilde{\nu} / \text{cm}^{-1}$): 3641w, 3518w, 3094b, 2839w, 2168w, 2037w, 1983w, 1589s, 1574sh, 1543m, 1520m, 1481m, 1458m, 1420m, 1358m, 1242s, 1180s, 1126w, 1018m, 818vs, 787sh, 741m, 648m, 617m.

UV-Vis / acetonitrile, $c_1=114\mu\text{M}$ and $c_2=11.4\mu\text{M}$, wavelength/nm (extinction coefficient/ $\text{cm}^{-1}\text{M}^{-1}$): 226 (93,600sh), 292 (72,000), 317 (66,300), 351 (51,100)sh, 467 (6,440), 581 (2,140)sh.

X-ray see appendix A.1 page 175.

7.3.6 [Nickel₂(4'-(4-methoxyphenyl)-4'''-(4-hydroxyphenyl)-2,2':6', 2'':6'', 2''':6''', 2''''-quinquepyridine)₂(OAc)][PF₆]₃, [Ni₂(mp)₂(OAc)][PF₆]₃

Turquoise $\text{Ni}(\text{OAc})_2 \cdot 4\text{H}_2\text{O}$ (9.8mg, 39 μmol) and beige ligand (21.8mg, 37.2 μmol) were alternatively sonicated and heated in relatively dry methanol (1ml) to give an intense brown solution. A solution of NH_4PF_6 (96mg, 59 $\cdot 10^{-4}\text{mol}$) in dry methanol (2ml) was added. First a light coloured precipitate formed. When the reaction flask was heated, the precipitate turned dark brown under an orange solution. Some more methanol (2ml) were added, and after heating for 5 min., the mixture was left standing at room temperature overnight. The precipitate was still brown, and the orange solution had turned lighter. After cooling down in the fridge, the precipitate was filtered off, washed with dry methanol (3ml) and dried *in vacuo* to yield 23mg 70%.

Microanalysis: found (calculated: $\text{C}_{78}\text{H}_{57}\text{N}_{10}\text{O}_6\text{Ni}_2\text{P}_3\text{F}_{18} \cdot 3,5 \text{H}_2\text{O}$) % C: 50.85 (50.76), % H: 3.52 (3.50), % N: 7.62 (7.59).

$^1\text{H-NMR}$, 600 MHz, acetonitrile- d_3 δ : 159 (vb), 139 (vb), 75.4 (b, 2H), 66.1 (b, 2H), 62.9 (b, 2H), 59.8 (b, 4H), 51.4 (b, 1H), 50.0 (b, 2H), 46.7 (sh, 2H), 45.8 (b, 2H), 45.0 (b, 2H), 40.9 (b, 2H), 14.86 (b, 2H), 13.63 (b, 2H), 11.01 (b, 4H), 9.69 (b, 3H), 8.09 (vb, 3H), 6.92-6.60 (m, phenyl, 8H), (3.91, 3.88 and 3.86) (m, CH_3CO , 6H).

Electrospray MS / acetonitrile, m/z: 1637 ($\text{M} - \text{PF}_6 + 2\text{H}$)⁺, 748, 725 ($\text{Ni}(\text{mp})(\text{H}_2\text{O})(\text{MeOH})_2$)⁺, 705 ($\text{Ni}_2(\text{mp}) + 4\text{H}$)⁺, 678, 662 ($\text{Ni}(\text{mp})(\text{H}_2\text{O})$)⁺, 634, 615 ($\text{Ni}(\text{mp})_2 + 2\text{H}$)²⁺/2, 450 ($\text{M} - 3\text{PF}_6 + 3\text{H}$)³⁺/3, 368 ($\text{Ni}(\text{mp})(\text{OAc})(\text{MeOH}) + 2\text{H}$)²⁺/2, 322 ($\text{Ni}(\text{mp}) + 2\text{H}$)²⁺/2.

IR diamond ($\tilde{\nu} / \text{cm}^{-1}$): 3641w, 3510w, 3190sh, 3078w, 2839w, 2168w, 1983w, 1597s, 1520m, 1482m, 1450m, 1420m, 1358m, 1242s, 1180s, 1126sh, 1080w, 1018m, 825vs, 787sh, 741s, 679sh, 648m.

7.3.7 Drying cobalt(II) acetate

In order to make the dinuclear, dihedral cobalt complex of mp, all water had to be removed from $\text{Co}(\text{OAc})_2 \cdot 4\text{H}_2\text{O}$. In order to accomplish this, the procedure described in the abstract CA 65, 18490g of a Japanese article of Kubo and Manabe¹⁵⁸ was followed. Cobalt(II) acetate $\cdot 4\text{H}_2\text{O}$ was dried for 5h at 60°C *in vacuo* (0.05mbar). The colour changed hereby from pink to marine blue.

IR diamond ($\tilde{\nu}$ / cm^{-1}): 3001w, 2932w, 1543vs, 1389vs, 1335vs, 1049m, 1026s.

IR nujol ($\tilde{\nu}$ / cm^{-1}): 2368w, 2199w, 2052w, 1574vs, 1558sh, 1543sh, 1528sh, 1420vs, 1342m, 1049m, 1018m.

7.3.8 [Cobalt₂(4'-(4-methoxyphenyl)-4'''-(4-hydroxyphenyl)-2,2':6',2'':6'',2''':6''', 2''''-quinquepyridine)₂(OH₂)(OH)][PF₆]₃, [Co₂(mp)₂(OH₂)(OH)][PF₆]₃

$\text{Co}(\text{OAc})_2 \cdot 4\text{H}_2\text{O}$ was dried at 60°C *in vacuo* until the pink colour had changed to blue completely (~3h). The IR spectrum was recorded, which confirmed that it was water free. $\text{Co}(\text{OAc})_2$ (7.1mg, $40\mu\text{mol}$) and predried ligand (20.6mg, $35.2\mu\text{mol}$) were then dried together again at 60°C *in vacuo* for three hours and let cool under argon to ambient temperature. Addition of dry methanol (3ml) (distilled twice from magnesium) and slight heating gave a dark brown solution. Dry NH_4PF_6 (96mg, $5.9 \cdot 10^{-4}\text{mol}$) was added as a solid, and after heating slightly and swirling, the mixture was left standing under argon at room temperature until all solvent had evaporated and only a brown solid was left. This was put in a predried sinter and washed with dry methanol. After drying *in vacuo*, 19mg of a brown powder was obtained (61% yield). The proton-NMR showed double helicate only.

Microanalysis: found (calculated: C₇₆H₅₇N₁₀O₆Co₂P₃F₁₈·3H₂O) % C: 50.67 (50.34), % H: 3.52 (3.50), % N: 7.75 (7.73).

¹H-NMR, 600 MHz, acetonitrile-d₃ measured immediately upon solvation δ : 266, 263, 261, 256, 141, 140, 139, 138, 117, 114, 113, 110, 80.6-74.0 (m), 70.2, 56.1-50.0 (m), 41.0 (weak), 34.4, 27.6 (weak), 24.5, 23.0 (weak), 21.0 (weak), 18.8 (weak), 14.8, 13.2 (weak), 12.5 (weak), 11.1 (weak), 9.7 (weak), 8.53, 6.78, 4.48, -0.6 (weak).

IR diamond ($\tilde{\nu}$ / cm^{-1}): 3634w, 3572w, 3495w, 3086w, 2978w, 2893w, 2839w, 2168w, 2014w, 1983w, 1767w, 1651sh, 1597s, 1520m, 1482m, 1450m, 1420m, 1358w, 1242s, 1180s, 1111sh, 1080w, 1018m, 825vs, 779sh, 740s, 702sh.

Differential pulse voltametry. Reduction potentials/V vs Fc⁺/Fc: -1.04, -1.50 (weak), -1.72, -2.24, -2.43, -2.74.

7.3.9 [Cobalt(4'-(4-methoxyphenyl)-4'''-(4-hydroxyphenyl)-2,2':6',2'':6'',2''':6''', 2''''-quinquepyridine)(H₂O)₂][PF₆]₂, [Co(mp)(OH₂)₂][PF₆]₂

The procedure from Whall⁵¹ was followed but no water added before precipitating. The ligand (19.8mg, $33.8\mu\text{mol}$) was suspended in methanol (12ml). Cobalt(II) acetate tetrahydrate was added to the suspension. It turned into an orange-brown solution. A solution of ammonium hexafluorophosphate (370mg, 2.27mmol) in methanol (3ml) was added and a golden precipitate formed after some of the solvent had been taken off *in vacuo*. It was filtered off, washed with water and ice-cold methanol and diethyl ether and dried *in vacuo* to give 160mg of a greenish-yellow solid. It contained excess ammonium hexafluorophosphate.

¹H-NMR, 600 MHz, acetonitrile-d₃ δ: 134 (b), 81.8, 76.1, 67.0, 74.0, 73.9, 70.2, 50.1, 21.0, 18.1, 13.3, 13.2, 8.32, 7.95, 4.46.

Electrospray MS / methanol, m/z: 995 (M + Na + 2H)⁺, 789 (M - PF₆ - 2H₂O)⁺, 679 (M - 2PF₆ - H)⁺, 663 (M - H₂O - 2PF₆ + H)⁺

IR diamond ($\tilde{\nu}$ / cm⁻¹): 3655w, 3067w, 2843w, 2162w, 2031w, 1601vs, 1574s, 1551m, 1520s, 1481s, 1454s, 1421m, 1389w, 1362w, 1304sh, 1283sh, 1242s, 1182s, 1118w, 1078m, 1014s, 970w, 829vs, 818vs, 789vs, 741s, 733s, 702s, 673w, 652m.

7.4 The synthesis of 1,17-Bis(4-(4'-(4-methoxyphenyl)-2,2':6',2'':6'', 2''':6''',2''''-quinquepyridyl)phenoxy)-3,6,9,12,15-pentaoxaheptadecane (mcm) and complexes

7.4.1 1,17-Bis(4-(4'-(4-methoxyphenyl)-2,2':6',2'':6'', 2''':6''',2''''-quinquepyridyl)phenoxy)-3,6,9,12,15-pentaoxaheptadecane (mcm)

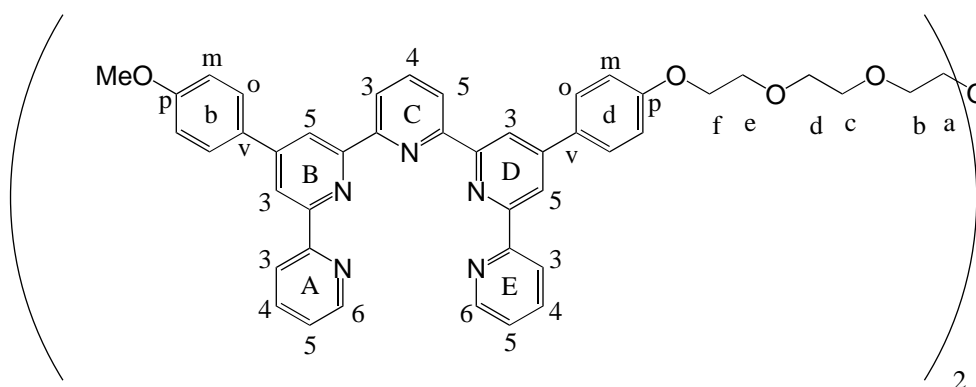


Figure 7.14: 1,17-Bis(4-(4'-(4-methoxyphenyl)-2,2':6',2'':6'', 2''':6''',2''''-quinquepyridyl)phenoxy)-3,6,9,12,15-pentaoxaheptadecane

All ingredients except DMF were dried *in vacuo*, over P₂O₅ for 3h. Then they were weighed and added to the predried reaction flask and kept under argon: 4'-(4-hydroxyphenyl)-4'''-(4-methoxyphenyl)-2,2':6',2'':6'', 2''':6''',2''''-quinquepyridine (mp) (353mg, 0.603mmol), Cs₂CO₃ (100mg, 0.307mmol) and tos₂heg (172mg, 0.291mmol). DMF (abs., 13ml) was added, and the mixture heated to 110 °C (oil bath-temperature). The mixture became a dark brown solution and the flask containing the mixture was left at that temperature overnight, attached with a reflux cooler. The TLC then showed that all starting mp was consumed, and the mixture was cooled to room temperature. A brown precipitate formed and could be filtered off. It was washed with methanol followed by diethyl ether and dried *in vacuo* to give 221mg crude product.

The crude product was purified by column chromatography, using Alox 90 (Merck) and DCM : MeOH : Et₂NH in a ratio of 200 : 10 : 0.1 as eluent. A solution of clean product was collected in the first yellow fraction, and after removing the solvent *in vacuo*, 213mg (53%) pure product was obtained.

Microanalysis: found (calculated): C₈₈H₇₆N₁₀O₉·2.5H₂O % C: 72.20 (72.26), % H: 5.45 (5.58), % N: 9.22 (9.58).

¹H-NMR, 600 MHz, CDCl₃ δ: 8.853 and 8.848 (two d, B5 and D3, J=1.5Hz, 4H), 8.71 (ddd, A6 or E6, J=4.7Hz, 1.8Hz and 0.9Hz, 2H), 8.69 (ddd, E6 or A6, J=4.4Hz, 1.7Hz and 0.9Hz, 2H), 8.67-8.62 (m, C3, B3, C5, D5, A3 and E3, 12H) with A3 and E3 at 8.65 and 8.63, B3 and D5 at 8.65 and 8.62 and C3 and C5 at 8.64 and 8.63, 7.98 (t, C4, J_{C4-C3/C5}=7.7Hz, 2H), 7.87-7.80 (m, A4, E4, bo and do, 12H) with A4 and E4 at 7.85 and 7.83, bo at 7.84 and do at 7.82, 7.32 (ddd, A5 or E5, J=1.2Hz, 7.4Hz and 7.4Hz, 2H), 7.31 (ddd, E5 or A5, J=1.2Hz, 7.4Hz and 7.3Hz, 2H), 7.01 (d, dm, J=8.7Hz, 4H), 7.00 (d, bm, J=8.7Hz, 4H), 4.18 (t, f, J_{f-e}=4.9Hz, 4H), 3.91 (t, e, J_{e-f}=4.8Hz, 4H), 3.88 (s, MeO, 6H), 3.77 (m, d, 4H), 3.71 (m, c, 4H), 3.69 (s, a and b, 8H).

¹³C-NMR, 150 MHz, CDCl₃ δ: 161.0 (bp), 160.0 (dp), 157.0, 156.2, 155.7, 149.3 (A6, E6), 138.0 (C4), 137.1 (4, E4, bo or do), 131.2, 128.7 (A4, E4, bo or do), 124.0 (A5, E5), 122.0, 121.0 (B3, D5, A3, E3, C3 or C5), 118.7 (B5, D3), 118.4 (B3, D5, A3, E3, C3 or C5), 115.1 (bm or dm), 114.5 (bm or dm), 71.3 (d), 71.1 (c), 71.0 (a, b), 70.0 (e), 67.9 (f), 55.8 (CH₃).

Maldi-TOF MS (matrix: α-Cyano-4-hydroxycinnamic acid) m/z: 1560, 1475 (M + K + H₂O + 2H)⁺, 1439 (M + Na)⁺, 949 (M – mp + 2K + 2H₂O)⁺, 889 (M – mp + K + H₂O)⁺, 657, 643, 551.

IR diamond ($\tilde{\nu}$ / cm⁻¹): 3533(w), 3063(w), 2924 (m), 2854(m), 2322(w), 2291(w), 2168(w), 2044(w), 1983(w), 1720(m), 1690(w), 1605(m), 1582(s), 1566(sh), 1543(s), 1512(vs), 1474(s), 1458(s), 1420(s), 1389(vs), 1296(sh), 1258(vs), 1180(s), 1111(vs), 1072(vs), 1041(vs), 987(m), 949(w), 887(m), 818(vs), 787(vs), 733(s), 694(w), 679(w), 663(m), 640(w), 617(m).

UV-Vis / chloroform, c=5.64 μM, wavelength/nm (extinction coefficient/cm⁻¹M⁻¹): 260 (99,900)sh, 284 (133,000), 310 (67,000)sh, 320 (45,500)sh.

7.4.2 [Cu₂(1,17-Bis(4-(4'-[4-methoxyphenyl]-2,2':6',2'':6'',2''':6''',2''''-quinque-pyridyl)phenoxy)-3,6,9,12,15-pentaoxaheptadecane)][PF₆]₄, [Cu₂mcm][PF₆]₃

1,17-Bis(4-(4'-[4-methoxyphenyl]-2,2':6',2'':6'',2''':6''',2''''-quinque pyridyl)phenoxy)-3,6,9,12,15-pentaoxaheptadecane (21.1g, 14.9 μmol) and copper(II) acetate · monohydrate (10.4mg, 52.1 μmol) were sonicated in methanol (~3ml) to yield a green solution. After filtration, a filtered solution of ammonium hexafluorophosphate (56mg, 344 μmol) in methanol (1ml) was added. A greenish brown solid was filtered from the turquoise solution. The solid was washed with ice cold methanol, and water (and at this point the colour of the solid turned brown), then ice cold methanol again, and finally diethyl ether. Drying *in vacuo* gave a brown powder (16mg, 54%).

Microanalysis: found (calculated: C₈₈H₇₆N₁₀O₉Cu₂P₄F₂₄ % C: 49.38 (49.75), % H: 3.89 (3.61), % N: 6.40 (6.59).

¹H-NMR, 250 MHz, CDCl₃ δ: 24.8 (vb), 17.5 (weak, vb), 12.8, 12.2, 9.14, 8.00 (b), 7.71, 6.49 (b), 4.10, 3.95, 3.91, 3.79, 3.77, 3.65, 3.63, 3.59, 3.58, 3.55, 3.54 (4.10-3.54 linker -CH₂O- and CH₃O protons).

Maldi-TOF MS (matrix: α-Cyano-4-hydroxycinnamic acid) m/z: 1688 (M – 2PF₆ + H)⁺, 1546, 1543 (M – 3PF₆)⁺, 1496, 1479 (M – 3PF₆ – Cu)⁺, 955, 939, 930, 662

IR diamond ($\tilde{\nu}$ / cm⁻¹): 3657w, 3581w, 3086b, 2870b, 2168w, 2029w, 1983w, 1597s, 1574m, 1543w, 1520m, 1481w, 1450m, 1427m, 1411sh, 1358m, 1304w, 1242s, 1188s, 1119b, 1080m, 1018m, 818vs, 787vs, 741s, 694sh, 648m, 617m.

UV-Vis / acetonitrile, $c_1=105\mu\text{M}$ and $c_2=10.5\mu\text{M}$, wavelength/nm (extinction coefficient/ $\text{cm}^{-1}\text{M}^{-1}$): 225 (92,500)sh, 292 (68,400), 320 (65,500)sh, 348 (54,300)sh, 468 (4,670), 576 (1,630)sh.

7.5 The Synthesis of 4'-(4-hydroxyphenyl)-4'''-phenyl-2,2':6',2'':6'', 2''':6''',2''''-quinquepyridine (pp) and complexes

7.5.1 2-[3-(4-Hydroxy)-1-oxoprop-2-enyl]-6-[3-phenyl-1-oxoprop-2-enyl]pyridine

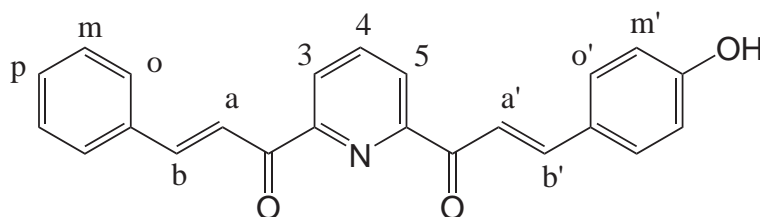


Figure 7.15: 2-[3-(4-Hydroxy)-1-oxoprop-2-enyl]-6-[3-phenyl-1-oxoprop-2-enyl]pyridine

2-Acetyl-6-[3-(4-hydroxyphenyl)-1-oxoprop-2-enyl]pyridine (6.771g, 25.33mmol) was suspended in 1-propanol (100ml). Addition of Et_2NH (30ml) caused a colour change to ruby red. The suspension was heated to 80°C and a solution of benzaldehyde (10.0ml, 10.5g, 98.9mmol) in 1-propanol (80ml) was added during ~ 10 min. In the heat, the suspension turned into a solution, that was refluxed at 135°C . Over night it turned brown. After cooling slightly, the solvent was removed *in vacuo* to give a brown oil.

The oil was added to a silica column and eluted with DCM : MeOH : Et_2NH (20:1:0.1). The product was collected as the second band and obtained as a yellow powder (3.35g, 37%).

Microanalysis found (calculated: $\text{C}_{23}\text{H}_{17}\text{N}_1\text{O}_3$) % C: 77.44 (77.73), % H: 5.10 (4.82), % N: 3.86 (3.94).

$^1\text{H-NMR}$, 250 MHz, CDCl_3 δ : 8.53-8.29 (m, H3, H5, Ha, Ha', 4H), 8.11-7.96 (m, H4, Hb, Hb', 3H), 7.81-7.73 (m, Ho, $\sim 2\text{H}$), 7.69 (d, Ho', $J_{\text{Ho}'-\text{Hm}'}=8.7\text{Hz}$, 2H), 7.49-7.45 (m, Hm, Hp, $\sim 3\text{H}$), 6.91 (d, Hm', $J_{\text{Hm}'-\text{Ho}'}=8.5\text{Hz}$, 2H).

EI-MS, 70eV, $\sim 250^\circ\text{C}$: $m/z=$ 355 M^+ , 278 ($\text{M} - \text{phenyl}$) $^+$, 147, 103.

IR diamond ($\tilde{\nu} / \text{cm}^{-1}$): 3356b, 3063w, 3024w, 1983w, 1882w, 1659s, 1597s, 1558vs, 1504s, 1443m, 1381w, 1335s, 1281m, 1234s, 1204s, 1165s, 1034vs, 980vs, $\sim 929\text{sh}$, 810vs, 764m, 741s, 702w, 679m.

7.5.2 4'-(4-Hydroxyphenyl)-4'''-phenyl-2,2':6',2'':6'', 2''':6''',2''''-quinquepyridine (pp)

The synthesis procedure from Whall's thesis⁵¹ was applied. 2-[3-(4-Hydroxy)-1-oxoprop-2-enyl]-6-[3-phenyl-1-oxoprop-2-enyl]pyridine (2.629g, 7.398mmol), PPI (4.834g, 14.82mmol) and NH_4OAc (5.98g, 77.6mmol) were dissolved in dry methanol (40ml) and heated to 100°C under argon. A brown solution formed, and was refluxed for 17h to give a beige precipitate. After cooling to room temperature, the precipitate was filtered off, washed with ice cold methanol and dried *in vacuo* to yield 3.64g (89%).

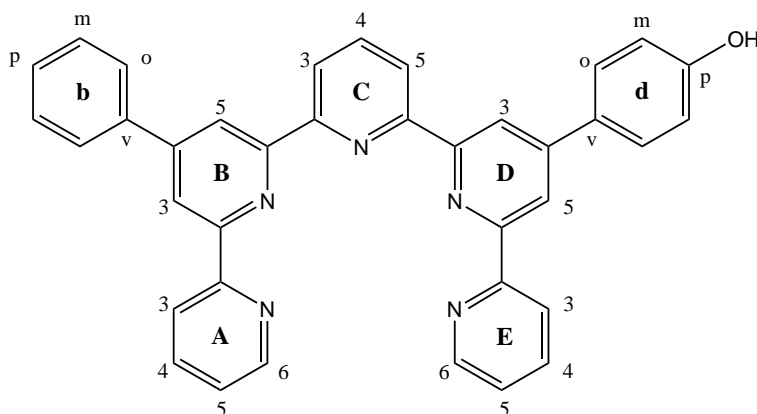


Figure 7.16: 4'-(4-Hydroxyphenyl)-4'''-phenyl-2,2':6',2'':6'',2''':6''',2''''-quinquepyridine

Microanalysis: found (calculated): $C_{37}H_{25}N_5O \cdot 0,5H_2O$ % C: 78.82 (78.70), % H: 4.62 (4.64), % N: 12.52 (12.40).

1H -NMR, 600 MHz DMSO- d_6 δ : 9.93 (s, OH, 1H), 9.04 (d, B5, $J_{B5-B3}=1.7$ Hz, 1H), 8.98 (d, D3, $J_{D3-D5}=1.9$ Hz, 1H), 8.78-8.67 (m, B3, C3, C5, A3, A6, D5, E3, E6, 8H) where B3 is at 8.77, C3 and C5 at 8.75 and 8.72 and D5 at 8.69, 8.27 (t, C4, $J_{C4-C3, C4-C5}=7.7$ Hz, 1H), 8.06-7.98 (m, A4, E4, bo, 4H) where A4 and E4 come at 8.04 and bo at 8.02, 7.89 (d, do, $J_{do-dm}=8.9$ Hz, 2H), 7.64 (t, bm, $J_{bm-bo}=7.4$ Hz, 2H), 7.59 (t, bp, $J_{bp-bm}=7.4$ Hz, 1H), 7.56-7.52 (m, A5, E5, 2H), 7.00 (d, dm, $J_{dm-do}=8.8$ Hz, 2H)

Maldi-TOF MS (no matrix) m/z: 616 (M + 4H + K + H₂O)⁺, 614 (M + 2H + K + H₂O)⁺, 579 (M + H + Na)⁺, 557 (M + 2H)⁺.

IR diamond ($\tilde{\nu}$ / cm⁻¹): 3549w, 3186b, 3055m, 2291w, 1983w, 1967w, 1952w, 1798w, 1666m, 1605m, 1566s, 1543vs, 1520s, 1474s, 1434m, 1389vs, 1273s, 1219m 1173m, 1126w, 1103m, 1072m, 1041m, 995m, 957sh, 887m, 833m, 818s, 787vs and 764vs, 733s, 694m, 678m, 656m, 640m, 617s.

UV-Vis / chloroform, c=20.16 μ M, wavelength/nm, (extinction coefficient/cm⁻¹M⁻¹): 257 (62,800), 279 (58,300), 308 (34,000)sh, 318 (27,000)sh.

7.5.3 [Cu₂(4'-(4-hydroxyphenyl)-4'''-phenyl-2,2':6',2'':6'',2''':6''',2''''-quinquepyridine)]₂[PF₆]₃, [Cu₂(pp)₂][PF₆]₃

4'-(4-Hydroxyphenyl)-4'''-phenyl-2,2':6',2'':6'',2''':6''',2''''-quinquepyridine (25.0mg, 45 μ mol) and Cu(OAc)₂·H₂O (9.3mg, 46.6 μ mol) were dissolved in methanol (20ml) to yield a dark brown solution. A solution of NH₄PF₆ (100mg, 613 μ mol) in methanol (2ml) was filtered through cotton wool and added to the solution. First there was a light coloured precipitate, but after part of the solvent was removed, a green precipitate formed. This green precipitate was redissolved, by heating. The solution was brown, but again the precipitate formed was green. It was filtered off, washed once with cold methanol, three times with water, twice with cold methanol and three times with ether. Upon drying *in vacuo*, the solid turned brown (28mg, 74%).

Microanalysis: found (calculated): $C_{74}H_{50}N_{10}O_2Cu_2P_3F_{18} \cdot 6H_2O$ % C: 50.02 (49.90), % H: 3.20 (3.51), % N: 7.87 (7.86).

¹H-NMR, 600 MHz, acetonitrile-d₃ δ: 24.9 (vb), 13.7 (vb), 10.4 (b), 9.29, 9.12, 8.92, 8.01-7.51 (m), 6.98 (d, J=49.9Hz), 6.38 (d, J=46.3Hz).

Maldi-TOF MS (no matrix) m/z: 1234 (M – 2H – 3PF₆)⁺, 1172 (M – H – Cu – 3PF₆)⁺, 1153 (2pp + Na + 2H + H₂O)⁺, 724, 618 (pp + Cu)⁺, 613 (pp + K + H + H₂O)⁺, 602, 600, 589, 524.

IR diamond ($\tilde{\nu}$ / cm⁻¹): 3641w and 3518w, 3094b, 1983w, 1597vs, 1573s, 1543s, 1520m, 1481m, 1458m, 1443m, 1358m, 1281sh, 1242s and 1180s, 1111w, 1080m, 1011m, 818vs and 787sh, 764s, 741s, 694m, 648m, 617m.

UV-Vis / acetonitrile, c₁=104 μM and c₂=9.32 μM, wavelength/nm (extinction coefficient/cm⁻¹M⁻¹): 222 (85,000)sh, 288 (72,400), 319 (49,900)sh, 351 (32,400)sh, 467 (4,150), 572 (1,700)sh.

7.6 The synthesis of 1,17-Bis-4-(4'-(4'''-phenyl-2,2':6',2''':6'',2''':6''',2''''-quinquepyridyl)phenoxy)-3,6,9,12,15-pentaoxaheptadecane (pcp) and complexes

7.6.1 1,17-Bis-4-(4'-(4'''-phenyl-2,2':6',2''':6'',2''':6''',2''''-quinquepyridyl)phenoxy)-3,6,9,12,15-pentaoxaheptadecane (pcp)

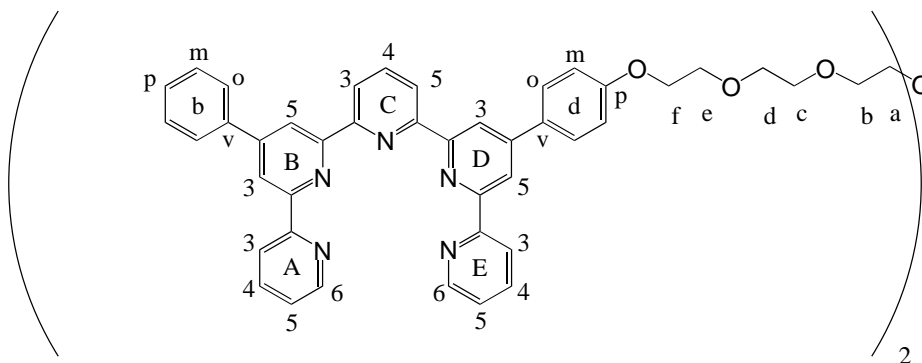


Figure 7.17: 1,17-Bis-4-(4'-(4'''-phenyl-2,2':6',2''':6'',2''':6''',2''''-quinquepyridyl)phenoxy)-3,6,9,12,15-pentaoxaheptadecane

Dry 4'-(4-hydroxyphenyl)-4'''-phenyl-2,2':6',2''':6'',2''':6''',2''''-quinquepyridine (319mg, 0.574mmol) and dry Cs₂CO₃ (107mg, 0.328mmol) were suspended in DMF (7ml) and heated in an oilbath at 100 °C under argon. To the brown solution, a solution of tos₂heg (169mg, 0.286mmol) in DMF (1ml) was added dropwise over a period of 5 min. The flask with the tos₂heg solution was rinsed with 3ml and the 1 ml of DMF, so there where 12 ml DMF in the reaction flask. The oilbath was cooled to 80 °C and after 20h of reaction some white precipitate was formed. A CaCl₂ drying tube was put on top of the reflux cooler. After 90h under reflux, under Argon, more precipitate had formed. The mixture was cooled to room temperature. The precipitate was filtered off, washed with DMF, water, methanol and diethyl ether, and dried *in vacuo* to yield 237mg (61%) of product.

The solid was sonicated in dilute NaOH_(aq) for half an hour at pH=11 and then extracted with chloroform. After reducing the amount of solvent *in vacuo*, the solution was added to an Alox 90 (Merck) column, and eluated with chloroform : Et₂NH (42 : 1). The crude product was collected as the first yellow band (202mg).

Microanalysis: found (calculated): $C_{86}H_{720}N_{10}O_7 \cdot 0.5 H_2O$ % C: 74.93 (75.09), % H: 5.33 (5.42), % N: 10.06 (10.18).

1H -NMR, 600 MHz, $CDCl_3$ δ : 8.92 (d, B5, $J=1.7$ Hz, 2H), 8.87 (d, D3, $J=1.6$ Hz, 2H), 8.73-8.62 (m, B3, C3, C5, D5, A3, E3, A6, E6, 16H) with A6 at 8.72, B3 at 8.71, E6 at 8.70, C3 and C5 at 8.67 and 8.65, A3 at 8.67, E3 at 8.64 and D5 at 8.63, 8.00 (t, C4, $J_{C4-C3/C5}=7.7$ Hz, 2H), 7.91-7.81 (m, bo, A4, E4 and do, 12H) with bo at 7.89, A4 at 7.87, E4 at 7.85 and do at 7.84, 7.53-7.46 (m, bm and bp, 6H) with bm and bp at 7.50 and 7.48, 7.34 (ddd, A5, $J=7.4$ Hz, 4.8Hz and 1.1Hz, 4H), 7.31 (ddd, E5, $J=7.4$ Hz, 4.7Hz and 1.1Hz, 4H), 7.01 (d, dm, $J_{dm-do}=8.6$ Hz, 4H), 4.19 (t, f, $J_{f-e}=4.8$ Hz, 4H), 3.91 (t, e, $J_{e-f}=4.8$ Hz, 4H), 3.77 (m, d, 4H), 3.72 (m, c, 4H), 3.69 (s, a and b, 8H).

^{13}C -NMR, 150 MHz, $CDCl_3$ δ : 160.0 (dp), 149.4 (A6, E6), 138.1 (C4), 137.2 (A4, E4), 129.3 (bm, bp), 128.7 (do), 127.4 (bo), 124.0 (A5, E5), 121.6 (C3, C5, A3 and E3), 119.3 (B5), 119.1 (B3), 118.7 (D3), 118.4 (D5), 115.0 (dm), 71.2 (d), 70.9 (a, b, and c), 69.9 (e), 67.7 (f). The sample was too dilute to see quaternary carbon resonances.

Maldi-TOF MS (matrix: α -Cyano-4-hydroxycinnamic acid) m/z: 1629, 1566, 1421 (M + Na + K + 2H)⁺, 1414 (M + K + H₂O + H)⁺, 1358 (M + 2H)⁺, 801, 618 (pp + K + Na)⁺, 613 (pp + K + H₂O + H)⁺, 556 (pp + H)⁺, 441, 379.

IR diamond ($\tilde{\nu}$ / cm^{-1}): 3549w, 3055m, 2870m, 1983w, 1967w, 1952w, 1798w, 1720w, 1605s, 1582vs, 1566sh, 1543vs, 1512vs, 1474s, 1443m, 1420m, 1389vs, 1358sh, 1296m, 1250vs, 1180m, 1111vs, 1072vs, 1041vs, 987s, 941m, 887s, 817vs, 794vs, 764vs, 733vs, 694vs, 663s, 640m, 617vs.

UV-Vis / chloroform, $c=7.366\mu M$, wavelength/nm (extinction coefficient/ $cm^{-1}M^{-1}$): 257 (102,000), 280 (97,600), 307 (57,500) sh, 316 (46,300) sh.

7.6.2 [Cu₂(1,17-di-4'(4'''-phenyl-2,2':6',2'':6'',2''':6''',2''''-quinquepyridyl)phenoxy)-3,6,9,12,15-pentaoxaheptadecane)][PF₆]₃, [Cu₂pcp][PF₆]₃

pcp ligand (21mg, 15.6 μ mol) and Cu(OAc)₂ · H₂O (7.6mg, 38.1 μ mol) were dissolved in methanol (approx. 3ml) in the sonicating bath to yield a green solution. To the filtered solution, a filtered solution of NH₄PF₆ (56mg, 34.4 μ mol) in methanol (1ml) was added. A green precipitate was filtered from the slightly greenish solution. It was washed with ice cold methanol, water, more ice cold methanol, diethyl ether and dried *in vacuo* to give a brown powder (22mg, 74%).

Microanalysis: found (calculated): $C_{86}H_{72}N_{10}O_7Cu_23.7 PF_6$ % C: 51.28 (51.11), % H: 3.62 (3.59), % N: 6.75 (6.93).

1H -NMR, 250 MHz, $CDCl_3$ δ : 25.0 (vb), 17.5 (weak, vb), 13.2 (weak, vb), 9.15 (b), 8.10-7.51 (m), 6.96, 6.50, 3.94, 3.79, 3.64, 3.63, 3.59, 3.56 (3.94-3.564 linker -CH₂O- protons).

Maldi-TOF MS (matrix: α -cyano-4-hydroxycinnamic acid) m/z: 1629 (M - 2PF₆ + 2H)⁺, 1484 (M - 3PF₆ + 2H)⁺, 1433, 1419 (M - 3PF₆ - Cu)⁺, 1359, 624, 568.

IR diamond ($\tilde{\nu}$ / cm^{-1}): 3657w, 3063b, 2870m, 1597s, 1574m, 1543m, 1520m, 1481m, 1450m, 1412m, 1381w, 1358w, 1304w, 1242s, 1188s, 1111b, 1080m, 1011m, 879sh, 833vs, 795s, 764s, 741s, 694m, 648m, 617m.

UV-Vis / acetonitrile, $c_1=122.4\mu\text{M}$ and $c_2=12.24\mu\text{M}$, wavelength/nm (extinction coefficient/ $\text{cm}^{-1}\text{M}^{-1}$): 224 (91,600) sh, 289 (78,900), 316 (63,800) sh, 351 (39,700) sh, 472 (250), 574 (102) sh.

X-ray see appendix A.2 page 186.

7.7 On the way to 5-(4-methoxyphenyl)-2,2':6',2'':6'',2''':6''',2''''-quaterpyridine (5qtpy)

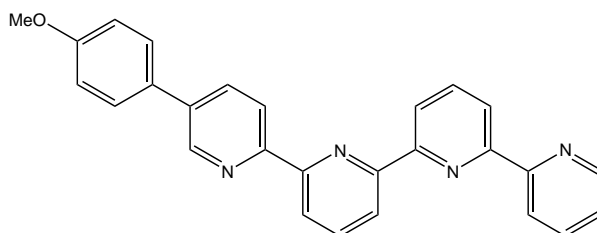


Figure 7.18: 5-(4-Methoxyphenyl)-2,2':6',2'':6'',2''':6''',2''''-quaterpyridine

7.7.1 3-*N,N*-Dimethylamino-1-oxo-1-(2-pyridyl)-2-propene

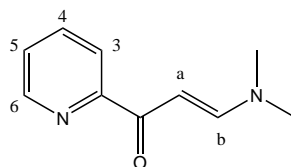


Figure 7.19: 3-*N,N*-Dimethylamino-1-oxo-1-(2-pyridyl)-2-propene

The literature procedure^{2,3} was followed. *N,N*-Dimethylformamide dimethyl acetal (13.2ml, 11.8g, 99.3mmol) and 2-acetyl pyridine (10.0ml, 10.8g, 88.6mmol) were dissolved in toluene (17ml) in a distillation apparatus and heated to 110°C. After 22h, the reaction mixture had turned black and the methanol formed by the reaction was separated off. To complete the reaction, the temperature was raised to 130°C for 1.5h and then cyclohexane (21ml) was added to the hot, black solution. From a red-brown solution, a yellow precipitate formed while cooling to room temperature. The precipitate was filtered off, washed twice with cyclohexane : toluene (2 : 1) and dried *in vacuo* to give neon-yellow needles (13.49g, 86%).

¹H-NMR, 250 MHz, CDCl₃ δ : 8.64 (d, H6, J=4.7Hz, 1H), 8.16 (d, H3, J=7.9Hz, 1H), 7.92 (d, Ha or Hb, J=13Hz, 1H), 7.82 (t, H4, J=7.7Hz, 1H), 7.37 (dd, H5, J=7.4 Hz and 4.8Hz, 1H), 6.46 (d, Hb or Ha, J=13Hz, 1H), 3.18 (s, CH₃, 3H), 3.01 (s, CH₃, 3H).

7.7.2 2-Acetyl-6-bromopyridine

The synthesis was consistent with the literature procedure.^{82, 159-163}

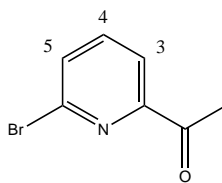


Figure 7.20: 2-Acetyl-6-bromopyridine

$^1\text{H-NMR}$, 250 MHz, CDCl_3 δ : 8.10-7.96 (m, 1H), 7.75-7.62 (m, 2H), 2.71 (s, 3H).

$^1\text{H-NMR}$, 250 MHz, MeOD δ : 8.01-7.96 (m, 1H), 7.88-7.76 (m, 2H), 2.64 (m, \sim 3H).

IR diamond ($\tilde{\nu}$ / cm^{-1}): 3371w, 3062w, 3047w, 1662w, 2530w, 2322w, 2006w, 1921w, 1836w, 1759w, 1697vs, 1574m, 1551vs, 1427s, 1396m, 1358vs, 1303vs, 1288sh, 1234vs, 1180sh, 1157s, 1126vs, 1095m, 1072s, 1026m, 987m, 957s, 802vs, 725m, 656m

7.7.3 2-Bromo-6-(3'-dimethylammonio-1'-oxopropyl)pyridine chloride

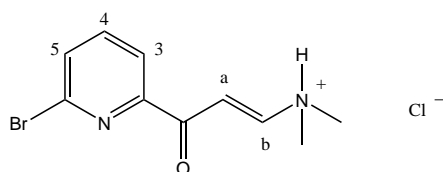


Figure 7.21: 2-Bromo-6-(3'-dimethylammonio-1'-oxopropyl)pyridine chloride

First, the procedure from my diploma work page 23¹³¹ was followed after the general method developed by Kröhnke,⁹² using DMF. But like Newkome¹³⁷ described the synthesis, ethanol proved to be the better solvent. 2-Acetyl-6-bromopyridine (503mg, 2.52mmol) and paraformaldehyde (90mg, 3.0mmol) were mixed with a solution of HCl (37%, \sim 30mg) in ethanol (16.0ml). The hygroscopic *N,N*-dimethylammonium chloride was added last, and the mixture stirred and heated for 40 minutes at 60-66°C while everything dissolved. The oilbath was removed, and the yellow solution was cooled in the fridge. Nothing precipitated. Addition of water (5ml) made a white solid fall out of solution. After renewed cooling in the fridge, the precipitate was filtered off, washed with ethanol : water (2 : 1) and dried *in vacuo* (72mg, 10%). The proton-NMR spectrum showed decomposition, the infrared spectrum showed a strong similarity to 2-acetyl-6-bromopyridine in the fingerprint region.

IR KBr ($\tilde{\nu}$ / cm^{-1}): 3854m, 3423b, \sim 2000b, 1699vs, 1655m, 1571m, 1551vs, 1430vs, 1397m, 1361vs, 1305vs, 1283sh, 1238vs, 1160s, 1126vs, 1100s, 1073vs, 987m, 959m 806s, 793m, 593vs

7.7.4 2-Ethylthiopyridine

The literature procedure¹⁶⁴ and the procedure described in my diploma thesis¹³¹ was followed. 2-Mercaptopyridine (11.14g, 0.100mmol), aqueous NaOH (1.0M, 105ml) and ethyl iodide (8.40ml, 16.2g, 0.104mol) were mixed to give a yellow solution. It was stirred under argon at room temperature over night. For protection from light, the reaction flask was wrapped in aluminium foil. The reaction mixture was then extracted four times with ether (4 · 60ml). The combined organic layers were washed three times with aqueous NaOH (2M). This caused a decolorisation. Then they were washed with water, dried

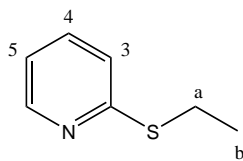


Figure 7.22: 2-Ethylthiopyridine

over magnesium sulfate and filtrated. The solvent was removed *in vacuo* and a yellow oil was obtained (12.02g, 86%).

¹H-NMR, 250 MHz, CDCl₃ δ: 8.43 (d, H6 J=4.3Hz, 1H), 7.47 (td, H4, J=7.7Hz and 2.1Hz, 1H), 7.16 (dt, H3, J=8.1Hz and 0.85Hz, 1H), 6.97 (ddd, H5, J=7.3Hz, 4.9Hz and 1.1Hz, 1H), 3.17 (q, CH₂, J=7.3Hz, >2H), 1.37 (t, CH₃, J=7.3Hz, >3H).

7.7.5 2-Bromo-6-(2-methyl-1,3-dioxolan-2-yl)pyridine

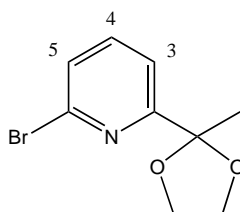


Figure 7.23: 2-Bromo-6-(2-methyl-1,3-dioxolan-2-yl)pyridine

The classical method^{131,165,166} was applied. 2-Acetyl-6-bromopyridine (2.287g, 11.43mmol), ethyleneglycol (4.79ml, 5.33g, 85.9mmol) and p-toluenesulfonic acid (0.72g, 3.3mmol) were dissolved in toluene (100ml). The mixture was refluxed using a water extractor and water was removed repeatedly over a period of 64h. The residue was washed with aqueous NaOH (1M, 20ml) and extracted back with DCM. The combined organic phases were dried over magnesium sulfate and filtered. Removing the solvent *in vacuo* gave a dark brown oil (2.550g).

The crude product can be purified by distillation.¹³¹

7.7.6 6-Bromo-2,2':6',2''-terpyridine

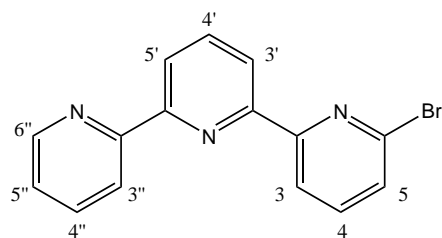


Figure 7.24: 6-Bromo-2,2':6',2''-terpyridine

Route 1: The literature procedure^{92,124,137} was followed. 2-Bromo-6-(3'-dimethylammonio-1'-oxopropyl)pyridine chloride (69mg, 0.24mmol), PPI (78mg, 0.24mmol) and ammonium acetate (200mg, 2.6mmol) were heated in methanol (p.a., 1.0ml) to give a yellow solution. The reaction mixture was refluxed for three hours. After cooling, water (1ml) was added and a white precipitate formed. It was filtered off (30mg). ¹H-NMR showed some product but mainly decomposition.

Route 2: The literature procedure^{2,3} to make terpy was followed. 2-Acetyl-6-bromopyridine (1.10g, 5.50mmol) and K^tBuO (2.157g, 19.22mmol) were dissolved in THF (abs., 40ml) and stirred at room temperature under argon. After 3.5h, a very small amount of white precipitate had formed in the reddish-beige solution. 3-*N,N*-Dimethylamino-1-oxo-1-(2-pyridyl)-2-propene (1.46g, 8.29mmol) was added and this caused an immediate colour change from brown to intense deep red and all precipitate dissolved again. The solution was stirred under argon for 41h without changing colour. After cooling in a ice-water bath, a mixture of ammonium acetate (6.2g, 80mmol) in acetic acid (99-100%, 21ml) was added. During a few minutes of stirring, the colour changed to brown. Methanol (4.1ml) was added, and the remaining THF removed by distillation, followed by methanol. The oilbath temperature reached 115 °C towards the end of the distillation. After 7.5h, the residual black oil was cooled to room temperature. It was poured into water (40ml) and neutralised with sodium carbonate (the pH reached 8). A black tarry material was obtained. It was mixed with celite (~20g) and heated to 80 °C in toluene (30ml). After two hours at that temperature, the mixture was cooled and filtered. The filtrate consisted of two phases. They were separated and the reddish-brown aqueous phase was extracted three times with toluene (20ml). Alox (I, neutral, 3.8g) were added to the combined orange organic phases, and after stirring for half an hour, this mixture was filtered. Removing the solvent from the filtrate *in vacuo* gave a black oily solid.

The black material was dissolved in DCM (10ml) and alox(III, neutral) was added. The solvent was removed on the rotavap to give a black powder. It was added to an alox (III, neutral) column and eluted with cyclohexane : ethyl acetate (20 : 1). Removing the solvent *in vacuo* of the first yellow fraction, yielded the product (0.368g, 21%).

¹H-NMR, 400 MHz, CDCl₃ δ: 8.73 (d, H6'', J=3.8Hz, 1H), 8.62-8.44 (m, H3, H3', H5' and H3'', 4H), 7.97 (t, H4', J=7.84Hz, 1H), 7.89 (t, H4'', J=7.8Hz, 1H), 7.71 (t, H4, J=7.8Hz, 1H), 7.52 (d, H5, J=7.8Hz, 1H), 7.34 (ddd, H5, J=7.4Hz, 4.6Hz and 1.5Hz, 1H)

7.7.7 6-(*n*-Butyl)-2,2':6',2''-terpyridine

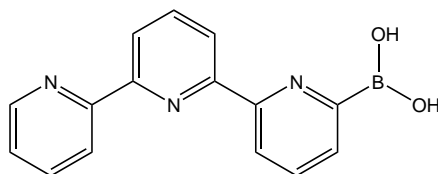


Figure 7.25: 6-2,2':6',2''-Terpyridylboronic acid

A suspension of 6-bromo-2,2':6',2''-terpyridine (90mg, 0.29mmol) in diethyl ether (abs., 20ml) was cooled to -80 °C under argon. *n*-BuLi (1.6M/hexane, 0.22ml, 0.35mmol) was added slowly, while the reaction mixture became a very dark, blue solution. The temperature was raised to -50 °C and after stirring at that temperature for 15 minutes, it was lowered to -100 °C. Triisopropyl borate (predried over molecular sieves of 4Å, 0.146ml, 0.121g, 0.641mmol) was added, and the reaction mixture was slowly rising in temperature. The colour stayed dark blue. At -20 °C water (100ml) was added. The phases were separated, and the brown aqueous phase (pH=7-8) was extracted three times with toluene, once with diethyl ether, once with *tert*-butylmethyl ether and once with THF. The combined organic layers were washed with brine, dried over sodium sulfate and filtered. Removing the solvent *in vacuo* left

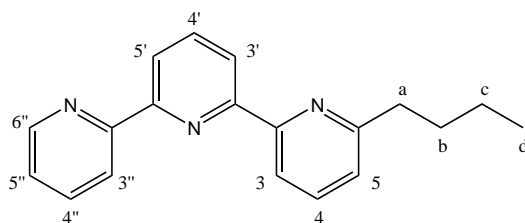


Figure 7.26: 6-(*n*-Butyl)-2,2':6',2''-terpyridine

164mg residue. Mass spectroscopy showed that to some extent, the *n*-butyl group had been added to the terpy instead of the boron group. No bromo-terpy was left, which supports that in the lithiation step had worked, but the *n*-butyl group had been added instead of the the lithium. Although the proton-NMR is rather messy in the aliphatic region, there are signals of the required multiplicity for Ha,Hc and Hd, when compared with *n*-butyl-6-(2,2':6',2''-terpyridine in a ChemDraw Ultra¹⁶⁷ simulation. Hb is covered by other signals. No 6-terpy-boronic acid was isolated under these reaction conditions.

¹H-NMR, 400 MHz, CDCl₃ + methanol-d₄ δ: 8.48 (d, H6'', J=4.0Hz, 1H), 8.42 (d, J=7.8Hz, 1H), 8.25 (dd, J=8.0Hz and J=2.1Hz, 1H), 8.18 (dd, J= 7.8Hz and J=3.0Hz 1H), 8.14 (d, J=7.8Hz, 1H), 7.82 (t, J=7.8Hz, 1H), 7.75 (td, J=7.7Hz and J=1.6Hz, 1H), 7.62 (t, J=7.6Hz, 1H), ~7.25Hz (under CDCl₃-signal), 7.06 (dd, H5, J=7.5Hz and J=2.9Hz, 1H), 2.71 (t, Ha, J=7.8Hz, 2H), 1.73-1.58 (m, containing Hb, >2H), 1.27 (q, Hc, J=7.4Hz, 2H), 0.80 (t, Hd, J=7.3Hz, >3H).

FAB-MS (NBA and KCl): 506 (terpy-B-O-B-terpy – H)⁺, 402 (diisopropoxy-6-terpyridyl borate + K + 2H)⁺, 352 (6-hydroxy terpy + 3H)⁺, 306 (isopropoxy-6-terpyridyl borate + 4H)⁺, 290 (*n*-butyl-6-terpy – H)⁺ (100%).

7.7.8 Test boronation reaction of 2-bromopyridine: comparing the effects of *n*-BuLi and PhLi

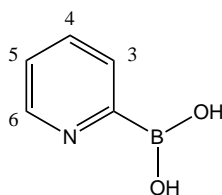


Figure 7.27: 2-Pyridylboronic acid

A general procedure for boronation¹⁴⁹ of aromatic rings was followed. THF was used instead of diethyl ether as a solvent so *n*-BuLi and PhLi should not form tetramers and react better.¹⁴¹ In two separate dry reaction flasks, 2-bromopyridine (1.00ml, 1.66g, 10.4mmol) was dissolved in THF (abs., 20ml) and cooled to -78°C under argon. To the first reaction flask, *n*-BuLi (1.6M, 7.00ml, 11mmol) was added dropwise, keeping the temperature below -70°C. At the same time PhLi (2.2M, 7.00ml, 15.4mmol) was added dropwise to the second reaction flask, also keeping the temperature below -70°C. Both mixtures turned brown. They were stirred at -76 to -78°C for 15 minutes before trimethoxyborate (3.00ml, 2.80g, 26.9mmol) was added to each. The solution in the reaction flask with the *n*-BuLi turned red-brown, while the one with the PhLi turned almost colourless, but slightly brown. After stirring another 40 minutes at that temperature, the colour of the first solution was red, and the colour of the second was slightly orange. The reactions were quenched by addition of HCl_{aq} (2.0M, 20ml). The first reaction

became an orange, the second a yellow suspension. They were warmed slowly to room temperature and extracted three times with diethyl ether each. The organic phases were dried over sodium sulfate and filtered. The solvent was removed *in vacuo*. The residue from the reaction with *n*-BuLi weighed 175mg. ¹H-NMR showed decomposition. The residue from the reaction with PhLi was a solid and weighed 335mg (10.3% anhydride). ¹H-NMR was nicely structured.

¹H-NMR, 250 MHz, CDCl₃ δ: 7.53-7.47 (m (=‘td’), 2H), 7.34-7.19 (m, ‘quintett: d’), ~2H (coincides with the solvent signal).

EI-MS, 70eV, ~200 °C: m/z= 388, 312 (3M – 3H₂O – 3H)⁺ (100%), 235 (3M – 3H₂O – pyridine)⁺, 208 (3M – 3H₂O – pyridine – B-OH)⁺, 164, 104 (M – OH – 2H)⁺

IR KBr ($\tilde{\nu}$ / cm⁻¹): 3854w, 3650w, 3448b, 2345w, 1736w, 1508w, 1441s, 1366vs, 1351vs, ~1698sh, 1024m, 699vs, 578m.

7.7.9 4-Methoxyphenylboronic acid

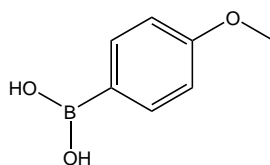


Figure 7.28: 4-Methoxyphenylboronic acid

The procedure via a Grignard compound from the literature was followed.¹⁴⁹ Under a nitrogen atmosphere, magnesium (54.9mg, 2.26mmol) and one pellet of iodine were mixed in the reaction apparatus and heated until violet vapour was visible, to activate the magnesium. THF (abs., 10ml) was added, followed by 4-bromoanisole. Refluxing for 30 minutes gave a white suspension. It was cooled to room temperature before it was added dropwise during 20 minutes to a solution of triisopropyl borate (1.04ml, 850mg, 4.51mmol) in THF (abs., 2ml) under nitrogen at -76 °C to -70 °C. After stirring for 10 more minutes at this temperature, it was warmed to room temperature overnight. The white suspension was treated with HCl_{aq} (10%, 10ml). It was stirred for 70 minutes, and during that time, the colour changed to yellow and then to orange. The orange solution was extracted three times with *tert*-butylmethyl ether. The combined organic layers were washed with water, dried over magnesium sulfate and filtered. The solvent was removed *in vacuo* to give a brown solid (419mg). The proton-NMR showed approximately product : 4-bromoanisole (2.5 :1).

The crude compound was recrystallised from hot water to give a white solid (84mg, 22%). A crystal structure was obtained.

¹H-NMR, 250 MHz, CDCl₃ δ: 8.16 (d, J=7,8Hz, 2H), 7.01 (d, 8.7Hz, 2H), 3.89 (s, 3H).

IR diamond ($\tilde{\nu}$ / cm⁻¹): 3005w, 2956m, 2935m, 2839m, 2048w, 2037w, 1597vs, 1566s, 1512s, 1512s, 1450m, 1412s, 1335vs, 1304vs, 1242vs, 1165vs, 1103s, 1080sh, 1022vs, 906s, 833vs, 806s, 744vs, 733vs, 683vs, 648s.

Melting point: 211 °C.

X-ray see appendix C page 211.

7.7.10 Dimethoxyl-4-methoxyphenyl boronate

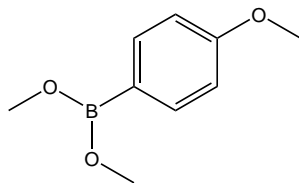


Figure 7.29: Dimethoxyl-4-methoxyphenyl boronate

The literature procedure¹⁴⁹ was followed, but for the hydrolysis. THF (abs., 80ml), magnesium (284mg, 11.7mmol) and a iodine pellet were mixed under an argon atmosphere. To this brown mixture, 4-bromoanisole (1.28ml, 10.3mmol) was added, and after refluxing for 3h after replacing the argon flux with a calcium chloride drying tube. The white suspension was cooled in a ice - ammonium chloride bath. It was added slowly to a colourless solution of trimethyl borate (2.3ml, 3.1mg, 20mmol) in THF (abs., 50ml) under argon at a temperature of $<-70^{\circ}\text{C}$. After the addition was complete, the solution was warmed to room temperature overnight. A white suspension had formed. Water ($\sim 100\text{ml}$) and a sodium carbonate (5%, $\sim 20\text{ml}$) was added. The latter caused a slight colour change to reddish. Finally the addition of brine ($\sim 20\text{ml}$) caused the phases to separate. The aqueous phase was extracted twice with *tert*-butyl methyl ether and twice with ethyl acetate. Both layers were clear now, but opalescent. The combined organic layers were washed with brine, dried over magnesium sulfate and filtered. The solvent was removed *in vacuo* and left a yellowish grey oily substance. Proton-NMR looked unpure.

$^1\text{H-NMR}$, 250 MHz, CDCl_3 δ : 7.85-7.63 (m, 2.0H), 7.50-7.28 (m, 2.1H), 4.40-4.00 (m, 6.4H)

It was redissolved in DCM and washed twice with water, dried over sodium sulfate and filtered. Removing the solvent *in vacuo* gave a yellow oily substance (824mg, 44%) The proton-NMR looked worse.

$^1\text{H-NMR}$, 250 MHz, CDCl_3 δ : 7.58-7.28 (m, 2H), 7.00-6.63 (m, 9H), 3.86-3.65 (m, 22H).

7.7.11 Diisopropyl-4-methoxyphenyl borate

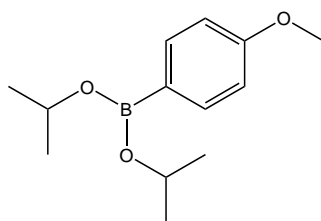


Figure 7.30: Diisopropyl-4-methoxyphenyl borate

Magnesium (1.139g, 46.86mmol) and one iodine pellet were suspended in THF (abs., 70ml) under argon. 4-bromoanisole (5.3ml, 7.9g, 42mmol) was added and stirred for 2h, before heating to reflux at 80°C for 1.5h. The white suspension was cooled in an ice- NaCl bath, before it was added in portions of 5ml during 1.5h to a solution of triisopropyl borate (19.6ml, 16.1g, 85.4mmol) in THF (30ml) at $70\pm 3^{\circ}\text{C}$. The resulting greyish white suspension was warmed to room temperature overnight. Brine (50ml) was added and stirred for 45 minutes. The phases were separated and the aqueous phase extracted twice with ethyl acetate. The combined opalescent white organic phases were dried over magnesium sulfate which caused a colour change to yellow. The solvent was removed *in vacuo* to give a yellow oily

substance (8.103g, 82%). Proton-NMR suggests that although hydrolysis had been mildly, the ether had at least partly hydrolysed to the corresponding boronic acid.

¹H-NMR, 250 MHz, CDCl₃ δ: 8.21 (m, 1.6H), 7.77 (d, J=8.9Hz, 1.0H), 7.06-6.74 (m, 4.8H), 3.93-3.68 (m, 8.2H).

Recrystallisation from hot diethyl ether gave a white powder (1.459g) of 4-methoxyphenylboronic acid or anhydride.

¹H-NMR, 250 MHz, CDCl₃ δ: 8.17 (d, J=8.17Hz, 2.0H), 7.02 J=8.6Hz, 2.0H), 3.92-3.69 (m, 4.8H).

7.7.12 Test on which side of the 2,5-dibromopyridine the lithiation occurs

The literature finding¹⁶⁸ that the 5 position is lithiated was confirmed. 2,5-Dibromopyridine (2.37g, 10.0mmol) was dissolved in THF (abs., 120ml) and cooled to -100°C to give a yellow solution. *n*-BuLi (1.6M/hexane, 6.8ml, 11mol) was added slowly, keeping the temperature of the between -100°C and -90°C. Three probes of each 10ml were taken and hydrolysed each separately with HCl_{aq} (10%, 50ml). There three probes were combined to 'probe 1'. Half an hour later, the rest of the reaction flask was distributed over 12 Erlenmeyer flasks with HCl_{aq} (10%, 50ml) and then combined to 'probe 2'. The probes were extracted twice with diethyl ether before and after adjusting the pH to 12-14 by addition of aqueous KOH (50%). The organic phases of each probe were combined, dried over magnesium sulfate and filtered. A small amount of methanol was added to both probes and then all solvent removed *in vacuo* at 40°C. 'Probe 1' yielded 471mg and 'probe 2' 967mg yellow oil. Proton-NMR showed exclusively 2-bromopyridine (91%).

¹H-NMR, 250 MHz, CDCl₃ δ: 8.38 (ddd, H6, J=4.7Hz, 1.3Hz and 0.9Hz, 1H), 7.60-7.46 (m, H3 and H4, 2H), 7.27 (ddd, H5, J=8.1Hz, 4.7Hz and 1.5Hz, ~1H).

7.7.13 2-Bromo-5-pyridylboronic acid

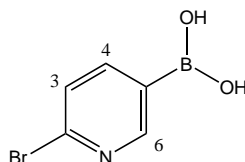


Figure 7.31: 2-Bromo-5-pyridylboronic acid

A general procedure for boronation¹⁴⁹ was followed. 2,5-Dibromopyridine (575mg, 2.22mmol) was dissolved in diethyl ether (abs., 40ml) under an argon atmosphere. Cooling to -90°C caused the 2,5-dibromopyridine to fall out of solution again. *n*-BuLi (1.6M/hexane, 1.53ml, 2.45mmol) was added, and the mixture cooled immediately to -100°C before warming slowly to -60°C. The yellowish suspension turned slowly into a dull, deep red mixture. It was cooled to -80°C before adding trimethyl borate and stirred at that temperature for 1.5h. The mixture was warmed slowly, and turned yellow at -25°C. At this point, HCl_{aq} (10%, 50ml) was added to give two phases. They were separated. The aqueous phase was red and the organic phase was colourless. Adjusting the pH of the aqueous phase with aqueous KOH (50%) and aqueous NaCO₃ (5%) to 8 caused a colour change to yellow. Extracting twice with *tert*-butyl methyl ether gave a yellow organic phase and an almost colourless aqueous phase. The combined organic phases were dried over sodium sulfate and filtered. The solvent was removed *in vacuo* to give a red solid (242g, 54%).

¹H-NMR, 250 MHz, DMSO δ : 8.64 (d, H6, J=2.0Hz, 1H), 8.50 (s, OH, 2.7H), 8.00 (dd, H4, J=7.9Hz and 2.0Hz, 1H), 7.62 (d, H3, J=7.9Hz, 1H)

EI-MS, 70eV, 450 °C: m/z= 551 (3M – 3H₂O)⁺, 472 (3M – 3H₂O – Br)⁺, 157 (bromopyridine)⁺, 78 (pyridine – H)⁺.

FAB-MS (NBA): 474 (3M – 3H₂O – Br + 2H)⁺, 154, 136.

IR KBr ($\tilde{\nu}$ / cm⁻¹): 3343b, 3271sh, 3252sh, 3238sh, 1584vs, 1554s, 1461m, 1446m, 1414s, 1381m, 1343vs, 1296m, 1178m, 1088s, ~1052 1028s, 802m, 739w, 644m.

Melting point: 187-189 °C.

7.7.14 Two approaches to 2-bromo-5-(4-methoxyphenyl)pyridine

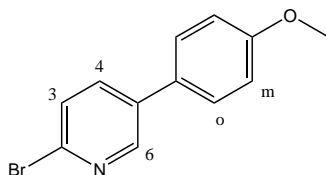


Figure 7.32: 2-Bromo-5-(4-methoxyphenyl)pyridin

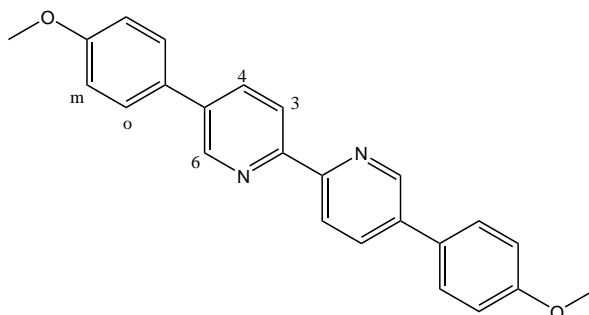


Figure 7.33: 5,5'-Di-(4-methoxyphenyl)-2,2'-bipyridine

Route 1 2,5-Dibromopyridine (102mg, 0.428mmol) was suspended in ether (abs., 4ml) and cooled to -75 °C under nitrogen. *n*-BuLi (1.6M/hexane, 0.29ml, 0.46mmol) was added while the temperature stayed below -70 °C. The colour changed to dark orange. A suspension of 4-methoxyboronic acid in diethyl ether (abs., 2ml) was added. The flask with the 4-methoxyboronic acid solution was rinsed twice with diethyl ether (abs., 1ml) and this was added to the reaction flask too. After stirring for 10 minutes below -70 °C an orange-white suspension had formed. It was warmed to 0 °C and hydrolysed with saturated aqueous NH₄Cl and extracted twice with ethyl acetate. The combined organic layers were washed with brine, dried over sodium sulfate and filtered. The solvent was removed *in vacuo* and a yellow oil was obtained. Proton-NMR showed apart from starting material, a new subspectrum that might possibly belong to 5,5'-di-(methoxyphenyl)-2,2'-bipyridine. Very possibly what is seen here is a mixture of several minor side products.

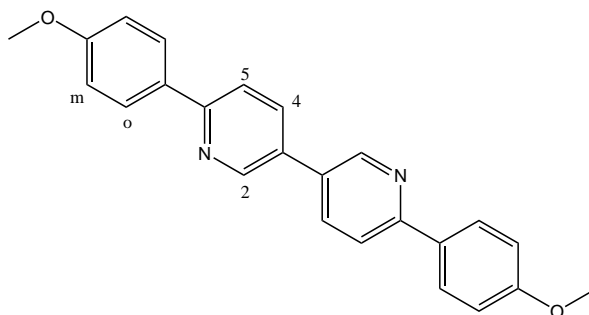


Figure 7.34: 6,6'-Di-(4-methoxyphenyl)-3,3'-bipyridine (dmp)

¹H-NMR, 300 MHz, CDCl₃ δ: 8.98 (d, 1H), 8.79 (s, 1H), 8.39 (d, 1H), 8.16 (d, 1H), 8.10-7.98 (m, >2H), 7.62-7.52 (m, >2H), 6.90 (dd, > m4H), 4.10 (q, > m4H), 3.92-3.70 (m, > m4H).

The oil was suspended in toluene : petrolether (1 : 1), filtered, put on a silica column and eluated with the same solvent mixture. A second side product could be collected in the second band. MS-analysis suggests that it is 6,6'-di-(4-methoxyphenyl)-3,3'-bipyridine (M). The proton-NMR shifts would support this, but for the integral values.

¹H-NMR, 500 MHz, CDCl₃ δ: 8.45 (dd, H6, J=2.5Hz and 0.5Hz, 3.7H), 7.67 (dd, Ho, J=8.4Hz and 2.6Hz, 4.0H), 7.48 (dt, H4, J=8.9Hz and 2.6Hz, 3.0H), 7.39 (dd, H3, J=8.4Hz and 0.6Hz, 4.4H), 6.96 (dt, Hm, J=5.9Hz and 2.6Hz, 2.9H), 3.85 (s, CH₃, 5.8H).

Maldi-TOF MS m/z: 368 (dmp)⁺, 291 (dmp-pyridine)⁺.

EI-MS, 70eV, ~300°C: m/z= 366(dmp – 2H)⁺, 290 (dmp – pyridine – H)⁺, 275 (dmp – pyridine – CH₄)⁺

Route 2 The general procedure of¹⁴⁹ was used. To a mixture of degassed benzene (65ml) and degassed aqueous Na₂CO₃ (2M, 50ml), 4-bromoanisole (0.10ml (0.15g, 0.80mmol) was added. The catalyst Pd(Ph₃P)₄ (24.5mg, 21μmol) was added. It was yellow but not lemon yellow. The organic phase became yellow, the aqueous phase stayed colourless. The mixture was heated to 90°C while a degassed solution of 2-bromo-5-pyridylboronic acid (55mg, 0.27mmol) was added slowly. This resulted in yellow solution with white solid. After 1.5h, TLC showed that all C had been consumed. The reaction mixture was cooled to room temperature before adding H₂O₂ (30%, 1ml) and stirring for 1h. No change was visible. After filtering, the phases were separated. The solid (1mg) was insoluble in chloroform. The organic phase was washed with water. Some of the solvent was removed from the filtrate and new precipitate formed. It was filtered off and washed with water to give a yellow solid (18mg). This substance could not be dissolved in DCM, methanol nor DMSO. All of the solvent was now removed from the filtrate, despite of the TLC proton-NMR showed was starting material.

Route 3 Like route 2, but with Pd(OAc)₂ as catalyst and potassium carbonate instead of sodium carbonate, and the reaction mixture was only heated to 60-62°C. 4-bromanisole was regained.

7.7.15 5-Bromo-2-(4-methoxyphenyl) pyridine

The reaction conditions¹⁶⁹ and work up procedure¹⁷⁰ from the literature were followed. 2,5-Dibromopyridine (313mg, 1.32mmol) and the catalyst Pd(Ph₃P)₄ (35mg, 30μmol, lemon yellow) were dissolved in degassed toluene (4.5ml) to give a light yellow solution. Degassed aqueous Na₂CO₃ (2M,

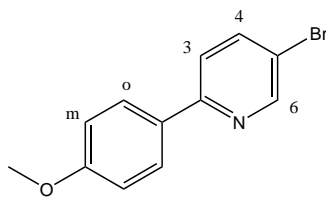


Figure 7.35: Main product: 5-bromo-2-(4-methoxyphenyl)pyridine

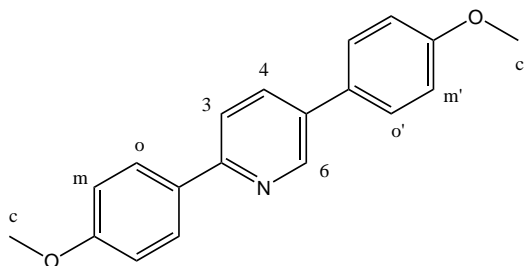


Figure 7.36: Side product: 2,5-di-(4-methoxyphenyl)pyridine

4.5ml) was added and this phase was colourless. A degassed solution of 4-methoxyphenylboronic acid (203mg, 1.52mmol (if trimer)) in methanol (5ml) was added last. The reaction mixture was heated in the oil bath at 90°C for 24h. After cooling for 3 minutes, saturated aqueous NaHCO₃ (50ml) was added. The phases were separated and the aqueous phase was extracted three times with ethyl acetate. A solid formed. It was filtered off and washed with ethyl acetate to give a yellow solid (side product 22mg.) The combined organic phases were washed with brine, dried over sodium sulfate and filtered. The solvent was removed in vacuo to give a yellow solid (303mg, 87%) see also the crystal structure in appendix C.3 on page 207. The crystal used for x-ray diffraction, crystallised from a solution in deuterated chloroform. The microanalysis however did not fit satisfactorily, even after recrystallising from methanol.

Main product:

Microanalysis: found (calculated): C₁₂H₁₀NOBr % C: 56.33 (54.57), % H: 4.22 (3.82), % N: 5.25 (5.30).

¹H-NMR, 250 MHz, CDCl₃ δ: 8.71 (d, H₆, J=2.4Hz, 1H), 7.94 (d, H_o, J=8.9Hz, 2H), 7.87 (dd, H₄, J=8.6Hz and 2.4Hz, 1H), 7.59 (d, H₃, J=8.5Hz, 1H), 7.00 (d, H_m, J=8.9Hz, 2H), 3.87 (s, CH₃, 3H).

EI-MS, 70eV, ~2300°C: m/z= 263/265 M⁺, 248/250 (M - CH₃)⁺, 220/222, 141.

Side product: 2,5-di-(4-methoxyphenyl)pyridine

¹H-NMR, 250 MHz, CDCl₃ δ: 8.87 (d, H₆, J=2.4Hz, 1H), 8.00 (d, H_o, J=8.9Hz, 2H), 7.91 (dd, H₄, J=8.3Hz and 2.5Hz, 1H), 7.73 (d, H₃, J=8.4Hz, 1H), 7.57 (d, H_{o'}, J=8.7Hz, 2H), 7.02 (dd, H_m and H_{m'}, J=8.9Hz and 1.5Hz, 4H), 3.88 (d, CH₃, J=1.7Hz, 6H).

EI-MS, 70eV, ~250°C: m/z= 291 M⁺, 276 (M - CH₃)⁺, 248 (M - 2CH₃ - O).

7.7.16 Diisopropyl-2-(4-methoxyphenyl)-5-pyridyl borate

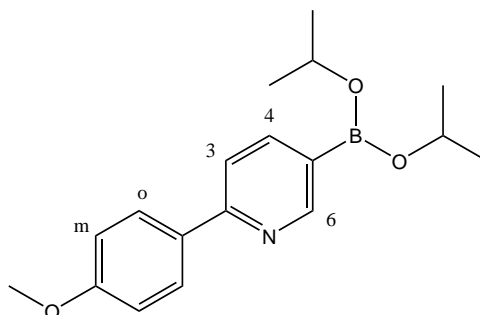


Figure 7.37: Diisopropyl-2-(4-methoxyphenyl)-5-pyridyl borate

The literature procedure for boronation^{149,168} was followed. 5-Bromo-2-(4-methoxyphenyl)pyridine (107mg, 4.5 μ mol) was suspended in diethyl ether (abs., 50ml) and cooled to -73 $^{\circ}$ C under argon. *n*-BuLi (1.6M / hexane, 0.30ml, 0.49mmol) was added and the yellow mixture warmed to -50 $^{\circ}$ C. This temperature was kept for 0.5h while all solid dissolved and the colour changed to red. This solution was cooled back to -65 $^{\circ}$ C before triisopropyl borate (abs., 0.47ml, 0.76g, 4.05mmol) was added. The mixture was stirred at -65 $^{\circ}$ C for 0.5h more, before warming to 0 $^{\circ}$ C. During the warming, the colour changed to yellow. Saturated aqueous NH₄Cl (20ml) was added, and after mixing for several minutes, the phases were separated and the aqueous phase extracted three times with diethyl ether. The combined organic layers were washed with brine, dried over sodium sulfate and filtered. The solvent was removed *in vacuo* to give a yellow oil (177mg).

¹H-NMR, 250 MHz, CDCl₃ and methanol-d₄ δ : 7.91 (d, H₆, J=2.4Hz, 1H), 7.49 (d, H_o, J=8.9Hz, 2H), 7.31 (d, H₃, J=8.7Hz, 1H), 7.04 (dd, H₄, J= 8.6Hz and 2.9Hz, 1H), 6.75 (d, H_m, J=8.9Hz, 2H), 3.63 (s, CH₃O, 3H), 3.75 (m, -CH-, ~2H), 0.93 (d, CH/3-C, J=6.2Hz, 6H).

7.8 The synthesis of 4-(4-methoxyphenyl)-2,2':6',2'':6'',2''':2'''-quaterpyridine (4MeOphqtpy)

7.8.1 6,6'-Dibromo-2,2'-bipyridine

The synthesis was consistent with the literature procedure.⁸² Dry 2,6-dibromopyridine (13.00g, 54.9mmol) was suspended in diethyl ether (freshly distilled from sodium, 100ml) and cooled in an acetone/dryice bath to $\leq -75^{\circ}\text{C}$ under argon. *n*-BuLi (1.6M in hexane, 38.4ml) was added slowly. Additional cooling with liquid nitrogen helped to keep the temperature below -75°C . After the addition was complete, the temperature was raised to -50°C and then kept between -50 and -60°C until everything dissolved, and the mixture became a yellow solution; this took about 30 min. The solution was cooled back to $\leq -75^{\circ}\text{C}$ and dry, brown CuCl_2 (3.73g, 27.7mmol) was added as a solid. The suspension was stirred at that temperature for 40min, and then dry air was bubbled through for 3h. The flask was left open to warm to room temperature, still protected from water by a P_2O_5 chamber and a gas wash flask filled with H_2SO_4 . Again the mixture was cooled to -65°C and dry air was bubbled through for 20 min. The colour changed from brown to greenish brown, and HCl (6.0M, 50ml) was added to quench the reaction. The mixture was stirred until it reached ambient temperature. A beige precipitate had formed, and it was filtered off, washed with HCl (2.0M) and dried *in vacuo* over P_2O_5 to give 4.81g pure product in 57.5% yield.

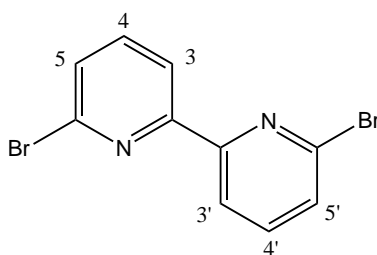


Figure 7.38: 6,6'-Dibromo-2,2'-bipyridine

$^1\text{H-NMR}$, 250 MHz, CDCl_3 δ : 8.38 (d, H3 7.7Hz, 2H), 7.67 (t, H4, J=7.78Hz, 2H), 7.51 (d, H5, 7.85Hz, 2H).

Melting point $220.3\text{-}220.9^{\circ}\text{C}$.

7.8.2 6-Bromo-2,2'-bipyridine

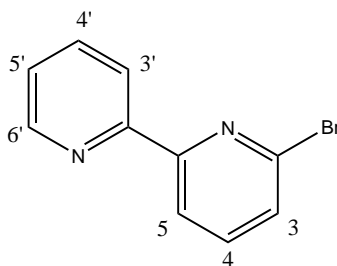


Figure 7.39: 6-Bromo-2,2'-bipyridine

A modified version of the literature procedure for the reaction from 6,6-dibromo-2,2-bipyridine was used.¹³⁵ While using the exact temperature given in the literature¹³⁵ only gave the starting material back (in good yield), a different reaction temperature was found to make this reaction work to produce a reasonable yield of the desired product. 2,6-Dibromopyridine (0.526g, 1.675mmol) and dry THF (50 ml, freshly distilled from sodium) were added to an argon-flushed reaction flask. The resulting orange suspension was cooled to -90°C. Phenyllithium solution (2.0 ml, 2.5 M, 5.0 mmol) was added dropwise, while the temperature was allowed to rise to -80°C. After the addition was complete, the temperature was kept between -95°C and -80°C for 15 min., and then between -75°C and -65°C for 45 min. The solution was cooled back to -90°C again and then let warm slowly to -70°C. This procedure was repeated, and then, when -70°C was reached the second time, the reaction was quenched by adding methanol (40 ml), and after two to three minutes, water (20 ml). THF and methanol were removed *in vacuo* from the clear orange solution. The residual suspension was cooled to room temperature, filtered, and the brown oily solid dried in a dessicator over P₂O₅ (345mg).

The solid was suspended in a small amount of DCM, filtered, and the filtrate added to a column of silica gel (0.04 - 0.06 mm). Elution with DCM : methanol : diethylamine (20:1:0.01) gave the compound as a white solid (333mg, 63%)

¹H-NMR, 250 MHz, CDCl₃ δ: 8.67 (ddd, H6', J=4.9Hz, 1.8Hz and 0.9Hz, 1H), 8.44-8.35 (m, H3 and H3', 2H), 7.82 (td, H4', J=7.7Hz and 1.8Hz, 1H), 7.67 (t, H4, J=7.8Hz, 1H), 7.49 (dd, H5, J=7.8Hz and 0.93Hz, 1H), 7.33 (ddd, H5', J=7.5Hz, 4.9Hz and 1.2Hz

7.8.3 6-*n*-Butyl-2,2'-bipyridine

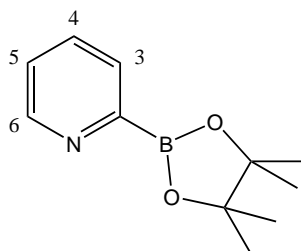


Figure 7.40: 6-Pyridyl-1,3,2-dioxaborolane

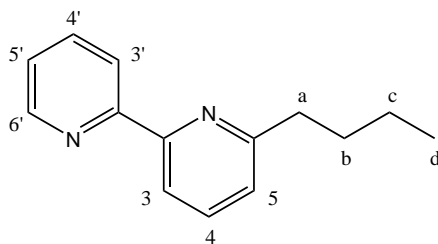


Figure 7.41: 6-*n*-Butyl-2,2'-bipyridine

The general procedures from the literature were followed.^{144, 146, 148, 149} 2-Bromopyridine (1.715g, 10.85mmol) was dissolved in diethyl ether (abs., ~100ml) and cooled to -75°C under argon. *n*-BuLi (1.6M/hexane, 8.52ml, 13.6mmol) was added while keeping the temperature below -70°C. After the addition was complete, the temperature was raised slowly to -50°C and upon arriving at that temperature, the reaction mixture was cooled back to -75°C immediately. Addition of tributyl borate (3.66ml, 13.6mmol) gave a red solution, which was warmed overnight to room temperature. Predried pinacol

(1.733g, 14.66mmol) was added under stirring, followed 10 minutes later by acetic acid (100%, 0.64ml, 11.2mmol). The neutralisation caused a colour change to yellow and a small amount of precipitate formed. The mixture was filtered through celite, and the ether in the filtrate removed *in vacuo*. The pH of the residue was adjusted to 8 with sodium carbonate and extracted three times with DCM. The solvent of the combined DCM layers was removed *in vacuo* to give a brown oil that was dried further *in vacuo*. NMR- and MS-analysis proved this to be a side product (137mg, 27%). No 6-pyridyl-1,3,2-dioxaborolane was isolated under these reaction conditions.

¹H-NMR, 600 MHz, CDCl₃ δ: 8.67 (ddd, H6' J=4.9Hz, 1.8Hz and 0.93Hz, 1H), 8.44 (td, H3', J=8.0Hz and 1.0Hz, 1H), 8.17 (dd, H3, J=7.9Hz and 0.84Hz, 1H), 7.80 (td, H4', J=7.5Hz and 1.8Hz, 1H), 7.71 (t, H4, J=7.7Hz, 1H), 7.28 (ddd, H5', J=7.5Hz, 4.9Hz and 1.3Hz, 1H), 7.16 (dd, H5, J=7.7Hz and 1.0Hz, 1H), 2.87 (t, Ha, J=7.8Hz, 2H), 1.79 (quintett, Hb, J=7.6Hz, 2H), 1.43 (sextett, Hc, J=7.5Hz, ~2H), 0.966 (t, Hd, J=7.3Hz, ~3H).

¹³C-NMR, 150 MHz, CDCl₃ δ: 162.7 (C6), 157.4 (C2'), 156.1 (C2), 149.7 (C6'), 137.7 (C4), 137.5 (C4'), 124.1 (C5'), 123.4 (C5), 121.9 (C3'), 118.8 (C3), 38.82 (Ca), 32.58 (Cb), 23.19 (Cc), 14.71 (Cd).

EI-MS, 70eV, ~100°C: m/z= 226, 211 (6-(*n*-butyl)-2,2'-bipyridine – H)⁺, 197 (6-(*n*-butyl)-2,2'-bipyridine – CH₃)⁺, 183 (6-(*n*-butyl)-2,2'-bipyridine – C₂H₅)⁺, 170 (100%), 6-methyl-2,2'-bipyridine)⁺, 155 (2,2'-bipyridine – H)⁺.

IR KBr (ν̄ / cm⁻¹): 3855w, 3677w, 3421b, 2957vs, 2926vs, 2870s, 1664b, 1582s, 1563sh, 1459s, 1430s, 1379m, 1260w, 1081b, 776m.

7.8.4 6-Tributylstannyl-2,2'-bipyridine

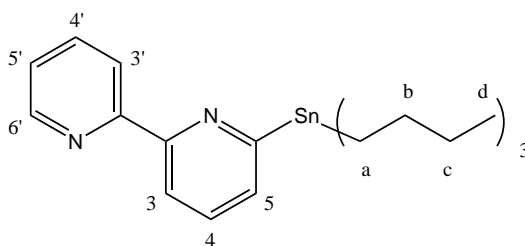


Figure 7.42: 6-Tributylstannyl-2,2'-bipyridine

The procedure of Hanan¹³⁴ was followed. Best results were obtained when the amount of BuLi added, was equivalent to the amount of 6-bromo-2,2'-bipyridine. The BuLi-solution was therefore titrated against HCl (0.20M) before use. 6-Bromo-2,2'-bipyridine (651mg, 2.77mmol) was suspended in diethyl ether and cooled to -100°C under argon. BuLi-solution (1.80ml, 1.69M, 3.05mmol) was added dropwise, while the temperature was kept below -100°C. During 40 minutes, the temperature was raised to -80°C. The black suspension, that followed the addition, turned slowly into a reddish-brown solution. After cooling back to -100°C tributyltin chloride (0.826ml, 0.992g 3.05mmol) was added and the solution turned black. The temperature was raised over 4h to -30°C to give an orange solution and with white precipitate. The contents of the reaction flask were transferred into a round bottomed flask, and the solvent removed *in vacuo* at 50°C to give a yellow oil.

¹H-NMR, 250 MHz, CDCl₃ δ: 8.65 (ddd, H6', J=4.9Hz, 1.8Hz and 0.83Hz, 1H), 8.53 (td, H3', J=8.0Hz and 1.0Hz, 1H), 8.24 (dd, H3, J=8.03Hz and 1.2Hz, 1H), 7.80 (td, H4', J=7.53Hz and 1.9Hz, 1H), 7.62 (t, H4, J=7.27Hz, 1H), 7.40 (dd, H5, J=7.4Hz and 1.4Hz, 1H), 7.28 (ddd, H5', J=8.70Hz, 4.9Hz and 1.2Hz, 1H), 1.68-1.55 (m, H_{a,borc}, 6H), 1.45-1.25 (m, H_{a,borc}, >6H), 1.22-1.10 (m, H_{a,borc}, 6H), 0.89 (t, H_d, J=7.2Hz, >9H).

7.8.5 3-(4'-Methoxyphenyl)-1-oxo-2-butenic acid

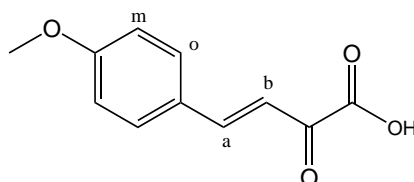


Figure 7.43: 3-(4'-Methoxyphenyl)-1-oxo-2-butenic acid

The synthesis was analogous to the literature preparation of 4-bromocinnamaldehyde,¹ except a different ratio of ethanol/water was used in the reaction.

Sodium pyruvate (12.4 g, 113 mmol) was dissolved in water (100 ml), and 4-methoxycinnamaldehyde (12 ml, g, mmol) was added. Ethanol (100 ml) was added in portions of 50ml, and an opalescent mixture formed first, then became a colourless solution. It was cooled in an ice-water bath to 4 °C and a potassium hydroxide solution (10%, 100ml) was added slowly, while the temperature was kept at 4 ± 1 °C. After the first few drops of potassium hydroxide solution, the reaction mixture turned yellow, and later, a precipitate formed. Towards the end of the addition, the quantity of precipitate prevented magnetic stirring, so the suspension was swirled every few minutes. The reaction mixture was acidified to pH 4 with hydrochloric acid, still in the cooling bath, and the colour became more intensely yellow. The mixture was filtered, and the yellow solid washed with water followed by diethyl ether, and dried over phosphorus pentoxide. Yield: 11.98g (58.9%).

¹H-NMR, 250 MHz, methanol-d₄ δ: 7.90 (s, 1H, COOH), 7.74 (d, 1H, alkene CH, J=16.2Hz), 7.65 (d, 2H, aromatic, J=1.01Hz), 7.01 (d, 1H, alkene CH, J=16.0Hz), 7.01 (d, 2H, aromatic, J=8.7Hz) and 3.88 (s, 3H, methoxy).

7.8.6 N-[1-Oxo-1-(6-bromo-2-pyridyl)eth-2-yl]pyridinium iodide (Br-PPI)

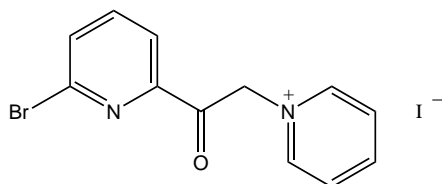


Figure 7.44: N-[1-Oxo-1-(6-bromo-2-pyridyl)eth-2-yl]pyridinium iodide (Br-PPI)

The synthesis was consistent with the literature procedure.¹³⁷ 2-Acetyl-6-bromo-pyridine (7.82g, 39.1mmol), iodine (10.6g, 41.7mmol) were mixed with pyridine (12.0ml, 11.8g, 149mmol) and heated in the oil bath to 60 °C while stirring. After ~30min the mixture turned solid and dark. Pyridine (1.5ml) was added, followed by water (35ml). Then the temperature of the oil-bath was raised to 100 °C. The mixture was stirred until all precipitate dissolved (~30min), and filtered hot. The filtrate was cooled in

the fridge, and a brown precipitate formed that was filtered off, washed with water and dried *in vacuo* to give a brown powder (12.6g), in 79.3% yield.

IR KBr ($\tilde{\nu}$ / cm^{-1}): 3402w, ~3125w, 3084m, 3033s, 2965s, 2884m, 2511w, 2366w, ~2060w, ~2028, ~1930w, 1712vs, 1633vs, 1577sh, 1570m, 1554s, 1493s, 1484vs, 1430vs, 1408s, 1400sh, 1362m, 1342s, 1297m, 1282m, 1268sh, 1232m, 1218s. 1195m, 1189m, 1158vs, 1148m, 1121s, 1077m, 1028m, 1008vs, 1003vs, 987s, 853m, 806s, 775s, 727w, 718s, 678vs, 642m, 569s, 461m.

7.8.7 6'-Bromo-4-(4-methoxyphenyl)-2,2'-bipyridine-6-carboxylic acid

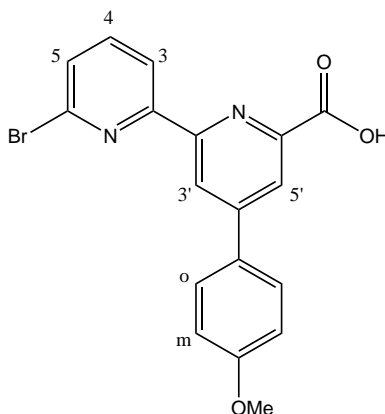


Figure 7.45: 6'-Bromo-4-(4-methoxyphenyl)-2,2'-bipyridine-6-carboxylic acid

For the synthesis of 6'-bromo-4-(4-methoxyphenyl)-2,2'-bipyridine-6-carboxylic acid, the literature procedure for the synthesis of 6'-bromo-4-(4-bromophenyl)-2,2'-bipyridine-6-carboxylic acid¹ was slightly altered. It is a Kröhnke cyclisation.⁹²

3-(4'-Methoxyphenyl)-1-oxo-2-butenic acid (5.043g, 24.94mmol), Br-PPI (10.130g, 25.01mmol) and NH_4OAc (14.5g, 188mmol) were suspended in water (166ml) and heated in the oilbath to 80°C. Ethanol (~3ml) was added and almost everything dissolved. The mixture was then heated to 100°C and after addition of more ethanol (~4ml), the reaction mixture was left to reflux for 16h. After cooling to room temperature, the cream beige precipitate was filtered off, washed with water and dried *in vacuo* to yield an off-white powder (9.25g, 96%).

Microanalysis: found calculated: $\text{C}_{18}\text{H}_{13}\text{N}_2\text{O}_3\text{Br}$ % C: 56.32 (56.12), % H: 3.45 (3.40), % N: 7.22 (7.27).

$^1\text{H-NMR}$, 250 MHz, CDCl_3 δ : 8.87 (d, H3', $J_{\text{H}3'-\text{H}5'}=1.85\text{Hz}$, 1H), 8.49 (d, H5', $J_{\text{H}5'-\text{H}3'}=1.68\text{Hz}$, 1H), 8.35 (dd, H3, $J_{\text{H}3-\text{H}5}=0.93\text{Hz}$, $J_{\text{H}3-\text{H}4}=7.78\text{Hz}$, 1H), 7.82 (d, Ho, $J_{\text{H}o-\text{H}m}=9.03\text{Hz}$, 2H), (7.76 (t, H4, $J_{\text{H}4-\text{H}3/\text{H}5}=7.78\text{Hz}$, 1H), 7.60 (dd, H5, $J_{\text{H}5-\text{H}3}=0.84\text{Hz}$, $J_{\text{H}5-\text{H}4}=7.86\text{Hz}$, 1H), 7.07 (d, Hm, $J_{\text{H}m-\text{H}o}=9.05\text{Hz}$, 2H), 3.90 (s, H(MeO), 3H).

$^{13}\text{C-NMR}$, 62.5 MHz, DMSO-d_6 δ : 166.8 (1C), 161.6 (1C), 156.8 (1C), 155.1 (1C), 150.3 (1C), 150.1 (1C), 141.9 (1C), 141.6 (1-2C), 129.8 (1C), 129.3 (2C), 122.7 (1C), 121.5 (1C), 120.8 (1C), 115.8 (2C), 56.2 (MeO, 1C).

IR diamond ($\tilde{\nu}$ / cm^{-1}): 2831w, 2646sh, 2592sh, 2523m, 2037w, 1821w, 1681vs, 1605s, 1574s, 1551s, 1512s, 1458s, 1427s, 1389s, 1350s, 1258vs, 1157s, 1126s, 1095w, 1065m, 1034s, 987m, 933m, 895s, 833s, 787vs, 733m, 694s.

EI-MS, 70eV, 500° C: m/z= 386/384 M⁺, 342/340 (M – CO₂)⁺, 130.

X-ray see Appendix C on page 209.

7.8.8 6-Bromo-4'-(4-methoxyphenyl)-2,2'-bipyridine

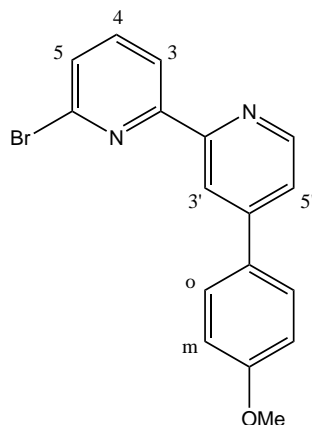


Figure 7.46: 6-Bromo-4'-(4-methoxyphenyl)-2,2'-bipyridine

After several approaches to decarboxylate 6'-Bromo-4-(4-methoxyphenyl)-2,2'-bipyridine-6-carboxylic acid in solution, the approach of Hammarström, Toftlund and Åkermark was used.¹³⁸ Small portions of 6'-Bromo-4-(4-methoxyphenyl)-2,2'-bipyridine-6-carboxylic acid (10-20mg) were heated with the heat gun in a round bottomed flask (10 ml). When the compound melted, a brown liquid formed and it degassed spontaneously. When cooled to room temperature, it became a brown glass that still contained some carboxylated material.

When recrystallised from hot THF, the carboxylated starting material could be filtered off and heated up again. The product crystallised upon cooling to give a brown powder (yield 51%).

Microanalysis: found (calculated): C₁₇H₁₃N₂OBr % C: 59.71 (59.84), % H: 3.89 (3.84), % N: 8.04 (8.21).

¹H-NMR, 250 MHz, CDCl₃δ: 8.68 (dd, H_{6'}, J_{H_{6'}-H_{5'}}=5.0Hz, J_{H_{6'}-H_{3'}}=0.75Hz, 1H), 8.63 (d, H_{3'}, J_{H_{3'}-H_{5'}}=1.5Hz, 1H), 8.49 (d (slightly broad), H₃, J_{H₃-H₄}=7.8Hz (coupling to the H₅ is not resolved), 1H), 7.74 (d, H_o, J_{H_o-H_m}=9.0Hz, 2H), 7.70 (t, H₄, J_{H₄-H₃/H₅}=7.9Hz, 1H), 7.56 (dd, H_{5'}, J_{H_{5'}-H_{6'}}=5.0Hz, J_{H_{5'}-H_{3'}}=2.0Hz, 1H), 7.52 (dd, H₅, J_{H₅-H₄}=7.6Hz, J_{H₅-H₃}=0.9Hz, 1H), 7.04 (d, H_m, J_{H_m-H_o}=9.2Hz, 2H), 3.89 (s, H(MeO), 3H).

EI-MS, 70eV, 350° C: m/z= 342/340 M⁺, 261 (M – Br)⁺, 218.

IR diamond (ν / cm⁻¹): 3348b, 3078w, 2932w, 2839w, 2577w, 2168w, 2037w, 1983w, 1628sh, 1597vs, 1574vs, 1504s, 1458m, 1427s, 1389m, 1312w, 1288w, 1250vs, 1165vs, 1119vs, 1080w, 1018vs, 987s, 903sh, 825vs, 795vs, 733w, 671m.

X-ray see Appendix C on page 204.

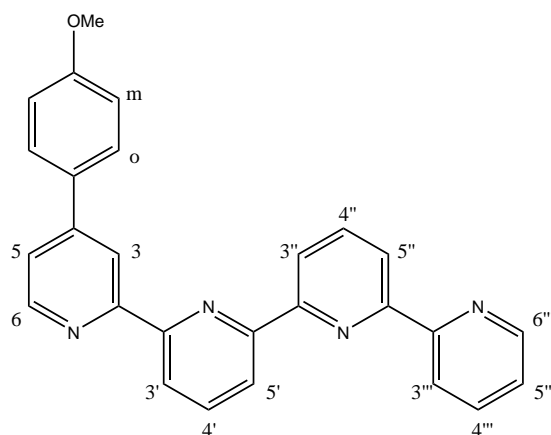


Figure 7.47: 4-(4-Methoxyphenyl)-2,2':6',2'':6'',2''':6''',2''''-quaterpyridine

7.8.9 4-(4-Methoxyphenyl)-2,2':6',2'':6'',2''':6''',2''''-quaterpyridine

The procedure of Stille coupling was followed as described by Hanan.¹³⁴ Dry DMF (10 ml) was degassed in a two necked flask for 50 min and Pd(OAc)₂ (6.0 mg, 26.7 mmol) was added. This gave an orange-brown solution. Triphenylphosphine (33.2 mg, 1.27 mmol) was added and the solution turned lemon yellow. This catalyst solution was kept under argon while a degassed solution of 4'-(4-methoxyphenyl)-6-bromo-2,2'-bipyridine (0.112g, 0.328 mmol) in dry DMF (10 ml) was prepared. This solution was added to the catalyst solution via cannula. The colour of the solution turned orange-brown. A solution of 6-tributylstannyl-2,2'-bipyridine (0.085g, 0.191 mmol) in dry DMF (6.0 ml) was degassed for 40 min in the same flask already used to prepare the solution of the 4'-(4-methoxyphenyl)-6-bromo-2,2'-bipyridine. This solution was added to the reaction flask, and the remainder rinsed out with more dry, degassed DMF (3 times 2.5 ml). The mixture was then heated at 90 °C for 25 hours. The brown reaction mixture was then cooled to room temperature. A saturated aqueous solution of sodium fluoride (20 ml) was added and the mixture was stirred at 60 °C overnight. The suspension was allowed to cool to room temperature, water (3–4 ml) was added and the white precipitate was filtered onto a sinter (P4) and washed with a small amount of DMF-water (1 : 1) mixture, followed by diethyl ether. The solvent of the filtrate was removed *in vacuo* to give the crude product as a brown powder (104 mg).

1. Step: chromatography on alox: eluents were used for a column: DCM : MeOH : Et₂NH (200:10:1). Product and tin salt were collected in the same fraction.
2. Step: chromatography on silica: eluent hexane : EtOAc : Et₂NH (100 :40 : 1). Pure product was collected in the third fraction. The yield of pure product was now reduced to 5.5%.

Microanalysis: found (calculated): C₂₇H₂₀N₄O % C: 77.55 (77.87), % H: 4.95 (4.84), % N: 13.21 (13.45).

¹H-NMR, 500MHz, CDCl₃δ: 8.84 (dd, H₃, J=3.5Hz and 0.75Hz, 1H), 8.72 (dd, H_{6'''} or H₆, J=5.0Hz and 1.0 MHz, 1H), 8.72 (dd, H₆ or H_{6'''}, J=5.25Hz and 0.75Hz, 1H), 8.69 and 8.68 (each a dd, H_{3'} or H_{5'} and H_{5''}, J=8.0Hz and 1.0Hz, 1H), 8.67 (dt, H_{3'''}, J=7.5Hz and 1.0Hz, 1H), 8.51 and 8.49 (each a dd, H_{3'} or H_{5'} and H_{3''}, or H J=7.5Hz and 1.0Hz, 1H), 8.02 (t, 4' and 4'', J=7.5Hz, 2H) 7.88 (td, H_{4'''}, J=7.75Hz and 1.83Hz, 1H), 7.77 (dt, H_{ortho}, J=8.5Hz and 2.0Hz, 2H) 7.53 (dd, H₅, J=5.0Hz and 2.0Hz, 1H), 7.35 (ddd, H_{5'''}, J=7.5Hz and 4.75Hz and 1.25Hz, 1H), 7.08 (dt, H_{meta}, J=9.0Hz and 2.25Hz, 2H), 3.90 (s, H(methoxy), 3H).

¹³C-NMR, 125 MHz, CDCl₃δ: 160.5 (quarternary, C(para)), 156.7 (quarternary, C_{6'} or C_{6''}), 156.2 (quarternary, C_{2'''} or C_{6'''}), 155.5 (quarternary), 155.4 (quarternary), 155.3 (quarternary), 149.5 (quar-

ternary), 149.1 (C6 and C6'''), 148.8 (quarternary, C2 or C2'''), 137.9 (C4' or C4''), 137.8 (C4' or C4''), 136.9 (C4'''), 130.9 (quarternary, C4 or C(phenyl1)), 128.4 (C(ortho)), 123.8 (C5'''), 121.3 and 121.2 and 121.1 and 121.0 (C3', C3'', C3''', C5, C5', C5''), 118.6 (C3), 114.5 (C(meta)), 55.4 (C(methoxy)).

EI-MS: 416 M⁺ (100.0%), 415 (M – H)⁺ (99.1%), 417.1, 402.1 (M – CH₃)⁺, 385.1 (M – OCH₃)⁺, 372.1 (M – 44)⁺, 208.1 M²⁺/2, 186.6 (M – 44)²⁺/2).

FAB-MS: 417 (100%) (M+H)⁺.

IR diamond ($\tilde{\nu}$ / cm⁻¹): 3055w, 3016w, 2932m, 2839w, 2044w, 1983w, 1906w, 1728w, 1674w, 1605m, 1566vs, 1512s, 1466sh, 1443s, 1420s, 1396s, 1296m, 1242vs, 1180s, 1149w, 1110m, 1072w, 1041s, 987s, 941w, 910w, 810vs, 771s, 733s, 687w, 656m.

Crystal structure The crystal structure was measured on a crystal that had crystallised from one small fraction off the silica column. The eluent had been EtOAc: hexane : Et₂NH (8:20:1). For a picture and further data on the structure see Figure B.1 on page 197 and the listed data below.

7.8.10 Alternative synthesis of 6-bromo-4'-(4-methoxyphenyl)-2,2'-bipyridine

4-Methoxycinnamaldehyde

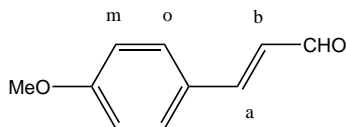


Figure 7.48: 4-Methoxycinnamaldehyde

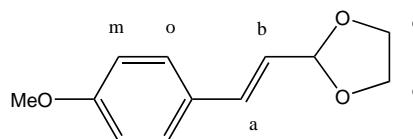


Figure 7.49: 1-(1,3-Dioxolan-2-yl)-2-(4-methoxyphenyl)ethene

The general procedure for Wittig reactions described in the literature¹³⁹ was followed, but the work-up conditions were altered in order to avoid Ph₃P = O impurity in the product. 1,3-Dioxolan-2-ylmethyltriphenylphosphonium bromide (10.055g, 22.422mmol) was predried in the reaction flask at 80-90°C at 1.5 · 10⁻¹ mbar for 2.5h and left to cool to room temperature under argon. In a two neck round bottomed flask MeOLi/methanol (15ml, 2.2M, 33mmol) and methanol (15ml) were frozen three times and evacuated, then let warm to room temperature under argon atmosphere. 4-Methoxybenzaldehyde was distilled *in vacuo* at ~100°C and stored under argon.

DMF (15ml, abs.) was added to the reaction flask already containing the 1,3-dioxolan-2-ylmethyltriphenylphosphonium bromide. Using a predried syringe from the dessicator, 4-methoxybenzaldehyde (1.81ml, 14.9mmol) from above was added over a period of 3h, making sure the reaction temperature stayed at 90°C always. The mixture was refluxed overnight. The clear solution was cooled to room temperature, and water (100ml) was added. Upon addition, the clear solution turned into a white suspension. Extraction with hexane gave a colourless organic phase and a yellow aqueous phase. The organic phase was washed with water, dried over sodium sulfate and filtered. The solvent was removed *in vacuo* to give a phosphine free, slightly yellowish oil (3.49g), containing the protected product 1-(1,3-dioxolan-2-yl)-2-(4-methoxyphenyl)ethene and some already deprotected product.

Protected: ¹H-NMR, 250 MHz, CDCl₃ δ: 9.65 (d, CHO, J_{CHO-Hb}=7.7Hz, 1H), 7.53 (d, Ho, J_{Ho-Hm}=8.5Hz, 2H), 7.43 (d, Ha, J_{Ha-Hb}=15.9Hz, 1H), 6.95 (d, Hm, J_{Hm-Ho}=8.9Hz, 2H), 6.61 (dd, Hb, J_{Hb-Ha}=15.9Hz, J_{Hb-CHO}=7.7Hz, 1H), 3.86 (s, MeO, 3H), 3.74 (s, Hc or Hd, 2H), 3.49 (s, Hd or Hc, 2H).

For deprotection, the oil was dissolved in THF (60ml) and HCL (100ml, 10%) was added. The mixture was stirred under argon for 2.5h at room temperature. The colour was more yellow than before. The mixture was extracted four times with hexane, together the organic layers were washed with a sodium hydrogencarbonate solution, then with brine and dried over sodium sulfate and filtered. The solvent was removed *in vacuo* and the residue dried in the deccicator to give clean product (2.307, 95%).

Deprotected: $^1\text{H-NMR}$, 250 MHz, CDCl_3 δ : 9.65 (d, CHO, $J_{\text{CHO}-\text{Hb}}=7.7\text{Hz}$, 1H), 7.53 (d, Ho, $J_{\text{Ho}-\text{Hm}}=8.5\text{Hz}$, 2H), 7.43 (d, Ha, $J_{\text{Ha}-\text{Hb}}=15.9\text{Hz}$, 1H), 6.95 (d, Hm, $J_{\text{Hm}-\text{Ho}}=8.9\text{Hz}$, 2H), 6.61 (dd, Hb, $J_{\text{Hb}-\text{Ha}}=15.8\text{Hz}$, $J_{\text{Hb}-\text{CHO}}=7.7\text{Hz}$, 1H), 3.86 (s, MeO, 3H).

6-Bromo-4'-(4-methoxyphenyl)-2,2'-bipyridine via 4-methoxycinnamaldehyde

See Figure 7.46 page 168.

Method B page 10 of Kröhnke⁹² was followed. 4-Methoxycinnamaldehyde (1.937g, 11.94mmol) was dried at 60°C at 0.2mbar. Br-PPI (4.867g, 12.02mmol) was added to the yellow oil and cooled to room temperature at the same pressure. Ammonium acetate (4.80g, 62.3mmol) was added to the reaction flask, and the flask with the reflux cooler was evacuated and flushed with argon three times. The mixture was heated to 100°C under argon while acetic acid (5.5ml) was added in portions until everything dissolved. The temperature was raised to 120°C and the reddish black solution was refluxed at that temperature for 4.5h. The reaction was quenched by the addition of HCl solution. At first, a brown oily precipitate formed. Stirring further, while cooling to room temperature, a beige powdery precipitate formed as well. The beige precipitate was filtered off, washed with HCl (2M) and dried *in vacuo*. The brown amorphous residue stuck to the walls of the reaction flask, and was dissolved in a minimum amount of DMF. Adding the same volume of HCL (2M) gave a beige precipitate. It was filtered off and washed first with HCL (2M) : DMF (10:1), then three times with water to remove all acetic acid. Both precipitates were product (913mg, 23%). For characterisation see 7.8.8 on page 168.

7.9 Alternative synthesis of 4-(4-methoxyphenyl)-2,2':6',2'':6''',2''''-quaterpyridine

7.9.1 (2,2'-bipyrid-6-yl)-4,4,5,5-tetramethyl-1,3,2-dioxaborolane

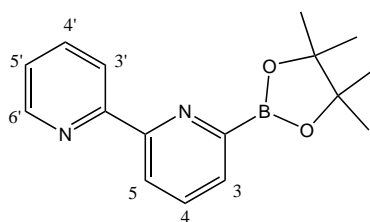


Figure 7.50: (2,2'-Bipyrid-6-yl)-4,4,5,5-tetramethyl-1,3,2-dioxaborolane

From the literature, the lithiation procedure with PhLi ^{135,141} and the reaction procedure for lithiated bipyridine with boronic esters¹⁴²⁻¹⁴⁶ was followed. 6-Bromo-2,2'-bipyridine (217mg, 0.923mmol) was suspended in THF (abs., 20ml) and cooled under argon until the internal thermometer showed -85°C. PhLi (2.0M / cyclohexane : ether (70 : 30)) was added slowly, and the reaction mixture turned black. Slowly the temperature was allowed to rise to -60°C. After cooling back to -80°C 2-isopropoxy-4,4,5,5-tetramethyl-1,3,2-dioxaborolan (0.5ml, 2.45mmol) was added dropwise, while the temperature was kept below -70°C. The solution was stirred in the cooling bath for another 2h and a test showed on TLC, that the starting material had gone, and four new signals showed; 45 min later, the colour was becoming

lighter and TLC showed six signals. The reaction was quenched at -70°C when HCl (2M, 20ml) was added. The internal temperature raised immediately to 0°C and the colour changed to orange. When 18°C was reached, the mixture was extracted with ether, but the colourless organic phase and yellow aqueous phase suggested the bipyridine type product to be in the aqueous phase, so water (25ml) was added, without effect. The pH of the aqueous phase at this point was 6. Saturated sodium carbonate was added and the pH raised to 7.5. Now the organic layer was a yellow solution and the aqueous layer a white suspension. The aqueous phase was extracted with ether two more times, the combined organic layers dried over sodium sulfate and filtered. After removing the solvent *in vacuo*, the residue was a yellow oil that slowly turned brown (277mg). After characterisation, the oil was left in air.

$^1\text{H-NMR}$, 250 MHz, CDCl_3 δ : 8.69 (ddd, H6', J=4.7Hz, 1.8Hz and 0.85Hz, 1H), 8.40 (dt, H3', J=8.0Hz and J=1.1Hz, 1H), 7.87-7.77 (m, H4' and H3, >2H), 7.44 (td, H4, J=6.6Hz and 2.0Hz, *sim* 1H), 7.40-7.27 (m, H5 and H5', >2H), 1.34 (s, CH_3 , *sim* 16H).

A flash column on alox, using toluene with traces of Et_2NH was not successful.

7.9.2 4-(4-Methoxyphenyl)-2,2':6',2'':6''',2'''- quaterpyridine

Figure, see 7.47 on page 169

The procedure from the literature¹⁴⁷ was followed. (2,2'-Bipyrid-6-yl)-4,4,5,5-tetramethyl-1,3,2-dioxaborolane (384mg, $\sim 1.0\text{mmol}$) and dioxane ($\sim 40\text{ml}$) were added to a reaction flask and frozen three times, evacuated ($3.6 \cdot 10^{-1}\text{mbar}$) and flushed with argon. 6-Bromo-4'-(4-methoxyphenyl)-2,2'-bipyridine (139mg, 0.408mmol) and potassium carbonate was added to the yellow solution. The freeze-pump cycle was repeated three more times, and then the catalyst: $\text{Pd}(\text{Ph}_3\text{P})_4$ (20mg, $17\mu\text{mol}$) was added to the yellow suspension. The reaction mixture was stirred at 90°C for 1h, then refluxed at 110°C for 24h. A test on TLC showed that no change had occurred. The catalyst was washed with ethanol and ether, and the same amount as before was added additionally. After 48h, the colour had changed to brown and water ($\sim 40\text{ml}$) was added to quench the reaction. Three extractions with ethyl acetate were combined and washed with brine, dried over sodium sulfate and filtered. Solvent was removed *in vacuo* to give a brown oil. The proton-NMR showed traces of product, some 6-bromo-4'-(4-methoxyphenyl)-2,2'-bipyridine and also 6-bromo-2,2'-bipyridine. The MS showed among other signals one matching the product and also one matching 6-bromo-4'-(4-methoxyphenyl)-2,2'-bipyridine.

EI-MS, 70eV, 400°C : $m/z=$ 586, 521, 450, 415($\text{M} - \text{H}$)⁺, 385 ($\text{M} - \text{MeO}$)⁺, 325, 309 ($\text{M} - \text{MeOphenyl}$)⁺, 261 ($\text{M} - \text{Br} - \text{bipy}$)⁺.

EI-MS, 70eV, 250°C : $m/z=$ 340 (bromophenyl bipy)⁺, 277, 261 (bromo-phenyl bipy - Br)⁺

For full characterisation see page 169.

7.10 General Experimental

NMR Spectroscopy ^1H -, ^{13}C - and ^{15}N -NMR spectroscopy were recorded on Bruker 250, 400, 500 and 600 MHz Avance spectrometers at ambient temperature (295-298K).

Mass Spectroscopy

- Fast-atom bombardment (FAB) spectra were recorded on a Finnigan MAT 312
- Electron Impact (EI) mass spectra were recorded on a VG 70 SE
- Electrospray mass spectroscopy was recorded on a Finnigan MAT LCQ
- Matrix-assisted laser desorption and ionisation time-of-flight (Maldi TOF) were recorded using a PerSeptive Biosystems Voyager-RP Biospectrometry or PerSeptive Biosystems Voyager-DETM PRO Biospectrometry workstation

Infrared Spectrometers Infrared spectra were recorded on

- Shimadzu Fourier-Transformation 8400S spectrophotometer directly as the solids
- Mattson Genesis Fourier-transform spectrophotometer with samples in compressed KBr disks

UV-Vis Spectroscopy UV-Vis spectra were recorded on a Varian Carry 5000 UV-Vis-NIR photospectrometer and processed with Microsoft Excel 97.

Micro Analysis Micro analysis was carried out at the 'Mikrolabor' at the Chemistry Department of the University of Basel on a LECO CHN-900.

Electrochemical measurements The potentiostat/galvanostat 'Autolab' model 'PGSTAT 30' was used for differential pulse voltammetry and cyclic voltammetry. In both methods, the potential is varied linearly over time. The former method gives the potentials accurately, while the latter gives information about the reproducibility. The voltammograms were recorded in absolute acetonitrile, using a conventional three electrode configuration, comprising a glassy carbon disc as working electrode, a platinum wire as counter electrode and a silver wire as pseudo reference. Tetrabutylammonium hexafluorophosphate was used as electrolyte in 0.1M concentration, and ferrocene was added as an internal standard, after gaining a full set of voltammograms. All solutions were degassed with argon for at least 15 minutes before measurement, and during the scans an inert atmosphere was maintained. The voltammograms were processed with the software 'GPES Manager' and 'Excel'97'.

Crystallography The crystal and molecular structures were viewed with the help of several computer programs.^{128,129,171} Torsion angles of the pyridine ring planes were measured with three atoms per ring forming a plane. Every second atom in a ring was used, one time comparing the planes using the nitrogen atoms and two carbon atoms from each ring, and a second time, using only carbon atoms, then forming the average.

Appendix A

Crystal Structures of Helicates

A.1 $[\text{Cu}_2(\text{mp})_2][\text{PF}_6]_3$

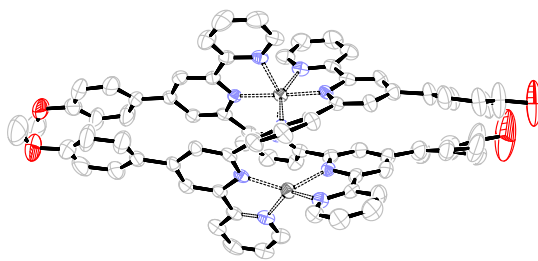


Figure A.1: Crystal structure of the complex cation in $[\text{Cu}_2(\text{mp})_2][\text{PF}_6]_3 \cdot 1.5$ acetone, ellipsoids enclose 50% probability. Hydrogen atoms, counterions and solvent molecules have been omitted for clarity.

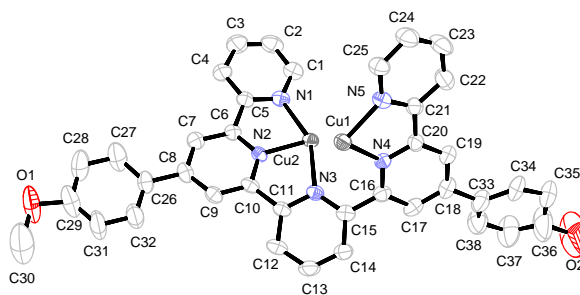


Figure A.2: Crystal structure of one of the ligand strands in $[\text{Cu}_2(\text{mp})_2][\text{PF}_6]_3 \cdot 1.5$ acetone, ellipsoids enclose 50% probability. Hydrogen atoms have been omitted for clarity.

$\text{C}_{76}\text{H}_{54}\text{N}_{10}\text{O}_7\text{Cu}_2\text{P}_3\text{F}_{18} \cdot 1.5\text{C}_3\text{H}_6\text{O}$, $M=1'820.43$, triclinic, cell volume= 3890.5\AA^3 , $T=173\text{K}$, space group $\text{P}\bar{1}$, $Z=2$, 85'712 reflections measured, 28'493 unique ($R_{int}=0.21$) from which 15'370 have been used in the refinement ($I > 3\sigma(I)$). The final R was 0.062.

Unit cell lengths (\AA)	$a=11.7086(11)$	$b=17.378(3)$	$c=19.3791(9)$
Unit cell angles (degree)	$\alpha=92.837(7)$	$\beta=92.355(6)$	$\gamma=98.490(12)$

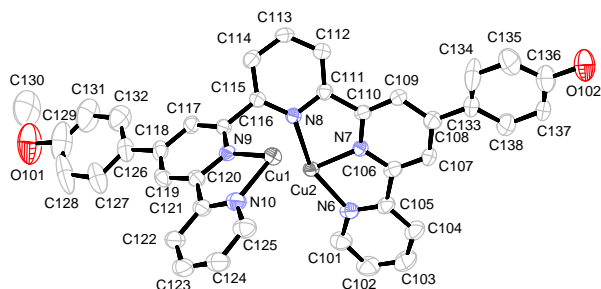


Figure A.3: Crystal structure of the other of the ligand strands in $[\text{Cu}_2(\text{mp})_2][\text{PF}_6]_3 \cdot 1.5$ acetone, ellipsoids enclose 50% probability. Hydrogen atoms have been omitted for clarity.

Table A.1: Bond distances for the non-hydrogen atoms of $[\text{Cu}_2(\text{mp})_2][\text{PF}_6]_3 \cdot 1.5$ acetone / (Å)

Atom A	Atom B	Distance	Atom A	Atom B	Distance	Atom A	Atom B	Distance
Cu1	N4	2.037(3)	Cu1	N5	1.986(3)	Cu1	N9	2.011(3)
Cu1	N10	2.011(3)	Cu2	N1	2.186(3)	Cu2	N2	1.963(3)
Cu2	N3	2.357(3)	Cu2	N6	2.104(3)	Cu2	N7	1.932(3)
Cu2	N8	2.243(3)	N1	C1	1.342(5)	N1	C5	1.340(5)
N2	C6	1.337(5)	N2	C10	1.339(5)	N3	C11	1.327(5)
N3	C15	1.345(5)	N4	C16	1.353(5)	N4	C20	1.326(5)
N5	C21	1.339(5)	N5	C25	1.324(5)	N6	C101	1.339(5)
N6	C105	1.337(5)	N7	C106	1.345(5)	N7	C110	1.340(5)
N8	C111	1.341(5)	N8	C115	1.342(5)	N9	C116	1.342(5)
N9	C120	1.355(5)	N10	C121	1.329(5)	N10	C125	1.338(5)
P1	F1	1.573(4)	P1	F2	1.529(4)	P1	F3	1.600(4)
P1	F4	1.524(4)	P1	F5	1.561(4)	P1	F6	1.571(5)
P1	F11	1.504(7)	P1	F12	1.596(6)	P1	F13	1.537(7)
P1	F14	1.577(7)	P1	F15	1.523(7)	P1	F16	1.606(6)
P2	F21	1.533(4)	P2	F22	1.558(4)	P2	F23	1.596(5)
P2	F24	1.515(6)	P2	F25	1.606(6)	P2	F26	1.522(6)
P2	F33	1.498(6)	P2	F34	1.614(6)	P2	F35	1.563(5)
P2	F36	1.570(6)	P3	F51	1.581(3)	P3	F52	1.561(3)
P3	F53	1.577(3)	P3	F54	1.540(3)	P3	F55	1.555(4)
P3	F56	1.570(4)	C1	C2	1.357(7)	C2	C3	1.338(8)
C3	C4	1.386(7)	C4	C5	1.379(6)	C5	C6	1.479(5)
C6	C7	1.392(5)	C7	C8	1.402(6)	C8	C9	1.384(6)
C8	C26	1.474(5)	C9	C10	1.365(5)	C10	C11	1.484(5)
C11	C12	1.383(5)	C12	C13	1.396(6)	C13	C14	1.345(6)
C14	C15	1.392(6)	C15	C16	1.473(6)	C16	C17	1.378(6)
C17	C18	1.389(6)	C18	C19	1.375(6)	C18	C33	1.483(6)
C19	C20	1.371(6)	C20	C21	1.478(6)	C21	C22	1.406(6)
C22	C23	1.369(7)	C23	C24	1.364(8)	C24	C25	1.373(6)
C26	C27	1.391(8)	C26	C32	1.366(7)	C27	C28	1.378(8)
C28	C29	1.426(9)	C29	O1	1.377(6)	C29	C31	1.306(8)
O1	C30	1.503(8)	C31	C32	1.361(7)	C33	C34	1.382(9)
C33	C38	1.392(8)	C33	C84	1.387(9)	C33	C88	1.395(8)
O50	C50	1.240(9)	O50	C500	1.247(8)	C101	C102	1.380(7)
C102	C103	1.376(8)	C103	C104	1.369(7)	C104	C105	1.384(6)
C105	C106	1.476(6)	C106	C107	1.374(6)	C107	C108	1.384(6)
C108	C109	1.397(6)	C108	C133	1.475(6)	C109	C110	1.368(5)

Table A.1: Bond distances for the non-hydrogen atoms of $[\text{Cu}_2(\text{mp})_2][\text{PF}_6]_3 \cdot 1.5 \text{ acetone}$ / (\AA)

Atom A	Atom B	Distance	Atom A	Atom B	Distance	Atom A	Atom B	Distance
C110	C111	1.482(5)	C111	C112	1.377(5)	C112	C113	1.380(6)
C113	C114	1.378(6)	C114	C115	1.380(5)	C115	C116	1.494(5)
C116	C117	1.371(5)	C117	C118	1.399(6)	C118	C119	1.405(6)
C118	C126	1.469(6)	C119	C120	1.376(6)	C120	C121	1.482(6)
C121	C122	1.377(5)	C122	C123	1.396(7)	C123	C124	1.338(7)
C124	C125	1.388(6)	C126	C127	1.384(7)	C126	C132	1.416(8)
C127	C128	1.401(9)	C128	C129	1.427(12)	C129	O101	1.357(7)
C129	C131	1.318(11)	O101	C130	1.531(9)	O101	C180	1.46(1)
C131	C132	1.390(8)	C133	C134	1.366(8)	C133	C138	1.404(8)
C133	C184	1.410(8)	C133	C188	1.392(7)	C34	C35	1.380(9)
C34	C84	0.638(15)	C34	C85	1.36(3)	C35	C36	1.367(9)
C35	C84	1.56(2)	C35	C85	0.38(3)	C36	O2	1.387(7)
C36	C37	1.403(9)	C36	C85	1.37(1)	C36	C87	1.418(9)
C37	C38	1.410(9)	C37	C87	1.294(19)	C38	C88	1.142(17)
C84	C85	1.380(9)	C87	C88	1.406(9)	C134	C135	1.370(9)
C134	C184	0.766(16)	C134	C185	1.623(17)	C135	C136	1.367(9)
C135	C184	1.540(19)	C135	C185	0.788(17)	C136	O102	1.387(6)
C136	C137	1.425(9)	C136	C185	1.393(8)	C136	C187	1.354(8)
C137	C138	1.406(9)	C137	C187	1.132(18)	C137	C188	1.625(16)
C138	C188	1.027(15)	C184	C185	1.388(9)	C187	C188	1.392(9)
F23	F33	1.07(1)	F23	F36	1.42(1)	F24	F34	1.22(1)
F24	F35	1.07(1)	F25	F33	1.23(1)	F25	F35	1.305(9)
F26	F34	1.32(1)	F26	F36	0.96(1)	C50	C51	1.49(1)
C50	C52	1.48(1)	C50	C500	0.531(12)	C50	C510	1.164(14)
C51	C510	1.02(2)	C52	C500	1.167(14)	C52	C510	1.67(2)
C52	C520	1.07(2)	C500	C510	1.49(1)	C500	C520	1.50(1)
F1	F11	1.196(12)	F1	F14	1.394(12)	F2	F12	1.296(11)
F2	F13	1.103(11)	F3	F13	1.310(12)	F3	F15	1.476(13)
F4	F14	1.100(11)	F4	F16	1.405(11)	F5	F12	1.505(11)
F5	F15	0.961(12)	F6	F11	1.280(11)	F6	F16	1.209(11)
C40	O40	1.298(8)	C40	C41	1.50(1)	C40	C42	1.49(1)

Table A.2: Bond angles for the non-hydrogen atoms of $[\text{Cu}_2(\text{mp})_2][\text{PF}_6]_3 \cdot 1.5 \text{ acetone}$ / (degrees)

Atom A	Atom B	Atom C	Angle	Atom A	Atom B	Atom C	Angle
N4	Cu1	N5	81.37(13)	N4	Cu1	N9	133.91(12)
N5	Cu1	N9	123.64(13)	N4	Cu1	N10	109.84(13)
N5	Cu1	N10	134.66(14)	N9	Cu1	N10	80.74(13)
N1	Cu2	N2	77.94(12)	N1	Cu2	N3	153.52(12)
N2	Cu2	N3	75.65(12)	N1	Cu2	N6	104.42(12)
N2	Cu2	N6	101.95(13)	N3	Cu2	N6	83.04(11)
N1	Cu2	N7	98.69(12)	N2	Cu2	N7	176.63(13)
N3	Cu2	N7	107.72(12)	N6	Cu2	N7	78.66(13)
N1	Cu2	N8	83.58(11)	N2	Cu2	N8	102.70(11)
N3	Cu2	N8	100.3(1)	N6	Cu2	N8	155.18(12)
N7	Cu2	N8	76.89(11)	Cu2	N1	C1	129.4(3)
Cu2	N1	C5	111.6(2)	C1	N1	C5	117.9(4)
Cu2	N2	C6	119.1(2)	Cu2	N2	C10	121.5(3)
C6	N2	C10	119.3(3)	Cu2	N3	C11	107.8(2)

Table A.2: Bond angles for the non-hydrogen atoms of
 $[\text{Cu}_2(\text{mp})_2][\text{PF}_6]_3 \cdot 1.5 \text{ acetone}$ / (degrees)

Atom A	Atom B	Atom C	Angle	Atom A	Atom B	Atom C	Angle
Cu2	N3	C15	129.2(2)	C11	N3	C15	118.5(3)
Cu1	N4	C16	127.4(3)	Cu1	N4	C20	113.0(3)
C16	N4	C20	117.7(3)	Cu1	N5	C21	113.5(3)
Cu1	N5	C25	128.5(3)	C21	N5	C25	118.0(4)
Cu2	N6	C101	127.8(3)	Cu2	N6	C105	113.3(3)
C101	N6	C105	118.9(4)	Cu2	N7	C106	119.8(3)
Cu2	N7	C110	121.0(2)	C106	N7	C110	119.2(3)
Cu2	N8	C111	108.3(2)	Cu2	N8	C115	128.0(2)
C111	N8	C115	117.8(3)	Cu1	N9	C116	128.1(2)
Cu1	N9	C120	114.4(3)	C116	N9	C120	117.2(3)
Cu1	N10	C121	115.3(3)	Cu1	N10	C125	125.8(3)
C121	N10	C125	118.8(4)	F1	P1	F2	175.3(4)
F1	P1	F3	87.8(3)	F2	P1	F3	87.7(3)
F1	P1	F4	89.4(3)	F2	P1	F4	95.2(3)
F3	P1	F4	177.1(3)	F1	P1	F5	90.2(3)
F2	P1	F5	91.0(3)	F3	P1	F5	87.6(3)
F4	P1	F5	93.0(3)	F1	P1	F6	87.3(3)
F2	P1	F6	91.2(3)	F3	P1	F6	88.0(3)
F4	P1	F6	91.2(3)	F5	P1	F6	175.1(3)
F1	P1	F11	45.7(5)	F2	P1	F11	130.8(5)
F3	P1	F11	66.5(5)	F4	P1	F11	111.0(5)
F5	P1	F11	126.6(5)	F1	P1	F12	134.9(5)
F2	P1	F12	48.9(4)	F3	P1	F12	117.2(4)
F4	P1	F12	65.4(4)	F5	P1	F12	56.9(4)
F1	P1	F13	133.1(5)	F2	P1	F13	42.2(4)
F3	P1	F13	49.3(5)	F4	P1	F13	133.1(5)
F5	P1	F13	103.7(5)	F1	P1	F14	52.5(5)
F2	P1	F14	132.2(5)	F3	P1	F14	136.1(5)
F4	P1	F14	41.5(4)	F5	P1	F14	76.1(4)
F1	P1	F15	72.6(5)	F2	P1	F15	105.8(5)
F3	P1	F15	56.4(5)	F4	P1	F15	123.2(5)
F5	P1	F15	36.3(5)	F1	P1	F16	107.7(4)
F2	P1	F16	74.1(4)	F3	P1	F16	127.2(5)
F4	P1	F16	53.3(4)	F5	P1	F16	140.2(5)
F6	P1	F11	49.1(5)	F6	P1	F12	127.4(5)
F11	P1	F12	175.6(5)	F6	P1	F13	75.1(5)
F11	P1	F13	93.5(5)	F12	P1	F13	87.7(4)
F6	P1	F14	105.6(5)	F11	P1	F14	91.1(5)
F12	P1	F14	87.4(5)	F13	P1	F14	174.2(6)
F6	P1	F15	138.8(5)	F11	P1	F15	93.9(5)
F12	P1	F15	90.2(5)	F13	P1	F15	92.6(5)
F14	P1	F15	90.5(5)	F6	P1	F16	44.7(4)
F11	P1	F16	88.8(4)	F12	P1	F16	87.0(4)
F13	P1	F16	89.7(5)	F14	P1	F16	87.0(4)
F15	P1	F16	176.3(6)	F21	P2	F22	179.6(3)
F21	P2	F23	92.3(3)	F22	P2	F23	87.6(3)
F21	P2	F24	89.0(3)	F22	P2	F24	91.1(3)
F23	P2	F24	175.0(5)	F21	P2	F25	93.5(3)
F22	P2	F25	86.2(3)	F23	P2	F25	86.1(4)
F24	P2	F25	89.0(4)	F21	P2	F26	89.9(3)
F22	P2	F26	90.4(3)	F23	P2	F26	89.5(4)

Table A.2: Bond angles for the non-hydrogen atoms of
 $[\text{Cu}_2(\text{mp})_2][\text{PF}_6]_3 \cdot 1.5 \text{ acetone} / (\text{degrees})$

Atom A	Atom B	Atom C	Angle	Atom A	Atom B	Atom C	Angle
F24	P2	F26	95.3(4)	F25	P2	F26	174.6(4)
F21	P2	F33	87.4(4)	F22	P2	F33	92.2(4)
F23	P2	F33	40.3(4)	F24	P2	F33	135.1(5)
F25	P2	F33	46.6(4)	F21	P2	F34	92.8(3)
F22	P2	F34	87.6(3)	F23	P2	F34	138.9(4)
F24	P2	F34	45.8(4)	F25	P2	F34	134.2(4)
F21	P2	F35	88.9(3)	F22	P2	F35	91.0(3)
F23	P2	F35	134.6(4)	F24	P2	F35	40.6(4)
F25	P2	F35	48.6(4)	F21	P2	F36	90.2(3)
F22	P2	F36	89.9(3)	F23	P2	F36	53.4(4)
F24	P2	F36	131.4(5)	F25	P2	F36	139.5(5)
F26	P2	F33	129.5(5)	F26	P2	F34	49.7(4)
F33	P2	F34	179.1(5)	F26	P2	F35	135.8(4)
F33	P2	F35	94.6(4)	F34	P2	F35	86.2(4)
F26	P2	F36	36.2(4)	F33	P2	F36	93.4(4)
F34	P2	F36	85.8(4)	F35	P2	F36	171.9(5)
F51	P3	F52	179.5(2)	F51	P3	F53	89.3(2)
F52	P3	F53	90.26(19)	F51	P3	F54	88.9(2)
F52	P3	F54	91.6(2)	F53	P3	F54	177.6(3)
F51	P3	F55	87.4(2)	F52	P3	F55	92.8(2)
F53	P3	F55	89.1(3)	F54	P3	F55	92.3(3)
F51	P3	F56	89.8(2)	F52	P3	F56	90.0(2)
F53	P3	F56	88.2(2)	F54	P3	F56	90.2(3)
F55	P3	F56	176.1(3)	N1	C1	C2	122.4(4)
C1	C2	C3	120.1(4)	C2	C3	C4	119.5(4)
C3	C4	C5	118.1(4)	N1	C5	C4	122.1(4)
N1	C5	C6	114.5(3)	C4	C5	C6	123.4(4)
N2	C6	C5	115.5(3)	N2	C6	C7	121.6(3)
C5	C6	C7	122.9(4)	C6	C7	C8	119.6(4)
C7	C8	C9	116.5(4)	C7	C8	C26	121.6(4)
C9	C8	C26	121.9(4)	C8	C9	C10	121.3(4)
N2	C10	C9	121.6(4)	N2	C10	C11	116.1(3)
C9	C10	C11	122.3(3)	N3	C11	C10	115.5(3)
N3	C11	C12	122.9(4)	C10	C11	C12	121.6(3)
C11	C12	C13	117.6(4)	C12	C13	C14	120.2(4)
C13	C14	C15	118.9(4)	N3	C15	C14	121.9(4)
N3	C15	C16	117.9(3)	C14	C15	C16	120.2(4)
N4	C16	C15	115.2(3)	N4	C16	C17	121.9(4)
C15	C16	C17	122.9(4)	C16	C17	C18	120.2(4)
C17	C18	C19	116.6(4)	C17	C18	C33	122.4(4)
C19	C18	C33	121.0(4)	C18	C19	C20	120.7(4)
N4	C20	C19	122.9(4)	N4	C20	C21	114.1(3)
C19	C20	C21	123.0(4)	N5	C21	C20	116.4(3)
N5	C21	C22	120.5(4)	C20	C21	C22	123.1(4)
C21	C22	C23	119.5(5)	C22	C23	C24	119.7(4)
C23	C24	C25	117.5(4)	N5	C25	C24	124.8(4)
C8	C26	C27	121.5(4)	C8	C26	C32	121.5(4)
C27	C26	C32	116.8(4)	C26	C27	C28	120.7(6)
C27	C28	C29	119.1(6)	C28	C29	O1	110.5(5)
C28	C29	C31	119.2(5)	O1	C29	C31	130.1(5)
C29	O1	C30	109.2(1)	C29	C31	C32	121.3(6)

Table A.2: Bond angles for the non-hydrogen atoms of
 $[\text{Cu}_2(\text{mp})_2][\text{PF}_6]_3 \cdot 1.5 \text{ acetone} / (\text{degrees})$

Atom A	Atom B	Atom C	Angle	Atom A	Atom B	Atom C	Angle
C26	C32	C31	122.9(5)	C18	C33	C34	124.3(7)
C18	C33	C38	121.5(6)	C34	C33	C38	113.0(8)
C18	C33	C84	118.4(7)	C34	C33	C84	26.7(7)
C38	C33	C84	106.7(8)	C18	C33	C88	118.2(6)
C34	C33	C88	105.8(8)	C38	C33	C88	48.4(8)
C84	C33	C88	122.3(8)	C50	O50	C500	24.6(5)
N6	C101	C102	121.8(5)	C101	C102	C103	118.9(4)
C102	C103	C104	119.7(4)	C103	C104	C105	118.5(5)
N6	C105	C104	122.2(4)	N6	C105	C106	114.7(3)
C104	C105	C106	123.1(4)	N7	C106	C105	113.1(3)
N7	C106	C107	121.2(4)	C105	C106	C107	125.7(4)
C106	C107	C108	120.3(4)	C107	C108	C109	117.3(4)
C107	C108	C133	121.9(4)	C109	C108	C133	120.8(4)
C108	C109	C110	119.8(4)	N7	C110	C109	121.8(3)
N7	C110	C111	114.0(3)	C109	C110	C111	124.2(3)
N8	C111	C110	114.0(3)	N8	C111	C112	123.3(3)
C110	C111	C112	122.7(3)	C111	C112	C113	117.7(4)
C112	C113	C114	120.1(4)	C113	C114	C115	118.2(4)
N8	C115	C114	122.6(3)	N8	C115	C116	116.6(3)
C114	C115	C116	120.6(3)	N9	C116	C115	113.2(3)
N9	C116	C117	124.4(3)	C115	C116	C117	122.4(3)
C116	C117	C118	119.1(4)	C117	C118	C119	116.6(4)
C117	C118	C126	122.6(4)	C119	C118	C126	120.8(4)
C118	C119	C120	120.8(3)	N9	C120	C119	121.9(4)
N9	C120	C121	114.5(3)	C119	C120	C121	123.6(3)
N10	C121	C120	114.8(3)	N10	C121	C122	122.3(4)
C120	C121	C122	122.9(4)	C121	C122	C123	118.2(4)
C122	C123	C124	119.7(4)	C123	C124	C125	119.3(4)
N10	C125	C124	121.8(4)	C118	C126	C127	122.5(5)
C118	C126	C132	120.4(4)	C127	C126	C132	117.0(5)
C126	C127	C128	119.5(7)	C127	C128	C129	121.2(6)
C128	C129	O101	111.9(6)	C128	C129	C131	119.2(6)
O101	C129	C131	128.9(6)	C129	O101	C130	109.1(1)
C129	O101	C180	109.04(11)	C130	O101	C180	140.4(5)
C129	C131	C132	120.4(8)	C126	C132	C131	122.7(6)
C108	C133	C134	120.4(5)	C108	C133	C138	118.1(5)
C134	C133	C138	121.5(7)	C108	C133	C184	123.1(6)
C134	C133	C184	32.0(7)	C138	C133	C184	108.9(7)
C108	C133	C188	123.2(5)	C134	C133	C188	101.0(8)
C138	C133	C188	43.1(6)	C184	C133	C188	112.7(7)
C33	C34	C35	129.6(12)	C33	C34	C84	77.1(12)
C35	C34	C84	93.6(21)	C33	C34	C85	120.4(12)
C35	C34	C85	16.1(14)	C84	C34	C85	78.1(22)
C34	C35	C36	109.7(11)	C34	C35	C84	24.2(7)
C36	C35	C84	109.6(9)	C34	C35	C85	79.4(41)
C36	C35	C85	82.7(23)	C84	C35	C85	56.3(35)
C35	C36	O2	114.2(8)	C35	C36	C37	121.0(9)
O2	C36	C37	118.3(8)	C35	C36	C85	16.1(14)
O2	C36	C85	118.9(9)	C37	C36	C85	108.3(11)
C35	C36	C87	114.1(11)	O2	C36	C87	122.0(9)
C37	C36	C87	54.6(9)	C85	C36	C87	116.6(11)

Table A.2: Bond angles for the non-hydrogen atoms of
 $[\text{Cu}_2(\text{mp})_2][\text{PF}_6]_3 \cdot 1.5 \text{ acetone}$ / (degrees)

Atom A	Atom B	Atom C	Angle	Atom A	Atom B	Atom C	Angle
C36	C37	C38	116.2(9)	C36	C37	C87	63.3(7)
C38	C37	C87	83.1(11)	C33	C38	C37	121.1(9)
C33	C38	C88	65.9(7)	C37	C38	C88	97.2(12)
C33	C84	C34	76.3(12)	C33	C84	C35	116.2(9)
C34	C84	C35	62.2(16)	C33	C84	C85	118.8(12)
C34	C84	C85	75.0(23)	C35	C84	C85	13.4(15)
C34	C85	C35	84.5(46)	C34	C85	C36	110.5(14)
C35	C85	C36	81.2(22)	C34	C85	C84	26.9(7)
C35	C85	C84	110.3(46)	C36	C85	C84	120.7(13)
C36	C87	C37	62.1(6)	C36	C87	C88	121.3(10)
C37	C87	C88	90.7(10)	C33	C88	C38	65.7(6)
C33	C88	C87	115.9(10)	C38	C88	C87	89.0(11)
C133	C134	C135	121.7(9)	C133	C134	C184	77.2(9)
C135	C134	C184	87.5(16)	C133	C134	C185	112.3(8)
C135	C134	C185	29.0(8)	C184	C134	C185	58.6(12)
C134	C135	C136	120.3(10)	C134	C135	C184	29.8(7)
C136	C135	C184	106.7(9)	C134	C135	C185	93.5(16)
C136	C135	C185	75.3(10)	C184	C135	C185	63.9(13)
C135	C136	O102	121.4(7)	C135	C136	C137	118.2(7)
O102	C136	C137	120.4(6)	C135	C136	C185	33.2(7)
O102	C136	C185	117.4(6)	C137	C136	C185	111.4(8)
C135	C136	C187	102.2(9)	O102	C136	C187	116.6(6)
C137	C136	C187	48.0(8)	C185	C136	C187	123.7(7)
C136	C137	C138	122.4(8)	C136	C137	C187	62.7(7)
C138	C137	C187	96.1(11)	C136	C137	C188	98.6(8)
C138	C137	C188	38.8(7)	C187	C137	C188	57.4(8)
C133	C138	C137	115.8(8)	C133	C138	C188	67.8(6)
C137	C138	C188	82.2(11)	C133	C184	C134	70.9(10)
C133	C184	C135	108.1(10)	C134	C184	C135	62.7(13)
C133	C184	C185	125.4(10)	C134	C184	C185	93.3(16)
C135	C184	C185	30.7(7)	C134	C185	C135	57.5(11)
C134	C185	C136	103.6(8)	C135	C185	C136	71.6(9)
C134	C185	C184	28.1(7)	C135	C185	C184	85.4(15)
C136	C185	C184	114.2(9)	C136	C187	C137	69.3(7)
C136	C187	C188	115.0(8)	C137	C187	C188	79.4(10)
C133	C188	C137	103.9(8)	C133	C188	C138	69.1(7)
C137	C188	C138	59.0(8)	C133	C188	C187	125.4(8)
C137	C188	C187	43.2(7)	C138	C188	C187	102.2(11)
P2	F23	F33	64.9(4)	P2	F23	F36	62.4(3)
F33	F23	F36	126.7(6)	P2	F24	F34	71.4(4)
P2	F24	F35	72.1(5)	F34	F24	F35	143.3(7)
P2	F25	F33	62.1(4)	P2	F25	F35	64.0(4)
F33	F25	F35	125.0(6)	P2	F26	F34	68.8(4)
P2	F26	F36	74.6(5)	F34	F26	F36	143.1(7)
P2	F33	F23	74.8(5)	P2	F33	F25	71.3(4)
F23	F33	F25	143.4(7)	P2	F34	F24	62.9(4)
P2	F34	F26	61.5(3)	F24	F34	F26	124.0(6)
P2	F35	F24	67.3(4)	P2	F35	F25	67.4(4)
F24	F35	F25	134.4(6)	P2	F36	F23	64.2(3)
P2	F36	F26	69.2(5)	F23	F36	F26	133.4(7)
O50	C50	C51	119.9(1)	O50	C50	C52	119.9(1)

Table A.2: Bond angles for the non-hydrogen atoms of
 $[\text{Cu}_2(\text{mp})_2][\text{PF}_6]_3 \cdot 1.5$ acetone / (degrees)

Atom A	Atom B	Atom C	Angle	Atom A	Atom B	Atom C	Angle
C51	C50	C52	119.9(1)	O50	C50	C500	78.5(13)
C51	C50	C500	158.9(18)	C52	C50	C500	44.9(14)
O50	C50	C510	162.6(11)	C51	C50	C510	42.8(10)
C52	C50	C510	77.3(10)	C500	C50	C510	118.8(17)
C50	C51	C510	51.0(9)	C50	C52	C500	18.7(7)
C50	C52	C510	42.8(5)	C500	C52	C510	60.5(9)
C50	C52	C520	102.7(10)	C500	C52	C520	84.0(13)
C510	C52	C520	141.0(17)	O50	C500	C50	76.9(13)
O50	C500	C52	155.1(15)	C50	C500	C52	116.3(20)
O50	C500	C510	119.9(1)	C50	C500	C510	43.0(13)
C52	C500	C510	76.6(11)	O50	C500	C520	119.9(1)
C50	C500	C520	161.6(15)	C52	C500	C520	45.2(11)
C510	C500	C520	119.9(1)	C50	C510	C51	86.2(12)
C50	C510	C52	59.9(9)	C51	C510	C52	145.9(13)
C50	C510	C500	18.1(6)	C51	C510	C500	103.8(9)
C52	C510	C500	42.9(6)	C52	C520	C500	50.8(8)
P1	F1	F11	64.1(4)	P1	F1	F14	63.9(3)
F11	F1	F14	116.1(7)	P1	F2	F12	68.2(4)
P1	F2	F13	69.3(5)	F12	F2	F13	129.5(8)
P1	F3	F13	62.9(3)	P1	F3	F15	59.2(3)
F13	F3	F15	105.0(6)	P1	F4	F14	71.8(5)
P1	F4	F16	66.3(4)	F14	F4	F16	121.4(8)
P1	F5	F12	62.7(3)	P1	F5	F15	69.7(5)
F12	F5	F15	125.8(8)	P1	F6	F11	62.7(4)
P1	F6	F16	69.1(4)	F11	F6	F16	121.9(8)
P1	F11	F1	70.2(4)	P1	F11	F6	68.2(4)
F1	F11	F6	122.5(8)	P1	F12	F2	62.8(3)
P1	F12	F5	60.4(3)	F2	F12	F5	103.5(6)
P1	F13	F2	68.5(4)	P1	F13	F3	67.8(4)
F2	F13	F3	127.7(8)	P1	F14	F1	63.6(4)
P1	F14	F4	66.7(4)	F1	F14	F4	121.3(7)
P1	F15	F3	64.4(4)	P1	F15	F5	74.0(5)
F3	F15	F5	126.5(9)	P1	F16	F4	60.4(3)
P1	F16	F6	66.1(4)	F4	F16	F6	115.4(6)
O40	C40	C41	119.9(1)	O40	C40	C42	119.9(1)
C41	C40	C42	119.8(1)	C51	H511	C510	63.661
C52	H522	C520	83.189	C51	H5102	C510	70.261
C51	H5103	C510	58.395	C52	H5201	C520	63.345
C34	H341	C84	30.094	C35	H351	C85	19.174
C35	H851	C85	23.069				

Table A.3: Atomic coordinates of the non-hydrogen atoms of
 $[\text{Cu}_2(\text{mp})_2][\text{PF}_6]_3 \cdot 1.5$ acetone

Atom	x/a	y/b	z/c	U(equiv)	occupancy
CU1	-0.00650(4)	0.34185(3)	0.86981(3)	0.0376	1
CU2	0.07523(4)	0.42279(3)	0.68885(2)	0.0315	1
N1	0.2347(3)	0.49342(19)	0.66010(16)	0.0372	1
N2	0.0452(3)	0.52901(17)	0.71188(15)	0.0308	1

Table A.3: Atomic coordinates of the non-hydrogen atoms of
 $[\text{Cu}_2(\text{mp})_2][\text{PF}_6]_3 \cdot 1.5$ acetone

Atom	x/a	y/b	z/c	U(equiv)	occupancy
N3	-0.1087(3)	0.40519(18)	0.73578(15)	0.0332	1
N4	-0.0555(3)	0.26359(17)	0.78840(16)	0.0338	1
N5	0.0969(3)	0.2645(2)	0.89160(17)	0.0401	1
N6	-0.0216(3)	0.3949(2)	0.59472(17)	0.0399	1
N7	0.1135(3)	0.32086(18)	0.66418(15)	0.0317	1
N8	0.1851(2)	0.39834(17)	0.78040(15)	0.0296	1
N9	0.0440(3)	0.45779(18)	0.87838(15)	0.0325	1
N10	-0.1471(3)	0.3745(2)	0.91212(17)	0.0412	1
P1	-0.23943(12)	0.64901(9)	0.56793(7)	0.0658	1
P2	-0.53040(14)	0.87754(12)	1.1837(1)	0.0855	1
P3	-0.41145(11)	0.64693(8)	0.87648(7)	0.0568	1
C1	0.3307(4)	0.4707(3)	0.6356(2)	0.046	1
C2	0.4317(4)	0.5201(3)	0.6342(3)	0.0592	1
C3	0.4383(4)	0.5942(3)	0.6581(3)	0.0692	1
C4	0.3405(4)	0.6206(3)	0.6824(3)	0.0552	1
C5	0.2398(3)	0.5682(2)	0.6822(2)	0.0372	1
C6	0.1297(3)	0.5889(2)	0.70670(19)	0.0353	1
C7	0.1137(4)	0.6653(2)	0.7231(2)	0.04	1
C8	0.0076(4)	0.6802(2)	0.7475(2)	0.0401	1
C9	-0.0765(3)	0.6162(2)	0.7530(2)	0.0378	1
C10	-0.0571(3)	0.5427(2)	0.73416(18)	0.0344	1
C11	-0.1470(3)	0.4734(2)	0.73743(18)	0.0336	1
C12	-0.2630(3)	0.4803(3)	0.7398(2)	0.0459	1
C13	-0.3420(3)	0.4116(3)	0.7390(3)	0.0527	1
C14	-0.3045(3)	0.3421(3)	0.7380(2)	0.0468	1
C15	-0.1862(3)	0.3399(2)	0.7369(2)	0.0377	1
C16	-0.1419(3)	0.2650(2)	0.7401(2)	0.0391	1
C17	-0.1856(4)	0.2004(3)	0.6978(2)	0.0459	1
C18	-0.1415(4)	0.1310(3)	0.7040(2)	0.0497	1
C19	-0.0539(4)	0.1312(2)	0.7536(2)	0.0456	1
C20	-0.0145(3)	0.1970(2)	0.7947(2)	0.0392	1
C21	0.0785(3)	0.2003(2)	0.8491(2)	0.0393	1
C22	0.1464(4)	0.1407(3)	0.8568(3)	0.0584	1
C23	0.2325(5)	0.1489(3)	0.9077(3)	0.0671	1
C24	0.2516(4)	0.2148(3)	0.9503(3)	0.0606	1
C25	0.1805(4)	0.2699(3)	0.9405(2)	0.0477	1
C26	-0.0120(4)	0.7599(2)	0.7680(2)	0.0476	1
C27	0.0786(6)	0.8217(3)	0.7755(3)	0.0782	1
C28	0.0597(7)	0.8947(3)	0.7990(4)	0.0874	1
C29	-0.0544(6)	0.9061(3)	0.8156(3)	0.0794	1
O1	-0.0551(4)	0.98159(19)	0.8407(2)	0.1033	1
C30	-0.1762(8)	0.9916(4)	0.8579(6)	0.144	1
C31	-0.1379(6)	0.8471(3)	0.8089(4)	0.0859	1
C32	-0.1187(5)	0.7754(3)	0.7849(3)	0.074	1
C33	-0.1863(4)	0.0596(3)	0.6604(3)	0.0615	1
O50	0.5470(5)	0.6903(5)	0.3625(3)	0.153	1
C101	-0.0854(4)	0.4398(3)	0.5603(2)	0.0518	1
C102	-0.1488(5)	0.4129(3)	0.5001(3)	0.0625	1
C103	-0.1454(5)	0.3379(3)	0.4746(3)	0.0653	1
C104	-0.0811(4)	0.2914(3)	0.5097(2)	0.0515	1
C105	-0.0181(3)	0.3224(3)	0.5692(2)	0.04	1

Table A.3: Atomic coordinates of the non-hydrogen atoms of
 $[\text{Cu}_2(\text{mp})_2][\text{PF}_6]_3 \cdot 1.5$ acetone

Atom	x/a	y/b	z/c	U(equiv)	occupancy
C106	0.0593(3)	0.2791(2)	0.60883(19)	0.0369	1
C107	0.0784(4)	0.2043(3)	0.5928(2)	0.043	1
C108	0.1556(3)	0.1706(2)	0.6331(2)	0.0433	1
C109	0.2172(3)	0.2171(2)	0.6870(2)	0.038	1
C110	0.1926(3)	0.2906(2)	0.70184(18)	0.0318	1
C111	0.2468(3)	0.3426(2)	0.76086(18)	0.0316	1
C112	0.3520(3)	0.3347(2)	0.7919(2)	0.0409	1
C113	0.3978(3)	0.3895(3)	0.8435(2)	0.0475	1
C114	0.3352(4)	0.4466(3)	0.8654(2)	0.0458	1
C115	0.2272(3)	0.4471(2)	0.83432(19)	0.0329	1
C116	0.1467(3)	0.4977(2)	0.86413(18)	0.0339	1
C117	0.1782(3)	0.5763(2)	0.8776(2)	0.0373	1
C118	0.0994(4)	0.6195(2)	0.90763(19)	0.0409	1
C119	-0.0076(4)	0.5777(2)	0.9234(2)	0.0407	1
C120	-0.0324(3)	0.4985(2)	0.90874(18)	0.0347	1
C121	-0.1432(3)	0.4509(2)	0.92406(19)	0.0385	1
C122	-0.2361(4)	0.4829(3)	0.9477(2)	0.0474	1
C123	-0.3368(4)	0.4327(3)	0.9599(2)	0.0555	1
C124	-0.3408(4)	0.3558(3)	0.9483(2)	0.052	1
C125	-0.2446(4)	0.3273(3)	0.9236(2)	0.0486	1
C126	0.1266(5)	0.7037(3)	0.9243(2)	0.0523	1
C127	0.0439(6)	0.7482(3)	0.9448(3)	0.0754	1
C128	0.077(1)	0.8274(4)	0.9640(3)	0.1113	1
C129	0.1945(8)	0.8634(4)	0.9615(4)	0.1088	1
O101	0.2082(6)	0.9403(2)	0.9815(3)	0.1285	1
C131	0.2732(8)	0.8209(3)	0.9421(4)	0.1023	1
C132	0.2418(6)	0.7422(3)	0.9232(3)	0.0745	1
C133	0.1729(4)	0.0888(2)	0.6203(2)	0.0554	1
F51	-0.2775(2)	0.6515(2)	0.8941(2)	0.0941	1
F52	-0.5437(2)	0.6417(2)	0.8586(2)	0.1061	1
F53	-0.4174(3)	0.5580(2)	0.8536(2)	0.1103	1
F54	-0.4008(4)	0.7344(2)	0.8974(3)	0.1416	1
F55	-0.4312(4)	0.6237(3)	0.95203(19)	0.1266	1
F56	-0.3853(4)	0.6666(3)	0.79998(17)	0.1238	1
C34	-0.1649(11)	-0.0143(5)	0.6746(7)	0.0674	0.5
C35	-0.1870(11)	-0.0828(7)	0.6339(6)	0.0695	0.5
C36	-0.2661(9)	-0.0756(4)	0.5816(5)	0.144	1
O2	-0.3033(11)	-0.1440(4)	0.5419(6)	0.2682	1
C37	-0.2673(16)	-0.0044(5)	0.5506(6)	0.0993	0.5
C38	-0.2333(12)	0.0635(6)	0.5937(5)	0.0762	0.5
C84	-0.1210(11)	-0.0008(6)	0.6581(8)	0.0685	0.5
C85	-0.1665(16)	-0.0701(9)	0.6225(11)	0.1118	0.5
C87	-0.341(1)	-0.0209(7)	0.5974(9)	0.1056	0.5
C88	-0.3006(8)	0.0503(7)	0.6343(8)	0.0856	0.5
C134	0.2239(14)	0.0509(6)	0.6704(5)	0.0734	0.5
C135	0.2352(14)	-0.0263(6)	0.6614(6)	0.0808	0.5
C136	0.2013(6)	-0.0666(3)	0.5998(4)	0.1071	1
O102	0.2144(6)	-0.1442(3)	0.5890(4)	0.1619	1
C137	0.1527(12)	-0.0264(6)	0.5463(6)	0.0989	0.5
C138	0.1363(12)	0.0520(6)	0.5553(5)	0.0712	0.5
C184	0.272(1)	0.0593(6)	0.6449(7)	0.072	0.5

Table A.3: Atomic coordinates of the non-hydrogen atoms of
 $[\text{Cu}_2(\text{mp})_2][\text{PF}_6]_3 \cdot 1.5$ acetone

Atom	x/a	y/b	z/c	U(equiv)	occupancy
C185	0.289(1)	-0.0180(6)	0.6383(8)	0.0751	0.5
C187	0.0937(8)	-0.0488(6)	0.5880(8)	0.0846	0.5
C188	0.0855(8)	0.0303(5)	0.5939(6)	0.0617	0.5
F21	-0.4027(3)	0.9132(4)	1.1942(2)	0.1728	1
F22	-0.6600(3)	0.8407(3)	1.1731(2)	0.1332	1
F23	-0.5263(7)	0.8314(4)	1.2528(3)	0.1159	0.5
F24	-0.5343(8)	0.9146(6)	1.1147(4)	0.1377	0.5
F25	-0.5022(6)	0.7995(4)	1.1444(4)	0.1186	0.5
F26	-0.5641(7)	0.9465(4)	1.2254(5)	0.1213	0.5
F33	-0.4965(7)	0.8032(4)	1.2081(6)	0.1543	0.5
F34	-0.5677(7)	0.9578(4)	1.1585(5)	0.1193	0.5
F35	-0.5095(6)	0.8584(5)	1.1060(3)	0.1023	0.5
F36	-0.5536(7)	0.9085(6)	1.2586(3)	0.1292	0.5
C50	0.502(1)	0.7325(7)	0.4033(6)	0.1548	0.5
C51	0.5281(17)	0.8191(8)	0.4012(11)	0.1647	0.5
C52	0.4116(16)	0.6972(13)	0.448(1)	0.1643	0.5
C500	0.491(1)	0.7049(6)	0.4138(6)	0.1332	0.5
C510	0.4735(16)	0.7867(9)	0.4317(9)	0.1437	0.5
C520	0.4313(13)	0.639(1)	0.4526(8)	0.1341	0.5
F1	-0.2589(5)	0.6693(4)	0.6461(2)	0.1091	0.7051
F2	-0.2126(5)	0.6255(4)	0.4940(2)	0.1179	0.7051
F3	-0.1179(3)	0.6252(3)	0.5924(2)	0.0834	0.7051
F4	-0.3569(4)	0.6718(4)	0.5485(3)	0.1231	0.7051
F5	-0.1747(4)	0.7333(2)	0.5610(3)	0.0978	0.7051
F6	-0.2965(5)	0.5634(3)	0.5799(4)	0.127	0.7051
F11	-0.245(1)	0.6037(7)	0.6322(5)	0.1111	0.2949
F12	-0.2437(9)	0.6941(7)	0.4983(5)	0.1006	0.2949
F13	-0.1623(9)	0.5968(6)	0.5316(6)	0.1032	0.2949
F14	-0.3247(9)	0.7031(6)	0.5978(6)	0.1024	0.2949
F15	-0.1361(8)	0.7076(7)	0.5957(6)	0.1172	0.2949
F16	-0.3521(7)	0.5919(6)	0.5367(5)	0.0895	0.2949
C130	0.337(1)	0.9741(5)	0.9815(7)	0.1325	0.7153
C180	0.0945(11)	0.9657(7)	0.9828(18)	0.1435	0.2847
C40	0.5472(7)	0.1683(6)	0.2695(6)	0.139	0.5
O40	0.6485(6)	0.1873(3)	0.3007(6)	0.1059	0.5
C41	0.442(1)	0.191(1)	0.303(1)	0.1576	0.5
C42	0.5370(13)	0.1329(9)	0.1975(8)	0.1568	0.5

A.2 [Cu₂pcp][PF₆]₃

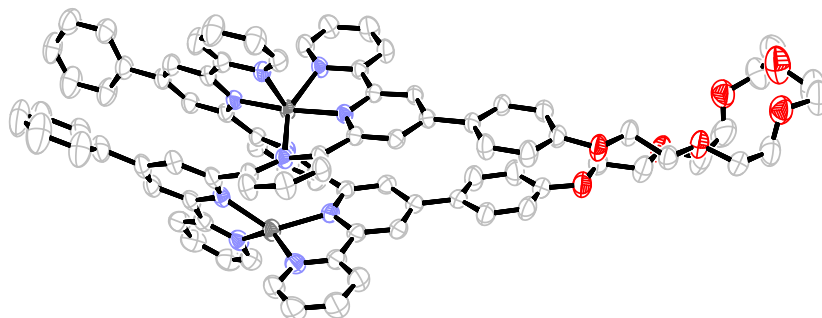


Figure A.4: Crystal structure of the complex cation of [Cu₂pcp][PF₆]₃ · 2.5 acetone, ellipsoids enclose 50% probability. Hydrogen atoms, counterions and solvent molecules have been omitted for clarity.

C₈₆H₇₂N₁₀O₇Cu₂P₃F₁₈ · 2.5 C₃H₆O, $M=2'064.76$, triclinic, cell volume= $4'659.0\text{\AA}^3$, $T=173\text{K}$, space group P $\bar{1}$ (no. 2), $Z=2$, 41'046 reflections measured, 21'247 unique ($R_{int}=0.02$) from which 12'623 have been used in the refinement ($I>3\sigma(I)$). The final R was 0.059.

Unit cell lengths (Å) $a=15.6921(2)$ $b=16.0207(2)$ $c=21.2804(3)$
 Unit cell angles (degree) $\alpha=103.9732(7)$ $\beta=102.0324(8)$ $\gamma=109.0858(7)$

Table A.4: Bond distances for the non-hydrogen atoms of [Cu₂(pcp)[PF₆]₃ · 2.5 C₃H₆O / (Å)

Atom A	Atom B	Distance	Atom A	Atom B	Distance	Atom A	Atom B	Distance
Cu1	N1	2.117(3)	Cu1	N2	1.950(3)	Cu1	N3	2.240(3)
Cu1	N6	2.202(3)	Cu1	N7	1.973(3)	Cu1	N8	2.354(3)
Cu2	N4	2.027(3)	Cu2	N5	2.005(3)	Cu2	N9	2.035(3)
Cu2	N10	2.001(3)	P1	F1	1.604(5)	P1	F2	1.566(5)
P1	F3	1.527(6)	P1	F4	1.615(6)	P1	F5	1.595(5)
P1	F6	1.535(5)	P1	F11	1.576(5)	P1	F12	1.598(6)
P1	F13	1.631(6)	P1	F14	1.504(6)	P1	F15	1.549(6)
P1	F16	1.596(6)	P2	F21	1.579(3)	P2	F22	1.588(3)
P2	F23	1.529(5)	P2	F24	1.620(5)	P2	F25	1.509(5)
P2	F26	1.647(5)	P2	F33	1.638(5)	P2	F34	1.512(5)
P2	F35	1.592(6)	P2	F36	1.566(5)	P3	F51	1.584(3)
P3	F51	1.584(3)	P3	F53	1.590(3)	P3	F53	1.590(3)
P3	F55	1.586(4)	P3	F55	1.586(4)	P4	F61	1.575(5)
P4	F61	1.575(5)	P4	F63	1.579(6)	P4	F63	1.579(6)
P4	F65	1.557(6)	P4	F65	1.557(6)	N1	C1	1.343(5)
N1	C5	1.349(4)	N2	C6	1.347(5)	N2	C10	1.348(4)
N3	C11	1.349(4)	N3	C15	1.342(5)	N4	C16	1.342(4)
N4	C20	1.354(4)	N5	C21	1.343(5)	N5	C25	1.346(5)
N6	C56	1.334(5)	N6	C60	1.343(4)	N7	C61	1.358(4)
N7	C65	1.348(4)	N8	C66	1.344(4)	N8	C70	1.344(4)
N9	C71	1.331(5)	N9	C75	1.353(4)	N10	C76	1.347(5)
N10	C80	1.343(5)	O1	C35	1.360(5)	O1	C38	1.415(5)
O2	C39	1.408(6)	O2	C40	1.403(6)	O3	C41	1.358(8)
O3	C42	1.408(7)	O5	C45	1.425(6)	O5	C46	1.385(7)
O6	C47	1.419(5)	O6	C48	1.405(5)	O7	C49	1.424(5)

Table A.4: Bond distances for the non-hydrogen atoms of
 $[\text{Cu}_2(\text{pcp})][\text{PF}_6]_3 \cdot 2.5 \text{C}_3\text{H}_6\text{O}$ / (Å)

Atom A	Atom B	Distance	Atom A	Atom B	Distance	Atom A	Atom B	Distance
O7	C50	1.363(4)	O8	C87	1.208(6)	O9	C90	1.239(8)
O10	C93	1.212(9)	C1	C2	1.363(6)	C2	C3	1.387(6)
C3	C4	1.385(6)	C4	C5	1.376(6)	C5	C6	1.475(5)
C6	C7	1.391(5)	C7	C8	1.393(5)	C8	C9	1.402(6)
C8	C26	1.486(5)	C9	C10	1.388(5)	C10	C11	1.480(5)
C11	C12	1.390(5)	C12	C13	1.380(6)	C13	C14	1.391(5)
C14	C15	1.389(5)	C15	C16	1.490(5)	C16	C17	1.388(5)
C17	C18	1.406(5)	C18	C19	1.396(5)	C18	C32	1.473(5)
C19	C20	1.385(5)	C20	C21	1.486(5)	C21	C22	1.397(5)
C22	C23	1.391(6)	C23	C24	1.368(7)	C24	C25	1.383(6)
C26	C27	1.364(6)	C26	C31	1.394(7)	C27	C28	1.397(6)
C28	C29	1.361(8)	C29	C30	1.363(8)	C30	C31	1.402(6)
C32	C33	1.397(5)	C32	C37	1.386(6)	C33	C34	1.382(6)
C34	C35	1.383(6)	C35	C36	1.387(6)	C36	C37	1.394(6)
C38	C39	1.508(6)	C40	C41	1.425(9)	C42	C43	1.480(9)
C43	O4	1.410(8)	C43	O40	1.443(8)	C45	C44	1.423(9)
C45	C440	1.444(8)	C46	C47	1.473(8)	C48	C49	1.494(5)
C50	C51	1.391(6)	C50	C55	1.378(5)	C51	C52	1.376(5)
C52	C53	1.395(5)	C53	C54	1.389(5)	C53	C63	1.480(4)
C54	C55	1.383(5)	C56	C57	1.379(6)	C57	C58	1.373(6)
C58	C59	1.391(5)	C59	C60	1.381(5)	C60	C61	1.483(5)
C61	C62	1.384(4)	C62	C63	1.392(5)	C63	C64	1.399(5)
C64	C65	1.379(4)	C65	C66	1.490(5)	C66	C67	1.388(5)
C67	C68	1.388(5)	C68	C69	1.378(5)	C69	C70	1.393(5)
C70	C71	1.492(4)	C71	C72	1.395(5)	C72	C73	1.402(5)
C73	C74	1.381(6)	C73	C81	1.480(6)	C74	C75	1.390(5)
C75	C76	1.487(6)	C76	C77	1.390(5)	C77	C78	1.390(7)
C78	C79	1.370(7)	C79	C80	1.387(6)	C81	C82	1.411(7)
C81	C86	1.381(7)	C82	C83	1.384(7)	C83	C84	1.37(1)
C84	C85	1.35(1)	C85	C86	1.401(8)	C87	C88	1.448(7)
C87	C89	1.449(7)	C90	C91	1.443(9)	C90	C92	1.457(9)
C93	C94	1.42(1)	C93	C95	1.46(1)	F1	F11	0.775(9)
F1	F16	1.64(1)	F2	F12	0.84(1)	F2	F15	1.57(1)
F3	F13	0.79(1)	F3	F15	1.632(12)	F4	F14	0.630(12)
F5	F14	1.640(11)	F5	F15	1.145(11)	F6	F12	1.639(11)
F6	F16	0.87(1)	F23	F33	1.197(9)	F23	F36	1.122(9)
F24	F34	0.901(9)	F24	F35	1.594(9)	F25	F33	1.446(9)
F25	F35	0.841(9)	F26	F34	1.36(1)	F26	F36	1.234(9)
C44	O4	1.42(1)	C44	C440	0.934(18)	C44	O40	1.101(12)
O4	C440	1.253(13)	O4	O40	0.752(13)	C440	O40	1.439(8)

Table A.5: Bond angles for the non-hydrogen atoms of
 $[\text{Cu}_2\text{pcp}][\text{PF}_6]_3 \cdot 2.5 \text{C}_3\text{H}_6\text{O}$ / (degrees)

Atom A	Atom B	Atom C	Angle	Atom A	Atom B	Atom C	Angle
Atom A	Atom B	Atom C	Angle	Atom A	Atom B	Atom C	Angle
N1	Cu1	N2	79.28(11)	N1	Cu1	N3	155.6(1)
N2	Cu1	N3	77.07(11)	N1	Cu1	N6	103.55(11)
N2	Cu1	N6	95.96(11)	N3	Cu1	N6	84.9(1)
N1	Cu1	N7	99.32(11)	N2	Cu1	N7	173.66(11)

Table A.5: Bond angles for the non-hydrogen atoms of $[\text{Cu}_2\text{pcp}][\text{PF}_6]_3 \cdot 2.5 \text{C}_3\text{H}_6\text{O}$ / (degrees)

Atom A	Atom B	Atom C	Angle	Atom A	Atom B	Atom C	Angle
N3	Cu1	N7	104.84(11)	N6	Cu1	N7	78.3(1)
N1	Cu1	N8	80.69(11)	N2	Cu1	N8	110.46(11)
N3	Cu1	N8	102.1(1)	N6	Cu1	N8	153.5(1)
N7	Cu1	N8	75.2(1)	N4	Cu2	N5	81.43(12)
N4	Cu2	N9	129.99(11)	N5	Cu2	N9	114.14(13)
N4	Cu2	N10	119.75(12)	N5	Cu2	N10	137.12(13)
N9	Cu2	N10	81.86(13)	F1	P1	F2	175.1(4)
F1	P1	F3	91.6(4)	F2	P1	F3	92.5(4)
F1	P1	F4	86.4(4)	F2	P1	F4	89.4(4)
F3	P1	F4	177.4(4)	F1	P1	F5	88.0(3)
F2	P1	F5	89.2(3)	F3	P1	F5	91.7(4)
F4	P1	F5	86.6(4)	F1	P1	F6	89.3(4)
F2	P1	F6	93.2(4)	F3	P1	F6	93.4(4)
F4	P1	F6	88.2(4)	F5	P1	F6	174.3(4)
F1	P1	F11	28.2(3)	F2	P1	F11	151.9(4)
F3	P1	F11	73.9(5)	F4	P1	F11	103.7(4)
F5	P1	F11	67.3(4)	F1	P1	F12	150.8(4)
F2	P1	F12	30.6(4)	F3	P1	F12	99.0(4)
F4	P1	F12	83.5(4)	F5	P1	F12	118.6(4)
F1	P1	F13	92.3(4)	F2	P1	F13	92.6(4)
F3	P1	F13	28.7(4)	F4	P1	F13	152.9(4)
F5	P1	F13	120.4(4)	F1	P1	F14	88.3(5)
F2	P1	F14	86.9(5)	F3	P1	F14	155.5(5)
F4	P1	F14	23.0(5)	F5	P1	F14	63.8(5)
F1	P1	F15	119.0(4)	F2	P1	F15	60.7(4)
F3	P1	F15	64.1(5)	F4	P1	F15	115.6(5)
F5	P1	F15	42.7(4)	F1	P1	F16	61.9(4)
F2	P1	F16	119.2(4)	F3	P1	F16	109.0(5)
F4	P1	F16	71.4(5)	F5	P1	F16	142.9(4)
F6	P1	F11	111.7(4)	F6	P1	F12	63.1(4)
F11	P1	F12	171.3(4)	F6	P1	F13	64.8(4)
F11	P1	F13	86.8(3)	F12	P1	F13	84.6(3)
F6	P1	F14	111.1(5)	F11	P1	F14	95.6(4)
F12	P1	F14	92.9(4)	F13	P1	F14	175.8(4)
F6	P1	F15	142.6(5)	F11	P1	F15	91.2(4)
F12	P1	F15	90.0(4)	F13	P1	F15	88.6(4)
F14	P1	F15	94.7(5)	F6	P1	F16	32.1(4)
F11	P1	F16	88.7(4)	F12	P1	F16	88.9(4)
F13	P1	F16	84.2(4)	F14	P1	F16	92.4(4)
F15	P1	F16	172.8(5)	F21	P2	F22	178.3(2)
F21	P2	F23	93.4(3)	F22	P2	F23	88.0(3)
F21	P2	F24	89.9(2)	F22	P2	F24	88.6(3)
F23	P2	F24	171.0(4)	F21	P2	F25	93.6(3)
F22	P2	F25	87.2(3)	F23	P2	F25	97.8(4)
F24	P2	F25	90.4(4)	F21	P2	F26	89.6(3)
F22	P2	F26	89.5(3)	F23	P2	F26	87.5(4)
F24	P2	F26	84.1(4)	F25	P2	F26	173.6(4)
F21	P2	F33	87.3(3)	F22	P2	F33	94.4(3)
F23	P2	F33	44.3(3)	F24	P2	F33	144.5(4)
F25	P2	F33	54.5(4)	F21	P2	F34	90.9(3)
F22	P2	F34	87.4(3)	F23	P2	F34	138.2(5)

Table A.5: Bond angles for the non-hydrogen atoms of
 $[\text{Cu}_2\text{pcp}][\text{PF}_6]_3 \cdot 2.5 \text{C}_3\text{H}_6\text{O}$ / (degrees)

Atom A	Atom B	Atom C	Angle	Atom A	Atom B	Atom C	Angle
F24	P2	F34	33.2(3)	F25	P2	F34	123.4(5)
F21	P2	F35	88.4(3)	F22	P2	F35	91.5(3)
F23	P2	F35	129.0(4)	F24	P2	F35	59.5(4)
F25	P2	F35	31.3(4)	F21	P2	F36	89.9(3)
F22	P2	F36	90.5(3)	F23	P2	F36	42.5(4)
F24	P2	F36	129.2(4)	F25	P2	F36	140.3(4)
F26	P2	F33	131.3(4)	F26	P2	F34	50.9(4)
F33	P2	F34	177.2(4)	F26	P2	F35	143.5(4)
F33	P2	F35	85.0(3)	F34	P2	F35	92.7(4)
F26	P2	F36	45.1(4)	F33	P2	F36	86.2(4)
F34	P2	F36	96.0(4)	F35	P2	F36	171.2(4)
F51	P3	F51	179.993	F51	P3	F53	88.87(17)
F51	P3	F53	91.13(17)	F51	P3	F53	91.13(17)
F51	P3	F53	88.87(17)	F53	P3	F53	179.993
F51	P3	F55	90.0(2)	F51	P3	F55	90.0(2)
F53	P3	F55	90.0(2)	F53	P3	F55	90.0(2)
F51	P3	F55	90.0(2)	F51	P3	F55	90.0(2)
F53	P3	F55	90.0(2)	F53	P3	F55	90.0(2)
F55	P3	F55	179.993	F61	P4	F61	179.993
F61	P4	F63	90.0(3)	F61	P4	F63	90.0(3)
F61	P4	F63	90.0(3)	F61	P4	F63	90.0(3)
F63	P4	F63	179.993	F61	P4	F65	91.8(3)
F61	P4	F65	88.2(3)	F63	P4	F65	88.8(4)
F63	P4	F65	91.2(4)	F61	P4	F65	88.2(3)
F61	P4	F65	91.8(3)	F63	P4	F65	91.2(4)
F63	P4	F65	88.8(4)	F65	P4	F65	179.993
Cu1	N1	C1	127.9(2)	Cu1	N1	C5	112.6(2)
C1	N1	C5	118.8(3)	Cu1	N2	C6	118.6(2)
Cu1	N2	C10	120.5(2)	C6	N2	C10	120.5(3)
Cu1	N3	C11	108.9(2)	Cu1	N3	C15	129.0(2)
C11	N3	C15	118.5(3)	Cu2	N4	C16	127.7(2)
Cu2	N4	C20	113.6(2)	C16	N4	C20	118.2(3)
Cu2	N5	C21	114.5(2)	Cu2	N5	C25	126.8(3)
C21	N5	C25	118.4(3)	Cu1	N6	C56	128.9(2)
Cu1	N6	C60	111.4(2)	C56	N6	C60	119.0(3)
Cu1	N7	C61	118.6(2)	Cu1	N7	C65	122.7(2)
C61	N7	C65	118.7(3)	Cu1	N8	C66	108.2(2)
Cu1	N8	C70	127.4(2)	C66	N8	C70	118.7(3)
Cu2	N9	C71	127.6(2)	Cu2	N9	C75	112.9(3)
C71	N9	C75	118.4(3)	Cu2	N10	C76	113.9(3)
Cu2	N10	C80	127.1(3)	C76	N10	C80	118.6(3)
C35	O1	C38	119.2(3)	C39	O2	C40	110.3(4)
C41	O3	C42	115.7(5)	C45	O5	C46	115.3(5)
C47	O6	C48	111.0(4)	C49	O7	C50	118.6(3)
N1	C1	C2	122.2(3)	C1	C2	C3	119.1(4)
C2	C3	C4	119.2(4)	C3	C4	C5	118.5(4)
N1	C5	C4	122.0(3)	N1	C5	C6	114.6(3)
C4	C5	C6	123.4(3)	N2	C6	C5	114.2(3)
N2	C6	C7	120.8(3)	C5	C6	C7	124.9(3)
C6	C7	C8	120.1(3)	C7	C8	C9	117.9(3)
C7	C8	C26	120.4(4)	C9	C8	C26	121.7(3)

Table A.5: Bond angles for the non-hydrogen atoms of
 $[\text{Cu}_2\text{pcp}][\text{PF}_6]_3 \cdot 2.5 \text{C}_3\text{H}_6\text{O}$ / (degrees)

Atom A	Atom B	Atom C	Angle	Atom A	Atom B	Atom C	Angle
C8	C9	C10	119.8(3)	N2	C10	C9	121.0(3)
N2	C10	C11	114.2(3)	C9	C10	C11	124.8(3)
N3	C11	C10	115.2(3)	N3	C11	C12	122.3(3)
C10	C11	C12	122.4(3)	C11	C12	C13	118.8(3)
C12	C13	C14	119.2(3)	C13	C14	C15	118.8(4)
N3	C15	C14	122.3(3)	N3	C15	C16	117.5(3)
C14	C15	C16	120.1(3)	N4	C16	C15	115.0(3)
N4	C16	C17	122.6(3)	C15	C16	C17	122.3(3)
C16	C17	C18	120.1(3)	C17	C18	C19	116.2(3)
C17	C18	C32	122.4(3)	C19	C18	C32	121.4(3)
C18	C19	C20	121.0(3)	N4	C20	C19	121.9(3)
N4	C20	C21	114.7(3)	C19	C20	C21	123.3(3)
N5	C21	C20	115.3(3)	N5	C21	C22	121.8(4)
C20	C21	C22	123.0(3)	C21	C22	C23	118.8(4)
C22	C23	C24	119.3(4)	C23	C24	C25	118.9(4)
N5	C25	C24	122.8(4)	C8	C26	C27	121.4(4)
C8	C26	C31	120.4(4)	C27	C26	C31	118.2(4)
C26	C27	C28	120.9(5)	C27	C28	C29	120.5(5)
C28	C29	C30	119.8(4)	C29	C30	C31	120.0(5)
C26	C31	C30	120.4(5)	C18	C32	C33	120.6(3)
C18	C32	C37	121.9(3)	C33	C32	C37	117.4(3)
C32	C33	C34	121.3(4)	C33	C34	C35	120.3(4)
O1	C35	C34	115.8(4)	O1	C35	C36	124.3(4)
C34	C35	C36	119.9(4)	C35	C36	C37	119.1(4)
C32	C37	C36	122.1(4)	O1	C38	C39	104.1(4)
O2	C39	C38	108.5(4)	O2	C40	C41	115.1(5)
O3	C41	C40	118.1(6)	O3	C42	C43	112.3(5)
C42	C43	O4	123.8(8)	C42	C43	O40	101.1(6)
O4	C43	O40	30.5(5)	O5	C45	C44	116.4(7)
O5	C45	C440	111.8(6)	C44	C45	C440	38.0(7)
O5	C46	C47	110.7(4)	O6	C47	C46	111.3(5)
O6	C48	C49	108.6(3)	O7	C49	C48	105.8(3)
O7	C50	C51	115.2(3)	O7	C50	C55	125.3(3)
C51	C50	C55	119.4(3)	C50	C51	C52	120.1(3)
C51	C52	C53	121.3(3)	C52	C53	C54	117.4(3)
C52	C53	C63	121.4(3)	C54	C53	C63	121.1(3)
C53	C54	C55	121.7(3)	C50	C55	C54	119.8(3)
N6	C56	C57	122.3(3)	C56	C57	C58	118.8(3)
C57	C58	C59	119.4(4)	C58	C59	C60	118.4(3)
N6	C60	C59	122.0(3)	N6	C60	C61	115.1(3)
C59	C60	C61	122.9(3)	N7	C61	C60	115.5(3)
N7	C61	C62	121.2(3)	C60	C61	C62	123.3(3)
C61	C62	C63	121.1(3)	C53	C63	C62	121.6(3)
C53	C63	C64	122.0(3)	C62	C63	C64	116.4(3)
C63	C64	C65	120.7(3)	N7	C65	C64	121.9(3)
N7	C65	C66	114.8(3)	C64	C65	C66	123.3(3)
N8	C66	C65	115.5(3)	N8	C66	C67	121.9(3)
C65	C66	C67	122.5(3)	C66	C67	C68	119.3(3)
C67	C68	C69	118.9(3)	C68	C69	C70	118.9(3)
N8	C70	C69	122.3(3)	N8	C70	C71	115.3(3)
C69	C70	C71	122.3(3)	N9	C71	C70	114.9(3)

Table A.5: Bond angles for the non-hydrogen atoms of $[\text{Cu}_2\text{pcp}][\text{PF}_6]_3 \cdot 2.5 \text{C}_3\text{H}_6\text{O}$ / (degrees)

Atom A	Atom B	Atom C	Angle	Atom A	Atom B	Atom C	Angle
N9	C71	C72	123.4(3)	C70	C71	C72	121.7(3)
C71	C72	C73	118.2(4)	C72	C73	C74	118.2(4)
C72	C73	C81	121.9(4)	C74	C73	C81	119.9(3)
C73	C74	C75	120.2(3)	N9	C75	C74	121.6(4)
N9	C75	C76	114.6(3)	C74	C75	C76	123.8(3)
N10	C76	C75	115.6(3)	N10	C76	C77	122.0(4)
C75	C76	C77	122.4(4)	C76	C77	C78	118.4(4)
C77	C78	C79	119.9(4)	C78	C79	C80	118.6(4)
N10	C80	C79	122.5(4)	C73	C81	C82	119.7(4)
C73	C81	C86	121.9(4)	C82	C81	C86	118.4(4)
C81	C82	C83	120.9(5)	C82	C83	C84	119.6(6)
C83	C84	C85	120.0(5)	C84	C85	C86	122.0(6)
C84	C85	H851	119.002	C81	C86	C85	118.9(6)
O8	C87	C88	122.0(6)	O8	C87	C89	120.2(6)
C88	C87	C89	117.8(6)	O9	C90	C91	116.8(8)
O9	C90	C92	122.9(9)	C91	C90	C92	119.8(7)
O10	C93	C94	107.7(10)	O10	C93	C95	129.6(11)
C94	C93	C95	119.4(9)	P1	F1	F11	73.9(6)
P1	F1	F16	58.8(3)	F11	F1	F16	129.3(9)
P1	F2	F12	76.8(6)	P1	F2	F15	59.1(3)
F12	F2	F15	132.6(8)	P1	F3	F13	83.1(7)
P1	F3	F15	58.6(4)	F13	F3	F15	130.0(9)
P1	F4	F14	68.6(8)	P1	F5	F14	55.4(3)
P1	F5	F15	66.5(4)	F14	F5	F15	106.2(6)
P1	F6	F12	60.3(3)	P1	F6	F16	77.8(6)
F12	F6	F16	123.3(10)	P1	F11	F1	78.0(6)
P1	F12	F2	72.6(6)	P1	F12	F6	56.6(3)
F2	F12	F6	128.1(7)	P1	F13	F3	68.3(6)
P1	F14	F4	88.4(10)	P1	F14	F5	60.8(3)
F4	F14	F5	148.6(12)	P1	F15	F2	60.2(3)
P1	F15	F3	57.3(3)	F2	F15	F3	88.3(5)
P1	F15	F5	70.8(4)	F2	F15	F5	108.4(7)
F3	F15	F5	106.3(6)	P1	F16	F1	59.3(3)
P1	F16	F6	70.1(5)	F1	F16	F6	119.6(8)
P2	F23	F33	72.7(4)	P2	F23	F36	70.5(4)
F33	F23	F36	141.6(6)	P2	F24	F34	66.8(5)
P2	F24	F35	59.4(3)	F34	F24	F35	126.2(6)
P2	F25	F33	67.3(3)	P2	F25	F35	79.8(6)
F33	F25	F35	144.0(8)	P2	F26	F34	59.4(3)
P2	F26	F36	64.0(3)	F34	F26	F36	123.4(5)
P2	F33	F23	63.1(3)	P2	F33	F25	58.2(3)
F23	F33	F25	119.8(5)	P2	F34	F24	80.0(5)
P2	F34	F26	69.7(4)	F24	F34	F26	149.5(7)
P2	F35	F24	61.1(3)	P2	F35	F25	68.9(5)
F24	F35	F25	129.0(7)	P2	F36	F23	67.0(4)
P2	F36	F26	70.9(4)	F23	F36	F26	137.7(6)
C45	C44	O4	110.3(9)	C45	C44	C440	72.2(9)
O4	C44	C440	60.0(9)	C45	C44	O40	135.1(11)
O4	C44	O40	31.5(6)	C440	C44	O40	89.7(12)
C43	O4	C44	116.5(9)	C43	O4	C440	127.0(9)
C44	O4	C440	40.2(8)	C43	O4	O40	77.2(9)

Table A.5: Bond angles for the non-hydrogen atoms of $[\text{Cu}_2\text{pcp}][\text{PF}_6]_3 \cdot 2.5 \text{C}_3\text{H}_6\text{O}$ / (degrees)

Atom A	Atom B	Atom C	Angle	Atom A	Atom B	Atom C	Angle
C44	O4	O40	49.8(9)	C440	O4	O40	88.0(11)
C45	C440	C44	69.8(8)	C45	C440	O4	120.0(9)
C44	C440	O4	79.8(10)	C45	C440	O40	108.3(7)
C44	C440	O40	49.9(8)	O4	C440	O40	31.5(6)
C43	O40	C44	142.3(12)	C43	O40	O4	72.3(9)
C44	O40	O4	98.8(11)	C43	O40	C440	111.6(6)
C44	O40	C440	40.4(9)	O4	O40	C440	60.5(10)

Table A.6: Atomic coordinates of the non-hydrogen atoms of $[\text{Cu}_2\text{pcp}][\text{PF}_6]_3 \cdot 2.5$ acetone

Atom	x/a	y/b	z/c	U(equiv)	occupancy
Atom	x/a	y/b	z/c	U(equiv)	occupancy
CU1	0.33693(3)	0.13084(3)	0.72256(2)	0.0348	1
CU2	0.37943(3)	-0.04188(3)	0.82193(2)	0.044	1
P1	-0.22483(8)	0.04297(9)	0.61022(6)	0.0613	1
P2	0.55289(11)	0.43389(9)	1.13068(7)	0.0689	1
P3	0	-0.5	0.5	0.0616	1
P4	0	0	1	0.1153	1
N1	0.4176(2)	0.1775(2)	0.66020(14)	0.0386	1
N2	0.44578(19)	0.23761(19)	0.79066(14)	0.0375	1
N3	0.31142(19)	0.12245(19)	0.82101(14)	0.0366	1
N4	0.2410(2)	-0.08064(19)	0.77009(14)	0.0378	1
N5	0.3541(2)	-0.1703(2)	0.76137(16)	0.0453	1
N6	0.2387(2)	0.2024(2)	0.71837(14)	0.0395	1
N7	0.22162(18)	0.03300(19)	0.65102(13)	0.034	1
N8	0.37828(19)	0.00239(19)	0.68781(14)	0.037	1
N9	0.4978(2)	0.0611(2)	0.82269(14)	0.0391	1
N10	0.4291(2)	0.0297(2)	0.92202(15)	0.0454	1
O1	-0.3463(2)	-0.3385(2)	0.55426(17)	0.064	1
O2	-0.5760(2)	-0.3347(2)	0.52622(19)	0.0675	1
O3	-0.7363(3)	-0.3118(3)	0.4474(2)	0.0889	1
O5	-0.7307(2)	-0.5284(3)	0.2445(2)	0.0738	1
O6	-0.54225(19)	-0.4867(2)	0.33006(16)	0.0607	1
O7	-0.28952(19)	-0.39706(19)	0.37562(15)	0.0556	1
O8	0.2102(3)	-0.1771(5)	0.9696(3)	0.1459	1
O9	-0.3657(5)	-0.1715(7)	0.7546(4)	0.1988	1
O10	0.1056(7)	-0.5099(9)	0.8195(7)	0.1405	0.5
C1	0.4002(3)	0.1368(3)	0.59320(19)	0.0478	1
C2	0.4659(3)	0.1638(4)	0.5612(2)	0.0643	1
C3	0.5525(3)	0.2378(4)	0.5983(2)	0.0744	1
C4	0.5701(3)	0.2822(3)	0.6670(2)	0.0611	1
C5	0.5021(2)	0.2489(3)	0.69663(18)	0.0424	1
C6	0.5145(2)	0.2880(2)	0.76978(17)	0.0409	1
C7	0.5890(3)	0.3698(3)	0.81530(19)	0.0466	1
C8	0.5929(3)	0.4010(3)	0.88328(18)	0.0453	1
C9	0.5200(3)	0.3476(3)	0.90342(18)	0.0442	1
C10	0.4472(2)	0.2665(2)	0.85597(17)	0.038	1
C11	0.3651(2)	0.2058(2)	0.87052(17)	0.037	1
C12	0.3445(3)	0.2330(3)	0.93076(18)	0.0474	1

Table A.6: Atomic coordinates of the non-hydrogen atoms of
 $[\text{Cu}_2\text{pcp}][\text{PF}_6]_3 \cdot 2.5$ acetone

Atom	x/a	y/b	z/c	U(equiv)	occupancy
C13	0.2648(3)	0.1737(3)	0.9394(2)	0.0523	1
C14	0.2095(3)	0.0872(3)	0.8889(2)	0.0491	1
C15	0.2364(2)	0.0633(2)	0.83110(18)	0.0389	1
C16	0.1860(2)	-0.0330(2)	0.78019(17)	0.0383	1
C17	0.0887(3)	-0.0718(2)	0.74782(18)	0.0415	1
C18	0.0438(3)	-0.1645(2)	0.70216(18)	0.0417	1
C19	0.1023(3)	-0.2130(2)	0.69319(19)	0.0447	1
C20	0.1991(3)	-0.1702(2)	0.72672(18)	0.0408	1
C21	0.2648(3)	-0.2180(3)	0.71882(19)	0.0442	1
C22	0.2368(3)	-0.3063(3)	0.6707(2)	0.058	1
C23	0.3033(4)	-0.3458(3)	0.6675(3)	0.0676	1
C24	0.3948(3)	-0.2961(3)	0.7098(2)	0.0623	1
C25	0.4181(3)	-0.2082(3)	0.7555(2)	0.0519	1
C26	0.6728(3)	0.4879(3)	0.9324(2)	0.0522	1
C27	0.7038(3)	0.4991(3)	0.9999(2)	0.0672	1
C28	0.7814(4)	0.5794(4)	1.0451(3)	0.0828	1
C29	0.8266(4)	0.6489(4)	1.0227(3)	0.0791	1
C30	0.7938(4)	0.6420(3)	0.9562(3)	0.0721	1
C31	0.7164(3)	0.5614(3)	0.9105(2)	0.0634	1
C32	-0.0588(3)	-0.2085(3)	0.66531(19)	0.0437	1
C33	-0.0983(3)	-0.2951(3)	0.6131(2)	0.0538	1
C34	-0.1939(3)	-0.3359(3)	0.5767(2)	0.0562	1
C35	-0.2531(3)	-0.2919(3)	0.5921(2)	0.0506	1
C36	-0.2160(3)	-0.2053(3)	0.6432(3)	0.065	1
C37	-0.1192(3)	-0.1648(3)	0.6790(3)	0.0626	1
C38	-0.4107(3)	-0.2960(3)	0.5647(3)	0.0608	1
C39	-0.5063(3)	-0.3703(3)	0.5193(3)	0.0652	1
C40	-0.6671(4)	-0.4058(4)	0.4924(5)	0.1126	1
C41	-0.7421(4)	-0.3741(5)	0.4813(5)	0.1037	1
C42	-0.8233(4)	-0.3205(5)	0.4055(3)	0.0877	1
C43	-0.8238(5)	-0.3309(4)	0.3344(3)	0.0895	1
C45	-0.8282(4)	-0.5432(4)	0.2215(3)	0.0932	1
C46	-0.7097(4)	-0.5766(4)	0.2874(3)	0.0786	1
C47	-0.6147(3)	-0.5772(3)	0.2932(3)	0.0739	1
C48	-0.4519(3)	-0.4885(3)	0.3374(2)	0.0516	1
C49	-0.3789(3)	-0.3903(3)	0.3698(2)	0.0557	1
C50	-0.2091(3)	-0.3201(3)	0.41497(19)	0.0458	1
C51	-0.1249(3)	-0.3333(3)	0.4205(2)	0.055	1
C52	-0.0400(3)	-0.2624(3)	0.4630(2)	0.0521	1
C53	-0.0360(2)	-0.1763(2)	0.50099(17)	0.038	1
C54	-0.1206(2)	-0.1635(2)	0.49224(19)	0.0439	1
C55	-0.2061(3)	-0.2339(3)	0.4490(2)	0.048	1
C56	0.2534(3)	0.2889(3)	0.75527(19)	0.0481	1
C57	0.1806(3)	0.3191(3)	0.7552(2)	0.0557	1
C58	0.0899(3)	0.2582(3)	0.7156(2)	0.0592	1
C59	0.0735(3)	0.1677(3)	0.6771(2)	0.0486	1
C60	0.1502(2)	0.1428(2)	0.67913(16)	0.0371	1
C61	0.1414(2)	0.0497(2)	0.63789(16)	0.0346	1
C62	0.0583(2)	-0.0165(2)	0.58862(17)	0.0365	1
C63	0.0538(2)	-0.1029(2)	0.55111(16)	0.0358	1
C64	0.1382(2)	-0.1171(2)	0.56450(17)	0.037	1

Table A.6: Atomic coordinates of the non-hydrogen atoms of
 $[\text{Cu}_2\text{pcp}][\text{PF}_6]_3 \cdot 2.5$ acetone

Atom	x/a	y/b	z/c	U(equiv)	occupancy
C65	0.2198(2)	-0.0489(2)	0.61362(16)	0.0348	1
C66	0.3127(2)	-0.0581(2)	0.62848(16)	0.0365	1
C67	0.3324(3)	-0.1217(3)	0.58292(18)	0.0453	1
C68	0.4226(3)	-0.1221(3)	0.5983(2)	0.0527	1
C69	0.4907(3)	-0.0584(3)	0.65817(19)	0.0481	1
C70	0.4656(2)	0.0018(2)	0.70257(17)	0.0399	1
C71	0.5323(2)	0.0669(3)	0.77111(18)	0.0429	1
C72	0.6234(3)	0.1289(3)	0.77929(19)	0.0463	1
C73	0.6805(3)	0.1903(3)	0.8451(2)	0.0498	1
C74	0.6446(3)	0.1838(3)	0.89853(19)	0.0475	1
C75	0.5535(3)	0.1191(2)	0.88636(18)	0.0422	1
C76	0.5096(3)	0.1068(3)	0.94081(18)	0.045	1
C77	0.5486(3)	0.1709(3)	1.0067(2)	0.0529	1
C78	0.5019(4)	0.1544(3)	1.0540(2)	0.0619	1
C79	0.4208(4)	0.0753(3)	1.0355(2)	0.0606	1
C80	0.3859(3)	0.0143(3)	0.9689(2)	0.0534	1
C81	0.7763(3)	0.2614(3)	0.8581(2)	0.061	1
C82	0.8082(3)	0.3505(4)	0.9079(2)	0.0676	1
C83	0.8981(4)	0.4176(4)	0.9220(3)	0.0844	1
C84	0.9583(4)	0.3964(5)	0.8887(3)	0.1039	1
C85	0.9275(5)	0.3126(6)	0.8392(4)	0.1123	1
C86	0.8364(4)	0.2434(5)	0.8227(3)	0.0859	1
F51	0.0982(2)	-0.5090(2)	0.5240(2)	0.0985	1
F53	0.0568(2)	-0.3908(2)	0.51658(19)	0.087	1
F55	-0.0051(3)	-0.4805(3)	0.57551(18)	0.1111	1
F61	0.0943(3)	-0.0174(4)	1.0099(3)	0.1465	1
F63	-0.0166(4)	-0.0267(6)	0.9207(3)	0.1716	1
F65	-0.0603(4)	-0.1045(5)	0.9884(5)	0.1968	1
C87	0.1253(4)	-0.2059(6)	0.9437(4)	0.1117	1
C88	0.0843(6)	-0.1942(7)	0.8804(4)	0.1234	1
C89	0.0611(5)	-0.2553(7)	0.9750(5)	0.1306	1
C90	-0.2969(6)	-0.1249(6)	0.8070(4)	0.1274	1
C91	-0.2740(7)	-0.1738(7)	0.8524(5)	0.1475	1
C92	-0.2329(7)	-0.0291(7)	0.8191(6)	0.1547	1
C93	0.1391(8)	-0.4457(8)	0.7994(6)	0.0938	0.5
C94	0.1131(12)	-0.4828(11)	0.7271(7)	0.1244	0.5
C95	0.2185(8)	-0.3551(9)	0.8361(7)	0.1028	0.5
F1	-0.1446(5)	0.1429(4)	0.6215(4)	0.0901	0.5
F2	-0.3096(5)	-0.0513(4)	0.5969(4)	0.0875	0.5
F3	-0.1655(6)	0.0343(6)	0.6731(4)	0.1155	0.5
F4	-0.2860(6)	0.0571(5)	0.5456(3)	0.0904	0.5
F5	-0.2723(5)	0.0976(4)	0.6549(4)	0.1008	0.5
F6	-0.1810(6)	-0.0045(5)	0.5622(4)	0.128	0.5
F11	-0.1537(5)	0.1458(4)	0.6562(3)	0.0895	0.5
F12	-0.2841(6)	-0.0659(4)	0.5675(4)	0.107	0.5
F13	-0.1467(5)	0.0082(5)	0.6463(4)	0.0889	0.5
F14	-0.2966(6)	0.0712(6)	0.5720(4)	0.1263	0.5
F15	-0.2720(6)	0.0315(7)	0.6664(4)	0.152	0.5
F16	-0.1673(6)	0.0498(6)	0.5567(4)	0.1363	0.5
F21	0.5196(2)	0.5000(2)	1.17850(14)	0.0887	1
F22	0.5840(3)	0.3671(2)	1.08070(18)	0.1032	1

Table A.6: Atomic coordinates of the non-hydrogen atoms of [Cu₂pcp][PF₆]₃ · 2.5 acetone

Atom	x/a	y/b	z/c	U(equiv)	occupancy
F23	0.5766(7)	0.3883(5)	1.1836(3)	0.0949	0.5
F24	0.5141(5)	0.4663(5)	1.0679(3)	0.0872	0.5
F25	0.6507(4)	0.5089(5)	1.1483(4)	0.1033	0.5
F26	0.4447(4)	0.3516(5)	1.1026(4)	0.1153	0.5
F33	0.6433(4)	0.4604(5)	1.1974(3)	0.0993	0.5
F34	0.4707(5)	0.4145(6)	1.0698(3)	0.1133	0.5
F35	0.6197(6)	0.5239(4)	1.1189(4)	0.099	0.5
F36	0.4994(6)	0.3505(4)	1.1530(4)	0.0959	0.5
C44	-0.8606(9)	-0.4899(9)	0.2673(8)	0.1146	0.5
O4	-0.7944(7)	-0.3947(7)	0.2961(6)	0.1098	0.5
C440	-0.8413(8)	-0.4564(7)	0.2389(4)	0.0664	0.5
O40	-0.8266(6)	-0.4244(5)	0.3111(4)	0.0611	0.5

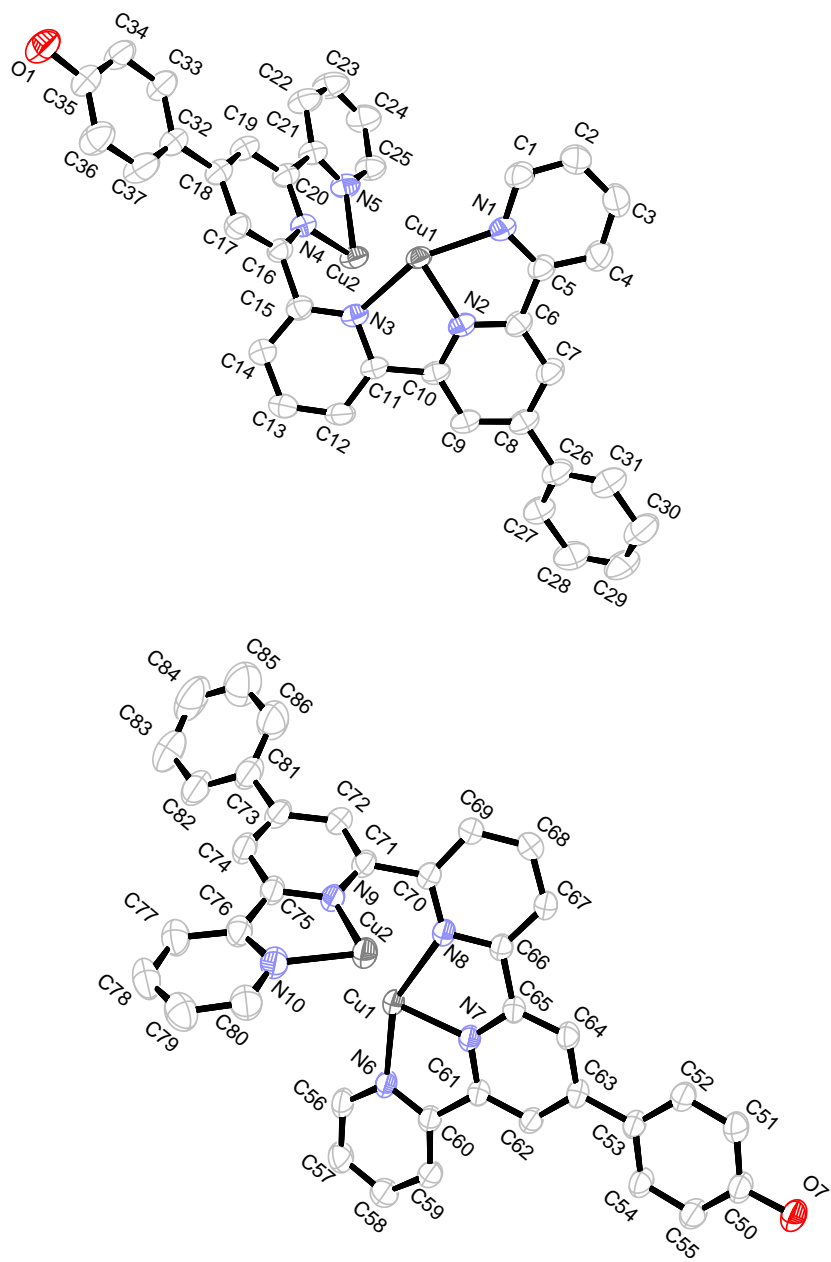


Figure A.5: Crystal structure of the two ligand strands of [Cu₂pep][PF₆]₃ · 2.5 acetone, ellipsoids enclose 50% probability. Hydrogen atoms have been omitted for clarity

Appendix B

Crystal Structures of the qtpy-ligand: 4MeOphqtpy

B.1 4MeOphqtpy

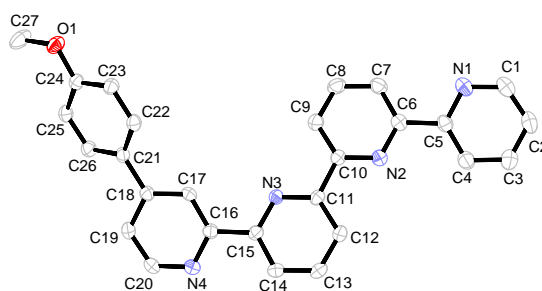


Figure B.1: Crystal structure of 4MeOphqtpy, ellipsoids enclose 50% probability. Hydrogen atoms have been omitted for clarity.

Crystals of 4MeOphqtpy were obtained as colourless plates from a solvent mixture of EtOAc: hexane : Et₂NH (8:20:1) as C₂₇H₂₀N₄O₁, *M*=416.48, monoclinic, cell volume=2'067.8Å³, *T*=173K, space group P 2₁/c, *Z*=4, 25'332 reflections measured, 4'726 unique (*R*_{int}=0.06) from which 2701 have been used in the refinement (*I*>2σ(*I*)). The final *R* was 0.044.

unit cell lengths (Å) a=10.087(8) b=8.666(9) c=23.684(3)
unit cell angles (degree) α=90 β=92.789(8) γ=90

Table B.3: Atomic coordinates of the non-hydrogen atoms of 4MeOphqtpy

Atom	x/a	y/b	z/c	U(equiv)	occupancy
O1	0.52871(12)	-0.01273(18)	0.43556(5)	0.0328	1
N1	-0.22599(19)	-1.0365(2)	0.15688(8)	0.0431	1
N2	-0.07376(15)	-0.68241(18)	0.11827(6)	0.0252	1
N3	0.10238(14)	-0.32289(18)	0.13187(6)	0.0229	1
N4	0.25341(17)	0.0325(2)	0.09411(7)	0.0355	1
C1	-0.3170(3)	-1.1357(3)	0.13638(11)	0.0535	1
C2	-0.3721(2)	-1.1299(3)	0.08208(11)	0.0491	1
C3	-0.3339(2)	-1.0145(3)	0.0473(1)	0.0424	1

Table B.3: Atomic coordinates of the non-hydrogen atoms of 4MeOphqtpy

Atom	x/a	y/b	z/c	U(equiv)	occupancy
C4	-0.2404(2)	-0.9092(2)	0.06760(9)	0.0348	1
C5	-0.18837(19)	-0.9240(2)	0.12229(8)	0.029	1
C6	-0.08751(18)	-0.8151(2)	0.14626(8)	0.0271	1
C7	-0.01471(19)	-0.8487(2)	0.19591(9)	0.0327	1
C8	0.07331(19)	-0.7410(2)	0.21780(9)	0.0344	1
C9	0.08663(19)	-0.6027(2)	0.19005(8)	0.03	1
C10	0.01121(17)	-0.5769(2)	0.14050(8)	0.0241	1
C11	0.01841(17)	-0.4283(2)	0.10950(8)	0.0241	1
C12	-0.05666(19)	-0.4026(2)	0.05960(8)	0.0305	1
C13	-0.0448(2)	-0.2632(3)	0.03250(9)	0.0357	1
C14	0.04257(19)	-0.1548(2)	0.05495(8)	0.031	1
C15	0.11495(18)	-0.1892(2)	0.10451(8)	0.0249	1
C16	0.21411(18)	-0.0786(2)	0.12888(8)	0.026	1
C17	0.26312(18)	-0.0929(2)	0.18444(8)	0.0235	1
C18	0.35695(17)	0.0108(2)	0.20616(8)	0.0249	1
C19	0.3992(2)	0.1241(2)	0.16988(8)	0.0343	1
C20	0.3453(2)	0.1297(3)	0.11534(9)	0.04	1
C21	0.40728(17)	0.0036(2)	0.26580(7)	0.0246	1
C22	0.32624(17)	-0.0503(2)	0.30747(8)	0.0264	1
C23	0.36911(18)	-0.0543(2)	0.36313(8)	0.0268	1
C24	0.49617(18)	-0.0046(2)	0.37910(8)	0.0246	1
C25	0.57884(18)	0.0487(2)	0.33857(8)	0.0269	1
C26	0.53380(18)	0.0518(2)	0.28273(8)	0.0279	1
C27	0.6569(2)	0.0399(3)	0.45466(9)	0.0468	1

Table B.1: Bond distances for the non-hydrogen atoms of 4MeOphqtpy / (Å)

Atom A	Atom B	Distance	Atom A	Atom B	Distance	Atom A	Atom B	Distance
O1	C24	1.363(2)	O1	C27	1.424(2)	N1	C1	1.332(3)
N1	C5	1.340(2)	N2	C6	1.338(2)	N2	C10	1.343(2)
N3	C11	1.338(2)	N3	C15	1.336(2)	N4	C16	1.339(2)
N4	C20	1.333(3)	C1	C2	1.377(3)	C2	C3	1.364(3)
C3	C4	1.382(3)	C4	C5	1.380(3)	C5	C6	1.481(3)
C6	C7	1.387(3)	C7	C8	1.372(3)	C8	C9	1.377(3)
C9	C10	1.385(3)	C10	C11	1.485(2)	C11	C12	1.390(3)
C12	C13	1.376(3)	C13	C14	1.377(3)	C14	C15	1.384(3)
C15	C16	1.482(3)	C16	C17	1.389(3)	C17	C18	1.386(3)
C18	C19	1.385(3)	C18	C21	1.479(2)	C19	C20	1.378(3)
C21	C22	1.392(2)	C21	C26	1.384(2)	C22	C23	1.368(3)
C23	C24	1.387(2)	C24	C25	1.382(3)	C25	C26	1.378(3)

Table B.2: Bond angles for the non-hydrogen atoms of 4MeOphqtpy / (degrees)

Atom A	Atom B	Atom C	Angle	Atom A	Atom B	Atom C	Angle
C24	O1	C27	117.83(15)	C1	N1	C5	117.2(2)
C6	N2	C10	118.06(17)	C11	N3	C15	118.24(16)
C16	N4	C20	116.32(17)	N1	C1	C2	123.9(2)
C1	C2	C3	118.6(2)	C2	C3	C4	118.8(2)
C3	C4	C5	119.2(2)	N1	C5	C4	122.38(19)
N1	C5	C6	116.05(18)	C4	C5	C6	121.57(18)
N2	C6	C5	116.35(17)	N2	C6	C7	122.51(18)
C5	C6	C7	121.12(18)	C6	C7	C8	118.93(19)
C7	C8	C9	119.22(19)	C8	C9	C10	118.85(18)
N2	C10	C9	122.41(18)	N2	C10	C11	116.22(15)
C9	C10	C11	121.36(17)	N3	C11	C10	116.20(15)
N3	C11	C12	122.37(18)	C10	C11	C12	121.43(17)
C11	C12	C13	118.77(18)	C12	C13	C14	119.17(19)
C13	C14	C15	118.80(19)	N3	C15	C14	122.64(18)
N3	C15	C16	116.74(16)	C14	C15	C16	120.60(17)
N4	C16	C15	116.08(16)	N4	C16	C17	123.02(18)
C15	C16	C17	120.90(17)	C16	C17	C18	119.93(18)
C17	C18	C19	117.03(17)	C17	C18	C21	121.58(17)
C19	C18	C21	121.38(17)	C18	C19	C20	119.17(19)
N4	C20	C19	124.5(2)	C18	C21	C22	120.34(16)
C18	C21	C26	122.21(17)	C22	C21	C26	117.45(17)
C21	C22	C23	121.51(17)	C22	C23	C24	119.98(18)
O1	C24	C23	115.27(16)	O1	C24	C25	125.04(16)
C23	C24	C25	119.69(17)	C24	C25	C26	119.44(17)
C21	C26	C25	121.92(18)				

Appendix C

Crystal Structures of Helicand precursors

C.1 2-Acetyl-6-[3-(4-methoxyphenyl)-1-oxoprop-2-enyl]pyridine

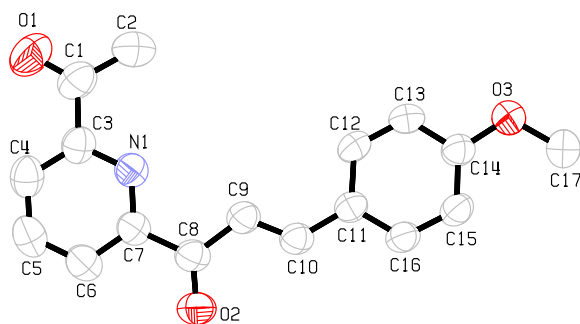


Figure C.1: Crystal structure of 2-acetyl-6-[3-(4-methoxyphenyl)-1-oxoprop-2-enyl]pyridine, ellipsoids enclose 50% probability. Hydrogen atoms were omitted for clarity.

Crystals of 2-Acetyl-6-[3-(4-methoxyphenyl)-1-oxoprop-2-enyl]pyridine were obtained as colourless plates from a solvent mixture of hexane : EtOAc : Et₂NH (50:10:1) as C₁₇H₁₅N₁O₃, *M*=281.31, monoclinic, cell volume=1'444.3Å³, *T*=293K, space group P 2₁/c, *Z*=4, 5'667 reflections measured, 2'494 unique (*R*_{int}=0.14) from which 1'877 have been used in the refinement (*I*>1σ(*I*)). The final *R* was 0.073.

Unit cell lengths (Å) a=12.394(7) b=4.032(4) c=28.900(16)
Unit cell angles (degree) α=90 β=90.73(4) γ=90

Table C.3: Atomic coordinates of the non-hydrogen atoms of 2-acetyl-6-[3-(4-methoxyphenyl)-1-oxoprop-2-enyl]pyridine

Atom	x/a	y/b	z/c	U(equiv)
O1	0.6830(2)	-0.4135(7)	0.52155(7)	0.1126
C1	0.7284(3)	-0.2450(9)	0.4933(1)	0.0826
C2	0.8464(3)	-0.1803(12)	0.49621(13)	0.1209
C3	0.6671(2)	-0.1034(7)	0.45362(8)	0.066
N1	0.72333(15)	0.0678(6)	0.42247(6)	0.0616

Table C.3: Atomic coordinates of the non-hydrogen atoms of 2-acetyl-6-[3-(4-methoxyphenyl)-1-oxoprop-2-enyl]pyridine

Atom	x/a	y/b	z/c	U(equiv)
C4	0.5569(2)	-0.1489(8)	0.4498(1)	0.0748
C5	0.5030(2)	-0.0162(8)	0.4128(1)	0.0784
C6	0.5595(2)	0.1605(8)	0.38059(9)	0.0717
C7	0.66977(19)	0.1952(7)	0.38622(8)	0.0594
C8	0.7333(2)	0.3845(8)	0.35164(8)	0.0637
O2	0.68696(14)	0.5176(6)	0.31924(6)	0.0845
C9	0.85063(19)	0.3980(7)	0.35781(8)	0.0631
C10	0.9118(2)	0.5705(7)	0.32937(8)	0.0607
C11	1.02854(19)	0.5961(7)	0.32991(7)	0.0575
C12	1.0937(2)	0.4735(7)	0.36541(8)	0.0685
C13	1.2035(2)	0.4898(8)	0.36315(8)	0.0733
C14	1.2520(2)	0.6281(7)	0.32497(8)	0.0624
C15	1.1904(2)	0.7547(7)	0.28967(8)	0.0632
C16	1.0795(2)	0.7409(7)	0.29294(8)	0.0618
O3	1.36202(14)	0.6215(6)	0.32529(6)	0.0799
C17	1.4150(2)	0.7652(9)	0.28687(9)	0.0825

Table C.1: Bond distances (Å) for the non-hydrogen atoms of 2-acetyl-6-[3-(4-methoxyphenyl)-1-oxoprop-2-enyl]pyridine

Atom A	Atom B	Distance	Atom A	Atom B	Distance
O1	C1	1.206(3)	C1	C2	1.487(4)
C1	C3	1.483(4)	C3	N1	1.337(3)
C3	C4	1.382(4)	N1	C7	1.336(3)
C4	C5	1.363(4)	C5	C6	1.372(4)
C6	C7	1.381(3)	C7	C8	1.491(4)
C8	O2	1.217(3)	C8	C9	1.464(3)
C9	C10	1.323(3)	C10	C11	1.451(3)
C11	C12	1.389(3)	C11	C16	1.378(3)
C12	C13	1.365(3)	C13	C14	1.381(3)
C14	C15	1.366(3)	C14	O3	1.363(3)
C15	C16	1.380(3)	O3	C17	1.421(3)

Table C.2: Bond angles (degrees) for the non-hydrogen atoms of 2-acetyl-6-[3-(4-methoxyphenyl)-1-oxoprop-2-enyl]pyridine

Atom A	Atom B	Atom C	Angle	Atom A	Atom B	Atom C	Angle
O1	C1	C2	121.9(3)	O1	C1	C3	120.1(3)
C2	C1	C3	118.0(3)	C1	C3	N1	117.0(2)
C1	C3	C4	120.4(3)	N1	C3	C4	122.6(3)
C3	N1	C7	117.9(2)	C3	C4	C5	118.9(3)
C4	C5	C6	119.2(3)	C5	C6	C7	119.0(3)
N1	C7	C6	122.3(3)	N1	C7	C8	117.5(2)
C6	C7	C8	120.2(2)	C7	C8	O2	119.6(2)
C7	C8	C9	118.0(2)	O2	C8	C9	122.4(2)
C8	C9	C10	121.3(2)	C9	C10	C11	127.6(2)
C10	C11	C12	123.6(2)	C10	C11	C16	119.3(2)
C12	C11	C16	117.1(2)	C11	C12	C13	121.2(2)
C12	C13	C14	120.2(2)	C13	C14	C15	120.2(2)
C13	C14	O3	115.6(2)	C15	C14	O3	124.2(2)
C14	C15	C16	118.8(2)	C11	C16	C15	122.5(2)
C14	O3	C17	117.3(2)				

C.2 6-Bromo-[4'-(4-methoxyphenyl)]-2,2'-bipyridine

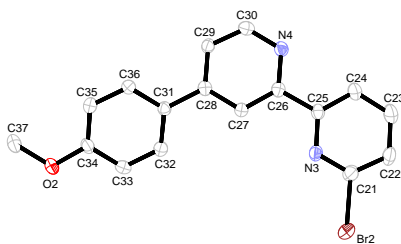


Figure C.2: Crystal structure of 6-bromo-4'-(4-methoxyphenyl)-2,2'-bipyridine, ellipsoids enclose 50% probability. Two molecules of almost identical conformation occupy the unsymmetrical unit cell. For clarity, only one of them is shown in the figure, and hydrogens were omitted.

Crystals of 6-bromo-4'-(4-methoxyphenyl)-2,2'-bipyridine were obtained as yellow plates from THF as two times $C_{17}H_{13}BrN_2O$, $M=682.41$, triclinic, cell volume= $1'432.5\text{\AA}^3$, $T=173\text{K}$, space group $P\bar{1}$, $Z=4$, 53'476 reflections measured, 6'899 unique ($R_{int}=0.07$) from which 4'215 have been used in the refinement ($I>3\sigma(I)$). The final R was 0.028.

unit cell lengths (\AA) $a=11.8229(3)$ $b=12.1488(4)$ $c=12.4098(3)$
 unit cell angles (degree) $\alpha=112.714(2)$ $\beta=115.6871(19)$ $\gamma=92.587(2)$

Table C.4: Bond distances for the non-hydrogen atoms of 6-bromo-4'-(4-methoxyphenyl)-2,2'-bipyridine (\AA)

Atom A	Atom B	Distance	Atom A	Atom B	Distance	Atom A	Atom B	Distance
Br1	C1	1.901(2)	N1	C1	1.311(3)	N1	C5	1.348(3)
N2	C6	1.337(3)	N2	C10	1.335(3)	O1	C14	1.371(3)
O1	C17	1.425(3)	C1	C2	1.379(3)	C2	C3	1.378(4)
C3	C4	1.379(4)	C4	C5	1.384(3)	C5	C6	1.488(3)
C6	C7	1.382(3)	C7	C8	1.391(3)	C8	C9	1.396(3)
C8	C11	1.477(3)	C9	C10	1.377(3)	C11	C12	1.388(3)
C11	C16	1.395(3)	C12	C13	1.373(3)	C13	C14	1.386(3)
C14	C15	1.376(3)	C15	C16	1.384(3)	Br2	C21	1.895(2)
N3	C21	1.314(3)	N3	C25	1.347(3)	N4	C26	1.338(3)
N4	C30	1.331(3)	O2	C34	1.364(3)	O2	C37	1.427(3)
C21	C22	1.379(4)	C22	C23	1.367(4)	C23	C24	1.380(4)
C24	C25	1.380(3)	C25	C26	1.486(3)	C26	C27	1.384(3)
C27	C28	1.390(3)	C28	C29	1.393(3)	C28	C31	1.484(3)
C29	C30	1.383(3)	C31	C32	1.389(3)	C31	C36	1.391(3)
C32	C33	1.379(3)	C33	C34	1.388(3)	C34	C35	1.378(3)
C35	C36	1.383(3)						

Table C.5: Bond angles for the non-hydrogen atoms of 6-bromo-4'-(4-methoxyphenyl)-2,2'-bipyridine / degrees)

Atom A	Atom B	Atom C	Angle	Atom A	Atom B	Atom C	Angle
C1	N1	C5	116.8(2)	C6	N2	C10	116.3(2)
C14	O1	C17	117.50(19)	Br1	C1	N1	115.83(18)
Br1	C1	C2	118.40(19)	N1	C1	C2	125.8(2)
C1	C2	C3	116.7(2)	C2	C3	C4	119.6(2)

Table C.5: Bond angles for the non-hydrogen atoms of 6-bromo-4'-(4-methoxyphenyl)-2,2'-bipyridine / degrees)

Atom A	Atom B	Atom C	Angle	Atom A	Atom B	Atom C	Angle
C3	C4	C5	118.7(2)	N1	C5	C4	122.4(2)
N1	C5	C6	116.3(2)	C4	C5	C6	121.4(2)
N2	C6	C5	114.9(2)	N2	C6	C7	123.7(2)
C5	C6	C7	121.5(2)	C6	C7	C8	119.8(2)
C7	C8	C9	116.4(2)	C7	C8	C11	122.1(2)
C9	C8	C11	121.5(2)	C8	C9	C10	119.7(2)
N2	C10	C9	124.0(2)	C8	C11	C12	122.5(2)
C8	C11	C16	120.1(2)	C12	C11	C16	117.3(2)
C11	C12	C13	121.6(2)	C12	C13	C14	119.9(2)
O1	C14	C13	115.5(2)	O1	C14	C15	124.4(2)
C13	C14	C15	120.2(2)	C14	C15	C16	119.3(2)
C11	C16	C15	121.8(2)	C21	N3	C25	117.0(2)
C26	N4	C30	116.61(19)	C34	O2	C37	116.69(19)
Br2	C21	N3	115.59(18)	Br2	C21	C22	118.75(18)
N3	C21	C22	125.6(2)	C21	C22	C23	116.7(2)
C22	C23	C24	119.8(2)	C23	C24	C25	119.1(2)
N3	C25	C24	121.9(2)	N3	C25	C26	116.5(2)
C24	C25	C26	121.7(2)	N4	C26	C25	115.10(19)
N4	C26	C27	123.3(2)	C25	C26	C27	121.6(2)
C26	C27	C28	119.8(2)	C27	C28	C29	116.9(2)
C27	C28	C31	121.9(2)	C29	C28	C31	121.19(19)
C28	C29	C30	119.1(2)	N4	C30	C29	124.2(2)
C28	C31	C32	121.7(2)	C28	C31	C36	120.5(2)
C32	C31	C36	117.9(2)	C31	C32	C33	121.1(2)
C32	C33	C34	120.1(2)	O2	C34	C33	116.1(2)
O2	C34	C35	124.2(2)	C33	C34	C35	119.7(2)
C34	C35	C36	119.7(2)	C31	C36	C35	121.5(2)

Table C.6: Atomic coordinates of the non-hydrogen atoms of 6-bromo-4'-(4-methoxyphenyl)-2,2'-bipyridine

Atom	x/a	y/b	z/c	U(equiv)
BR1	0.09430(3)	0.53634(2)	0.23969(3)	0.0321
N1	0.28429(18)	0.41306(17)	0.25084(19)	0.0233
N2	0.5401(2)	0.26357(19)	0.2560(2)	0.0285
O1	0.49389(17)	0.21418(16)	0.89697(16)	0.0297
C1	0.2064(2)	0.4608(2)	0.1788(2)	0.0268
C2	0.1987(3)	0.4593(2)	0.0641(3)	0.0331
C3	0.2802(3)	0.4023(3)	0.0221(3)	0.036
C4	0.3656(2)	0.3528(2)	0.0961(3)	0.0312
C5	0.3651(2)	0.3596(2)	0.2098(2)	0.0241
C6	0.4560(2)	0.3094(2)	0.2948(2)	0.0238
C7	0.4503(2)	0.3092(2)	0.4037(2)	0.0227
C8	0.5348(2)	0.2588(2)	0.4789(2)	0.0219
C9	0.6254(2)	0.2150(2)	0.4411(2)	0.0276
C10	0.6241(2)	0.2192(2)	0.3313(3)	0.0309
C11	0.5273(2)	0.2487(2)	0.5906(2)	0.0218
C12	0.4751(2)	0.3263(2)	0.6616(2)	0.0266
C13	0.4666(2)	0.3138(2)	0.7634(2)	0.0279
C14	0.5093(2)	0.2209(2)	0.7961(2)	0.0247

Table C.6: Atomic coordinates of the non-hydrogen atoms of 6-bromo-4'-(4-methoxyphenyl)-2,2'-bipyridine

Atom	x/a	y/b	z/c	U(equiv)
C15	0.5617(2)	0.1423(2)	0.7281(2)	0.0274
C16	0.5705(2)	0.1567(2)	0.6264(2)	0.0261
C17	0.5360(3)	0.1198(3)	0.9338(3)	0.0352
BR2	-0.26691(3)	-0.58574(3)	0.16665(3)	0.0478
N3	-0.09831(19)	-0.35806(18)	0.3444(2)	0.0251
N4	0.12803(18)	-0.06460(17)	0.59321(19)	0.024
O2	0.14720(17)	-0.07494(16)	-0.08305(16)	0.0322
C21	-0.1659(2)	-0.4507(2)	0.3390(3)	0.0298
C22	-0.1705(3)	-0.4558(2)	0.4462(3)	0.0357
C23	-0.0974(3)	-0.3557(3)	0.5683(3)	0.0409
C24	-0.0235(3)	-0.2568(2)	0.5791(3)	0.033
C25	-0.0259(2)	-0.2606(2)	0.4655(2)	0.0228
C26	0.0524(2)	-0.1575(2)	0.4707(2)	0.0212
C27	0.0479(2)	-0.1604(2)	0.3563(2)	0.0204
C28	0.1273(2)	-0.0651(2)	0.3662(2)	0.0201
C29	0.2064(2)	0.0316(2)	0.4938(2)	0.0227
C30	0.2012(2)	0.0282(2)	0.6017(2)	0.0255
C31	0.1302(2)	-0.0664(2)	0.2474(2)	0.0212
C32	0.0946(2)	-0.1759(2)	0.1333(2)	0.027
C33	0.1000(2)	-0.1761(2)	0.0245(2)	0.0289
C34	0.1420(2)	-0.0657(2)	0.0277(2)	0.025
C35	0.1776(2)	0.0440(2)	0.1398(2)	0.0268
C36	0.1716(2)	0.0432(2)	0.2484(2)	0.0251
C37	0.1996(3)	0.0367(3)	-0.0771(3)	0.0367

C.3 5-Bromo-2-(4-methoxyphenyl)pyridine

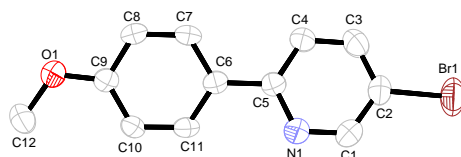


Figure C.3: Crystal structure of 5-bromo-2-(4-methoxyphenyl)pyridine, ellipsoids enclose 50% probability. Hydrogen atoms were omitted for clarity

Crystals of 5-bromo-2-(4-methoxyphenyl)pyridine were obtained as yellow blocks from chloroform- d_1 as $C_{12}H_{10}Br_1N_1O_1$, $M=264.12$, orthorhombic, cell volume= $1'086.1\text{\AA}^3$, $T=293\text{K}$, space group $Pn\ a\ 2_1$, $Z=4$, 7'349 reflections measured, 2'745 unique ($R_{int}=0.03$) from which 1'675 have been used in the refinement ($I>3\sigma(I)$). The final R was 0.036.

Unit cell lengths (\AA) $a=6.2143(8)$ $b=7.2729(4)$ $c=24.032(2)$
 Unit cell angles (degree) $\alpha=90$ $\beta=90$ $\gamma=90$

Table C.7: Bond distances for the non-hydrogen atoms of 5-bromo-2-(4-methoxyphenyl)pyridine / (\AA)

Atom A	Atom B	Distance	Atom A	Atom B	Distance
Br1	C2	1.881(3)	O1	C9	1.353(4)
O1	C12	1.408(4)	N1	C1	1.330(5)
N1	C5	1.340(4)	C1	C2	1.370(6)
C2	C3	1.357(6)	C3	C4	1.365(5)
C4	C5	1.384(5)	C5	C6	1.478(4)
C6	C7	1.395(4)	C6	C11	1.390(5)
C7	C8	1.367(4)	C8	C9	1.393(5)
C9	C10	1.382(5)	C10	C11	1.371(4)

Table C.8: Bond angles for the non-hydrogen atoms of 5-bromo-2-(4-methoxyphenyl)pyridine / (degrees)

Atom A	Atom B	Atom C	Angle	Atom A	Atom B	Atom C	Angle
C9	O1	C12	118.5(3)	C1	N1	C5	118.2(3)
N1	C1	C2	123.5(4)	Br1	C2	C1	121.0(3)
Br1	C2	C3	120.7(3)	C1	C2	C3	118.2(3)
C2	C3	C4	119.6(4)	C3	C4	C5	119.7(3)
N1	C5	C4	120.8(3)	N1	C5	C6	117.6(3)
C4	C5	C6	121.5(3)	C5	C6	C7	122.0(3)
C5	C6	C11	121.1(3)	C7	C6	C11	116.9(3)
C6	C7	C8	121.6(3)	C7	C8	C9	120.2(3)
O1	C9	C8	115.1(3)	O1	C9	C10	125.6(3)
C8	C9	C10	119.3(3)	C9	C10	C11	119.6(3)
C6	C11	C10	122.4(3)				

Table C.9: Atomic coordinates of the non-hydrogen atoms of 5-bromo-2-(4-methoxyphenyl)pyridin

Atom	x/a	y/b	z/c	U(equiv)
BR1	0.30726(8)	-0.01327(6)	-0.20913(4)	0.081
O1	0.9614(4)	0.0076(3)	0.1811(1)	0.0517
N1	0.7230(5)	-0.0343(4)	-0.07652(13)	0.0564
C1	0.6346(7)	-0.0381(5)	-0.12693(16)	0.0609
C2	0.4219(6)	-0.0005(5)	-0.13678(13)	0.0537
C3	0.2947(6)	0.0426(5)	-0.09278(16)	0.0598
C4	0.3813(6)	0.0484(5)	-0.04060(15)	0.0508
C5	0.5972(6)	0.0084(4)	-0.03311(12)	0.0379
C6	0.6965(5)	0.0084(4)	0.02277(11)	0.0358
C7	0.5993(5)	0.0945(4)	0.06814(12)	0.0382
C8	0.6908(5)	0.0913(4)	0.11989(12)	0.0387
C9	0.8852(6)	0.0004(4)	0.12844(13)	0.0373
C10	0.9845(5)	-0.0863(4)	0.08417(12)	0.0385
C11	0.8904(5)	-0.0813(4)	0.03258(12)	0.0394
C12	1.1591(6)	-0.0788(7)	0.19296(16)	0.0672

C.4 6'-Bromo-6-carboxyl-4-(4-methoxyphenyl)-2,2'-bipyridine

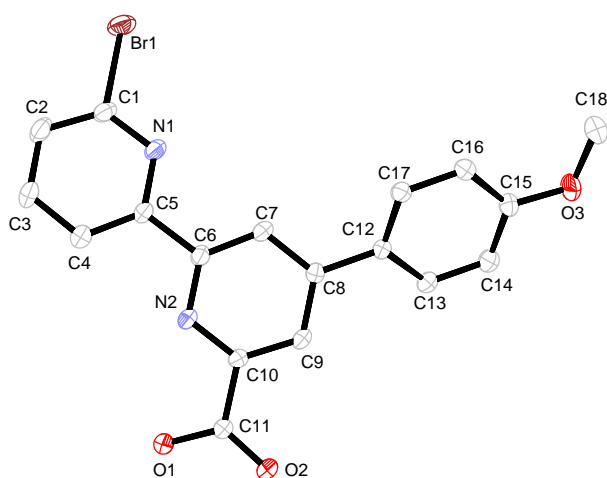


Figure C.4: Crystal structure of 6'-bromo-6-carboxyl-4-(4-methoxyphenyl)-2,2'-bipyridine, ellipsoids enclose 50% probability. Hydrogen atoms were omitted for clarity.

Crystals of 6'-bromo-6-carboxyl-4-(4-methoxyphenyl)-2,2'-bipyridine were obtained as colourless plates from chloroform- d_1 as $C_{18}H_{13}BrN_2O_3$, $M=385.22$, triclinic, cell volume= 761.4\AA^3 , $T=173\text{K}$, space group $P\bar{1}$, $Z=2$, 28'172 reflections measured, 4'778 unique ($R_{int}=0.12$) from which 2'979 have been used in the refinement ($I>3\sigma(I)$). The final R was 0.042.

Unit cell lengths (\AA) $a=3.8887(14)$ $b=10.473(3)$ $c=18.993(6)$
 Unit cell angles (degree) $\alpha=93.80(3)$ $\beta=93.60(2)$ $\gamma=98.44(3)$

Table C.10: Bond distances for the non-hydrogen atoms of 6'-bromo-6-carboxyl-4-(4-methoxyphenyl)-2,2'-bipyridine / (\AA)

Atom A	Atom B	Distance	Atom A	Atom B	Distance
Br1	C1	1.900(2)	N1	C1	1.316(3)
N1	C5	1.347(3)	N2	C6	1.337(3)
N2	C10	1.338(3)	O1	C11	1.283(3)
O2	C11	1.236(3)	O3	C15	1.355(3)
O3	C18	1.422(4)	C1	C2	1.378(4)
C2	C3	1.372(4)	C3	C4	1.385(3)
C4	C5	1.383(4)	C5	C6	1.484(3)
C6	C7	1.388(3)	C7	C8	1.394(3)
C8	C9	1.393(3)	C8	C12	1.474(3)
C9	C10	1.382(3)	C10	C11	1.487(3)
C12	C13	1.400(3)	C12	C17	1.384(3)
C13	C14	1.377(4)	C14	C15	1.390(4)
C15	C16	1.390(4)	C16	C17	1.386(3)

Table C.11: Bond angles for the non-hydrogen atoms of 6'-bromo-6-carboxyl-4-(4-methoxyphenyl)-2,2'-bipyridine / (degrees)

Atom A	Atom B	Atom C	Angle	Atom A	Atom B	Atom C	Angle
C1	N1	C5	116.3(2)	C6	N2	C10	116.5(2)
C15	O3	C18	117.5(2)	Br1	C1	N1	116.3(2)
Br1	C1	C2	117.64(18)	N1	C1	C2	126.0(2)
C1	C2	C3	117.0(2)	C2	C3	C4	119.2(3)
C3	C4	C5	119.0(2)	N1	C5	C4	122.5(2)
N1	C5	C6	116.6(2)	C4	C5	C6	121.0(2)
N2	C6	C5	115.6(2)	N2	C6	C7	123.0(2)
C5	C6	C7	121.4(2)	C6	C7	C8	120.0(2)
C7	C8	C9	117.0(2)	C7	C8	C12	121.9(2)
C9	C8	C12	121.1(2)	C8	C9	C10	118.7(2)
N2	C10	C9	124.7(2)	N2	C10	C11	115.9(2)
C9	C10	C11	119.4(2)	O1	C11	O2	123.7(2)
O1	C11	C10	116.5(2)	O2	C11	C10	119.8(2)
C8	C12	C13	120.6(2)	C8	C12	C17	121.2(2)
C13	C12	C17	118.1(2)	C12	C13	C14	121.2(2)
C13	C14	C15	120.0(2)	O3	C15	C14	115.9(2)
O3	C15	C16	124.5(2)	C14	C15	C16	119.6(2)
C15	C16	C17	119.8(2)	C12	C17	C16	121.3(2)

Table C.12: Atomic coordinates of the non-hydrogen atoms of 6'-bromo-6-carboxyl-4-(4-methoxyphenyl)-2,2'-bipyridine

Atom	x/a	y/b	z/c	U(equiv)
BR1	0.41973(8)	0.14678(3)	0.225874(17)	0.0314
N1	0.2453(6)	0.37190(19)	0.28677(12)	0.0217
N2	0.1009(6)	0.66925(19)	0.37659(11)	0.0209
O1	0.1490(7)	0.8540(2)	0.48042(11)	0.0357
O2	-0.1319(7)	0.97741(19)	0.41361(11)	0.0363
O3	-0.6887(6)	0.8007(2)	-0.03182(11)	0.0317
C1	0.3615(7)	0.2649(2)	0.30300(14)	0.0233
C2	0.4503(8)	0.2326(2)	0.37020(16)	0.029
C3	0.4144(8)	0.3201(3)	0.42527(16)	0.0293
C4	0.2903(7)	0.4338(3)	0.41094(15)	0.0262
C5	0.2097(7)	0.4566(2)	0.34139(14)	0.0206
C6	0.0802(6)	0.5777(2)	0.32338(13)	0.0197
C7	-0.0537(7)	0.5929(2)	0.25551(13)	0.0209
C8	-0.1649(6)	0.7091(2)	0.23983(13)	0.0189
C9	-0.1414(7)	0.8050(2)	0.29512(13)	0.0215
C10	-0.0119(7)	0.7796(2)	0.36133(13)	0.0211
C11	0.0005(7)	0.8785(2)	0.42167(13)	0.0239
C12	-0.3055(6)	0.7299(2)	0.16833(13)	0.0202
C13	-0.2536(7)	0.8531(2)	0.14275(14)	0.0239
C14	-0.3823(8)	0.8736(2)	0.07594(15)	0.0269
C15	-0.5717(7)	0.7714(2)	0.03298(13)	0.0233
C16	-0.6257(7)	0.6484(2)	0.05750(13)	0.0233
C17	-0.4916(7)	0.6289(2)	0.12461(13)	0.0212
C18	-0.8974(8)	0.7000(3)	-0.07604(15)	0.0315

C.5 4-Methoxyphenylboronic acid

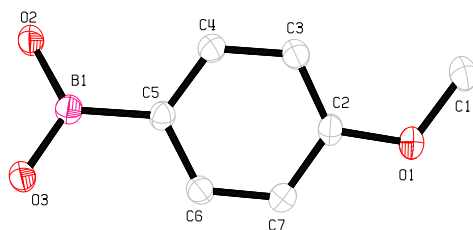


Figure C.5: Crystal structure of 4-methoxyphenylboronic acid, ellipsoids enclose 50% probability. Hydrogen atoms were omitted for clarity.

Crystals of 4-methoxyphenylboronic acid were obtained as colourless blocks from a solvent mixture of diethyl ether and EtOAc as $C_7H_9B_1O_3$, $M=151.96$, monoclinic, cell volume= 721.4\AA^3 , $T=173\text{K}$, space group $P 2_1/n$, $Z=2$, 3'442 reflexions measured, 1'721 unique ($R_{int}=0.01$) from which 1'095 have been used in the refinement ($I > 3\sigma(I)$). The final R was 0.034.

Unit cell lengths (\AA) $a=11.0475(2)$ $b=5.0442(1)$ $c=13.8833(3)$
 Unit cell angles (degree) $\alpha=90$ $\beta=111.1818(11)$ $\gamma=90$

Table C.13: Bond distances (\AA) for the non-hydrogen atoms of 4-methoxyphenylboronic acid

Atom A	Atom B	Distance	Atom A	Atom B	Distance
O1	C1	1.4327(19)	O1	C2	1.3715(15)
O2	B1	1.3722(18)	O3	B1	1.3649(18)
O3	H3	0.897	C2	C3	1.390(2)
C2	C7	1.3951(19)	C3	C4	1.3926(18)
C4	C5	1.3986(18)	C5	C6	1.3986(18)
C5	B1	1.5592(19)	C6	C7	1.3878(17)

Table C.14: Bond angles (degrees) for the non-hydrogen atoms of 4-methoxyphenylboronic acid

Atom A	Atom B	Atom C	Angle	Atom A	Atom B	Atom C	Angle
C1	O1	C2	116.72(11)	O1	C2	C3	124.36(12)
O1	C2	C7	115.45(12)	C3	C2	C7	120.19(12)
C2	C3	C4	119.15(12)	C3	C4	C5	122.19(13)
C4	C5	C6	117.00(11)	C4	C5	B1	122.40(12)
C6	C5	B1	120.60(12)	C5	C6	C7	122.02(12)
C2	C7	C6	119.44(12)	O2	B1	O3	118.34(12)
O2	B1	C5	122.91(12)	O3	B1	C5	118.74(12)

Table C.15: Atomic coordinates of the non-hydrogen atoms of 4-methoxyphenylboronic acid

Atom	x/a	y/b	z/c	U(equiv)
O1	0.0245(1)	0.5348(2)	0.14977(7)	0.0316
O2	0.2583(1)	0.6423(2)	0.65921(7)	0.0284
O3	0.1940(1)	0.19607(19)	0.63074(7)	0.029
C1	0.06811(17)	0.7489(3)	0.10270(11)	0.035
C2	0.07230(13)	0.5265(3)	0.25566(9)	0.0242
C3	0.16064(14)	0.7074(3)	0.3186(1)	0.0265
C4	0.20111(13)	0.6802(3)	0.4254(1)	0.0247
C5	0.15809(12)	0.4730(3)	0.47187(9)	0.022
C6	0.07034(12)	0.2933(3)	0.4060(1)	0.024
C7	0.02696(13)	0.3178(3)	0.2994(1)	0.0256
B1	0.20469(15)	0.4392(3)	0.59141(11)	0.0229

Appendix D

Crystal structures of minor quality

D.1 2,6-di-[3-*tert*-butylphenyl]-1-oxoprop-2-enylpyridine

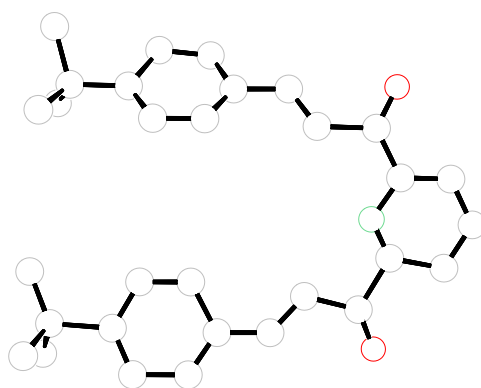


Figure D.1: Pluto plot (without hydrogen atoms) of 2,6-di-[3-*tert*-butylphenyl]-1-oxoprop-2-enylpyridine.

Crystal of 2-[3-(4-*tert*-butylphenyl)-1-oxoprop-2-enyl]-6-[3-(4-hydroxyphenyl)-1-oxoprop-2-enyl]pyridine were obtained as colourless crystals from methanol, as a byproduct in the synthesis of 2-[3-(4-*tert*-butylphenyl)-1-oxoprop-2-enyl]-6-[3-(4-hydroxyphenyl)-1-oxoprop-2-enyl]pyridine, see page 133. Unfortunately, the crystals were of poor quality and the dataset collected permitted only the confirmation of the connectivity in the molecule. Discussion of bond lengths and angles is pointless. The R value varies between 13 and 27%, depending on the settings used to refine the structure. However, it can be trusted that in solid form, the molecule actually bends in the U-form visible in Figure D.1.

The structure was solved in the space group $P2_1$. The asymmetric unit contains four independent molecules in this space group. The attempt to refine in $P2_1/c$ gave a considerably worse R value, even if it is very probable that the correct space group is centrosymmetric. Another attempt to reduce the number of parameters would have been to shorten one axis by 1/2 as the major part of the molecule would nicely superimpose, but the peripheral phenyl rings do not overlap well enough to make this attempt look promising. Therefore the structure stays in a state of preliminary refinement.

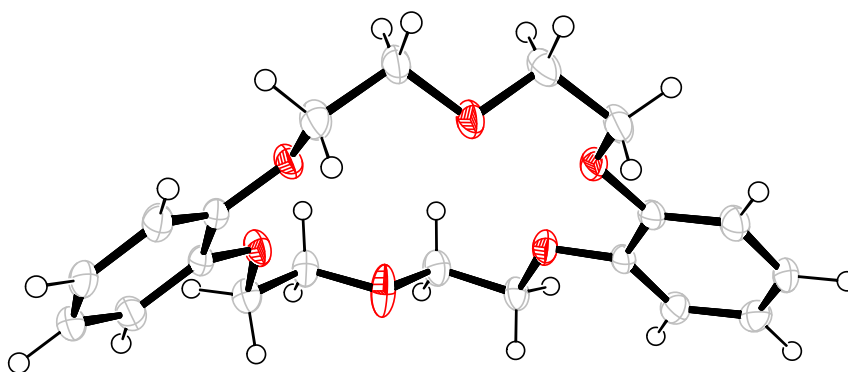


Figure D.2: Crystal structure of dibenzo-18-crown-6, ellipsoids enclose 50% probability.

D.2 Dibenzo-18-crown-6

This structure was obtained from a very small and thin crystal, that had grown in a sample of mcm in a mixture of diethyl ether and acetone. The quality of the dataset is not optimal. Although the connectivity of the dibenzo-18-crown-6 could be determined, the exact composition of the crystal, that included further small chemical entities, could not be determined exactly. Refining, without trying to interpret the residual electron density, gave the result presented in the plot.

Bibliography

- [1] M. Montalti, S. Wadhwa, W. Y. Kim, R. A. Kipp, and R. H. Schmehl. Luminescent ruthenium(II) bipyridyl-phosphonic acid complexes: pH-dependent photophysical behavior and quenching with divalent metal ions. *Inorg. Chem.*, **2000**, 39, 76–84.
- [2] D. Jameson, L. Guise, C. A. Bessel, and K. Takeuchi. *Inorg. Synth.*, chapter Biomimetic and Special Property Ligands, 46–50. 1998.
- [3] D. Jameson and L. Guise. An improved, two-step synthesis of 2,2':6',2''-terpyridine. *Tetrahedron Lett.*, **1991**, 32, 1999–2002.
- [4] O.-A. Neumüller and H. Römpp. *Römpps Chemie-Lexikon*. Franckh'sche Verlagshandlung, W. Keller & Co., Stuttgart, 8 edition, **1983**.
- [5] H. Beyer and W. Walter. *Lehrbuch der Organischen Chemie*. S. Hirzel Verlag, Stuttgart, Germany, 22 edition, **1991**.
- [6] H. Ringsdorf, B. Schlarb, and J. Venzmer. Molekulare Architektur und Funktion von polymeren orientierten Systemen – Modelle für das Studium von Organisation, Oberflächenerkennung und Dynamik bei Biomembranen. *Angew. Chem.*, **1988**, 100, 117–162.
- [7] J. M. Lehn. *Supramolecular Chemistry – Concepts and Perspectives*. VCH, Weinheim, **1995**.
- [8] F. Vögtle. *Supramolecular Chemistry*. Wiley, Chichester, **1993**.
- [9] J.-M. Lehn. Supramolekulare Chemie – Moleküle, Übermoleküle und molekulare Funktionseinheiten (Nobel-Vortrag). *Angew. Chem.*, **1988**, 100, 91–116.
- [10] E. Schrödinger. *Was ist Leben*. Francke, Bern, 2. edition, **1951**.
- [11] J. Collinge. Prion diseases of humans and animals: their causes and molecular basis. *Ann. Rev. of Neurosci.*, **2001**, 24, 519–550.
- [12] J. Tatzelt, R. Voellmy, and W. Welch. Abnormalities in stress proteins in prion diseases. *Cellular and Molecular Neurobiology*, **1998**, 18, 721–729.
- [13] L. C. Serpell, M. Sunde, and C. C. F. Blake. The molecular basis of amyloidosis. *Cellular and Molecular Life Sciences*, **1997**, 53, 871–887.
- [14] J. Breivik. Self-organization of template-replicating polymers and the spontaneous rise of genetic information. *Entropy*, **2001**, 3, 273–279.
- [15] U. P. Wild, S. Bernet, B. Kohler, and A. Renn. From supramolecular photochemistry to the molecular computer. *Pure Appl. Chem.*, **1992**, 64, 1335–1342.
- [16] D. Philip and J. F. Stoddart. Self-assembly in natural and unnatural systems. *Angew. Chem. Int. Ed. Engl.*, **1996**, 35, 1154–1196.

- [17] R. Ballardini, V. Balzani, M. Clemente-León, A. Credi, M. T. Gandolfi, L. Ishow, J. Perkins, J. F. Stoddart, H.-R. Tseng, and S. Wenger. Photoinduced electron transfer in a triad that can be assembled/disassembled by two different external inputs. toward molecular-level electrical extension cables. *J. Am. Chem. Soc.*, **2002**, *124*, 12786–12795.
- [18] R. F. Ziessel. Photoinduced energy or electron transfer in supramolecular systems: applications to molecular wires and light-harvesting sensors. an advanced chemistry project on kinetics using fast laser spectroscopy. *J. Chem. Ed.*, **1997**, *74*, 673–679.
- [19] H. L. Anderson. Building molecular wires from the colours of life: conjugated porphyrin oligomers. *Chem. Commun.*, **1999**, 2323–2330.
- [20] N. Kimizuka, N. Oda, and T. Kunitake. Self-assembling molecular wires of halogen-bridged platinum complexes in organic media. mesoscopic supramolecular assemblies consisting of a mixed valent Pt(II)/Pt(IV) complex and anionic amphiphiles. *Inorg. Chem.*, **2000**, *39*, 2684–2689.
- [21] K. Kuroiwa, T. Shibata, A. Takada, N. Nemoto, and N. Kimizuka. Heat-set gel-like networks of lipophilic Co(II) triazole complexes in organic media and their thermochromic structural transitions. *J. Am. Chem. Soc.*, **2004**, *126*, 2016–2021.
- [22] A. Shanzer, J. Libman, and L. Zelikovich. Molecular redox switches based on chemical triggering of iron translocation in triple-stranded helical complexes. *Nature*, **1995**, *374*, 790–792.
- [23] F. Vögtle, W. M. Müller, U. Müller, M. Bauer, and K. Rissanen. Photoswitchable catenanes. *Angew. Chem., Int. Ed. Engl.*, **1993**, *32*, 1295–1297.
- [24] A. R. Pease, J. O. Jeppesen, J. F. Stoddart, Y. Luo, C. P. Collier, and J. R. Heath. Switching devices based on interlocked molecules. *Acc. Chem. Res.*, **2001**, *34*, 433–444.
- [25] V. Balzani, G. Denti, W. Serroni, S. Campagna, and V. Ricevuto. Made-to-order control of the direction of electronic energy transfer in tetranuclear luminescent metal complexes. *Coord. Chem. Rev.*, **1991**, *111*, 227–236.
- [26] C. Piguet. Toward programmed molecular lanthanide probes and sensors. *Chimia*, **1996**, *50*, 144–153.
- [27] J.-M. Lehn. Toward self-organization and complex matter. *Science*, **2002**, *295*, 2400–2403.
- [28] J.-M. Lehn. Perspektiven der Supramolekularen Chemie – von der molekularen Erkennung zur molekularen Informationsverarbeitung und Selbstorganisation. *Angew. Chem.*, **1990**, *102*, 1347–1362.
- [29] E. Constable. Metallosupramolecular chemistry. *Chem. & Ind.*, **1994**, 56–59.
- [30] T. Kulke. *Chiral Oligopyridines for Metallosupramolecular Chemistry*. PhD thesis, Philosophisch-Naturwissenschaftliche Fakultät der Universität Basel, **1998**.
- [31] L. H. Gade. *Koordinationschemie*. Wiley-VCH Verlag GmbH, Weinheim, **1998**.
- [32] A. Werner. *Z. Anorg. Allg. Chem.*, **1893**, *3*, 267–330.
- [33] M. Gerloch and E. C. Constable. *Transition Metal Chemistry: The Valence Shell in d-Block Chemistry*. VCH, Weinheim, **1994**.
- [34] D. F. Shriver, P. W. Atkins, and C. H. Langford. *Anorganische Chemie: Ein weiterführendes Lehrbuch*. VCH, Weinheim, **1992**.
- [35] M. D. Ward. *The Coordination Chemistry of some Polynucleating Oligopyridines*. PhD thesis, University of Cambridge, **1989**.

- [36] E. C. Constable, S. M. Elder, M. J. Hannon, A. Martin, P. R. Raithby, and D. A. Tocher. 2,2':6',2'':6'',2''':6'''-Quaterpyridine (qtpy): a versatile ligand in metallosupramolecular chemistry; crystal and molecular structures of [Ni(qtpy)(OH)₂][BF₄]₂, [Pd(qtpy)][PF₆]₂, [Cu₂(qtpy)₂][PF₆]₂ and [Ag₂(qtpy)₂][BF₄]₂. *J. Chem. Soc., Dalton Trans.*, **1996**, 2423–2433.
- [37] K. T. Potts, M. Keshavarz-K, F. S. Tham, H. D. Abruña, and C. R. Arana. Metal ion-induced self-assembly of functionalized 2,6-oligopyridines. 2. Copper-containing double-stranded helicates derived from functionalized quaterpyridine and quinquopyridine: Redox state-induced transformations and electron communication in mixed-valence systems. *Inorg. Chem.*, **1993**, *32*, 4422–4435.
- [38] E. C. Constable, M. J. Hannon, A. Martin, P. Raithby, and D. A. Tocher. Self-assembly of double-helical complexes of 2,2':6',2'':6'',2''':6'''-quaterpyridine (qtpy); the X-ray crystal structures of [Cu₂(qtpy)₂][PF₆]₂ and [Ag₂(qtpy)₂][BF₄]₂. *Polyhedron*, **1992**, *11*, 2967–2971.
- [39] K.-M. Lam, K.-Q. Wong, S.-M. Yang, and C.-N. Che. Cobalt and nickel complexes of 2,2':6',2'':6'',2''':6'''-quaterpyridine as catalysts for electrochemical reduction of carbon dioxide. *J. Chem. Soc., Dalton Trans.*, **1995**, 1103–1107.
- [40] E. C. Constable, M. G. B. Drew, and M. D. Ward. Molecular helicity in inorganic complexes; the preparation, crystal and molecular structure of bis(2,2':6',2'':6'',2''':6''',2''''-quinquepyridine)acetatodicopper(II) hexafluorophosphate monohydrate. *J. Chem. Soc., Chem. Commun.*, **1987**, 1600–1601.
- [41] M. Barley, E. C. Constable, S. A. Corr, R. C. S. McQueen, J. C. Nutkins, M. D. Ward, and M. G. B. Drew. Molecular helicity in inorganic complexes; double helical binuclear complexes of 2,2':6',2'':6'',2''':6''',2''''-quinquepyridine (I): Crystal structures of acetato-di-m-(quinquepyridine)dicopper(II) tris(hexafluorophosphate) monohydrate and di m-(quinquepyridine)dicopper(I)(II) tris(hexafluorophosphate)-acetonitrile (1/2). *J. Chem. Soc., Dalton Trans.*, **1988**, 2655–2662.
- [42] E. C. Constable, S. M. Elder, P. Raithby, and M. D. Ward. The preparation and structural characterization of a double-helical binuclear dicobalt(II) complex of 2,2':6',2'':6'',2''':6''',2''''-quinquepyridine; the X-ray crystal structure of acetato(*o*, *o'*)bis(2,2':6',2'':6'',2''':6''',2''''-quinquepyridine)dicobalt(II)hexafluorophosphate tris-acetonitrile solvate. *Polyhedron*, **1991**, *10*, 1395–1400.
- [43] E. C. Constable, A. J. Edwards, P. R. Raithby, D. R. Smith, J. V. Walker, and L. Whall. Heterodimetallic double helicates from redistribution reactions. *Chem. Commun.*, **1996**, 2551–2552.
- [44] J. H. Brewster. *Topics in Current Chemistry*, volume 47. Springer-Verlag, Berlin, **1974**.
- [45] E. C. Constable. *Comprehensive Supramolecular Chemistry*, volume 9. Pergamon, Oxford, **1996**.
- [46] R. B. Corey and L. Pauling. Molecular models of amino acids, peptides, and proteins. *Rev. Sci. Instr.*, **1953**, *24*, 621–627.
- [47] L. Pauling and R. B. Corey. Compound helical configurations of polypeptide chains; structure of proteins of the α -keratin type. *Nature*, **1953**, *171*, 59–61.
- [48] H. Hart. *Organische Chemie: Ein kurzes Lehrbuch*. VCH, Weinheim, Germany, **1989**.
- [49] J. D. Watson and F. H. C. Crick. Molecular structure of nucleic acids; a structure for deoxyribose nucleic acid. *Nature*, **1953**, *171*, 737–738.
- [50] J. D. Watson and F. H. C. Crick. Genetical implications of the structure of deoxyribonucleic acid. *Nature*, **1953**, *171*, 964–967.
- [51] L. A. Whall. *Synthesis and Transition Metal Complexes of Novel Hydrophobic Asymmetric and Linked Oligopyridines*. PhD thesis, Philosophisch-Naturwissenschaftliche Fakultät der Universität Basel, **1998**.

- [52] A. Klug, A. C. Bloomer, J. N. Champness, G. Bricogne, and R. Staden. Protein disk of tobacco mosaic virus at 2.8Å resolution showing the interactions within and between subunits. *Nature*, **1978**, 276, 362–368.
- [53] K. Namba and G. Stubbs. Structure of tobacco mosaic virus at 3.6Å resolution: implications for assembly. *Science*, **1986**, 231, 1401–1406.
- [54] J.-M. Lehn, A. Rigault, J. Siegel, J. Harrowfield, B. Chevrier, and D. Moras. Spontaneous assembly of double-stranded helicates from oligobipyridine ligands and copper(I) cations: Structure of an inorganic double helix. *Proc. Natl. Acad. Sci. USA*, **1987**, 84, 2565–2569.
- [55] J.-M. Lehn, J.-P. Sauvage, J. Simon, R. Ziessel, C. Piccinni-Leopardi, G. Germain, J.-P. Declercq, and M. V. Meerssche. Synthesis and metal complexes of a conformationally restricted quaterpyridine. Crystal structure of its dimeric dinuclear Cu(I) complex, $[\text{Cu}_2(\text{pQP}_2)]^{2+}$. *New J. Chem.*, **1983**, 7, 413–420.
- [56] P. N. W. Baxter, J.-M. Lehn, B. O. Kneisel, and D. Fenske. Self-assembly of a symmetric tetra-copper box-grid with guest trapping in the solid state. *Chem. Commun.*, **1997**, 2231–2232.
- [57] J. C. Jeffery, P. L. Jones, K. L. V. Mann, E. Psillakis, J. A. McClevery, M. D. Ward, and C. M. White. Copper(II)-templated assembly of tetranuclear grid-like complexes from simple pyridine-pyrazole ligands. *Chem. Commun.*, **1997**, 175–176.
- [58] B. Hasenknopf, J.-M. Lehn, B. O. Kneisel, G. Baum, and D. Fenske. Self-assembly of a circular double helicate. *Angew. Chem., Int. Ed. Engl.*, **1996**, 35, 1838–1840.
- [59] B. Hasenknopf, J.-M. Lehn, N. Boumediene, A. Dupont-Gervais, A. Van Dorsselaer, B. Kneisel, and D. Fenske. Self-assembly of tetra- and hexanuclear circular helicates. *J. Am. Chem. Soc.*, **1997**, 119, 10956–10962.
- [60] D. P. Funeriu, J.-M. Lehn, G. Baum, and D. Fenske. Double subroutine self-assembly; spontaneous generation of a nanocyclic dodecanuclear Cu(I) inorganic architecture. *Chem. Eur. J.*, **1997**, 3, 99–104.
- [61] C. Piguet, G. Hopfgartner, A. F. Williams, and B. Bocquet. Formation of the first isomeric [2]-catenates by self-assembly about two different metal ions. *Angew. Chem., Int. Ed. Engl.*, **1995**, 34, 582–584.
- [62] C. Piguet, G. Bernardinelli, and G. Hopfgartner. Helicates as versatile supramolecular complexes. *Chem. Rev.*, **1997**, 97, 2005–2062.
- [63] R. Krämer, J.-M. Lehn, and A. Marquis-Rigault. Self-recognition in helicate self-assembly: Spontaneous formation of helical metal complexes from mixtures of ligands and metal ions. *Proc. Natl. Acad. Sci. USA*, **1993**, 90, 5394–5398.
- [64] W. Dai, H. Hu, X. Wei, S. Zhu, D. Wang, K. Yu, N. K. Dalley, and X. Kou. The double helical binuclear copper complex of 6,6'''-dimethyl-4',4'''-diphenylquinquepyridine and monohelical cadmium complex of 6,6'''-dimethylquinquepyridine. syntheses, crystal and molecular structure of $[\text{Cu}_2(\text{L}2)_2][\text{ClO}_4]_3 \cdot 2\text{CH}_3\text{CN}$ and $[\text{CdL1}][\text{ClO}_4]_2$. *Polyhedron*, **1997**, 16, 2059–2065.
- [65] E.C.Constable, M.Neuburger, L.A.Whall, and M.Zehnder. A tetranuclear meso-helicate. *New J.Chem.*, **1998**, 22, 219–220.
- [66] E. C. Constable, J. V. Walker, D. A. Tocher, and M. A. M. Daniels. Interconversion and ligand dependence in mononuclear and dinuclear cobalt(II)helicate complexes of 2,2':6'',2''':6''',2''''-quinquepyridines; crystal and molecular structure of aqua(methanol)[4',4'''-bis(4-chlorophenyl)-2,2':6',2'':6'',2''':6''',2''''-quinquepyridine] cobalt(II)bis(hexafluorophosphate). *J. Chem. Soc., Chem. Commun.*, **1992**, 768–771.

- [67] E. C. Constable, M. A. M. Daniels, M. G. B. Drew, D. A. Tocher, J. V. Walker, and P. D. Wood. Mono- and di-nuclear helical complexes of 2,2':6',2'':6'',2''':6''',2''''-quinquepyridine (qpy) and its 4',4''-disubstituted derivatives crystal and molecular structures of [Co(bcpqpy)(H₂O)(MeOH)][PF₆]₂ and [Ni₂(bmtqpy)₂(O₂CMe)][PF₆]₃ [bcpqpy and bmtqpy = bis(*p*-chlorophenyl) and bis(methylthio) derivatives]. *J. Chem. Soc., Dalton Trans.*, **1993**, 1947–1958.
- [68] K. T. Potts, M. Keshavarz-K, F. S. Tham, H. D. Abruña, and C. Arana. Metal ion-induced self-assembly of functionalized 2,6-oligopyridines. 3. Metal-metal interaction and redox state-induced transformations in double-stranded helicates derived from functionalized quinquepyridine and sexipyridine. *Inorg. Chem.*, **1993**, 32, 4436–4449.
- [69] Y. Fu, J. Sun, Q. Li, Y. Chen, W. Dai, D. Wang, T. Mak, W. Tang, and H. Hu. Substituent-controlled assembly of helical complexes: synthesis, crystal and molecular structures of double helical silver(I) complexes with substituted quinquepyridines. *J. Chem. Soc., Dalton Trans.*, **1996**, 2309–2313.
- [70] E. C. Constable, S. M. Elder, J. Healy, and M. D. Ward. Helical and nonhelical palladium(II) complexes of oligopyridine ligands: The ligand-directed assembly of polynuclear complexes. *J. Am. Chem. Soc.*, **1990**, 112, 4590–4592.
- [71] E. N. Maslen, C. L. Raston, and A. H. White. Crystal structure of aqua(2,2':6',2'':6'',2'''-quaterpyridyl)sulphito cobalt(III) nitrate monohydrate. *J. Chem. Soc., Dalton Trans.*, **1975**, 323–326.
- [72] W. Henke, S. Kremer, and D. Reinen. High-spin low-spin behaviour of cobalt(II) in octahedral coordination. I. Structure and bonding in tetrapyrindine complexes (M(II)(tetrapy)X₂ · 2H₂O (M(II)= Cu²⁺, Co²⁺). *Z. Anorg. Allg. Chem.*, **1982**, 491, 124–136.
- [73] E. C. Constable, M. J. Hannon, P. Harverson, M. Neuburger, D. R. Smith, V. F. Wanner, L. A. Whall, and M. Zehnder. Synthesis and coordination chemistry of 4',4''-disubstituted 2,2':6',2'':6'',2'''-quaterpyridines and crystal and molecular structures of nickel(II) and cobalt(II) complexes. *Polyhedron*, **2000**, 19, 23–34.
- [74] C.-M. Che, C. W. Chan, S.-M. Yang, C.-X. Guo, C.-Y. Lee, and S.-M. Peng. Synthesis, properties and crystal structures of iron-(II) and -(III) complexes of 2,2':6',2'':6'',2'''-quaterpyridine. *J. Chem. Soc. Dalton Trans.*, **1995**, 2961–2966.
- [75] S. Yang, K. Cheung, and C. M. Che. Preparation and crystal structure of a seven-coordinated oxotungsten(IV) complex of 2,2':6',2'':6'',2'''-quaterpyridine. *J. Chem. Soc., Dalton Trans.*, **1993**, 3515–3517.
- [76] C. Chan, C. Che, and S. Peng. Six- and seven-coordinated manganese(II) complexes of quaterpyridine, synthesis, X-ray crystal structure and catalyst for alkene epoxidation. *Polyhedron*, **1993**, 12, 2169–2173.
- [77] C. Che, Y. Wang, K. Yeung, K. Wong, and S. Peng. Synthesis and molecular structures of novel seven-coordinated oxo- and nitrido-rhenium(V) complexes of 2,2':6',2'':6'',2'''-quaterpyridine. *J. Chem. Soc., Dalton Trans.*, **1992**, 2675–2677.
- [78] E. C. Constable, M. G. B. Drew, G. Forsyth, and M. D. Ward. A near-planar pentadentate silver(I) complex; the crystal and molecular structure of (2,2':6',2'':6'',2''':6''',2''''-quinquepyridine)silver(I) hexafluorophosphate. *J. Chem. Soc., Chem Commun.*, **1988**, 1450–1451.
- [79] W.-Y. Sun, W.-N. Dai, M.-H. Shu, F. Xue, D.-F. Wang, T. C. W. Mak, and H.-W. Tang, Wen-Xia; Hu. Structure and properties of a novel OH-bridged dimetal helical complex with 6,6''-dimethyl-2,2':6',2'':6'',2''':6''',2''''-quinquepyridine ligand. *Inorg. Chim. Acta*, **1999**, 290, 127–132.

- [80] F. H. Burstall. Researches on the polypyridyls. *J. Chem. Soc.*, **1938**, 1662–1672.
- [81] W. Walter. *Lehrbuch der Organischen Chemie*. S. Hirzel Verlag, Stuttgart, Germany, 22 edition, **1991**.
- [82] J. E. Parks, B. E. Wagner, and R. H. Holm. Syntheses employing pyridyllithium reagents: New routes to 2,6-disubstituted pyridines and 6,6'-disubstituted 2,2'-bipyridyls. *J. Organomet. Chem.*, **1973**, 56, 53–66.
- [83] E. C. Constable, S. M. Elder, J. Healy, and D. A. Tocher. A convenient preparation of 2,2':6',2'':6'',2''':6'''-quaterpyridine; the crystal and molecular structures of 2,2':6',2'':6'',2''':6'''-quaterpyridine and bis(acetonitrile)-(2,2':6',2'':6'',2''':6'''-quaterpyridine) nickel(II)-hexafluorophosphate-acetonitrile(1/1). *J. Chem. Soc., Dalton Trans.*, **1990**, 1669–1674.
- [84] E. C. Constable and R. Chotalia. A templated synthesis of a dinickel(II) double-helicate and its demetallation to free 2,2':6',2'':6'',2''':6''':6''''-sexipyridine. *J. Chem. Soc., Chem. Commun.*, **1992**, 64–66.
- [85] T. Laue and A. Plagens. *Namen- und Schlagwort-Reaktionen der Organischen Chemie*. B. G. Teubner, Stuttgart, **1988**.
- [86] C. Mannich, W. Koch, and F. Borkowsky. Über den Aufbau von β -Dekalon aus Cyclohexanon. *Ber. dtsch. chem. Ges.*, **1937**, 70, 355–359.
- [87] H. Hellmann. Kohlenstoff-Alkylierung mit tertiären Aminen und quartären Ammoniumsalzen. Über die Kondensationsreaktionen tertiärer Mannich-Basen. *Angew. Chem.*, **1953**, 65, 473–396.
- [88] J. Thesing and A. Müller. Synthese des Nicotellins. *Angew. Chem.*, **1956**, 68, 577–578.
- [89] K. T. Potts, M. J. Cipullo, P. Ralli, and G. Theodoridis. Synthesis of 2,6-disubstituted pyridines, polypyridinyls, and annulated pyridines. *J. Org. Chem.*, **1982**, 47, 3027–3038.
- [90] E. C. Constable, P. Harverson, D. R. Smith, and L. A. Whall. 4-*tert*-Butylphenyl solubilized oligopyridines. *Tetrahedron*, **1994**, 50, 7799–7806.
- [91] J. V. Walker. *The Metal Directed Assembly of Helical Arrays*. PhD thesis, University of Cambridge, **1993**.
- [92] F. Kröhnke. The specific synthesis of pyridines and oligopyridines. *Synthesis*, **1976**, 1–24.
- [93] D. R. Smith PhD. copy of lab journal.
- [94] G. Mei. Improved method for preparation of 2,6-diacetylpyridine. *Guangdong Yaoxueyuan Xuebao*, **2001**, 17, 166–167.
- [95] Synthesis of 2,6-dicarbonylpyridines. Patent US 2003187271 A1, 2003. Boulder Scientific Company, USA, Inventor: Daniel A. Gately.
- [96] E. Pretsch, J. Seibl, and W. Simon. *Strukturaufklärung organischer Verbindungen mit spektroskopischen Methoden*. Springer-Verlag, Berlin Heidelberg, 2 edition, **1990**.
- [97] M. Hesse, H. Meier, and B. Zeeh. *Spektroskopische Methoden in der organischen Chemie*. George Thieme Verlag Stuttgart, New York, 3 edition, **1991**.
- [98] A. J. Boulton and A. McKillop, editors. *Comprehensive Heterocyclic Chemistry*, volume 2 Part A. Pergamon Press, Oxford, 1. edition, **1984**.
- [99] C. R. Woods, M. Benaglia, F. Cozzi, and J. S. Siegel. Enantioselective synthesis of copper(I) bipyridine based helicates by chiral templating of secondary structure: transmission of stereochemistry on the nanometer scale. *Angew. Chem., Int. Ed. Engl.*, **1996**, 35, 1830–1833.

- [100] Mikio, Y. Inoue, Y. Liu, S. Nagamune, S. Nakamura, K. Wada, and T. Hakushi. Convenient and efficient tosylation of oligoethylene glycols and the related alcohols in tetrahydrofuran-water in the presence of sodium hydroxide. *Bull. Chem. Soc. Jpn.*, **1990**, *63*, 1260–1262.
- [101] E. Weber, F. Vögtle, H.-P. Josel, G. R. Newkome, and W. E. Puckett. Hochselektive Clathrat-Wirtmoleküle für verzweigte Alkohole, insbesondere für 2-Propanol und Ethanol. *Chem. Ber.*, **1983**, *116*, 1906–1913.
- [102] E. Weber, H.-P. Josel, H. Puff, and S. Franken. Solid-state inclusion compounds of new host macrocycles with uncharged organic molecules. host synthesis, inclusion properties, and X-ray crystal structure of an inclusion compound with 1-propanol. *J. Org. Chem.*, **1985**, *50*, 3125–3132.
- [103] E. Weber, H.-J. Köhler, and H. Reuter. Synthese und Moleküleinschluss von Naphto- und Benzonaphto-kondensierten Pyridinokronen — Kristallstruktur eines Dioxan-Clathrats. *Chem. Ber.*, **1989**, *122*, 959–967.
- [104] W. H. Kruizinga and R. M. Kellogg. Preparation of macrocyclic lactones by ring closure of cesium carboxylates. *J. Am. Chem. Soc.*, **1981**, *103*, 5183–5189.
- [105] H. Friebolin. *Ein- und zweidimensionale NMR-Spektroskopie*. Wiley-VCH Verlag GmbH, Weinheim, 3 edition, **1999**.
- [106] J. Kohout, M. Kbešová, and J. Gažo. Studium des gegenseitigen Einflusses der Bindungen in Thiocyanat–Kupfer(II)-Komplexen mit Methyl- und Dimethylpyridinen mittels Infrarotspektroskopie. *Monatsh. Chem.*, **1977**, *108*, 1011–1018.
- [107] P. Drożdżewski and E. Kordon. Isotopic studies of the metal-ligand vibrations in histamine complexes with copper(II). *Spectrochim. Acta, Part A*, **2000**, *56*, 1299–1304.
- [108] I. Persson, M. Sandström, A. T. Steel, M. J. Zapatero, and R. Åkesson. A large-angle X-ray scattering, XAFS, and vibrational spectroscopic study of copper(I) halide complexes in dimethyl sulfoxide, acetonitrile, pyridine, and aqueous solutions. *Inorg. Chem.*, **1991**, *30*, 4075–4081.
- [109] N. W. Alcock, P. R. Barker, J. M. Haider, M. J. Hannon, C. L. Painting, Z. Pikramenou, E. A. Plummer, K. Rissanene, and P. Saarenketo. Red and blue luminescent metallo-supramolecular coordination polymers assembled through π - π interactions. *J. Chem. Soc., Dalton Trans.*, **2000**, 1447–1461.
- [110] B. Whittle, E. L. Horwood, L. H. Rees, S. R. Batten, J. C. Jeffery, and M. D. Ward. Crystal structures of a series of Co(II), Cu(II) and Zn(II) complexes of 4'-(3,4-dihydroxyphenyl)-2,2':6',2''-terpyridine and 4'-(3,4-dimethoxyphenyl)-2,2':6',2''-terpyridine. *Polyhedron*, **1998**, *17*, 373–379.
- [111] M. I. Arriortua, T. Rojo, J. M. Amigo, G. Germain, and J. P. Declercq. Bis(2,2':6',2''-terpyridine)copper(II) hexafluorophosphate. *Acta Crystallogr., Sect. B: Struct. Crystallogr. Cryst. Chem.*, **1982**, *38*, 1323–1324.
- [112] E. C. Constable. The coordination chemistry of 2,2':6',2''-terpyridine and higher oligopyridine. *Adv. Inorg. Chem. Radiochem.*, **1987**, *30*, 69–121.
- [113] M. H. Chisholm, J. C. Huffman, I. C. Rothwell, P. G. Bradley, and W. H. N. Kress. Bis(2,2'-bipyridyl)diisopropoxymolybdenum(II). structural and spectroscopic evidence for molybdenum-to-bipyridyl π^* bonding. *J. Am. Chem. Soc.*, **1981**, *103*, 4945–4947.
- [114] M. Munakata, S. Kitagawa, A. Asahara, and H. Masuda. Crystal structure of bis(2,2'-bipyridine)copper(I) perchlorate. *Bull. Chem. Soc. Jpn.*, **1987**, *60*, 1927–1929.
- [115] C. A. Bessel, R. F. See, D. L. Jameson, M. R. Churchill, and K. J. Takeuchi. Structural considerations of terdentate ligands: crystal structures of 2,2':6',2''-terpyridine and 2,6-bis(pyrazol-1-yl)pyridine. *J. Chem. Soc., Dalton Trans.*, **1992**, 3223–3228.

- [116] A. J. Bard and L. R. Faulkner. *Electrochemical Methods Fundamentals and Applications*. John Wiley & Sons, Inc., New York, 2. edition, **2001**.
- [117] K. T. Potts, M. P. Wentland, D. Ganguly, G. D. Storrer, S. K. Cha, J. Cha, and H. Abruña. Multimetallic, double-stranded helical complexes derived from hexa(*n*-propylthia)novipyridine: synthesis, structure and redox properties. *Inorg. Chim. Acta*, **1999**, 288, 189–199.
- [118] K. T. Potts, M. Keshavarz-K, F. S. Tham, K. A. G. Raiford, C. Arana, and H. D. Abruña. Di-, tri-, and tetrametallic double-stranded helical complexes derived from alkylthio-substituted septipyridines: Synthesis, structure, and redox properties. *Inorg. Chem.*, **1993**, 32, 5477–5484.
- [119] R. Hogg and R. G. Wilkins. Exchange studies of certain chelate compounds of the transitional metals. part VIII. 2,2',2''-terpyridine complexes. *J. Chem. Soc. (I)*, **1962**, 341–350.
- [120] A. Pfeil and J.-M. Lehn. Helicate self-organisation: Positive cooperativity in the self-assembly of double-helical metal complexes. *J. Chem. Soc., Chem. Commun.*, **1992**, 838–840.
- [121] E. C. Constable and J. V. Walker. The systematic synthesis of heterobimetallic double-helical complexes of 2,2':6',2'':6'',2''':6''',2''''-quinquepyridines. *J. Chem. Soc., Chem. Commun.*, **1992**, 884–886.
- [122] M. J. Hannon. *Metal Ion Control in Oligopyridine Coordination Chemistry*. PhD thesis, University of Cambridge, **1993**.
- [123] K. Nakamoto. *Infrared and Raman Spectra of Inorganic and Coordination Compounds*, volume B. John Wiley & Sons, Inc., New York, 5 edition, **1997**.
- [124] R. Chotalia, E. Constable, M. Neuburger, D. Smith, and M. Zehnder. A convenient high yield synthesis of 2,2':6',2'':6'',2''':6''',2''''-sexipyridine and helical transition-metal complexes of substituted sexipyridines. *J. Chem. Soc., Dalton Trans.*, **1996**, 4207–4216.
- [125] R. Prasad and D. B. Scaife. Electro-oxidation and electro-reduction of some iron(II), cobalt(II) and nickel(II) polypyridyl complexes in acetonitrile. *J. Electroanal. Chem.*, **1977**, 84, 373–386.
- [126] R. C. Weast, M. J. Astle, and W. H. Beyer, editors. *Handbook of Chemistry and Physics*. CRC press, Inc., Florida, 69 edition, **1988-1989**.
- [127] K. A. Gheysen, K. T. Potts, H. C. Hurrell, and H. D. A. na. Helical heptacoordinate complexes of cobalt derived from 2,2':6',2'':6'',2''':6''',2''''-quinquepyridine derivatives. *Inorg. Chem.*, **1990**, 29, 1589–1592.
- [128] L. J. Farrugia. Ortep32. University of Glasgow, 1997. Programme.
- [129] Cambridge Crystallographic Data Centre. Mercury version 1.1.2, 2001-2002. Programme.
- [130] E. Constable, F. Heitzler, M. Neuburger, and M. Zehnder. Steric control of directional isomerism in dicopper(I) helicates of asymmetrically substituted 2,2':6',2'':6'',2'''-quaterpyridine derivatives. *J. Am. Chem. Soc.*, **1997**, 119, 5606–5617.
- [131] I. A. Hougen. Helixbildende Oligothieryl-Bipyridin Liganden und ihre Komplexe. Diploma thesis, University of Basel, Switzerland, Institute of Inorganic Chemistry, 1996.
- [132] J. K. Stille. Palladium-katalysierte Kupplungsreaktionen organischer Elektrophile mit Organozinn-Verbindungen. *Angew. Chem.*, **1986**, 98, 504–519.
- [133] D. Milstein and J. K. Stille. A general, selective, and facile method for ketone synthesis from acid chlorides and organotin compounds catalyzed by palladium. *J. Am. Chem. Soc.*, **1978**, 100, 3636–3638.
- [134] G. Hanan. *Auto-assemblage de structures supramoléculaires polymétalliques*. PhD thesis, l'Université Louis Pasteur de Strasbourg, **1995**.

- [135] T. Garber and D. P. Rillema. Efficient preparative routes to 6,6'-dibromo-2,2'-bipyridine and 6-bromo-2,2'-bipyridine. *Synth. Commun.*, **1990**, *20*, 1233–1239.
- [136] H. G. O. Becker, W. Berger, G. Domschke, E. Fanghänel, J. Faust, M. Fischer, F. Gentz, K. Gewalt, R. Gluch, R. Mayer, K. Müller, D. Pavel, H. Schmidt, K. Schollberg, K. Schwetlick, E. Seiler, G. Zeppenfeld, R. Beckert, W. D. Habicher, P. Metz, and D. Pavel. *Organikum*. Wiley-VCH, Weinheim, 21. edition, **2001**.
- [137] G. Newkome, D. Hager, and G. Kiefer. Synthesis of halogenated terpyridines and incorporation of the terpyridine nucleus into a polyetheral macrocycle. *J. Org. Chem.*, **1986**, *51*, 850–853.
- [138] K. E. Berg, A. Tran, M. K. Raymond, M. Abrahamsson, J. Wolny, S. Redon, M. Andersson, L. Sun, S. Styring, L. Hammarström, H. Toftlund, and B. Åkermark. Covalently linked ruthenium(II)-manganese(II) complexes: Distance dependence of quenching and electron transfer. *Eur. J. Inorg. Chem.*, **2001**, 1019–1029.
- [139] T. M. Cresp, M. V. Sargent, and P. Vogel. A synthesis of $\alpha\beta$ -unsaturated aldehydes. *J. Chem. Soc., Perkin Trans. 1*, **1974**, 37–41.
- [140] J. J. Li. *Name Reactions*. Springer, Berlin, 1. edition, **2002**.
- [141] W. Bauer, W. R. Winchester, and P. von Ragué Schleyer. Monomeric organolithium compounds in tetrahydrofuran: *tert*-butyllithium, *sec*-butyllithium, supermesityllithium, mesityllithium, and phenyllithium. Carbon-lithium coupling constants and the nature of carbon-lithium bonding. *Organometallics*, **1987**, *6*, 2371–2379.
- [142] N. Miyaura and A. Suzuki. Palladium-catalyzed cross-coupling reactions of organoboron compounds. *Chem. Rev.*, **1995**, *95*, 2457–2483.
- [143] A. Suzuki. Recent advances in the cross-coupling reactions of organoboron derivatives with organic electrophiles, 1995–1998. *J. Organomet. Chem.*, **1999**, *576*, 147–168.
- [144] C. Coudret. Efficient syntheses of 4-iodopyridine and of 4-pyridylboronic acid pinacol ester. *Synth. Commun.*, **1996**, *26*, 3543–3547.
- [145] T. I. Wallow and B. M. Novak. Highly efficient and accelerated Suzuki aryl couplings mediated by phosphine-free palladium sources. *J. Org. Chem.*, **1994**, *59*, 5034–5037.
- [146] F. Raymond, 2001. ADS American Dye Source, Inc., Baie d'Urfé, Quebec, Canada, confidential note.
- [147] R. D'Alessio and A. Rossi. Short synthesis of undecylprodigiosine. a new route to 2,2'-bipyrrylpyromethene systems. *Synlett*, **1996**, 513–514.
- [148] S. Martina, V. Enkelmann, G. Wegner, and A.-D. Schlüter. *N*-protected pyrrole derivatives substituted for metal-catalyzed cross-coupling reactions. *Synthesis*, **1991**, 613–615.
- [149] G. W. Gray, M. Hird, D. Lacey, and K. J. Toyne. The synthesis and transition temperatures of some fluoro-substituted 4-cyanophenyl and 4-cyanobiphenyl-4'-yl 4-pentyl- and 4-butoxybenzoates. *Mol. Cryst. Liq. Cryst.*, **1989**, *172*, 165–189.
- [150] O. Baudoin, D. Guénard, and F. Guéritte. Palladium-catalyzed borylation of ortho-substituted phenyl halides and application to the one-pot synthesis of 2,2'-disubstituted biphenyls. *J. Org. Chem.*, **2000**, *65*, 9268–9271.
- [151] W. Goodall, K. Wild, K. J. Arm, and J. A. G. Williams. The synthesis of 4'-aryl substituent terpyridines by Suzuki cross-coupling reactions: substituent effects on ligand fluorescence. *J. Chem. Soc., Perkin Trans.*, **2002**, *2*, 1669–1681.

- [152] J.-P. Gisselbrecht, M. Gross, J.-M. Lehn, J.-P. Sauvage, R. Ziessel, C. Piccinni-Leopardi, J. M. Arrieta, G. Germain, and M. V. Meerssche. *p*-Quaterpyridine complexes: Crystal structure of the mononuclear Cu(II) complex. Electrochemical studies of the monomeric Cu(II) and dimeric Cu(I) complexes, of their interconversion, and of the *bis*-Ru(II)(bipy)₂ complex. *Nouveau Journal de Chimie*, **1984**, 8, 661–667.
- [153] G. Baum, E. C. Constable, D. Fenske, C. E. Housecroft, and T. Kulke. Stereoselective double-helicate assembly from chiral 2,2':6',2'':6'',2''':6''',2''''-quaterpyridines and tetrahedral metal centres. *Chem. Eur. J.*, **1999**, 5, 1862–1873.
- [154] E. I. Levkoeva, M. L. I., D. M. Krasnokutskaya, M. I. Evstratova, Y. S. Karpman, I. S. Tubina, I. L. Ivanova, and L. N. Yakhontov. *Khim. Geterotsykl. Soedin.*, **1976**, 233–237.
- [155] F. Kröhnke. Neuere Methoden der präparativen organischen Chemie: Synthesen mit Hilfe von Pyridinium-Salzen. *Angew. Chem.*, **1963**, 75, 181–194.
- [156] F. Kröhnke. Synthesen mit Hilfe von Pyridiniumsalzen. *Angew. Chem.*, **1953**, 65, 605–626.
- [157] L. C. King. The reaction of iodine with some ketones in the presence of pyridine. *J. Am. Chem. Soc.*, **1944**, 66, 894–895.
- [158] T. Kubo and K. Manabe. Solid-phase reactions of organometallic compounds. IV. thermal decomposition of cobaltous acetate tetrahydrate 2. verification of a new intermediate. *Kogyo Kagaku Zasshi*, **1966**, 69, 612–617.
- [159] L. J. Charbonnière, N. Weibel, and R. F. Ziessel. Synthesis of mono-, bis- and tris-tridentate ligands based on 5'-substituted-2,2'-bipyridine-6-carboxylic acid. *Tetrahedron Lett.*, **2001**, 42, 659–662.
- [160] G. M. P. Giblin, P. C. Box, I. B. Campell, A. P. Hancock, S. Roomans, G. I. Mills, C. Molloy, G. E. Tranter, A. L. Walker, S. R. Doctrow, K. Huffman, and B. Malfroy. 6,6'-bis(2-hydroxyphenyl)-2,2'-bipyridine manganese(III) complexes: A novel series of superoxide dismutase and catalase mimetics. *Bioorganic & Medicinal Chemistry Letters*, **2001**, 11, 1367–1370.
- [161] D. Lötscher, S. Rupprecht, H. Stoeckli-Evans, and A. von Zelewsky. Enantioselective catalytic cyclopropanation of styrenes by copper complexes with chiral pinene-[5,6]-bipyridine ligands. *Tetrahedron: Asymmetry*, **2000**, 11, 4341–4357.
- [162] E. C. Constable and J. Lewis. The preparation and coordination chemistry of 2,2':6',2''-terpyridine macrocycles-1. *Polyhedron*, **1982**, 1, 303–306.
- [163] J. Uenishi, T. Tanaka, K. Nishiwaki, S. Wakabayashi, S. Oae, and H. Tsukube. Synthesis of ω -(bromomethyl)bipyridines and related ω -(bromomethyl)pyridinoheteroaromatics: Useful functional tools for ligands in host molecules. *J. Org. Chem.*, **1993**, 58, 4382–4388.
- [164] J. McKenney, Jr. and R. N. Castle. The synthesis of [1]benzothieno[2,3-c]quinolines, [1]benzothieno[2,3-c][1,2,4]triazolo[4,3-a]quinoline, and [1]benzothieno[2,3-c]tetrazolo[1,5-a]quinoline. *J. Heterocycl. Chem.*, **1987**, 24, 1525–1529.
- [165] G. R. Newkome, J. D. Sauer, and G. L. McClure. Chemistry of heterocyclic compounds. 10. ketalization of 2-pyridylketones under basic conditions. *Tetrahedron Lett.*, **1973**, 18, 1599–1602.
- [166] E. Salmi. Untersuchungen über ätherartige Verbindungen, I. Mitteil.: Zur Darstellung der Acetale und Ketale. *Berichte der Deutschen Chemischen Gesellschaft*, **1938**, 71, 1803–1808.
- [167] CambridgeSoft Corporation. ChemDraw Ultra, version 7.0.1, 2002. Programme.
- [168] W. E. Parham and R. M. Piccirilli. Selective halogen-lithium exchange in 2,5-dibromobenzenes and 2,5-dibromopyridine. *J. Org. Chem.*, **1977**, 42, 257–260.

- [169] C. Dietrich-Buchecker, M. C. Jiménez, and J.-P. Sauvage. Selective and efficient syntheses of di-, tri- and tetrasubstituted 1,10-phenanthrolines. *Tetrahedron Lett.*, **1999**, *40*, 3395–3396.
- [170] Substituierte Benzoylguanidine, Verfahren zu ihrer Herstellung, ihre Verwendung als Medikament oder Diagnostikum sowie sie enthaltendes Medikament. Patent DE 4325822 A1, 1995. Hoechst AG, 65929 Frankfurt, DE, Inventor: Dr. Heinz-Werner Kleeman, Dr. Hans-Jochen Lang, Dr. Jan-Robert Schwark, Dr. Andreas Weichert, Dr. Wolfgang Scholz, and Dr. Udo Albus.
- [171] T. E. Gunda. Mol2mol version 5.2. University of Debrecen, Debrecen, Hungary, 2003. Programme.
- [172] A. J. Boulton and A. McKillop, editors. *Comprehensive Heterocyclic Chemistry*. Pergamon Press, Oxford, 1. edition, **1984**.
- [173] K. Nakamoto and P. J. McCarthy. *Spectroscopy and Structure of Metal Chelate Compounds*. John Wiley & Sons, inc., New York, London, Sydney, 1. edition, **1968**.
- [174] A. F. Holleman, E. Wieberg, and N. Wiberg. *Lehrbuch der Anorganischen Chemie*. Walter de Gruyter & Co., Berlin, Germany, 33. edition, **1985**.